HYDROGEN-BOND DRIVEN SUPRAMOLECULAR CHEMISTRY FOR MODULATING PHYSICAL PROPERTIES OF PHARMACEUTICAL COMPOUNDS

by

SAFIYYAH FORBES

B.S., Long Island University, 2004

AN ABSTRACT OF A DISSERTATION

submitted in partial fulfillment of the requirements for the degree

DOCTOR OF PHILOSOPHY

Department of Chemistry
College of Arts and Sciences

KANSAS STATE UNIVERSITY
Manhattan, Kansas

2010

Abstract

The ability to predict and control molecular arrangements without compromising the individual molecules themselves still remains an important goal in supramolecular chemistry. This can be accomplished by establishing a hierarchy of intermolecular interactions such as hydrogen and halogen bond, which may facilitate supramolecular assembly processes.

Several acetaminopyridine/acetaminomethylpyridine supramolecular reactants (SR's) were prepared with aliphatic carboxylic acids in order to determine patterns of molecular recognition preferences of the N-H moiety. The results obtained revealed the formation of molecular cocrystals through heteromeric O-H…N/N-H…O hydrogen bonds with the acetaminopyridine/acetaminomethylpyridine binding site. Furthermore, the SR's also reacted with metal ions resulting in robust 1D and 2D metal-containing architectures.

A series of pyridyl/pyrazine mono-*N*-oxide compounds were synthesized and reacted with a variety of halogenated benzoic acids, in order to assess the ability of these molecules to establish binding selectivity when both a hydrogen and halogen bond donor is present. The results obtained revealed that the pyridyl/carboxylic acid synthon formed 7/7 times and halogen bonds (N-O…I or N-O…Br) extended the SR/acid dimers into 1D and 2D networks. These results were rationalized via charge calculations as well as through the hierarchical view of intermolecular interactions consisting of hydrogen and halogen bonds.

Furthermore, a series of thienyl compounds were synthesized and allowed to react with halogen bond donors to determine whether the halogen bond is purely electrostatic or based on the hard and soft acids and bases principles. The results obtained showed that of the 34 reactions between a halogen bond donor and thienyl compounds, the halogen bond is predominantly electrostatic in nature.

Finally, as a result of our improved understanding on molecular recognition, we were able to carry out systematic structure-property studies on a series of cocrystals of anti-cancer drug molecules with aliphatic carboxylic acids. This study revealed that systematic changes to the molecular nature of the co-crystallizing agent combined with

control over the way individual building blocks are organized within the crystalline lattice makes it possible to establish predictable links between molecular structure and macroscopic physical properties, such as melting behavior, solubility, dissolution rate, etc.

HYDROGEN-BOND DRIVEN SUPRAMOLECULAR CHEMISTRY FOR MODULATING PHYSCIAL PROPERTIES OF PHARMACEUTICAL COMPOUNDS

by

SAFIYYAH FORBES

B.S., Long Island University, 2004

A DISSERTATION

submitted in partial fulfillment of the requirements for the degree

DOCTOR OF PHILOSOPHY

Department of Chemistry
College of Arts and Sciences

KANSAS STATE UNIVERSITY
Manhattan, Kansas

2010

Approved by:

Major Professor
Dr. Christer Aakeröy

Abstract

The ability to predict and control molecular arrangements without compromising the individual molecules themselves still remains an important goal in supramolecular chemistry. This can be accomplished by establishing a hierarchy of intermolecular interactions such as hydrogen and halogen bond, which may facilitate supramolecular assembly processes.

Several acetaminopyridine/acetaminomethylpyridine supramolecular reactants (SR's) were prepared with aliphatic carboxylic acids in order to determine patterns of molecular recognition preferences of the N-H moiety. The results obtained revealed the formation of molecular cocrystals through heteromeric O-H…N/N-H…O hydrogen bonds with the acetaminopyridine/acetaminomethylpyridine binding site. Furthermore, the SR's also reacted with metal ions resulting in robust 1D and 2D metal-containing architectures.

A series of pyridyl/pyrazine mono-*N*-oxide compounds were synthesized and reacted with a variety of halogenated benzoic acids, in order to assess the ability of these molecules to establish binding selectivity when both a hydrogen and halogen bond donor is present. The results obtained revealed that the pyridyl/carboxylic acid synthon formed 7/7 times and halogen bonds (N-O…I or N-O…Br) extended the SR/acid dimers into 1D and 2D networks. These results were rationalized via charge calculations as well as through the hierarchical view of intermolecular interactions consisting of hydrogen and halogen bonds.

Furthermore, a series of thienyl compounds were synthesized and allowed to react with halogen bond donors to determine whether the halogen bond is purely electrostatic or based on the hard and soft acids and bases principles. The results obtained showed that of the 34 reactions between a halogen bond donor and thienyl compounds, the halogen bond is predominantly electrostatic in nature.

Finally, as a result of our improved understanding on molecular recognition, we were able to carry out systematic structure-property studies on a series of cocrystals of anti-cancer drug molecules with aliphatic carboxylic acids. This study revealed that systematic changes to the molecular nature of the co-crystallizing agent combined with

control over the way individual building blocks are organized within the crystalline lattice makes it possible to establish predictable links between molecular structure and macroscopic physical properties, such as melting behavior, solubility, dissolution rate, etc.

Table of Contents

List of Figures

List of Tables

List of Abbreviations

I_3F_3B	1,3,5-trifluorotriiodobenzene
I_2F_4B	1,4-diiodotetrafluorobenzene
FBA	3-fluorobenzoic acid
F_2BA	2,4-difluorobenzoic acid
ABA	4-aminobenzoic acid
BrF_4BA	4-bromotetrafluorobenzoic acid
$BrIF_4B$	1-bromo-4-iodotetrafluorobenzene
HBA	4-hydroxybenzoic acid
IF_4BA	4-iodotetrafluorobenzoic acid
IBA	4-iodobenzoic acid
ADI	adipic acid
CSD	cambridge structural database
DCC	dicyclohexylcarbodimide
DOD	dodecanedioic acid
FUM	fumaric acid
GLU	glutaric acid
HEP	heptanoic acid
HEX	hexanoic acid
HG	hydrogenglutarate
LAU	lauric acid
OCT	octanoic acid
OXA	oxalic acid
MAL	malonic acid
NBA	4-nitrobenzoic acid
SEB	sebacic acid
SUB	suberic acid
SUC	succinic acid
API	active pharmaceutical ingredient
PIM	pimelic acid

py	pyridine
TPP	triphenyl phosphite

Acknowledgements

First I would like to thank my mom, Jannett for always believing in me and encouraging me to pursue my dreams. Most importantly, I would like to thank my best friend and husband Olajide for always having my back and for being very supportive and understanding. I would also like to thank my two brothers Danion and Kadian, for their endless love and support and for always keeping me grounded. Your love and continuous support constantly makes me know that I can accomplish whatever I set my mind to. All of you are and will always be an inspiration to me.

I would like to thank my advisor Christer Aakeröy for his continuous support and guidance over the past five years. I have blossomed into a more confident individual as well as an excellent chemist during my time under your supervision. I have learned a lot from you and will always hold on to those lessons, I couldn't have asked for a better advisor.

To both past and present members of the Aakeröy research group, thanks for all the helpful suggestions and advice. You have all made the lab an enjoyable place to work.

I would also like to thank my committee members, Professors Eric Maatta, Sundeep Rayat, Dolores Takemoto and Michael Apley for always having an open door policy.

Special thanks to Dr. John Desper for solving all the single crystal X-ray structures, without which, most of the results in this dissertation would not have been possible.

Thanks to the various people behind the scenes in the department for their assistance, especially, Jim Hodgson, Tobe Eggers, and Ron Jackson for always willing to help in fixing whatever needs to be fixed without any hesitation, you all have made my work in the lab a little less stressful.

Finally I would like to thank my undergraduate mentor Dr. Aderemi Oki for his encouragement to continue my education.

Dedication

Over the years there has being many shoulders that have held me up in order for me to be where I am today and the past five years would not have being possible without the never-ending support and love of my family. This accomplishment and others to come is as much yours as it is mine.

To my mother Jannett, you are one of the strongest women I have had the privilege to come to know and love, without your countless sacrifice and belief in me I would not be where I am today. Thank you for your endless support, love, encouragement and prays. I love you mommy!!

I would especially like to dedicate this dissertation to my husband Olajide. You have shared all my pains and frustrations; your love, complete understanding and belief in me is what kept me focused and driven. I love you very much!!

To my bothers Danion and Kadian, thanks for your support and love, but most importantly thanks for holding things down and allowing me to pursue my dream, I love you both!!!

To the other members of my family Iyabo, Adesola, Adenike, Lanre, Adeyemi Jr., and Bethnia, you guys rock. You all are an inspiration and I couldn't have asked for a better support system. Thank you all for putting up with me and surrounding me with your continuous love and support. I love you all!!

Preface

Research carried out at Kansas State University for this dissertation led to the following publications in scientific journals.

Aakeröy, C.B.; Forbes, S.; Desper, J. "Using Cocrystals to Systematically Modulate Aqueous Solubility and Melting Behavior of an Anticancer Drug" *J. Am. Chem. Soc*. **2009**, 131, 17048.

Aakeröy, C.B.; Hussain, I.; Forbes, S.; Desper, J. "Versatile Ligands for the Construction of Layered Metal-Containing Networks" *Aust. J. Chem*. **2009**, 62, 899.

Aakeröy, C.B.; Hussain, I.; Forbes, S.; Desper, J. "Exploring the hydrogen-bond preference of N–H moieties in co-crystals assembled via O–H(acid)…N(py) intermolecular interactions" *CrystEngComm*. **2007**, 9, 46.

CHAPTER 1 - From molecular recognition to fine-tuning physical properties of pharmaceutical compounds

1.1 Introduction

1.1.1 Molecular recognition

Molecular recognition[1] *i.e.* the way in which molecules interact and communicate with each other through non-covalent intermolecular forces[2] is essential in biological systems as well as in areas of pharmaceutics, materials science and polymer chemistry. According to Jean-Marie Lehn, recognition involves *complementarity* interactions between associating partners, *i.e*. the information content of a receptor with respect to a given substrate.[1] In essence, the recognition process extends over energetic features as well as over geometrical ones, which has being eloquently illustrated by Emil Fischer's concept of the steric fit "lock and key" model.[1,3] Further illustrating Lehn concept that recognition is binding with a purpose, similarly receptors are ligands with a purpose[1] Figure 1.1.

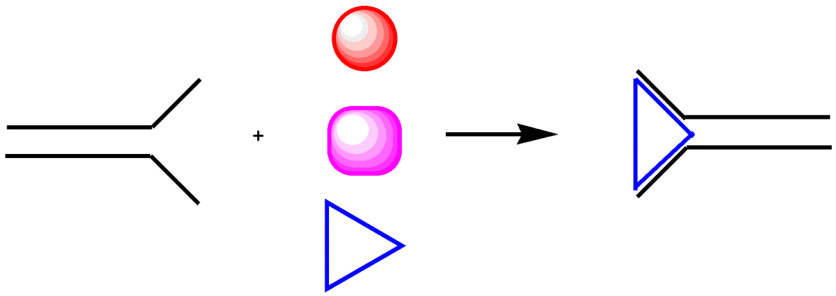

Figure 1.1 Example of selective molecular recognition.

Thus it is important to have a comprehensive understanding of non-covalent interactions, in order to reliably predict molecular organization, assembly and connectivity in the solid state as this will ultimately aid in controlling physical properties of bulk materials.[4]

1.1.2 Generation of complementarity through self-assembly

Self-assembly is a process of organizing molecular units into ordered structures through non-covalent interactions thereby generating supermolecules.[5] It is a powerful

strategy for the generation of structural and functional complexity. Several studies have shown that extended supramolecular architectures can be synthesized with the aid of complementary intermolecular interactions.[6] Most of these supramolecular synthetic strategies employed are based on the combination of functional groups located on different molecules that prefer to interact with each other rather than with themselves.[7,8]

Furthermore, the organization of different functional groups results from the molecular information stored in the component and from the active groups, which they bear. Thus generating molecular order is based on recognition-directed spontaneous assembly of one functional group from complementary molecular components, each of which presents two identical recognition sites,[9] Figure 1.2.

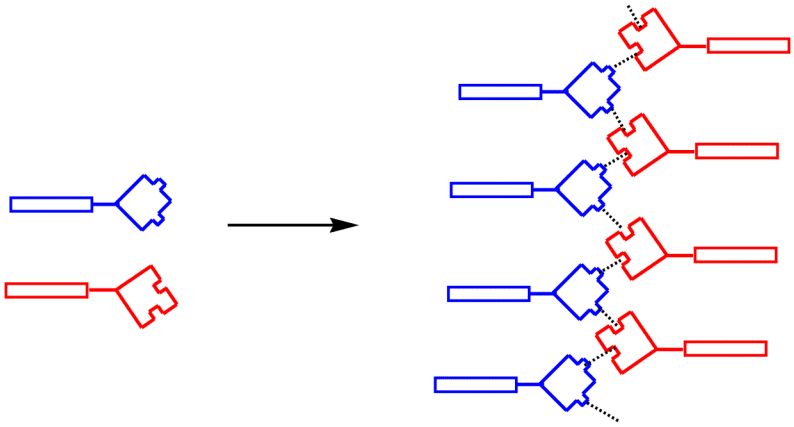

Figure 1.2 Schematic representation of the formation of an ordered structure through molecular-recognition assembly of two different molecular units.[9]

The most famous and well-known example of self-assembly is the DNA double helix, a self-assembly of two complementary helical strands, held together through hydrogen bonding between base pairs,[10] Figure 1.3.

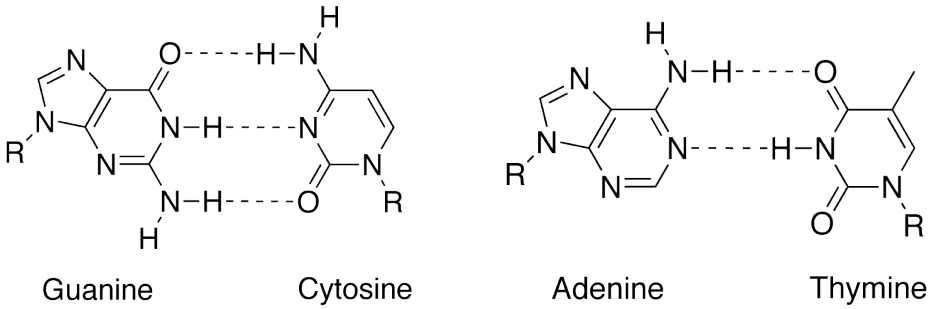

Figure 1.3 Example of self-assembly.

Other examples of self-assembly include inorganic and hydrogen-bonded multicomponent entities.[11] Furthermore, these examples provide us with more insight into controlling molecular recognition and self-assembly, thereby allowing for further construction of supermolecules.

1.1.3 Hydrogen bond in crystal engineering

Hydrogen bonding, the master key for molecular recognition,[12] is the most reliable directional interaction in supramolecular construction, and is highly significant in crystal engineering;[13] the latter has been defined as "*…the understanding of intermolecular interactions in the context of crystal packing and in the utilization of such understanding in the design of new solids with desirable physical and chemical properties*."[14]

The field of crystal engineering is greatly indebted to the pioneering work of Etter and co-workers who began to focus attention on the ability of hydrogen bonds to help control molecular crystallizations.[15] Moreover, this early work revealed that reliable hydrogen-bonding motifs are formed by many elementary functional groups frequently encountered in simple molecules. Together, these observations along with the hydrogen-bond rules provide useful information about preferred connectivity patterns, hydrogen-bond selectivity, and stereoelectronic properties.[16]

The hydrogen-bond rules proposed by Etter are very useful and can be applied to organic hydrogen-bonded structures. The general rules state:

1. all acidic hydrogens available in a molecule will be used in hydrogen bonding in the crystal structure of that compound.[17]
2. all good acceptors will be used in hydrogen bonding when there are available hydrogen-bond donors.[18]
3. the best hydrogen-bond donor and the best hydrogen-bond acceptor will preferentially form hydrogen bonds to one another.[19]

These guidelines have set the stage for important advances in crystal engineering where structures are built from more sophisticated molecules, specifically designed to incorporate multiple sites of hydrogen bonding and oriented in arrays favoring the assembly of networks with predictable architectures,[20] Figure 1.4.

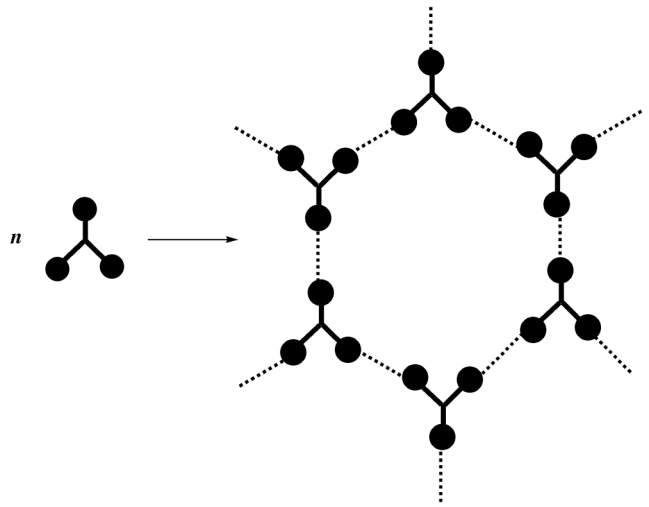

Figure 1.4 Formation of a hexagonal network, broken lines represent directional intermolecular interactions.[21]

Hydrogen bonds are usually written as D-H…A and normally involve an electronegative atom such as O or N as the acceptor (A) and an atom, as the donor (D) where D is more electronegative than A.[22] Normal hydrogen bonds typically range in strength from approximately 4-60 kJ mol^{-1}, although certain highly acidic compounds such as HF_2^- have hydrogen bond energies of up to 120 kJ mol^{-1}.[23] Whereas, the typical hydrogen bond distances are 2.50-2.80 Å (H…A), interactions in excess of 3.0 Å may also be significant.[23]

The design step of crystal engineering utilizes the knowledge of non-covalent forces that mediate the formation of supramolecular synthons, which are *"structural units within supermolecules which can be formed and/or assembled by known or conceivable intermolecular interactions."*[24]

Hydrogen-bonded supramolecular synthons are commonly used in crystal engineering, and an improved understanding of their geometries, and their frequency of occurrence in the presence of other hydrogen-bonding groups, will allow us to design and synthesize novel cocrystals. Supramolecular synthons are divided into two categories; homosynthons,[25] which are composed of self-complementary functional groups, as exemplified by the carboxylic acid dimer **1** and the amide-amide dimer **2**, and heterosynthons,[25,26] which are composed of different but complementary functional groups **3-6**, Figure 1.5.

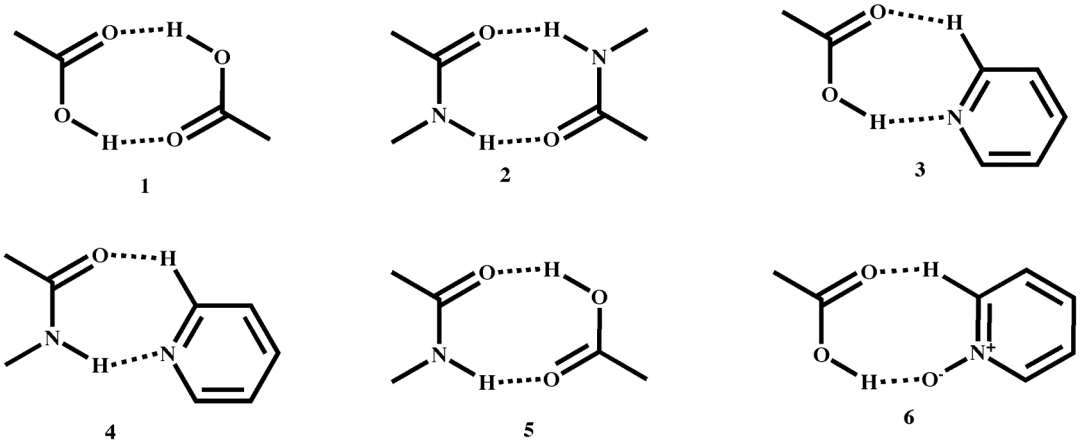

Figure 1.5 Few examples of supramolecular synthons selected from the recent literature: homosynthons (**1-2**) and heterosynthons (**3-6**).[25,26]

1.1.4 Co-crystallization a tool for probing intermolecular interaction

Co-crystallization plays a vital role in probing intermolecular interactions between different molecules; these involve the deliberate bringing together of different molecular species within the same crystalline lattice without making or breaking covalent bonds.[27] The overall aim of a co-crystallization reaction is to obtain a heteromeric compound, rather than a homomeric species (recrystallization), Figure 1.6.

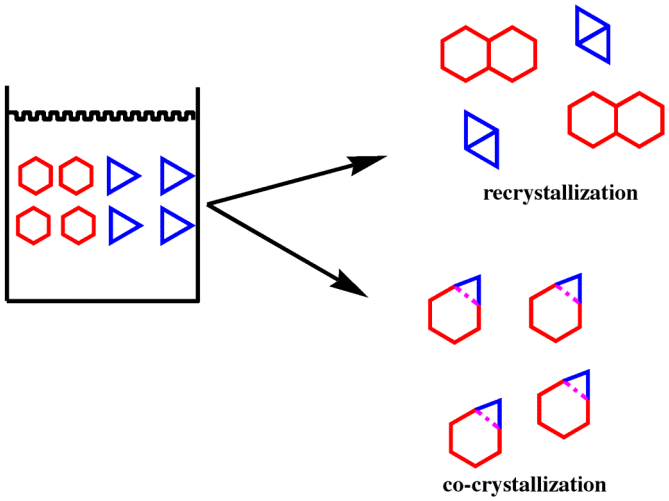

Figure 1.6 Recrystallization (homomeric intermolecular forces dominates) and co-crystallization (heteromeric intermolecular forces dominates).

Obtaining a heteromeric compound is easier said than done, because molecules by nature are inherently selfish and tend to stick with themselves. However, by developing

new systematic strategies we can increase the chances of obtaining a heteromeric product. With this in mind, one of the major goals of this dissertation is to probe for intermolecular recognition by conducting systematic studies on series of cocrystals. A cocrystal is a "*structurally homogeneous crystalline material that contains two or more neutral building blocks that are present in definite stoichiometric amounts.*"[27,28] Two examples of a cocrystal are shown in Figure 1.7.

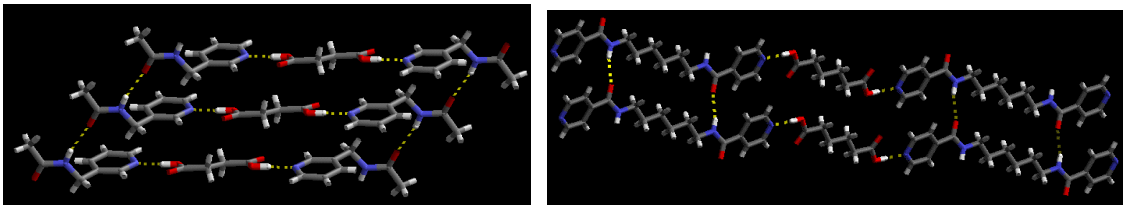

(a) (b)

Figure 1.7 Two examples of a cocrystal (a) 3-(acetaminomethyl)pyridine succinic acid (1:1),[11] (b) N,N'-1,6-hexanediylbis-4-pyridinecarboxamide suberic acid (1:1).[29]

1.1.5 Molecular electrostatic potential as a tool for ranking hydrogen/halogen bond donor and acceptor strength

According to one of Etter's rules "*the best hydrogen bond donor and the best hydrogen-bond acceptor will preferentially form hydrogens to one another.*"[19] Therefore, it begs the question, how do we determine the strength of a given donor or acceptor molecule in order to determine the best donor and best acceptor?

Hunter has shown that hydrogen bonding mainly involves electrostatic interactions and the molecular electrostatic potentials (MEP) of a given functional group which can be determined using low level of theoretical calculations provides a useful method for ranking different donors/acceptors.[30] The association constants (K) have been measured for a wide variety of intermolecular interactions both in the gas phase and in solution. Furthermore, simple molecules such as benzoic acid or amino benzoic acid can be analyze in terms of pair-wise hydrogen-bonding interactions between the functional groups. These results can then be accounted for by the following relationship, Equation 1.[30]

$$\log K = c_1\alpha_2^{H}\beta_2^{H} + c_2 \qquad \textbf{Equation 1}$$

"Where c_1 and c_2 are constants that depend on the solvent and α_2^H and β_2^H are functional group constants that relate to the hydrogen-bond donor and hydrogen-bond acceptor properties of the molecules."[30]

Therefore equation 1 can be correlated to the electrostatics of the hydrogen-bonding interaction.[31] Moreover, computed molecular properties such as atomic charge and electrostatic potential have been correlated to the values obtained for α_2^H and β_2^H.[32]

Furthermore, AM1 molecular electrostatic potential calculations carried out by Hunter, established that values obtained for α_2^H and β_2^H can be correlated with the experimentally determined values. Additionally, values of α (hydrogen bond donor) and β (hydrogen bond acceptor) can be calculated from the MEP by dividing by a correction factor of 52 kJ mol^{-1} resulting in:

$$\alpha = E_{max}/52 \text{ kJ mol}^{-1} = \text{hydrogen bond donor constant}$$

$$\beta = -E_{min}/52 \text{ kJ mol}^{-1} = \text{hydrogen bond acceptor constant.}$$ [30]

Hence MEPs can be used to rank the strength of hydrogen-bond donors and acceptors of a variety of functional groups, thus allowing us to probe the best-donor/best-acceptor hypothesis.

1.2 Halogen bonding as a complement to hydrogen bonding in crystal engineering

The hydrogen bond occupies a position of central importance in chemistry, biology and materials science. Its properties, which include well-defined directionality and strength, as mentioned earlier, have lead to profound consequences for supramolecular chemistry in general. Although the hydrogen bond is generally accepted to be unique, recently Resnati and co-workers have demonstrated that noncovalent interactions of strength and directionality comparable to the hydrogen bond can be accomplished via halogen bonding (XB).[33]

The term XB indicates any D…X-Y interaction in which X is an electrophilic halogen atom (Lewis acid, XB donor), D is a donor of electron density (Lewis base, XB acceptor), and Y is carbon, nitrogen, or halogen, Figure 1.8.[34]

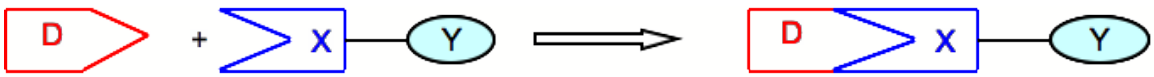

D = N, O, S, Se **X = I, Br, Cl** **Y = C, Halogen, N**

Figure 1.8 Schematic representation of XB. XB acceptors (D) are neutral or anionic species, while donors (X) are halogen atoms bound to a wide diversity of molecular arrays (Y).[34]

Normally the energy of XB interaction spans a very wide range from 5-180 $kJmol^{-1}$, the weak Cl…Cl interaction between chlorocarbons and the very strong $I^-...I_2$ interaction in the I^-_3 being the extremes.[33] Moreover the interaction between the donor and the acceptor results in a shortening of the D…X distances and the stronger the interaction the shorter the D…X distance.[33]

In addition, Hunter and co-workers have also used MEP calculations to show that XB have molecular recognition properties comparable to a moderate hydrogen-bond donor, and should therefore form complexes with strong hydrogen-bond acceptors such as pyridine.[35]

1.3 The role of crystal engineering in pharmaceutical science

Crystal engineering[15,16,36] strategies have been used in understanding and predicting hydrogen-bonding interactions in active pharmaceutical ingredients (API). Pharmaceuticals are generally comprised of an API, a formulation containing inactive ingredients as a carrier system, and a package for market performance and appeal.

A crystalline form of the API is strongly preferred because of their relative ease of isolation, and the physico-chemical stability that the crystalline solid state affords. The vast majority of API's occur as solids; these include, salts, polymorphs, cocrystals and hydrates/solvates, [37] Figure 1.9. Nevertheless the use of crystalline materials can result in problems such as poor solubility properties or the existence of more than one crystalline form of an API. However, crystal engineering affords a paradigm for rapid development of a fourth class of API's; pharmaceutical cocrystals.

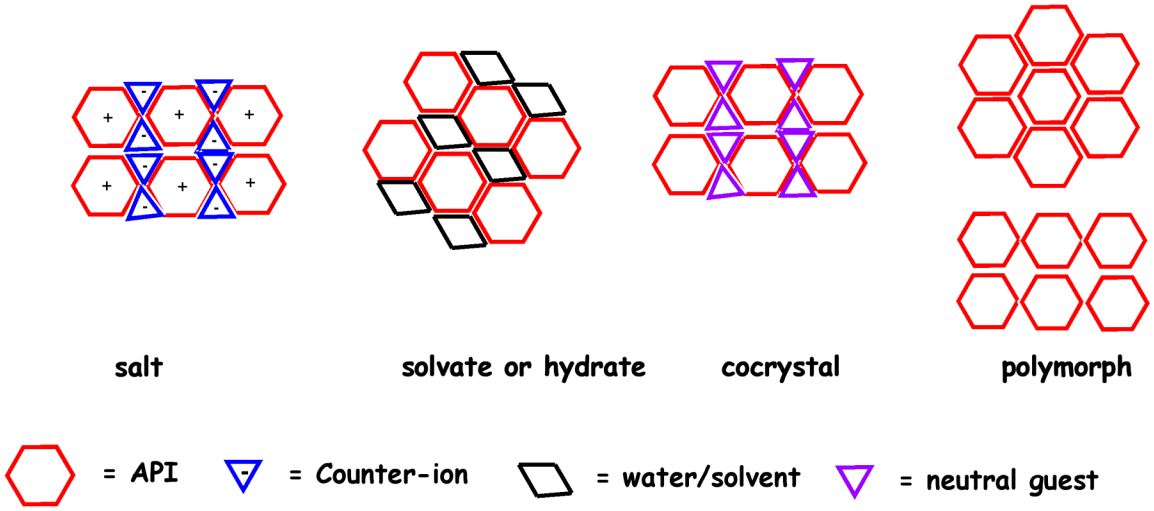

Figure 1.9 Pictures displaying the more common solid-state strategies and their respective components.[38]

The form "pharmaceutical cocrystal" is commonplace and usually applies when an API is one of the molecules in the multicomponent crystal.[37,38] Two examples of pharmaceutical cocrystals are shown in Figure 1.10.

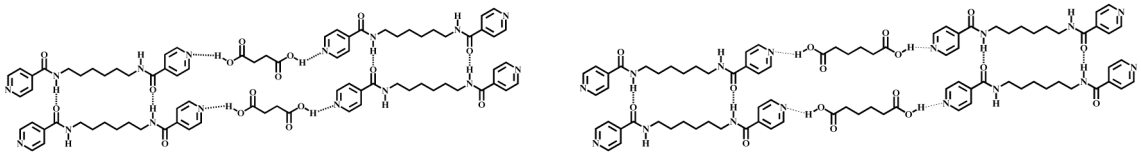

(a) (b)

Figure 1.10 Examples of pharmaceutical cocrystals: (a) N,N'-1,6-hexanediylbis-4-pyridinecarboxamide succinic acid;[29] (b) N,N'-1,6-hexanediylbis-4-pyridinecarboxamide adipic acid.[29]

1.3.1 Problems encountered during the development of API

During the development and formulation of any API, several stringent performance parameters (e.g. solubility, dissolution rate, thermal stability, etc.) need to be carefully considered.[39] It is thus not surprising that poor biopharmaceutical properties (opposed to toxicity or lack of efficacy, Figure 1.11)[40] are the main reason that less than 1% of active compounds eventually make it into the marketplace.[41]

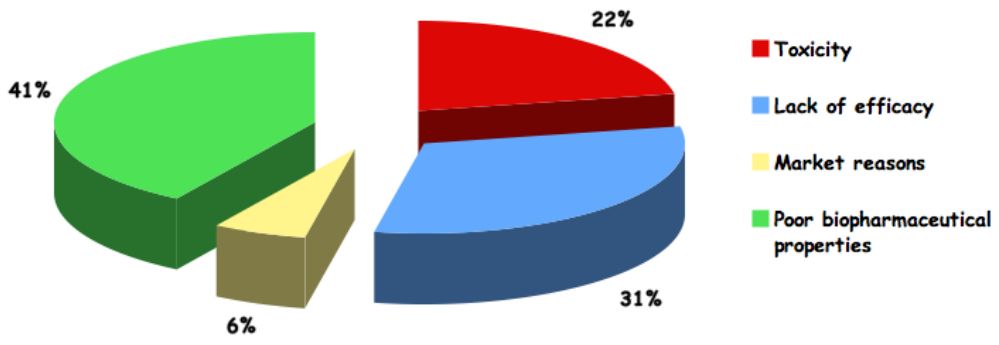

Figure 1.11 Reasons why compounds fail and slow down in development.[39]

1.3.2 Fine tuning physico-chemical properties by pharmaceutical cocrystal formation

It has been well established that issues ranging from poor solubility and inadequate dissolution properties to lack of crystallinity and attendant instability plague the pharmaceutical industry.[42] Recent studies, have shown that an opportunity exists to use co-crystallization to replace the solid forms of API that are being used, by taking advantage of supramolecular synthons.[37]

1.3.2.1 Fine-tuning melting point behavior via co-crystallization

The thermal stability (*i.e.* melting point) is a fundamental physical property. There have been several literature reports where co-crystallization was used as a tool in fine-tune melting point behavior of an API. These results showed that the API melting point can typically be fine-tuned according to which coformer is chosen; therefore if a higher melting cocrystal is desired then a higher melting coformer should be selected and vice versa.[43]

1.3.2.2 Modulating solubility via co-crystallization

The aqueous solubility of a drug substance is one of the fundamental properties evaluated early in discovery. Majority of APIs fall into Biopharmaceutical Classification Scheme[44] (BCS) classification II[45] (low solubility, high permeability) furthermore aqueous solubility is a major indicator of the solubility in the intestinal fluids.[46] To

generally describe solubility the Pharmacopoeia (USP) uses seven different solubility expressions as shown in Table 1.1.

Table 1.1 Solubility Definitions[46,47]

Descriptive term (solubility definition)	Parts of solvent required for one part of solute	Solubility range (mg/mL)	Solubility assigned (mg/mL)
Very soluble (vs)	<1	>1000	1000
Freely soluble (fs)	From 1 to 10	100-1000	100
Soluble (s)	From 10 to 30	33-100	33
Sparingly soluble (sps)	From 30 to 1000	10-33	10
Slightly soluble (ss)	From 100 to 1000	1-10	1
Very slightly soluble (vss)	From 1000 to 10,000	0.1-1	0.1
Practically insoluble (pi)	≥10,000	<0.1	0.01

Pharmaceutical cocrystals have been demonstrated to profoundly modify the solubility of the parent API,[29,**Error! Bookmark not defined.**43,44,47,48,49] and at least 90 APIs have been studied in the context of co-crystallization. Often APIs that are targeted for pharmaceutical co-crystallization display undesirable solubility and possess multiple hydrogen bonding sites.[50]

In fact, Bak and co-workers highlighted the ability of a series of pharmaceutical cocrystals for improving the solubility of the parent API. It was found that oral administration of the cocrystal showed a maximum plasma concentration 8 times greater compared to the oral administration of the pure API.[43,51] Similarly, Childs *et al*[48] highlighted a cocrystal that exhibited approximately 4-fold increase in plasma concentration over the pure API after a single oral dose.

1.4 Goals

Understanding molecular recognition is important in the construction of new molecules. This can result in gaining control of intermolecular interactions, thereby providing opportunities to fine-tune specific properties (thermal stability, solubility, hygroscopicity, etc) of a variety of compounds.

Therefore, this dissertation will focus on:

I. Understanding molecular recognition through systematic studies of acetamidopyridine

Acetamidopyridine were of interest because pyridine derivatives exhibit high biological activity as is demonstrated in wide variety of pharmaceutical compounds.[52] Moreover the acetamide derivatives have shown to be effective inducers of cell growth.[53] Furthermore, by understanding the molecular recognition processes of this small molecule will provide us with valuable information, which can be used to understand larger and more complicated molecules. Therefore a series of acetamidopyridine derivatives will be designed and synthesized. Subsequent co-crystallizations with hydrogen-bond donors, will allow for a systematic study of molecular recognition preferences. Additionally, these supramolecular reagents will also be employed for organizing coordination complexes into extended architectures, using robust self-complementary hydrogen-bonding capability.

II. Balancing intermolecular hydrogen and halogen bonding

Halogen bonding has been shown to have similar strength and directionality as the hydrogen bond. To probe the strength of the halogen bond a collection of supramolecular reagents having the capability to participate in both hydrogen and halogen bonding will be tested. Additionally, Etter's rule which states that the best hydrogen-bond donor will interact with the best hydrogen-bond acceptor, will be tested using MEPs in ranking the strength of the hydrogen and halogen bond, thus allowing for better predictability.

III. Establishing the interaction of preference of the XB with thienyl compounds

A series of supramolecular reagents containing sulfur atoms will be synthesized. Subsequent co-crystallization reactions will be carried on these supramolecular reagents using a variety of halogen bond donors, in order to determine whether XB in these series is strictly electrostatic or a hard/soft acid and base interaction.

IV. Applying molecular recognition in fine-tuning physicochemical properties

Finally, systematic studies will be carried out on a series of API's with the ultimate goals of fine-tuning the melting behavior and aqueous solubility.

References

[1] (a) Lehn, J.-M. *Supramolecular Chemistry*. Weinheim: Wiley-VCH, 1995; (b) Gellman, S.H. *Chem. Rev.*, **1997**, 97, 1231.

[2] (a) MacGillivray, L. *CrystEngComm*., **2004**, 6, 77; (b) Lehn, J.–M. *Science*, **2002**, 295, 2400; (c) Etter, M. C. *J. Phys. Chem*., **1991**, 95, 4601; (d) Moulton, B.; Zaworotko, M.J. *Chem. Rev*., **2001**, 101, 1629; (e) Pauling, L. The Nature of the Chemical Bond, Cornell University Press: Ithaca, NY, 1939; (f) Lehn, J.–M. *Angew. Chem.Int. Ed. Engl*., **1990**, 29, 1304; (g) Steed J. W.; Atwood, J. L. *Supramolecular Chemistry*, John Wiley and Sons Ltd, Chichester, 2000.

[3] Fischer, E. *Ber. Deutsch. Chem. Ges*. **1894**, 3, 267.

[4] (a) Bernstein, J. *J. Phys D: Appl. Phys*., **1993**, 26, B66; (b) Bernstein, J. *Organic Solid State Chemistry*, Desiraju G.R. Ed. Elsevier: New York, 1987, 32, 471.

[5] (a) Reference 2b; (b) Hosseini, M.-W. *Chem. Commun*. **2005**, 5825.

[6] (a) Aakeröy, C. B. *Acta Crystallogr., Sect. B: Struct. Sci*., **1997**, 53, 569; (b) Desiraju, G. R. *Acc. Chem. Res*., **2002**, 35, 565; (c) Hosseini, M. W. *CrystEngComm*, **2004**, 6, 318; (d) Brammer, L. *Chem. Soc. Rev*., **2004**, 33, 476; (e) Aakeröy C. B.; Beatty, A. M. *Aust. J. Chem*., **2001**, 54, 409; (f) Caulder D. L.; Raymond, K. N. *Acc. Chem. Res*., **1999**, 32, 975; (g) Reinhoudt D. N.; Crego-Calama, M. *Science*, **2002**, 295, 2403; (h) Braga, D.; Desiraju, G. R; Miller, J. S.; Orpen A. G.; Price, S. L. *CrystEngComm*, **2002**, 4, 500; (i) Braga, D.; Maini, L.; Polito M.; Grepioni, F. *Struct. Bond*., **2004**, 111, 1; (j) Lewis G.; Orpen, A. G. *Chem. Commun*., **1998**, 1873; (k) Prins, L. J.; Reinhoudt D. N.; Timmerman, P. *Angew. Chem. Int. Ed*., **2001**, 40, 2382; (l) Zimmerman, S. C. and Corbin, P. S. *Struct. Bond*., **2000**, 96, 63.

[7] (a) Aakeröy, C. B.; Desper, J.; Helfrich, B. A. *CrystEngComm*, **2004**, 6, 19–24; (b) Aakeröy, C. B.; Desper, J.; Scott, B. M. T. *Chem. Commun*., **2006**, 1445; (c) Aakeröy, C. B.; Schultheiss, N.; Desper, J.; Moore, C. *New J. Chem*., **2006**, 30, 1452; (d) Aakeröy, C. B.; Fasulo, M. E.; Desper, J. *CrystEngComm*, **2006**, 8, 586; (e) Steed, J.W.; Turner, D.R.; Wallace, K.J. *Core Concepts in Supramolecular Chemistry and Nanochemistry*, John Wiley & Sons, Ltd, 2007.

[8] (a) Moulton B.; Zaworotko, M. J *Chem. Rev*., **2001**, 101, 1629; (b) Desiraju, G. R. *Acc. Chem. Res*., **2002**, 35, 565; (c) Hosseini, M. W. *CrystEngComm*, **2004**, 6, 318; (d) MacGillivray, L. R. *CrystEngComm*, **2004**, 6, 77; D. Braga, *Chem. Commun*., **2003**, 2751; (e) Brammer, L. *Chem. Soc. Rev*., **2004**, 33, 476.

[9] Lehn, J.-M. *Angew. Chem. Int. Ed. Engl*. **1990**, 29, 1304.

[10] Watson, J.D.; Crick, F.H.C. *Nature* (Landon) **1953**, 171, 737.

[11] (a) Aakeröy, C.B.; Hussain, I.; Forbes, S.; Desper, J. *Aust. J. Chem*. **2009**, 62, 899; (b) Fujita, M.; Kwon, Y.-J.; Washizu, S.; Ogura, K. *J. Am. Chem. Soc*. **1994**, 116, 1151; (c) Yaghi, O.M.; Li, H. *J. Am. Chem. Soc*. **1996**, 118, 295; (d) Aakeröy, C.B.; Beatty, A.M. Leinen, D.S. *J. Am. Chem. Soc*. **1998**, 120, 7383.

[12] (a) Reference 2f; (b) Whitesides, G.M.; Simanek, E.E.; Mathias, J.P.; Seto, C.T.; Chin, D.N.; Mammen, M.; Gordon, D.M. *Acc. Chem. Res*. **1995**, 28, 37.

[13] Desiraju, G.R. *Angew. Chem. Int. Ed. Engl*. **1995**, 34, 2311.

[14] (a) Nangia, A.; Desiraju, G.R. *Topics in Current Chemistry* "Supramolecular Synthons and Pattern Recognition" **1998**, 198/1998, 57; (b) Aakeröy, C.B. *Acta Cryst*. **1997**, B53, 569.

[15] (a) Etter, M.C. *Acc. Chem. Rev*. **1990**, 23, 120; (b) Taylor, R.; Kennard, O. *Acc. Chem. Res*. **1984**, 17, 320.

[16] (a) Wuest, J.D. *Chem. Commun*. **2005**, 5830; (b) Etter, M.C. *J. Phys. Chem*. **1991**, 95, 4601.

[17] Donohue, J. *J. Phys. Chem*. **1952**, 56, 502.

[18] Etter, M.C. *J. Am. Chem. Soc*. **1982**, 104, 1095.

[19] Reference 15b

[20] Burrows, A.D. *Struct. Bond* **2004**, 108, 55.

[21] Reference 14a

[22] Aakeröy, C.B.; Seddon, K.R. *Chem. Soc. Rev*. **1993**, 22, 397.

[23] Steed, J.W.; Atwood, J.L. *Supramolecular Chemistry*, 2nd Ed. John Wiley & Sons, Ltd. 2009.

[24] (a) Reference 12a; (b) Reference 11

[25] Walsh, R.D.B.; Bradner, M.W.; Fleischman, S.; Morales, L.A.; Moulton, B.; Rodriguez-Hornedo, N.; Zaworotko, M.J. *Chem. Commun*. **2003**, 186.

[26] (a) Bis, J.; Zaworotko, M.J. *Cryst. Growth Des.* **2005**, 5, 1169; (b) Steiner, T. *Acta Crystallogr. Sect. B: Struct. Sci*. **2001**, 57, 103; (c) Vishweshwar, P.; Nangia, A.; Lynch, V.M. *Cryst. Growth Des*. **2003**, 3, 783; (d) Etter, M.C.; Adsmond, D.A. *J. Chem. Soc. Chem. Commun*. **1990**, 8, 589; (e) Aakeröy, C.B.; Beatty, A.M.; Helfrich. A. *Cryst. Growth Des*. **2002**, 2, 325; (f) Vangala, V.R.; Mondal, R.; Broder, C.K.; Howard, J.A.K.; Desiraju, G.R. *Cryst. Growth Des.* **2005**, 5, 99; (g) Videnova-Adrabinska, V.; Etter, M.C. *J. Chem. Crystallogr.* **1995**, 25, 823.

[27] Aakeröy, C.B.; Salmon, D.J. *CrystEngComm.* **2005**, 7, 439.

[28] (a) Stahly, G.P. *Cryst. Growth Des*. **2007**, 7, 1007; (b) Vishweshwar, P.; McMahon, J.A.; Bis, J.A.; Zaworotko, M.J. *J. Pharm. Sci*. **2006**, 95, 499.

[29] Aakeröy, C.B.; Forbes, S.; Desper, J. *J. Am. Chem. Soc*. **2009**, 131, 17048.

[30] Hunter, C.A. *Angew. Chem. Int. Ed*. **2004**, 43, 5310.

[31] Pauling, L. *Proc. Natl. Acad. Sci. USA* **1928**, 14, 349.

[32] (a) Hagelin, H.; Murray, J.S.; Brinck, T.; Berhelot, M.; Politzer, P. *Can. J. Chem*. **1995**, 73, 483; (b) Dearden, J.C.; Ghafourian, T. *J. Chem. Inf. Comput. Sci.* **1999**, 39, 321; (c) Platts, J.A. *Phys. Chem. Chem. Phys.* **2000**, 2, 973; (d) Platts, J.A. *Phys. Chem. Chem. Phys.* **2000**, 2, 3115; (e) Zissimos, A.M.; Abraham, M.H.; Klamt, A.; Eckert, F.; Wood, J. *J. Chem. Inf. Comput. Sci.* **2002**, 42, 1320.

[33] (a) Metrangolo, P.; Neukirch, H.; Pilati, T.; Resnati, G. *Acc. Chem. Res*. **2005**, 38, 386; (b) Metrangolo, P.; Resnati, G. *Chem. Eur. J.* **2001**, 7, 2511.

[34] (a) Metrangolo, P.; Resnati, G.; Pilati, T.; Biella, S. *Struct. Bond*, **2008**, 126, 105; (b) Metrangolo, P.; Pilati, T.; Resnati, G. *CrystEngComm*. **2006**, 8, 946; (c) Pennington, W.T.; Hanks, T.W.; Arman, H.D. *Struct. Bond* **2008**, 126, 65.

[35] Cabot, R.; Hunter, C.A. *Chem. Commun*. **2009**, 2005.

[36] (a) Desiraju, G.R. *Crystal Engineering-The Design of Organic Solids*, Elsevier, Amsterdam, 1989; Desiraju, G.R. *Angew. Chem. Int. Ed. Engl.* **1995**, 34, 2311; (c) Moulton, B.; Zaworotko, M.J. *Chem. Rev.* **2001**, 101, 1629.

[37] Almarsson, Ö.; Zaworotko, M.J. *Chem. Commun*. **2004**, 1889.

[38] Schultheiss, N.; Newman, A. *Cryst. Growth Des*. **2009**, 9, 2950.

[39] (a) Kerns, E.H.; Di, L. *Drug-Like Properties: Concepts, Structure Design and Methods: from ADME to Toxicity Optimization*; Elsevier, Amsterdam, **2008**, pp 7-9; (b) Basavoju, S.; Boström, D.; Velaga, S.P. *Pharm. Res*. **2008**, 25, 530.

[40] Lipper, R.B. *Mod. Drug Discovery* **1999**, 2, 55.

[41] (a) *Pharmaceutical Industry Profile* 2006 & 2007; PhRMA: Washington, DC, 2006 & 2007; (b) *Mass Spectrometry in Drug Metabolism and Pharmacokinetics*; Ramanathan, R., Ed.; Wiley: Hoboken, NJ, 2009, pp 1-4.

[42] Almarsson, Ö.; Gardner, C.R. *Current Drug Discovery* **2003**, 21.

[43] Stanton, M.K.; Bak, A. *Cryst. Growth Des.* **2008**, 8, 3856.

[44] Takagi, T.; Ramachandran, C.; Bermejo, M.; Yamashita, S.; Yu, L.X.; Amidon, G.L. *Mol. Pharmaceutics* **2006**, 3, 631.

[45] Hiten, J.S.; Gunta, S.; Dasharath, M.P.; Chhagan, N.P. *Biopharm. Drug Dispos.* **2009**, 30, 524.

[46] Stegemann, S.; Leveiller, F.; Franchi, D.; de Jong, H.; Lindén, H. *Eur. J. Pharm. Sci*. **2007**, 31, 249.

[47] Takagi, T.; Ramachandran, C.; Bermejo, M.; Yamashita, S.; Yu, L.X.; Amidon, G.L. *Molecular Pharmaceutics* **2006**, 3, 631.

[48] McNamara, D.P.; Childs, S.L.; Giordano, J.; Iarricco, A.; Cassidy, J.; Manjunath, S.-S.; Mannion, R.; O'Donnell, E.; Park, A. *Pharm. Res.* **2006**, 23, 1888.

[49] (a) Shan, N.; Zaworotko, M.J. *Drug Disc. Today* **2008**, 8, 3856; (b) Reutzel-Edens, S.M.; Bush, J.K.; Magee, P.A.; Stephenson, G.A.; Byrn, S.R. *Cryst. Growth Des*. **2003**, 3, 897; (c) Hickey, M.B.; Peterson, M.L.; Manas, E.S.; Alvarez, J.; Haeffner, F.; Almarsson, Ö. *J. Pharm. Sci*. **2007**, 96, 1090; (d) Jayasankar, A.; Reddy, S.L.; Bethune, S.J.; Rodríguez-Hornedo, N. *Cryst. Growth Des*. **2009**, 9, 889; (e) Trask, A.V.; Motherwell, W.D.S.; Jones, W. *Int. J. Pharm*. **2006**, 320, 114.

[50] Cheney, M.L.; Shan, N.; Healey, E.R.; Hanna, M.; Wojtas, L.; Zaworotko, M.J.; Sava, V.; Song, S.; Sanchez-Ramos, J.R. *Cryst. Growth Des*. **2010**, 10, 394.

[51] Bak, A.; Gore, A.; Yanez, E.; Stanton, M.; Tufekcic, S.; Syed, R.; Akrami, A.; Rose, M.; Surapaneni, S.; Bostick. T.; King, A.; Neervannan, S.; Ostovic, D.; Koparkar, A.; *J. Pharm. Sci.* **2008**, 97, 3942.

[52] Lukevits, È. *Chemistry of Heterocyclic Compounds*, **1995**, 31, 639.

[53] Andreeff, M.; Stone, R.; Michaeli, J.; Young, C. W.; Tong, W. P.; Sogoloff, H.; Ervin, T.; Kufe, D.; Rifkind, R.A.; Marks, P. A. *Blood*, **1992**, 80, 2604.

CHAPTER 2 - Exploring the hydrogen-bond preference of N-H moieties in cocrystals of acetamidopyridine/acetamidomethylpyridine

2.1 Introduction

2.1.1 Molecular recognition through intermolecular interaction

In recent years, several efforts have been made to identify robust supramolecular synthons, and the reliability of homomeric self-complementary pair-wise hydrogen bonds, for example, amide…amide, carboxylic acid…carboxylic acid and oxime…oxime, have been established through extensive structural[1] or database studies.[2] Some heteromeric pair-wise interactions are particularly robust, for example, carboxylic acid…pyridine,[3] hydroxy…pyridine,[4] and hydroxy…amine,[5] which have allowed for the assembly of a wide range of binary cocrystals.

However, to add more versatility and refinement to crystal engineering, it is necessary to further explore the possibility of "ranking" different supramolecular synthons. Thus to expand on this area we have employed a combination of two well-known and robust synthons,[6] the heteromeric carboxylic acid…pyridine interaction and the N-H…O (amide…carbonyl) interaction in an attempt to prepare binary cocrystals. The initial assembly of these cocrystals will be achieved by locating a carboxylic acid and a pyridyl moiety on different molecular fragments. Once this interaction is locked into place, the resulting binary aggregates can be further organized through N-H…O interactions. However, complications occur since the N-H donor has a choice of three different potential hydrogen-bond acceptors, it is not obvious how the competition between those three oxygen atoms will play out.

We have carried out a systematic structural study on a family of acetamidopyridine compounds comprising of an amide moiety and an N-heterocyclic fragment, Figure 2.1. This study will allow us to determine patterns of molecular recognition preferences of the N-H moiety based upon analysis of several new cocrystals as well as of relevant data obtained from the Cambridge Structural Database (CSD).[7]

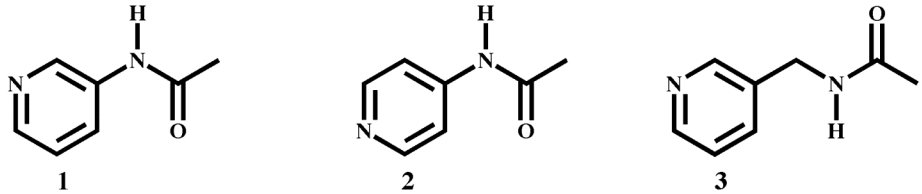

Figure 2.1 Target compounds 3-acetamidopyridine **1**, 4-acetamidopyridine **2**, and 3-acetamidomethylpyridine, **3**.

2.1.2 Controlling supramolecular structures through hydrogen and coordination bonds

Majority of crystal engineering has primarily focused on the syntheses of extended organic networks and transition metal based coordination polymers. Not enough work has been done on the construction of inorganic-organic hybrid materials with intermolecular forces;[8] this is as a result of the daunting task of having precise control over its structural motifs. The composite of inorganic-organic materials is important because it brings together synthetic flexibility as well as properties and reactivities inherent to the metal ions. Some of the common reasons for incorporating metal ions into supramolecular networks are metal ions give access to physical properties that are less common in organic solids, such as magnetic properties, conductivity and catalytic activity.

Metal ions also display a range of coordination geometries allowing for greater flexibility in constructing materials with specific dimensions and topologies. In fact, many reliable strategies based upon coordinate-covalent bonds have been employed in the syntheses of inorganic polymeric networks with predictable connectivity and dimensionality, typically through the use of bridging ligands such as 4,4-biypyridine, dicarboxylates, bis(amides), bis(lactams) and bis(pyridines).[9] In addition, the strength and directionality of the hydrogen bond have offered supramolecular pathways towards the directed assembly of extended organic networks and multicomponent supermolecules.[10] This approach may in some case have certain advantages, as it combines the strength of the coordinate-covalent bond with the flexibility of the softer hydrogen-bond interactions, which can offer desirable physical properties such as enhanced solubility in a range of

organic solvents. An important role in this approach is played by versatile bifunctional ligands that contain both metal-coordinating sites and functionalities that provide opportunities for organizing complex molecules into infinite architectures through supramolecular chemistry and non-covalent interactions.

Compounds **1-3** were investigated for their ability to organize coordination complexes into extended architectures, using the robust self-complementary hydrogen-bonding capability of the amide functionality (as a result of the strong N-H…O=C hydrogen bonds), and the reliable metal-coordinating ability of pyridine. Copper(II) 1,1,1,5,5,5-hexafluoro-2,4-pentanedione [Cu(II)(hfacac)$_2$], cobalt(II) 1,3-diphenyl-1,3-propanedione [Co(II)(DBM)$_2$] and nickel(II) 1,3-diphenyl-1,3-propanedione [Ni(II)(DBM)$_2$] were utilized in this study due to the two dione anions occupying the four equatorial sites around the metal ion thereby producing an overall neutral metal-containing building block. Therefore leaving the two remaining axial sites to be utilized in constructing extended linear supramolecular architectures with the appropriate ligand, Figure 2.2.

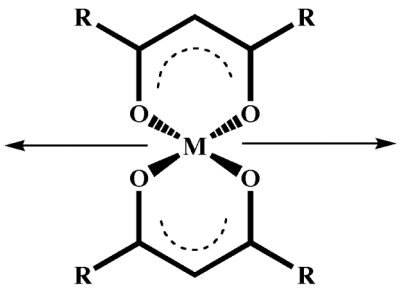

R = CF_3, Phenyl

M = Ni, Co, Cu

Figure 2.2 Metal(II) "paddlewheel" complexes with arrows indicating the two axial coordination sites.

2.2 Experimental

2.2.1 Synthesis

All chemicals were purchased from Aldrich, Fisher Scientific and used without further purification. Copper(II) 1,1,1,5,5,5-hexafluoro-2,4-pentanedione [Cu(II)(hfacac)$_2$] was purchased from Alfa Aesar, whereas cobalt(II) 1,3-diphenyl-1,3-propanedione [Co(II)(DBM)$_2$] and nickel(II) 1,3-diphenyl-1,3-propanedione [Ni(II)(DBM)$_2$] were prepared according to the literature.[11] Melting points were determined on a GallenKamp melting point apparatus in a capillary tube and are reported uncorrected. ^{1}H and ^{13}C NMR spectra were recorded on a Varian Unity plus 400 MHz or 200 MHz spectrometers in $CDCl_3$ or DMSO-d$_6$. Compounds were prepared for infrared spectroscopic (IR) analysis as a mixture in KBr or on a ZnSe ATR crystal.

2.2.1.1 Synthesis of 3-acetamidopyridine, 1

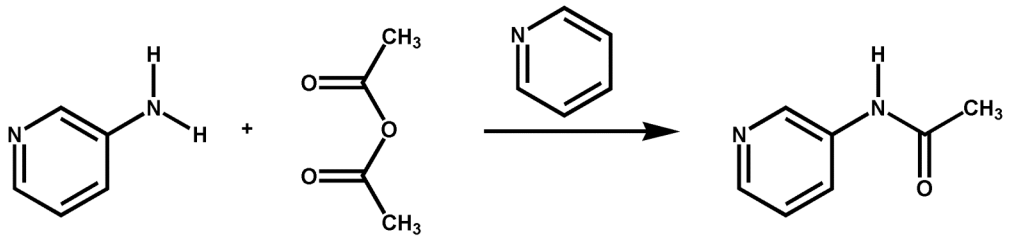

1 was prepared by a previously reported method.[12] 3-Aminopyridine (1.882g, 20.0 mmol) was dissolved in a mixture of pyridine (10 mL) and acetic anhydride (10 mL) and the resulting solution was stirred under a nitrogen atmosphere at room temperature for 24 h. Water (10 mL) was added and the solution was evaporated *in vacuo* to dryness. The precipitate obtained was washed thoroughly with diethyl ether and recrystallized from methanol. The product isolated was a light peach solid (1.738g, 64%). M.p.: 133-134°C. ^{1}H NMR (δ_H; 200 MHz, $CDCl_3$) 9.09 (br s, 1H), 8.6 (s, 1H), 8.34 (d, J = 4.8Hz, 1H), 8.21 (d, J = 6.96Hz, 1H), 7.32 (m, J = 8.42Hz, 1H), 2.21 (s, 3H). IR (KBr pellet) υ 1695 cm^{-1} (C=O, s), 1533 cm^{-1} (Amide II, s).

2.2.1.2 Synthesis of 4-acetamidopyridine, 2

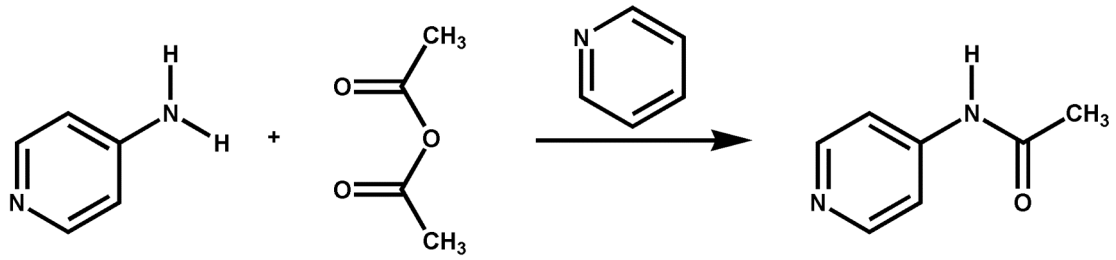

4-Aminopyridine (1.882g, 20 mmol) was dissolved in a mixture of pyridine (10.00 mL) and acetic anhydride (10.8g, 106 mmol, 10 mL). The mixture was left to stir at room temperature for 24 h under a nitrogen atmosphere. Water (10 mL) was added and the solution was evaporated under reduced pressure to dryness. The precipitate obtained was washed thoroughly with diethyl ether and recrystallized from methanol. The product isolated was a light yellow solid (1.76g, 65%). M.p.: 144-146°C. ^{1}H NMR (δ_H; 400 MHz, $CDCl_3$): 8.52 (d, J = 12Hz, 1H), 7.5 (d, J = 12Hz, 1H), 2.23 (s, 3H); IR (KBr pellet) υ 1689 cm^{-1} (C=O), 1515cm^{-1} (Amide II, s).

2.2.1.3 Synthesis of 3-(acetamidomethyl)pyridine, 3

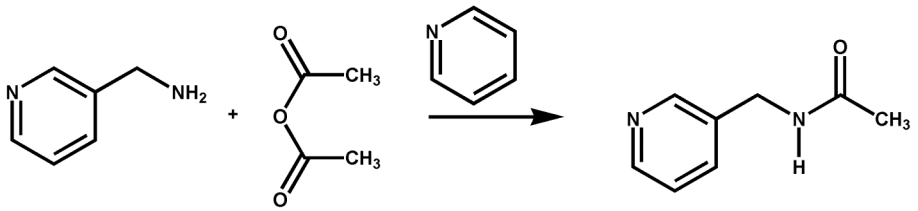

3-(Acetamidomethyl)pyridine was prepared by employing a modification of the previously reported procedure.[13] Acetic anhydride (10 mL) was added very slowly into a mixture of pyridine (10 mL) and 3-(aminomethyl)pyridine (5.00 mL, 50.0 mmol) with continuous stirring and the resulting solution was refluxed for 1 h. Excess of acetic anhydride and acetic acid produced during the reaction were evaporated under reduced

pressure and the product thus obtained was recrystallized from diethyl ether. The product isolated was brown liquid (7.5g, 77%). ^{1}H NMR (δ_H; 400 MHz, $CDCl_3$): 8.45 (s, 1H), 8.39 (d, J = 5.08 Hz 1H), 7.69 (d, J = 49.4 Hz, 1H), 7.40 (br s, 1H), 7.29 (m, J = 7.81Hz, 1H), 4.362 (d, 2H), 1.98 (s, 3H).

2.2.2 Synthesis of cocrystals and salts

2.2.2.1 Synthesis of 4-acetamidopyridinium hydrogenglutarate (1:2), 2HG

2 (0.030g, 0.22mmol) was dissolved in 4 mL of acetonitrile. To this solution was added **GLU** (0.015g, 0.11 mmol) in 4 mL of acetonitrile. The resulting solution was heated and allowed to stand at room temperature for slow evaporation. Colorless prisms were obtained after five days. M.p.: 119-121°C; IR (KBr pellet) υ 2500 cm^{-1}, 1850 cm^{-1} (O-H…N), 1652 cm^{-1} (C=O acid, s), 1555 cm^{-1} (Amide II, s).

2.2.2.2 Synthesis of 4-acetamidopyridine suberic acid (1:1), 2SUB

2 (0.030g, 0.22 mmol) was dissolved in 5 mL of acetonitrile. To this solution was added **SUB** (0.038g, 0.22 mmol) in 5 mL of acetonitrile. The resulting solution was heated and left at room temperature for slow evaporation. Colorless plates were obtained after five days. M.p.: 129-130°C; IR (KBr pellet) υ 2520 cm^{-1}, 1940 cm^{-1} (O-H…N), 1691 cm^{-1} (C=O acid, s), 1589 cm^{-1} (C=O amide I, s), 1511 cm^{-1} (Amide II, s).

2.2.2.3 Synthesis of 4-acetamidopyridine sebacic acid (1:1), 2SEB

2 (0.03g, 0.22 mmol) was dissolved in 5 mL of acetonitrile. **SEB** (0.044g, 0.22 mmol) dissolved in 7 mL of acetonitrile was added to the solution. The mixture was heated and left to evaporate at room temperature for five days; at which time colorless prisms were obtained. M.p.: 120-123°C; IR (KBr pellet) υ 2500 cm^{-1}, 1850 cm^{-1} (O-H…N, br), 1698 cm^{-1} (C=O acid, s), 1597 cm^{-1} (C=O amide I, s), 1514 cm^{-1} (Amide II, s).

2.2.2.4 Synthesis of 3-(acetamidomethyl)pyridine succinic acid (1:1), 3SUC

3 (0.015g, 0.099 mmol) was dissolved in 4 mL of ethanol and mixed with a solution of **SUC** (0.012g, 0.099 mmol) in 4 mL of ethanol was added and allowed to

stand at room temperature under slow evaporation. Colorless plates were obtained after ten days. M.p.: 79-81°C; IR (ZnSe ATR crystal) υ 2423cm^{-1}, 1956cm^{-1} (O-H…N, br), 1707cm^{-1} (C=O acid, s), 1543cm^{-1} (C=O amide, s).

2.2.2.5 Synthesis of 3-(acetamidomethyl)pyridine 4-hydroxybenzoic acid (1:1), 3HBA

A solution of **3** (0.015g, 0.099 mmol) in 4 mL of ethanol was mixed with a solution of **HBA** (0.014g, 0.099 mmol) in 4 mL of ethanol and allowed to stand at room temperature for slow evaporation. Transparent orange-brownish plates were obtained after eleven days. M.p.: 113-117°C; IR (ZnSe ATR crystal) υ 2627cm^{-1}, 1928cm^{-1} (O-H…N, br), 1675cm^{-1} (C=O acid, s), 1548cm^{-1} (C=O amide, s).

2.2.3 Synthesis of Metal Complexes

5.2.1.1 Synthesis of Co(3-acetamidopyridine)$_2$(1,3-diphenyl-1,3-propanedionato)$_2$, 1a

A mixture of **1** (0.027 g, 0.200 mmol) in 7 mL of ethanol-acetonitrile (1:1) was added to a solution of Cobalt(II) 1,3-diphenyl-1,3-propanedione (0.028g, 0.010 mmol) in 7 mL of ethanol-acetonitrile (1:1). The mixture was heated for 5 minutes to reduce the volume to 5 mL and then allowed to stand in screw cap vial at room temperature for ten days, at which time dark orange crystals appeared. IR (KBr pellet, cm^{-1}) 3409m [υ (NH)], 1672[υ(C=O)], 1570, 1553vs[υ(amide II)]. The confirmation of this complex was made from the X-ray structural results.

2.2.3.2 Synthesis of Ni(3-acetamidopyridine)$_2$(1,3-diphenyl-1,3-propanedionato)$_2$, 1b

A solution of **1** (0.027g, 0.200 mmol) in 7 mL of methylene chloride was added to a mixture of Nickel(II) 1,3-diphenyl-1,3-propanedione (0.049g, 0.010 mmol) in 7 mL methylene chloride. The mixture was heated for 5 minutes and then allowed to stand at room temperature in a screw cap vial. After ten days light green crystals were obtained.

IR (ZnSe ATR crystal, cm^{-1}) 3301m [υ(NH)], 1670[υ(C=O)], 1589, 1547vs [υ(amide II)]. The confirmation of this complex was made from the X-ray structural results.

2.2.3.3 Synthesis of Cu(4-acetoamidopyridine)$_2$(1,1,1,5,5,5-hexafluoro-2,4-pentanedione)$_2$, 2a

2 (0.03g, 0.20 mmol) was dissolved in 10 mL of methanol-acetonitrile (1:1) and was added to a solution of Cu(1,1,1,5,5,5-hexafluoro-2,4-pentanedione)$_2$ (0.049g, 0.010 mmol) in 10 mL methanol-acetonitrile (1:1). The resulting solution was shifted to a screw cap vial and allowed to stand at room temperature. Bright green needles were afforded in 4 weeks. IR (ZnSe ATR crystal, cm^{-1}) 3260m [υ (NH)], 1672[υ(C=O)], 1596, 1514vs[υ(amide II)]. The confirmation of this complex was made from the X-ray structural results.

2.2.3.4 Synthesis of Co(3-acetamidomethyl)pyridine)$_2$(1,3-diphenyl-1,3-propanedionato)$_2$, 3a

A solution of **3** (0.015g, 0.099 mmol) was dissolved in 4 mL acetonitrile and a solution of Co(II) 1,3-diphenyl-1,3-propanedione (0.023g, 0.049 mmol) in 4 mL of acetonitrile. The solution was heated and allowed to stand at ambient temperature in a screw cap vial. After 4 weeks transparent orange plates were obtained. IR (ZnSe ATR crystal, cm^{-1}) 3436m [υ (NH)], 1652[υ(C=O)], 1554, 1521vs [υ(amide II)]. The confirmation of this complex was made from the X-ray structural results.

2.3 Results

A summary of the crystallographic information for **2HG, 2SUB, 2SEB**, **3SUC, 3HBA** and **1a-b**, **2a, 3a** are displayed in Table C.1 and all hydrogen-bond geometries for **2HG, 2SUB, 2SEB**, **3SUC, 3HBA** and **1a-b**, **2a, 3a** are listed in Table 2.1.

Table 2.1 Hydrogen-bond geometries for **2HG, 2SUB, 2SEB, 3SUC, 3HBA, 1a-b, 3a**

Structure	D-H…A	d(D-H)/Å	d(H…A)/Å	d(D…A)/Å	<(DHA)/°
2HG[i]	N(11)-H(11)...O(21)	0.88(3)	1.79(3)	2.677(2)	177(2)
	O(25)-H(25)...O(21)#1	0.96(3)	1.58(3)	2.5309(19)	170(2)
	N(14)-H(14)...O(26)#2	0.86(2)	1.97(2)	2.824(2)	177(2)
2SUB[ii]	N(17)-H(17)...O(39)#1	0.877(13)	1.950(13)	2.8142(10)	168.4(12)
	N(27)-H(27)...O(32)#2	0.900(13)	2.018(13)	2.9156(9)	174.2(12)
	O(31)-H(31)...N(11)	1.036(19)	1.517(19)	2.5484(10)	172.8(17)
	O(38)-H(38)...N(21)	1.07(2)	1.48(2)	2.5454(9)	173.8(18)
2SEB[iii]	O(21)-H(21)...N(11)	1.136(19)	1.421(19)	2.5516(15)	172.5(17)
	N(17)-H(17)...O(22)#2	0.845(19)	2.012(19)	2.8494(15)	170.8(17)
3SUC[iv]	O(21)-H(21)...N(11)	0.965(13)	1.652(13)	2.6145(9)	174.0(12)
	N(17)-H(17)...O(18)#2	0.878(13)	1.971(13)	2.8259(10)	164.3(12)
3HBA[v]	N(17)-H(17)...O(22)#1	0.858(16)	2.012(17)	2.8678(12)	175.1(16)
	O(21)-H(21)...O(18)	0.92(2)	1.63(2)	2.5467(11)	175(2)
	O(24)-H(24)...N(11)#2	0.82(2)	1.92(2)	2.7081(13)	160(2)
1a[vi]	N(47)-H(47)...O(47)#2	0.875(19)	2.052(19)	2.9245(14)	174.5(18)
1b[vii]	N(13)-H(13)...O(17)#2	0.88(2)	2.10(2)	2.9696(18)	173(2)
3a[viii]	N(48)-H(48)...O(48)#2	0.868(14)	2.191(15)	3.0576(12)	176.0(13)

i) #1 -x,-y,-z+2 #2 x+1,y+1,z-1 ii) #1 x-1/2,-y+1/2,z+1/2 #2 x+1/2,-y+3/2,z-1/2 iii) #2 -x+1/2,y-1/2,-z+1 iv) #2 x,y-1,z v) #2 x,-y+1/2,z-1/2 vi) #2 x,-y+3/2,z+1/2 vii) #2 x,-y+1/2,z-1/2 viii) #2 x,-y+3/2,z+1/2

2.3.1 Description of cocrystals

2.3.1.1 Crystal structure 4-acetamidopyridinium hydrogenglutarate (1:2), 2HG

The crystal structure determination of **2HG** showed that a salt had formed resulting from proton transfer from one of the acid moieties of glutaric acid to the pyridine ring leading to a charge assisted N-H^{+}…O^{-} hydrogen bond as the driving force for the formation of the salt, Figure 2.3. Also one oxygen is bifurcated and is participating in an O-H…O hydrogen bond with the remaining neutral carboxylic acid moiety resulting in a tetrameric pair of ions, Figure 2.4. The N-H amide moiety forms a hydrogen bond with a C=O moiety at the neutral end of the anion (N14-H14…O26, 2.823 Å). These interactions connect adjacent tetramers into an infinite chain.

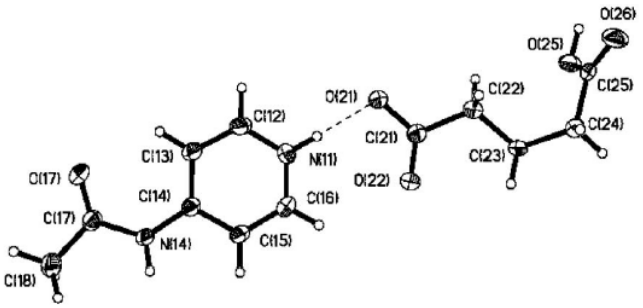

Figure 2.3 Thermal ellipsoids (50%) and labeling scheme of the supramolecular 1:2 trimer in **2HG**.

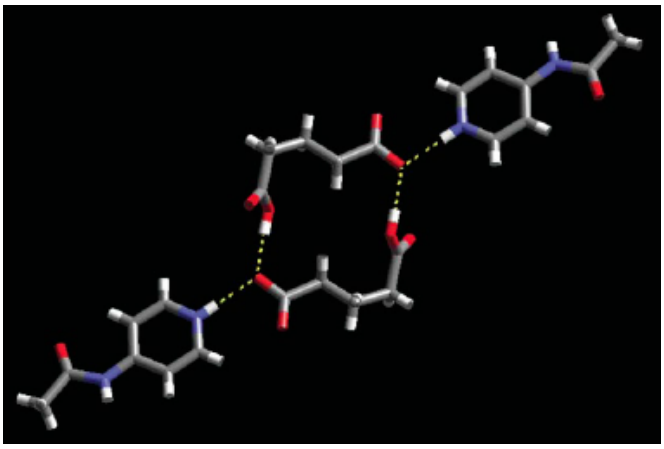

Figure 2.4 Two ion pairs connected into a tetramer in **2HG**.

2.3.1.2 Crystal structure of 4-acetamidopyridine suberic acid (1:1), 2SUB

The asymmetric unit of **2SUB** contains two molecules of **2** and one molecule of **SUB**. The primary synthons in this structure are two unique O-H…N hydrogen bonds

resulting from the interactions between the dicarboxylic acid and the two acetamidopyridine molecules O(31)-H(31)...N(11), 2.5484(10)Å; and O(38)-H(38)...N(21), 2.5454(9) Å, Figure 2.5. Adjacent trimeric supermolecules are interconnected via an amide-carbonyl hydrogen bond with the C=O moiety as the acceptor located on the carboxylic acid. The result of this interaction is an infinite 2-D layer of orthogonal supermolecules Figure 2.6.

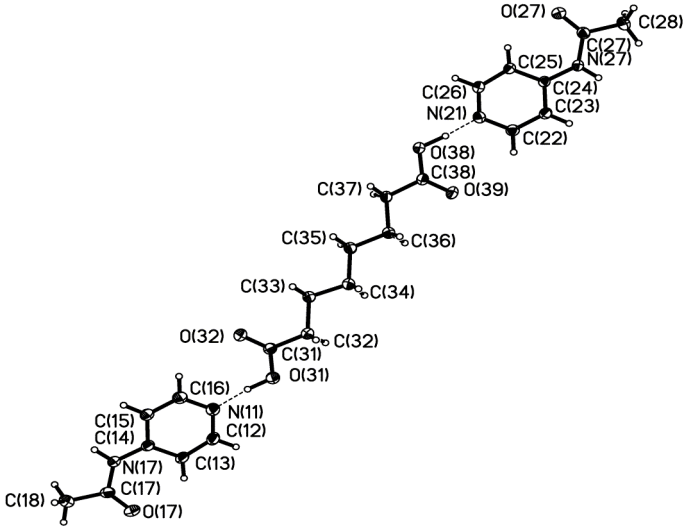

Figure 2.5 Thermal ellipsoids and labeling scheme of **2SUB**.

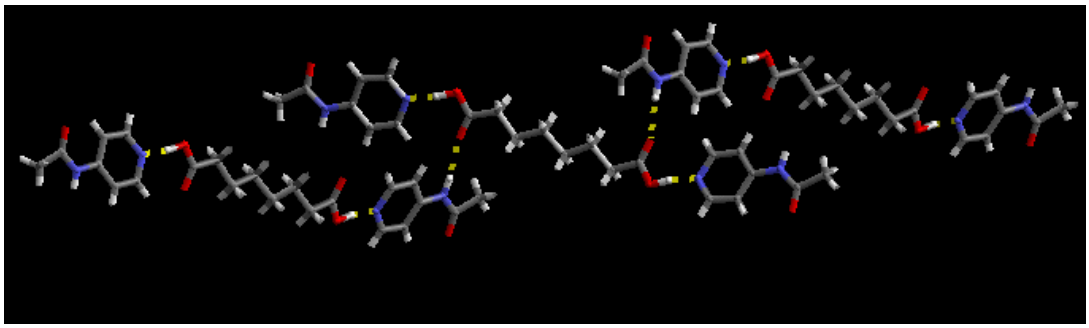

Figure 2.6 2-D layer of **2SUB** formed via N-H…O hydrogen bonds.

2.3.1.3 Crystal structure of 4-acetaminopyridine sebacic acid (1:1), 2SEB

The crystal structure of **2SEB** has one molecule of **2** and half a molecule of **SEB** in the asymmetric unit. The trimeric supermolecule is constructed from symmetry related O-H..N hydrogen bonds between the O-H of the dicarboxylic acid and the pyridine atom (O21…N11, 2.5516(16) Å), Figure 2.7. Adjacent trimers are interconnected via an

amide-carbonyl hydrogen bond with the C=O moiety as the acceptor located on the carboxylic acid. The result of this interaction is an infinite 2-D layer of orthogonal supermolecules, Figure 2.8.

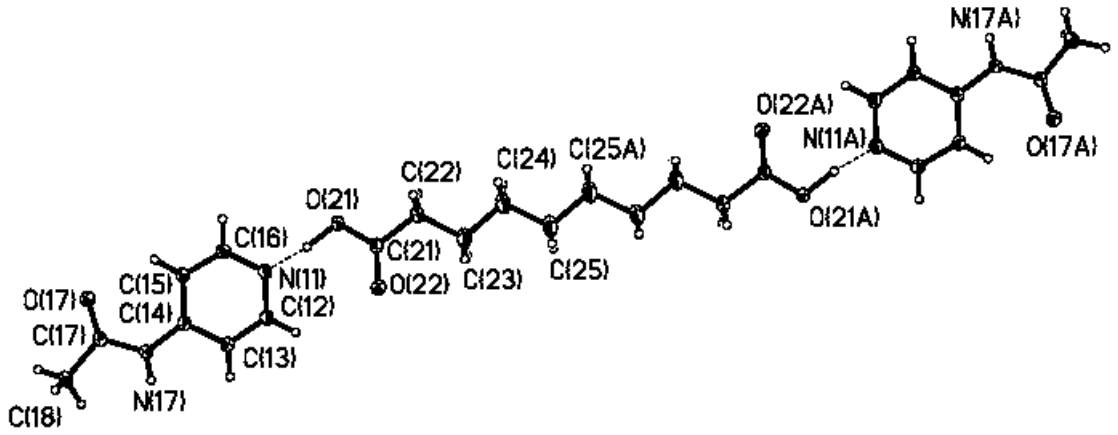

Figure 2.7 Thermal ellipsoids (50%) and labeling scheme of the supramolecule 2:1 trimer in **2SEB**.

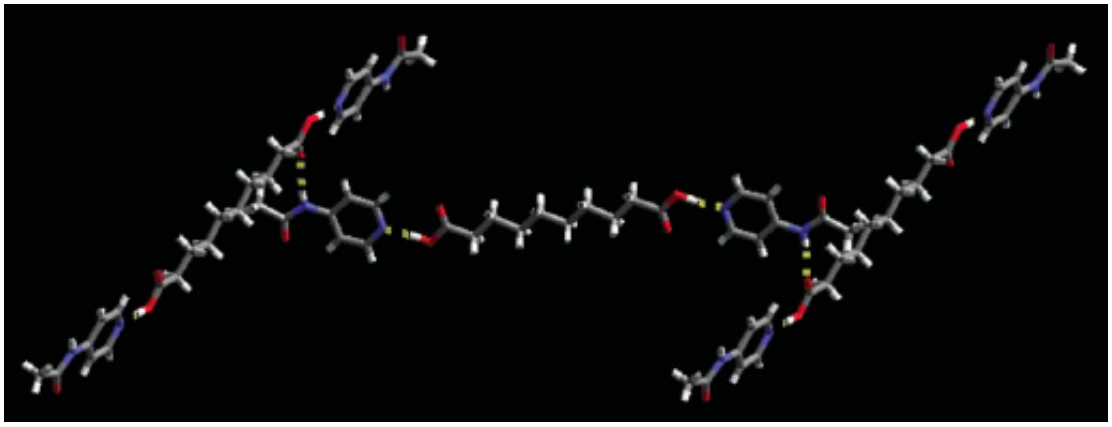

Figure 2.8 Orientation of adjacent supramolecular trimer in **2SEB**.

2.3.1.4 Crystal structure of 3-(acetaminomethyl)pyridine succinic acid (1:1), 3SUC

The asymmetric unit of **3SUC** contains one molecule of **3** and half a molecule of **SUC**. Two symmetry related O-H…N hydrogen bonds are formed through the two O-H groups of the dicarboxylic acid and pyridine nitrogen atoms (O(21)-H(21)...N(11), 2.6145(9) Å). The two pyridine rings in the trimer are coplanar with respect to one another as well as with the plane of **SUC** but the amide groups at both ends are

positioned in an up-down arrangement, Figure 2.9. Adjacent trimeric supermolecules produced from the primary hydrogen bonds are connected to one another via symmetry related hydrogen bonds involving H17 from the amide N-H group of one molecule and O18(#2) to an adjacent amide C=O group, N17...O18#2, 2.8259(10)Å. The overall result is an infinite 1-D ladder of trimers, Figure 2.10.

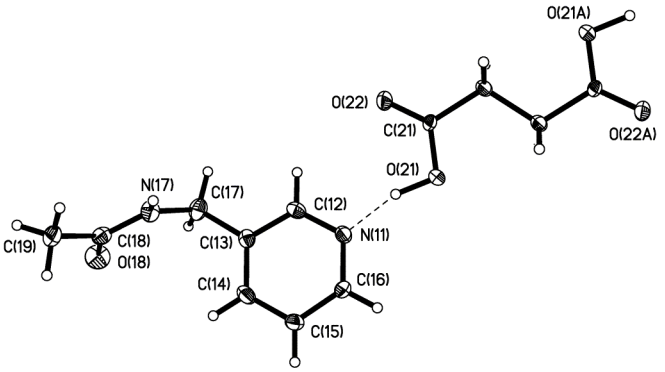

Figure 2.9 Thermal ellipsoids (50%) and labeling scheme of the supramolecular 2 : 1 trimer in **3SUC**.

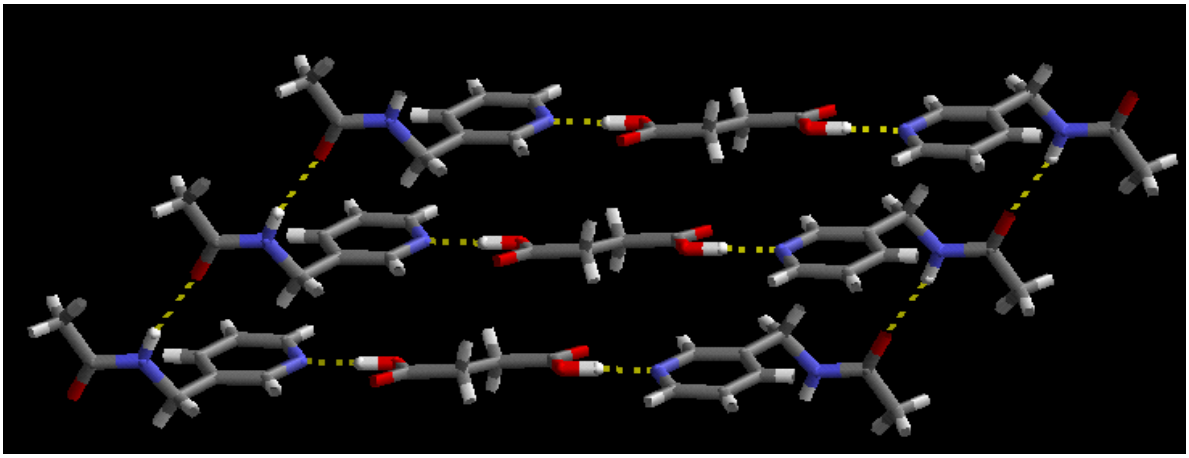

Figure 2.10 Alignment of trimers by N-H…O hydrogen bonds resulting in infinite 2-D ladders in **3SUC**.

2.3.1.5 Crystal structure of 3-(acetamidomethyl)pyridine 4-hydroxybenzoic acid (1:1), 3HBA

In the crystal structure of **3HBA**, the asymmetric unit comprises two molecules of **3** and one molecule of **HBA**. The primary synthons are the two unique O-H…N hydrogen bonds resulting from the interactions between the 4-hydroxybenzoic acid and

the 3-(acetamidomethyl)pyridine molecules (O(21)-H(21)...O(18), 2.5467(11) Å and O(24)-H(24)...N(11), 2.7081(13) Å, Figure 2.11. Adjacent trimeric supermolecules produced from the primary hydrogen bonds are further connected with one another via two unique hydrogen bonds, involving H17 from the amide N-H group and O22 on the acid C=O group N(17)-H(17)...O(22)#1, 2.7081(13) Å, resulting in an infinite 2-D ladder, Figure 2.12.

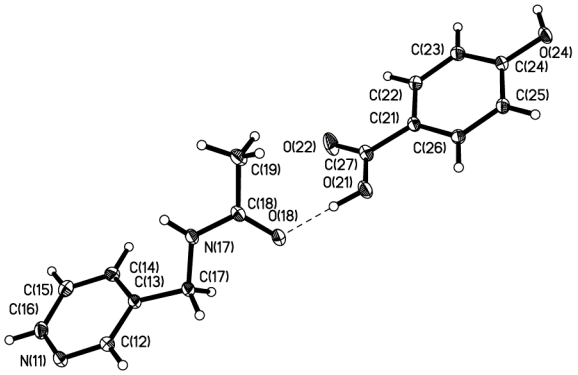

Figure 2.11 Thermal ellipsoids (50%) and labeling scheme of the supramolecular trimer in **3HBA**.

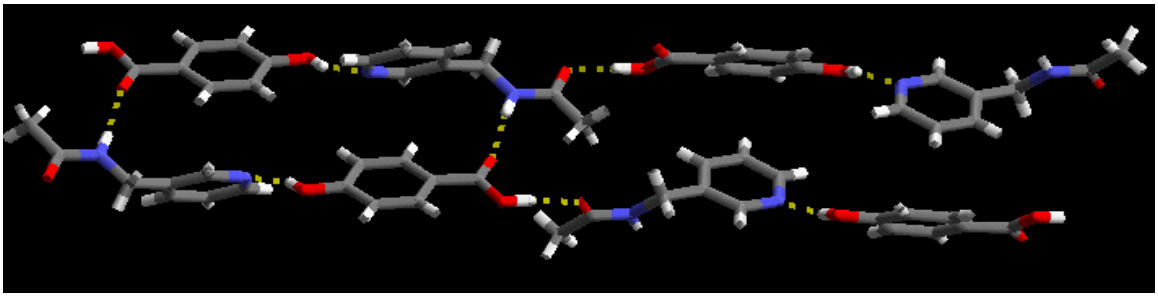

Figure 2.12 Orientation of adjacent supramolecular trimers in **3HBA** affected by N-H…O=C (amide) hydrogen bonds.

2.3.2 Description of Metal Complexes

Table 2.2 Selected bond distances and angles for compounds **1a-b, 2d, 3c**

Compounds	M(II)-N (Å)	<N-M(II)-N (°)
1a	Co1-N41, 2.1865(10)	180.0
1b	Ni1-N11, 2.1189(2)	180
2a	Cu1-N11, 1.994(3)	179.999(1)
3a	Co1-N41, 2.1746(8)	180.0

2.3.2.1 Crystal structure of Co(3-acetamidopyridine)$_2$(1,3-diphenyl-1,3-propanedionato)$_2$, 1a

The centerpiece in the crystal structure of **1a** is a hexa-coordinated cobalt(II) complex. Each metal complex is located on a crystallographic inversion center with an octahedral geometry constructed from two chelating 1,3-diphenyl-1,3-propanedionato anions and two 3-acetamidopyridine molecules coordinating through their pyridine nitrogen atoms with a Co-N distance of 2.1865(10) Å, Figure 2.13.

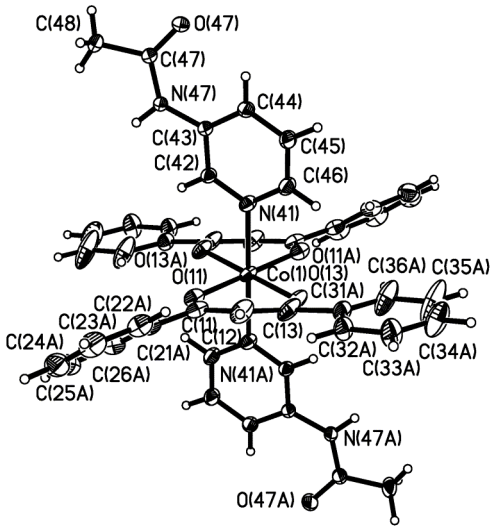

Figure 2.13 Molecular geometry and thermal ellipsoids (50%) for the complex ion in **1a**.

The pyridine rings of the two-amide ligands are planar with respect to one another and the amide groups in the complex are facing opposite directions. The chelate rings formed by the 1,3-diphenyl-1,3-propanedionato ligands have *cis*-angles ranging from 88.88^{o} to 91.12^{o}, with the short angle, as expected, being associated with the bite of the chelate ring. The N-H group of one amide ligand and C=O group of the other group, in each metal complex, engages in self-complementary N-H…O hydrogen bonds with the neighboring molecules (N47...O47, 2.9245(14) Å), arranging in 1-D chain of complex molecules. The remaining amide N-H and carbonyl group, in each metal complex form symmetry related hydrogen bonds with neighboring chains producing an infinite 2-D sheet structure Figure 2.14.

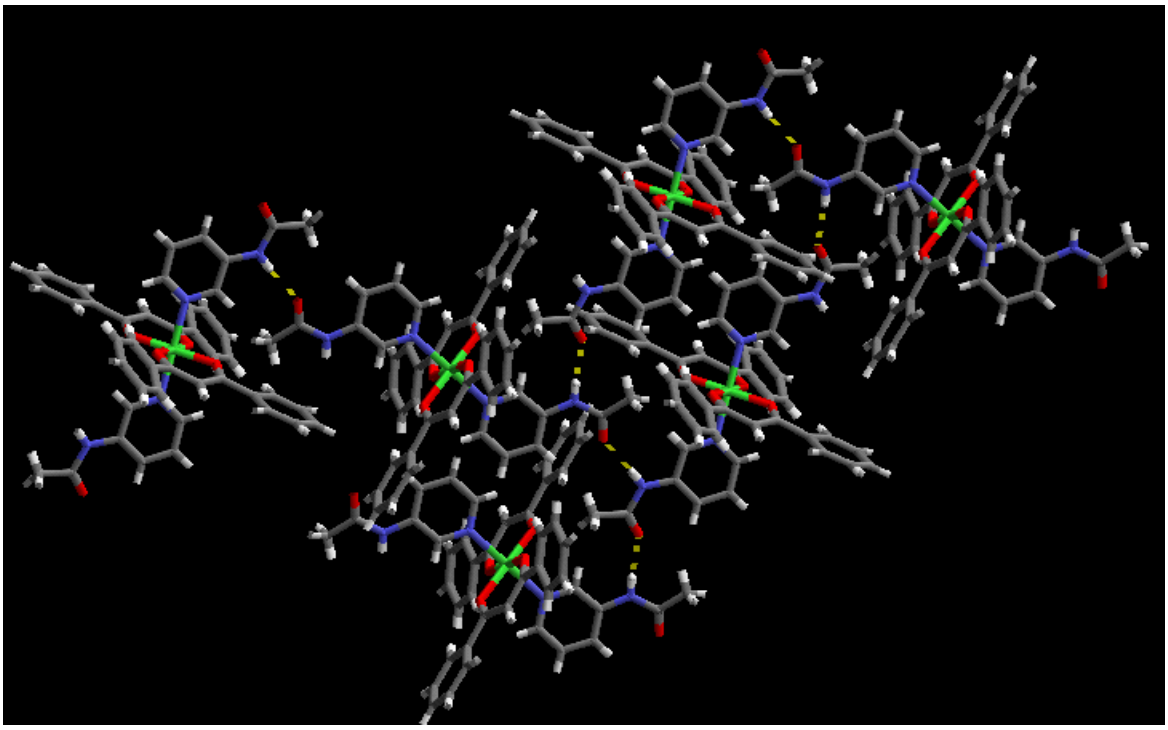

Figure 2.14 2-D layer in the structure of **1a** generated by symmetry-related N-H…O hydrogen bonds.

2.3.2.2 Crystal structure of Ni(3-acetamidopyridine)$_2$(1,3-diphenyl-1,3-propanedionato)$_2$, 1b

The crystal structure of **1b** has the nickel ions coordinated octahedrally by two unique 1,3-diphenyl-1,3-propanedionato ions and two 3-acetamidopyridine molecules. The two symmetry-related axial ligands display Ni-N distances of 2.1188(12) Å and the amide groups arranged in a trans fashion, Figure 2.15.

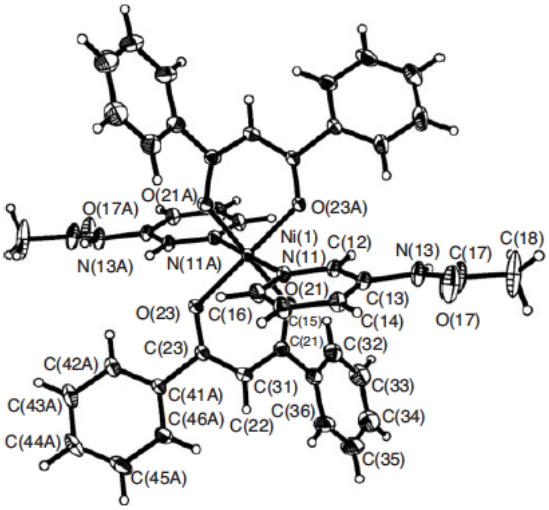

Figure 2.15 Molecular geometry and thermal ellipsoids (50%) for the complex **1b**.

Pyridine-based ligands on adjacent complex ions form intermolecular N-H···O=C hydrogen bonds, N13···O17, 2.9696(18) Å, resulting in a 2-D sheet structure, Figure 2.16.

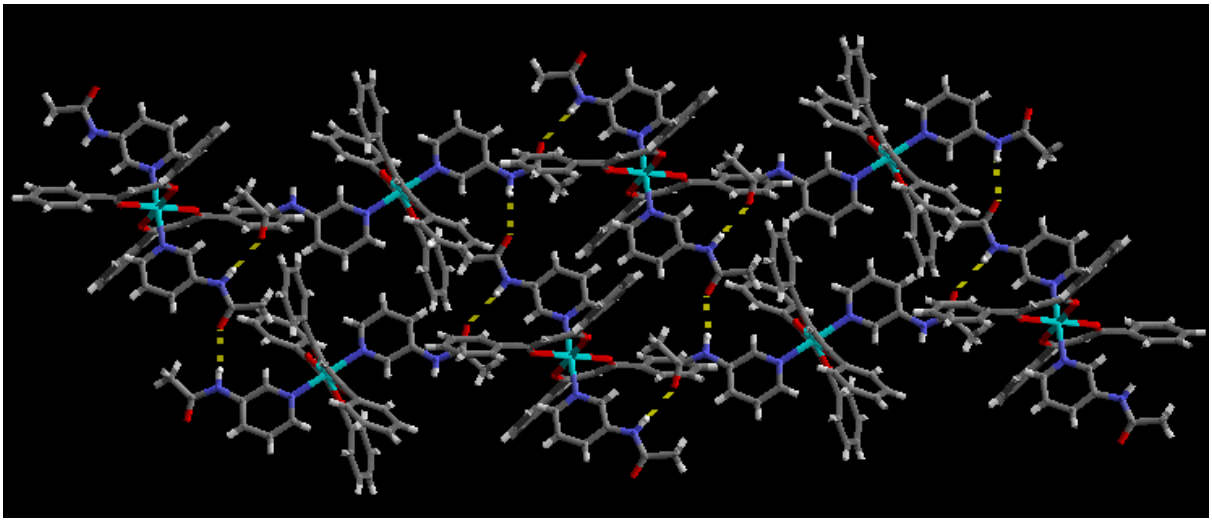

Figure 2.16 2-D layer in the crystal structure of **1b** generated by symmetry-related N-H···O hydrogen bonds.

2.3.2.3 Crystal structure of Cu(4-acetamidopyridine)$_2$(1,1,1,5,5,5-hexafluoro-2,4-pentanedione)$_2$, 2a

The crystal structure of **2a** contains the expected six-coordinated copper (II) complex as well as one molecule of methanol and acetonitrile. The geometry at the Cu(II) center is a 4 + 2 coordination, resulting from two *O,O'*-chelating hexafluoro-2,4-pentanedionato ions and two 4-acetamidopyridine ligands coordinated through their pyridine nitrogen atoms in trans positions, with Cu-N distance of 1.994(4) Å, Figure 2.17.

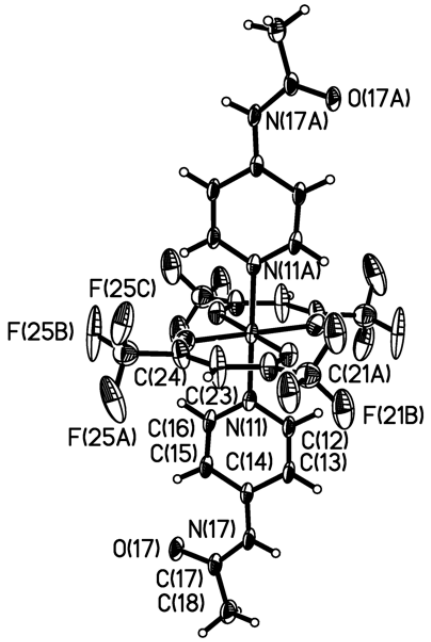

Figure 2.17 Molecular geometry and thermal ellipsoids (50%) for the complex ion in **2a** (solvent molecules not shown).

The N-H groups on both ligands engage in N-H…O hydrogen bonds with a C=O moiety from a ligand on a neighboring complex, producing an infinite 2-D layer, Figure 2.18.

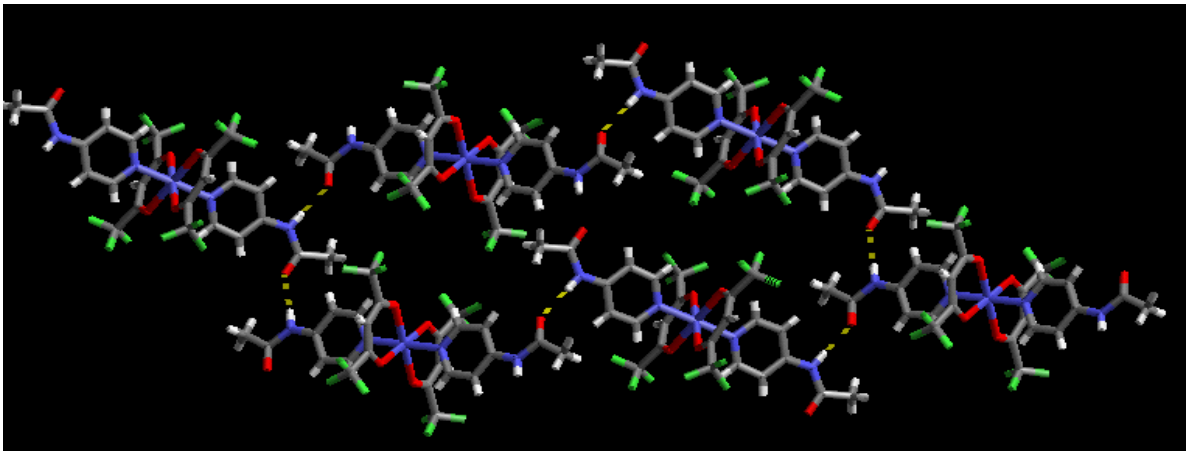

Figure 2.18 2-D layer in the structure of **2a** generated by symmetry-related N-H···O hydrogen bonds.

2.3.2.4 Crystal structure of Co((3-acetamidomethyl)pyridine)$_2$(1,3-diphenyl-1,3-propanedionato)$_2$, 3a

The central motif in the crystal structure of **3a** is a 4 + 2 hexa-coordinate cobalt(II) complex where the metal ion is located on an inversion center. The two chelating 1,3-diphenyl-1,3-propanedionato anions occupy the equatorial plane, whereas the two 3-(acetamidomethyl)pyridine molecules complete the complex ion by coordinating through their pyridine nitrogen atoms with a Co-N of 2.1746(8) Å, Figure 2.19.

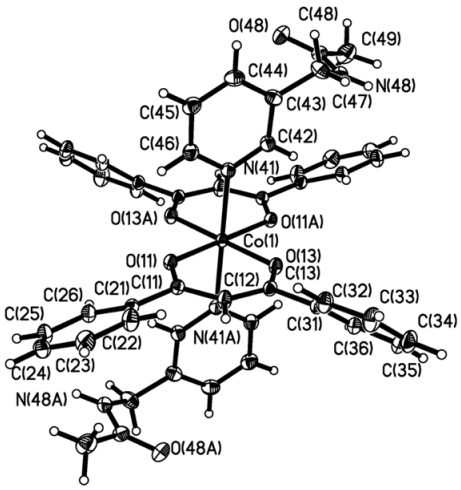

Figure 2.19 Molecular geometry and thermal ellipsoids (50%) for the complex ion in **3a**.

The pyridine rings of two amide ligands are coplanar and the amide groups in the complex are oriented trans with respect to the N-M(II) –N axis. The chelate rings formed by the anionic *acac* ligands have *cis* angles ranging from 89° to 92°, with the short angle, as expected, being associated with the bite of the chelate ring. The N-H group of one amide ligand and the C=O group on a pyridyl ligand on an adjacent complex engage in self-complementary N-H…O hydrogen bonds, N48…O48, 2.191(15), resulting in an infinite 2-D sheet structure, Figure 2.20.

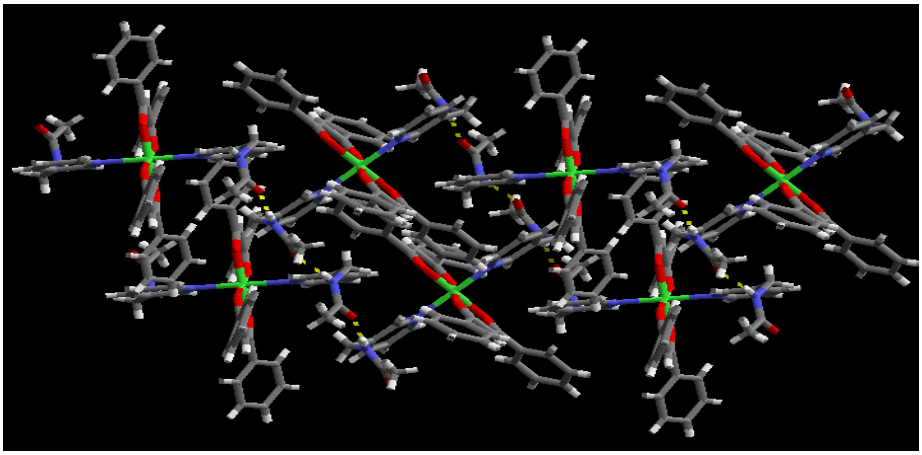

Figure 2.20 2-D layer in the structure of **3a** generated by symmetry-related N-H···O hydrogen bonds.

2.4 Discussion

2.4.1 Formation of acetamido/acetamidomethyl-pyridine cocrystals and salts

Infrared spectroscopy plays a vital role in screening the formation of cocrystal; since the interaction between a N-heterocyclic compound and carboxylic acid show two broad stretches near 2450 cm^{-1} and 1900 cm^{-1}, characteristic of O-H…N(py) hydrogen bonds.[14] These stretches appeared in the vibrational spectra of all five compounds suggesting the presence of COOH….py intermolecular interactions. However, if the formation of a salt occurs it can be eliminated by looking at the conversion of the carbonyl to the carboxylate anion (COO^{-}). In the vibrational spectra of compounds **2SUB**, **2SEB**, **3SUC,** and **3HBA** the carbonyl stretch appears above 1670 cm^{-1}; whereas, in compound **2HG** the carbonyl stretch is shifted to a lower wavenumber, below 1660

cm^{-1} suggesting the presence of COO^- anions, Table 2.3. Furthermore, single-crystal structural determinations carried out on **2HG, 2SUB**, **2SEB, 3SUC,** and **3HBA** confirmed the assignments made on the basis of the vibrational spectroscopy.

Table 2.3 Summary of IR data for compounds **2HG, 2SUB, 2SEB, 3SUC,** and **3HBA**

Compounds	2HG	2SUB	2SEB	3SUC	3HBA
Observed COOH/COO- Stretch (cm^{-1})	1652	1691	1698	1707	1675
Product	Salt	Cocrystal	Cocrystal	Cocrystal	Cocrystal

The distinction between cocrystal and salts can also be determined upon selective intermolecular distances and angles. In the crystal structures of **2SUB**, **2SEB, 3SUC,** and **3HBA** each carboxylic acid contains distinctly different C-O bond distances corresponding to the C=O (1.217-1.224 Å) and C-O(H) (1.300-1.317 Å) covalent bonds. Furthermore, the C-N-C endocyclic bond angle of the heterocyclic moieties fall in the range of 114.4^o-119.6^o, which is indicative of a non-ionized pyridine unit. In contrast, in the structure of **2HG** the carboxylate C-O bond distances are more similar (1.27/1.23 Å). In addition, the C-N-C endocyclic bond angle of the heterocyclic moiety is 121.1^o, which is typical for a pyridinium cation.[14]

2.4.2 Intermolecular interactions

The five crystal structures obtained exhibit similar primary trimeric supermolecules constructed through the expected intermolecular O-H…N synthon between the dicarboxylic acid and pyridine except for structure **3HBA**. In addition to the primary hydrogen bonding within each trimer, the N-H moiety in each acetamido group is further involved in the formation of hydrogen bonds with a neighboring molecule; in all five structures the amide C=O moiety act as the hydrogen bond acceptor. Besides the primary interaction that takes place between the carboxylic acid or carboxylate and acetamido/acetamidomethylpyridine, four other types of motifs are possible in this series of compounds, Figure 2.21. The frequency of occurrence of each type of motif is summarized in Table 2.4.

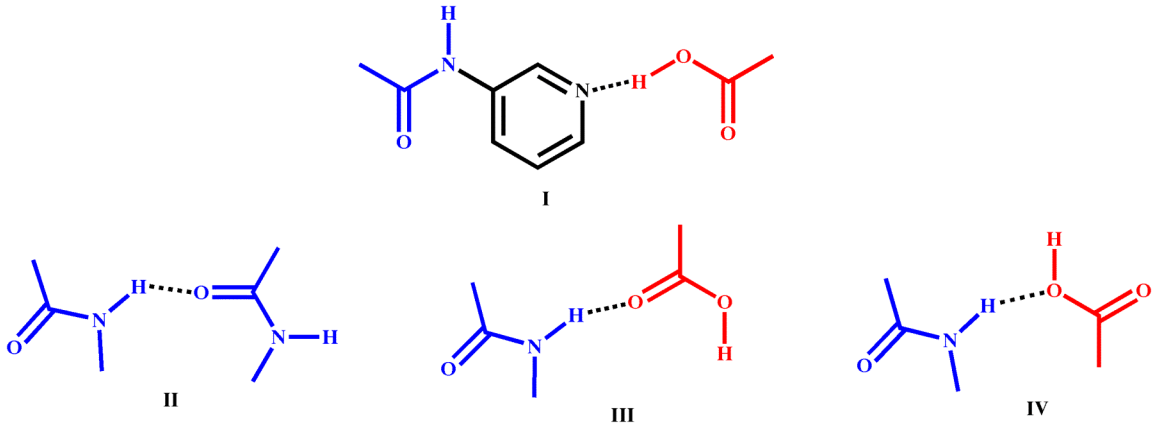

Figure 2.21 Expected primary acid···pyridine synthons (**I**). Three possible interactions involving the N-H hydrogen bond with the amide C=O (**II**), with the acid C=O (**III**), with the acid O-H (**IV**).

The binding motif in the crystal structure of **3HBA** is different when compared to the other cocrystals mentioned above, in that the phenolic hydroxy group forms a hydrogen bond to the pyridyl-N, while the carboxylic acid forms a hydrogen bond with the amide (N-H) group on the ligand. This binding preference is not surprising based on the molecular electrostatic potential (MEP) charge calculation carried out indicating that the phenolic hydroxy group is a better donor when compare to the carboxylic acid.[15] Moreover, there have been other similar cases of this interaction between phenolic hydroxy groups and isonicotinamide, where the phenol…pyridine interaction prevailed in the presence of COOH groups.[16] This 'low-yield' adduct **3HBA** provides more examples with acid…amide synthon **III** (Figure 2.21) without acid…pyridine recognition **I** (Figure 2.21). Furthermore, MEP charge calculations can be employed for assigning (and ranking) the relative hydrogen-bond donor/acceptor strengths across a wide range of chemical functionalities.

Overall, pyridine…carboxylic acid intermolecular interactions were observed approximately 90% of the time in this study. Thus this interaction may be employed in subsequent supramolecular synthetic strategies.

Table 2.4 Summary of structural motifs

Ligands	Carboxylic acid/carboxylate	Structure	Structural motif
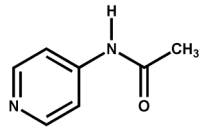	hydrogenglutarate	2HG	I, III
	suberic acid	2SUB	I, III
	sebacic acid	2SEB	I, III
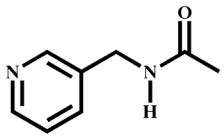	succinic acid	3SUC	I, II
	4-hydroxybenzoic acid	3HBA	III

2.4.3 Structural comparison with CSD

A search for relevant pyridine…carboxylic acid cocrystals in the CSD[7] revealed that this interaction occurs around 91% of the time, which was demonstrated in four out of the five structures herein. The self-complementarity of monoacetylated amides is generally a reliable motif with the combination of functionalities present. This intermolecular compability of the amide N-H and the amide C=O may therefore be employed in subsequent supramolecular synthetic strategies based upon a hierarchy of hydrogen bond interactions even in the presence of potentially competitive hydrogen bond acceptors.

2.4.4 Metal coordination abilities of acetamido/acetamidomethyl-pyridine moieties

Single-crystal X-ray analysis of **1a-b, 2a,** and **3a,** has demonstrated that the self-complementary N-H…O=C intermolecular ligand…ligand hydrogen bond interaction is present. The *O,O'*-chelating anions employed, hexafluoro-2,4-pentanedionate and 1,3-diphenyl-1,3-propanedionate, occupy the four equatorial positions around the metal(II) ions, when the amide moiety is located further away from the equatorial plane as demonstrated by the *meta*- and *para*-substituted pyridine-based ligands, it gives the N-H moiety the structural freedom to select a hydrogen bond acceptor, the carbonyl moiety the preferred interaction site in each of the complexes, Figure 2.22.

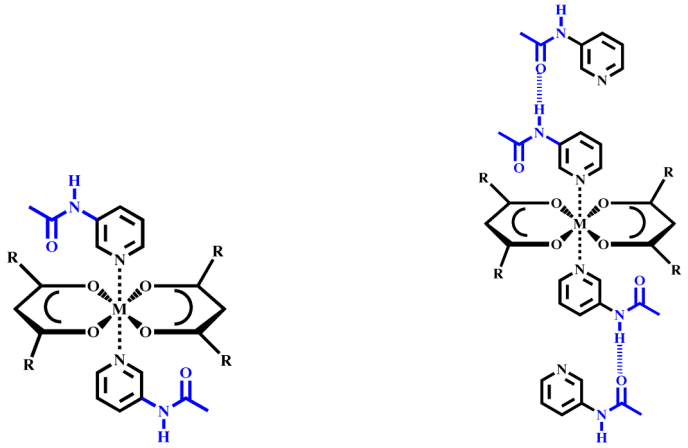

Figure 2.22 Pictorial representation of the desired coordination chemistry around the M(II) centers after compound binds; as well as the possible hydrogen bond interactions.

The nature of the metal ion does not affect the resulting structure notably because in each case, the metal ion is 'strapped into' a fixed geometry dictated by the two anionic chelating ligands. The importance of using chelating ligands for controlling the coordination geometry, and thereby the structural role of the complex ion itself, is illustrated by a previously reported crystal structure of a five coordinate Cu(II) complex compromising of two 4-acetamidopyridine, two acetate ions and a water molecule in the first coordination sphere; in this case the amide…amide hydrogen bond is disrupted by the water molecule, and the result is a complex 3-D architecture.[17]

The self-complementary acetamido moiety has also been demonstrated in the preparation of a series of silver(I)-containing 2-D architectures,[18] indicating that the particular supramolecular synthon is robust enough to organize relatively large complex ions into desired extended networks. A search of the CSD showed other examples of amido functional groups containing Ag(I) ions, where those structures also contained extended networks assembled via self-complementary N-H…O=C hydrogen bonds.[19] Other examples include nicotinamide and isonicotinamide with Cu(II) ions to produce 2-D network and similar 2-D networks with open channels have been constructed from Ni(II), Cu(II) and Co(II).[20]

The structures presented here support the idea that control at both the molecular and supramolecular level can be achieved by combining reliable supramolecular reagents

with coordination complexes where the coordination geometry is strictly controlled by the aid of suitable chelating ligands.

2.5 Conclusion

In summary the self-complementarity of monoacetylated amides is generally a reliable motif for the construction of other supermolecules, with the combination of functionalities present in **2HG, 2SUB, 2SEB**, **3SUC,** and **3HBA** despite the potential competition from a C=O moiety located on the carboxylic acid. This intermolecular compatibility of the amide N-H and the amide C=O may therefore be employed in subsequent supramolecular synthetic strategies based upon a hierarchy of hydrogen bond interactions.

References

[1] (a) Leiserowitz, L. *Acta Crystallogr*., **1976**, B32, 775; (b) Leiserowitz, L.; Tuval, M. *Acta. Crystallog*r., **1978**, B34, 1230; (c) Dunitz, J. D. *Pure Appl. Chem*., **1991**, 63, 177.

[2] Allen, F. H.; Motherwell, W.D.S.; Raithby, P.R.; Shields, G.P.; Taylor, R. *New J. Chem*., **1999**, 1, 25.

[3] (a) Kane, J. J.; Liao, R.-F.; Lauher, J.W.; Fowler, F.W. *J. Am. Chem. Soc*. **1995**, 117, 12003; (b) Grunert, M.; Howie, R.A.; Kaeding, A.; Imrie, C.T. *J. Mater. Chem*. **1997**, 7, 211; (c) Vishweshwar, P.; Nangia, A.; Lynch, V.M. *J. Org. Chem*. **2002**, 67, 556; (d) Palmore, G.T.R.; Luo, T.-J.M.; McBride-Wieser, M.T.; Picciotto, E.A.; Reynoso-Paz, C.M. *Chem. Mater*. **1999**, 11, 3315; (e) Aakeröy, C.B.; Beatty, A.M.; Tremayne, M.; Rowe, D. *Cryst. Growth Des*. **2001**, 1, 377; (f) Sharma, C.V.K.; Zaworotko, M. J. *Chem. Commun*. **1996**, 2655, (g) Pedireddi, V.R.; Chatterjee, S.; Ranganathan, A. *Tetrahedron* **1998**, 54, 9457, (h) Amai, M.; Endo, T.; Nagase, H.; Ueda, H.; Nakagaki, M. *Acta Crystallogr*. **1998**, C54, 1367.

[4] (a) Huang, K.-S.; Britton, D.; Etter, M.C.; Byrn, S.R. *J. Mater. Chem*. **1997**, 7, 713; (b) MacGillivray, L.R.; Reid, J.L.; Ripmeester, J.A. *J. Am. Chem. Soc*. **2000**, 122, 7817.

[5] Ermer, O.; Eling, A. *J. Chem. Soc., Perkin Trans. 2* **1994**, 925.

[6] Desiraju, G.R. *Angew. Chem. Int. Ed. Engl*., **1995**, 34, 2311.

[7] Allen, F. H. *Acta Crystallogr., Sect. B: Struct. Sci*., **2002**, 58, 380.

[8] (a) Beatty, A.M. *CrystEngComm*., **2001**, 51, 1; (b) Aakeröy, C.B.; Beatty, A.M. *Aust. J. Chem.,* **2001**, 54, 409.

[9] (a) Fujita, M.; Kwon, Y.-J.; Washizu, S.; Ogura, K. *J. Am. Chem. Soc.* **1994**, *116*, 1151; (b) Subramanian, S.; Zaworotko, M. J. *Angew. Chem. Int. Ed. Engl.* **1995**, *34*, 2127; (c) Yaghi, O. M.; Li, H. *J. Am. Chem. Soc.* **1996**, *118*, 295; (d) Fujita, M.; Kwon, Y.-J.; Sasaki, O.; Yamaguchi, K.; Ogura, K. *J. Am. Chem. Soc.* **1995**, *117*, 7287; (e) Goodgame, D. M. L.; Grachvogel, D. A.; Hussain, I.; White, A. J. P.; Williams, D. J. *Inorg. Chem.* **1999**, *38*, 2057; (f) Chatterton, N. P.; Goodgame, D. M. L.; Grachvogel, D. A.; Hussain, I.; White, A. J. P.; Williams D. J., *Inorg. Chem.* **2001**, *40*, 312; (g) Goodgame, D. M. L.; Menzer, S.; Smith, A. M.; Williams, D. J. *J. Chem. Soc., Dalton Trans.* **1997**, 3213; (h) Doyle, G. A.; Goodgame, D. M. L.; Hill, S. P. W.; Menzer, S.; Sinden, A.; Williams, D. J. *Inorg. Chem*. **1995**, *34*, 2850.

[10] (a) Aakeröy, C. B.; Salmon, D. J.; Smith, M. M.; J. Desper, *Cryst. Growth Des*. **2006**, *6*, 1033; (b) Basavoju, S.; Boström, D.; Velaga, S. P. *Cryst. Growth Des.* **2006**, *6*, 2699; (c) Aakeröy, C. B.; Salmon, D. J. *CrystEngComm* **2005**, *7*, 439; (d) Saha, B. K.; Nangia, A.; Jaskolski, M. *CrystEngComm* **2005**, *7*, 355; (e) Vishweshwar, P.; McMahon, J. A.; Peterson, M. L.; Hickey, M. B.; Shattock T. R.; Zaworotko, M. *Chem. Commun.* **2005**, 4601; (f) Bhogala, B. R.; Basavoju, S.; Nangia A., *Cryst. Growth Des.* **2005**, *5*, 1683.

[11] Soldatov, D.V.; Ripmeester, J A. *Chem. Eur. J.* **2001**, *7*, 2979.

[12] Li, C.; Rittmann, L. S.; Tsiftsoglou, A.S.; Bhargava, K.K.; Sartorelli, A.C. *J. Med. Chem*., **1978**, 21, 874-877.

[13] Singh, T.; Stein R.G.; Biel, J.H. *J. Med. Chem*., **1969**, 12, 949-950.

[14] Cowan, J.A.; Howard, A.K.; McIntyre, G.J.; Lo, S.M.-F.; Williams, I.D. *Acta Crystallogr., Sect. B: Struct. Sci.,* **59**, 794.

[15] Hunter, C. *Angew. Chem. Int. Ed*. **2004**, 43, 5310.

[16] Vishweshwar, P.; Nangia, A.; Lynch, V.M. *CrystEngComm*., **2003**, 5, 164.

[17] Emsley, J.; Arif, M.; Bates, P.A.; Hursthouse, M.B. *J. Chem. Soc., Dalton Trans*., **1988**, 1493.

[18] Schauer, C.L.; Matwey, E.; Fowler, F.W.; Lauher, J.W. *J. Am. Chem. Soc*., **1997**, 119, 10245.

[19] (a) Muthu, S.; Yip J.H.K.; Vittal, J.J. *J. Chem. Soc. Dalton Trans*., **2002**, 4561; (b) Muthu, S.; Yip, J.H.K.; Vittal, J.J. *J. Chem. Soc. Dalton Trans*., **2001**, 3577.

[20] (a) Ma, Z.; Moulton, B. *Cryst. Growth and Des.*, **2007**, 7, 196; (b) Aakeröy, C.B.; Desper, J. and Valdes-Martinez, J. *CrystEngComm*., **2004**, 6, 413; (c) Aakeröy, C.B.; Beatty, A.M.; Desper, J.; O'Shea, M.; Valdes-Martinez, J. *Dalton Trans*., **2003**, 3956.

CHAPTER 3 - Balancing intermolecular hydrogen and halogen bonding interactions using pyridine/pyrazine mono-N-oxides

3.1 Introduction

An important aspect of organic supramolecular chemistry is the design of discrete building blocks with intermolecular preferences that can be utilized for the directed assembly of homomeric[1] and heteromeric[2] solid-state architectures with predictable and desirable connectivities. In supramolecular chemistry, carboxylic acids have traditionally been used because they readily aggregate as homomeric dimers. However, the acid…pyridine heterosynthon is the most frequently occurring hydrogen bond motif in the Cambridge Structural Database (CSD), and has occurrence probability of over 90%[3] compared to <50% frequency for other hydrogen bond synthons[4] such as, acid…acid, amide…amide and acid…amide, Figure 3.1.

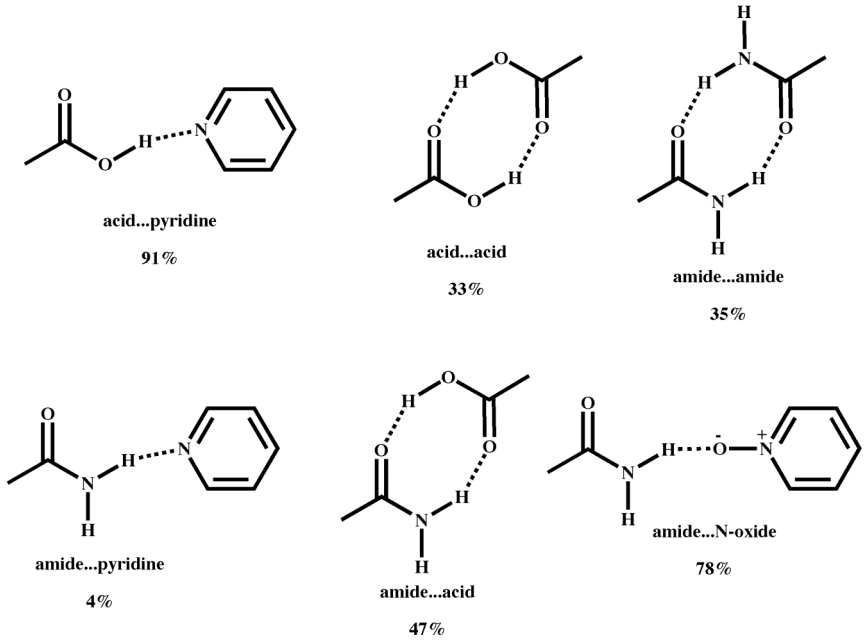

Figure 3.1 Strong hydrogen bond homosynthons and heterosynthons with their frequency.

Although the above synthons are well established and dependable tools within crystal engineering, other synthons such as pyrazine/4,4'-bipyridine mono N-

oxide…carboxylic acid and mono N-oxide…halogen (I or Br) have not been utilized, although they can form extended supramolecular architectures.[5]

Constructing new supramolecular products is often predictable when there are only two individual entities, containing only one complementary moiety; however predictability becomes more complicated when the number of interactive moieties on each reactant leads to an increased possibility of synthons. A 2010 search of the CSD[6] reported no assembly formed through a combination of hydrogen and halogen bonds with mono N-oxide derivatives; however there are approximately twenty examples of self assembly involving a dioxide moiety and a hydrogen-bond, and only one example where self assembly is through halogen bonding.[6]

A notable example is the carboxamide–pyridine N-oxide synthon, which takes advantage of the strong N-H…O^- hydrogen bond.[7] In fact pyridine N-oxide (N^+-O^-) is a stronger acceptor than pyridyl N because of its anionic character; for example the pK_{HB} values of pyridine N, and N-oxide O^- are 1.86 and 2.70 (increasing basicity)[7] and moreover, electrostatic surface potential charges at the electronegative atoms N -43.7, O -47.4, and O^- -53.3 kcal mol^{-1} parallel the same trend.[5] Hence in terms of energy, the amide…N-oxide two point heterosynthon of N-H…O^- and C-H…O hydrogen bond is more stable than the constituent N-H…O amide dimer, Figure 3.2.

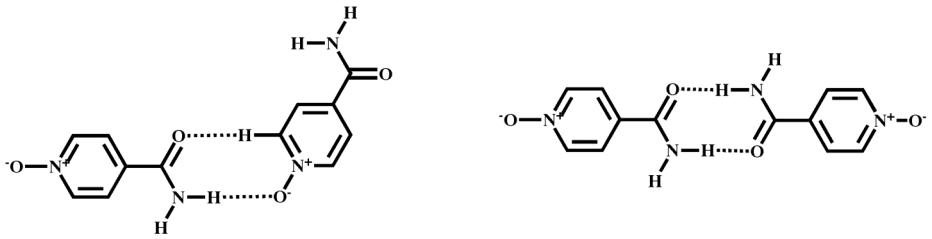

Figure 3.2 Two point heterosynthon of N-H…O^- and N-H…O amide dimer.

Another notable example is the case of 4,4'-bipyridine and 4,4'-bipyridine dioxide hydrocarbon modules where the electron donor moiety (i.e. oxygen atom) can effectively drive the perfluorocarbon halides-hydrocarbon self-assembly processes, as well as be more effective in the formation of the halogen bonded adducts than corresponding nitrogen substituted modules, Figure 3.3.[8]

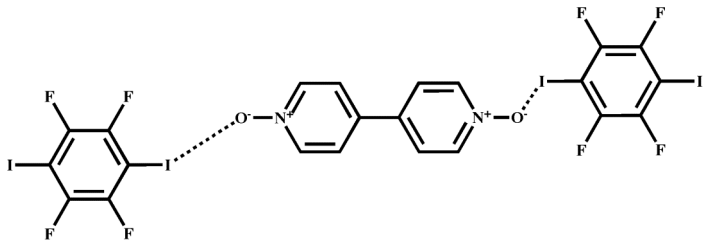

Figure 3.3 Halide-hydrocarbon self-assembly processes.

Furthermore, the strength of the halogen bond donor can be reinforced upon fluorination of the molecule, which can lead to an increase in the electron-acceptor capabilities of the iodine or bromine atoms.[9]

With the above concepts in mind, pyrazine and 4,4'-bipyridine mono N-oxide moieties have the capabilities to provide ideal molecular recognition sites for promoting both hydrogen and halogen bonding in a controllable and predictable manner. Therefore, we will focus on the design and synthesis of supramolecular architectures formed through hydrogen and halogen bonds using pyrazine and 4,4'-bipyridine mono N-oxide derivatives. Based on electrostatic surface potentials the higher charge will determine the interaction preferences between the different species. Therefore, we synthesized three mono N-oxide moieties **4**, **5**, and **6,** Figure 3.4, and allowed them to react with a variety of hydrogen and halogen donor species.

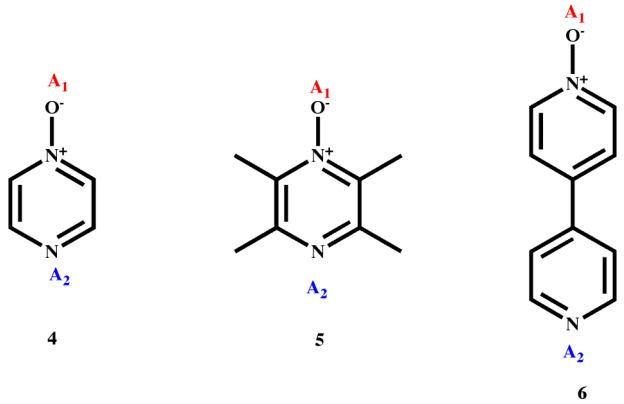

Figure 3.4 Target compounds showing best acceptor site (A_1) and second best acceptor site (A_2).

A series of semi-empirical PM3[10] calculations will be employed to calculate the charges on **4**, **5**, and **6** as well as on the hydrogen and halogen bond reactants. The overall goals of this chapter are:

1. To carry out a series of semi-empirical PM3 calculations in order to rank the binding sites in terms of charge.
2. To determine whether the combination of hydrogen and halogen bonds can be use to construct predictable assemblies with mono N-oxide derivatives.
3. Establish a balance between the hydrogen bond and halogen bond.

3.2 Experimental

3.2.1 Synthesis

All chemicals, unless noted, were purchased from Aldrich and used without further purification. Column chromatography was carried out on silica gel (150 Å pore size) from Analtech Inc. Melting points were determined on a GallenKamp melting point apparatus in a capillary tube and are reported uncorrected. ^{1}H and ^{13}C NMR spectra were recorded on a Varian Unity plus 400 MHz or 200 MHz spectrometers in DMSO-d_6. Compounds were prepared for infrared spectroscopic (IR) analysis as a mixture in KBr or on a ZnSe ATR crystal.

3.2.1.1 Synthesis of pyrazine mono N-oxide, 4[11]

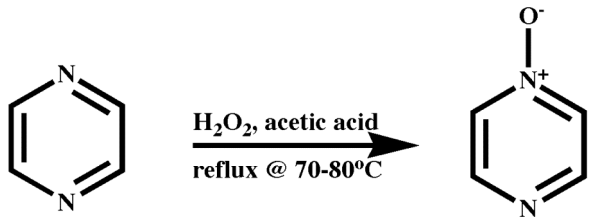

A solution of 30% hydrogen peroxide (1.42g, 0.042 mol) in 10 mL of acetic acid was added dropwise using a drop funnel over a period of 2.5 hr to a solution of pyrazine (1.00g, 0.013 mol) in 12.5 mL of acetic acid at 70-80°C. Heating was continued for about

5 hours. Acetic acid was removed on a rotary evaporator, and then 10 mL of water was added followed by evaporation. The residue was dissolved in 50 mL of hot chloroform and dried with a mixture of sodium sulfate and sodium carbonate and the solvent removed on a rotary evaporator. The residue was chromatographed on silica with 9:1 chloroform-methanol as the eluant. Product **4** was isolated as a white powder and recrystallization from methanol gave needle-like crystals, (1.2g, 72%). M.p.: 113-115°C (Lit. m.p.: 113-114°C);[11] ^{1}H NMR (δ_H; 400 MHz, DMSO-d_6): 8.66 (d, 2H, J = 4Hz), 8.36 (d, 2H, J = 4Hz); ^{13}C NMR (δ_C; 200 MHz, DMSO-d_6): 158, 144; IR (KBr pellet): υ 3430, 2914, 1596, 1470, 1433, 1312(N^+-O^-), 1213, 1005, 861, 540, 477 cm^{-1}.

3.2.1.2 Synthesis of tetramethylpyrazine mono N-oxide, 5[11]

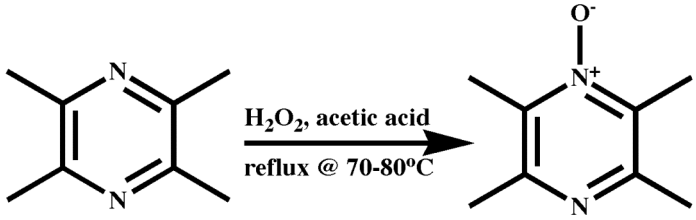

A solution of 30% hydrogen peroxide (1.42g, 0.042 mol) in 10 mL of acetic acid was added dropwise using a drop funnel over a period of 2.5 hr to a solution of tetramethylpyrazine (1.77g, 0.013 mol) in 12.5 mL of acetic acid at 70-80°C, with heating continued for about 5 hr. Acetic acid was removed using a rotary evaporator, 10 mL of water was added followed by evaporation. The residue was dissolved in 50 mL of hot chloroform and dried with a mixture of sodium sulfate and sodium carbonate and the solvent removed on a rotary evaporator. The residue was chromatographed on silica with 9:1 chloroform-methanol as the eluant. Product **5** was isolated as a white powder and recrystallization from methanol gave micro size crystalline particles, (1.2g, 61%). M.p.: 98-100°C; ^{1}H NMR (δ_H; 200 MHz, DMSO-d_6): 2.43 (d, 6H), 2.32 (d, 6H); ^{13}C NMR (δ_C; 200 MHz, DMSO-d_6): 150, 138, 21, 12; IR (KBr pellet): υ 3462, 2914, 1572, 1472, 1320 (N^+-O^-), 1138, 1004, 922, 691 cm^{-1}.

3.2.1.3 Synthesis of 4,4'-bipyridine mono N-oxide, 6[11]

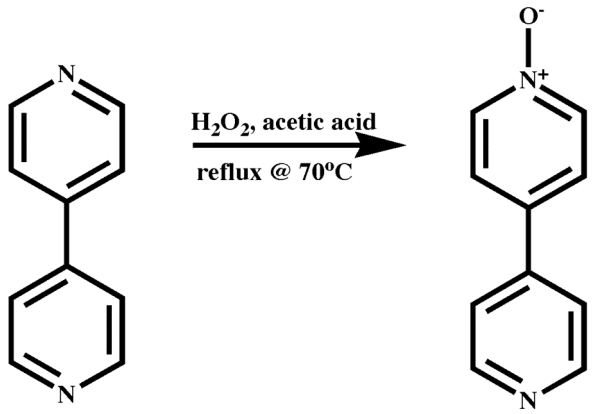

6 was prepared by employing a modification of the previously reported procedure.[11] A mixture of 4,4′-bipyridine (2.00g, 12.82 mmol), 30% hydrogen peroxide (1.33g, 39 mmol) and glacial acetic acid (8 mL) was stirred in a round bottom flask for 18 hours at 70°C. After cooling the reaction mixture the solvent was removed via a rotary evaporator and diluted with 20 mL water. The solution was basified with excess sodium carbonate (2g) and extracted with chloroform (3 x 50 mL). The organic layers were combined and then concentrated under reduced pressure using a rotary evaporator. **6** was further purified via column chromatography with a 3:1 ethyl acetate-methanol mixture producing an off-white solid, (1.1g, 52%). M.p.: 170-171°C; ^{1}H NMR (δ_H; 400 MHz, DMSO-d_6): 8.70 (d, 2H, J = 12Hz), 8.36 (d, 2H, J = 12Hz), 7.94 (d, 2H, J = 12 Hz), 7.83 (d, 2H, J = 21 Hz); ^{13}C NMR (δ_C; 400 MHz, DMSO-d_6): 150, 142, 139, 133, 124 120; IR (KBr pellet): υ 3222, 2910, 1600, 1515, 1482, 1410, 1253 (N^+-O^-), 1228, 1191, 1029, 851, 821, 714, 651, 580 cm^{-1}.

3.2.2 Synthesis of cocrystals

3.2.2.1 Synthesis of pyrazine mono N-oxide 4-iodotetrafluorobenzoic acid (1:1), 4IF$_4$BA

4 (15 mg, 0.163 mmol) and **IF$_4$BA** (52 mg, 0.163 mmol) were placed in a beaker and dissolved in 4 mL of acetonitrile. After five days of slow evaporation, light yellow needle-shaped crystals were obtained. M.p.: 122-124°C; IR (KBr pellet) υ 2561 and 1931 cm^{-1} (O-H…N, br), 1712 cm^{-1} (C=O, s), 1293 cm^{-1} (N^+-O^-, s), 1022 and 979 cm^{-1} (C-I, s)

3.2.2.2 Synthesis of pyrazine mono N-oxide 1,3,5-trifluorotriiodobenzene (1:1), $4I_3F_3B$

4 (15 mg, 0.163 mmol) and **I_3F_3B** (166 mg, 0.163 mmol) were placed in a beaker and dissolved in 4 mL of ethyl acetate. After ten days of slow evaporation, transparent plate-like crystals were obtained. M.p.: 155-156°C; IR (ZnSe crystal) υ 1292 cm^{-1} (N^+-O^-, s), 1046 cm^{-1} (C-I, s).

3.2.2.3 Synthesis of pyrazine mono N-oxide 4-hydroxybenzoic acid (1:1), 4HBA

4 (15 mg, 0.163 mmol) and **HBA** (45 mg, 0.163 mmol) were placed in a beaker and dissolved in 4 mL of acetonitrile and 2.00 mL methanol. After fifteen days of slow evaporation, transparent plate-like crystals were obtained. M.p.: 194-196°C; IR (KBr pellet) υ 2484 and 1928 cm^{-1} (O-H…N, br), 1695 cm^{-1} (C=O, s), 1244 cm^{-1} (N^+-O^-, s).

3.2.2.4 Synthesis of tetramethylpyrazine mono N-oxide 4-iodotetrafluorobenzoic acid (1:1), $5IF_4BA$

5 (15 mg, 0.110 mmol) and **IF_4BA** (35 mg, 0.110 mmol) were placed in a beaker and dissolved in 5 mL of ethanol. After thirteen days of slow evaporation, transparent plate-like crystals were obtained. M.p.: 177-178°C; IR (ZnSe crystal) υ 2441 and 1918 cm^{-1} (O-H…N, br), 1732 cm^{-1} (C=O, s), 1298 cm^{-1} (N^+-O^-, s), 979 cm^{-1} (C-I, s).

3.2.2.5 Synthesis of tetramethylpyrazine mono N-oxide 4-bromotetrafluorobenzoic acid (1:1), $5BrF_4BA$

5 (15 mg, 0.110 mmol) and **BrF_4BA** (30 mg, 0.110 mmol) were placed in beaker a and dissolved in 5 mL of ethanol. After fifteen days of slow evaporation, transparent plate-like crystals were obtained. M.p.: 113-115°C; IR (KBr pellet) υ 2448 and 1911 cm^{-1} (O-H…N, br), 1732 cm^{-1} (C=O, s), 1301 cm^{-1} (N^+-O^-, s), 990 cm^{-1} (C-Br, s).

3.2.2.6 Synthesis of tetramethylpyrazine mono N-oxide 4-aminobenzoic acid (1:2), 5ABA

5 (15 mg, 0.110 mmol) and **ABA** (30 mg, 0.220 mmol) were placed in a beaker and dissolved in 5 mL of ethanol. After thirteen days of slow evaporation, transparent plate-like crystals were obtained. M.p.: 178-179°C; IR (KBr pellet) υ 2554 and 1900 cm^{-1} (O-H…N, br), 1655 cm^{-1} (C=O, s), 1290 cm^{-1} (N^+-O^-, s).

3.2.2.7 Synthesis of 4,4'-bipyridine mono N-oxide 4-iodobenzoic acid (1:1), 6IBA

6 (15 mg, 0.091 mmol) and **IBA** (23 mg, 0.091 mmol) were placed in a beaker and dissolved in 2 mL of acetonitrile. After ten days of slow evaporation, transparent needle-like crystals were obtained. M.p.: 168-170°C; IR (KBr pellet) υ 2550 and 1926 cm^{-1} (O-H…N, br), 1680 cm^{-1} (C=O, s), 1220 cm^{-1} (N^{+}-O^{-}, s), 815 cm^{-1} (C-I, s).

3.2.2.8 Synthesis of 4,4'-bipyridine mono N-oxide 4-aminobenzoic acid (1:1), 6ABA

6 (15 mg, 0.091 mmol) and **ABA** (13 mg, 0.091 mmol) were placed in a beaker and dissolved in 2 mL of acetonitrile. After fifteen days of slow evaporation, transparent needle-like crystals were obtained. M.p.: 197-198°C; IR (KBr pellet) υ 2448 and 1961 cm^{-1} (O-H…N, br), 1662 cm^{-1} (C=O, s), 1265 cm^{-1} (N^{+}-O^{-}, s).

3.2.2.9 Semi-empirical PM3 calculations

Compounds **4**(pyrazine mono N-oxide) **5**(tetramethylpyrazine mono N-oxide) and, **6**(4,4'-bipyridine mono N-oxide) molecular structures were constructed using Spartan ’06 (Wavefunction, Inc. Irvine, CA). All three molecules were optimized using Semi-empirical PM3 with the maxima and minima in the electrostatic potential surface (0.002 e/au isosurface) determined using a positive point charge in the vacuum as a probe.

3.3 Results

A summary of the crystallographic information for **4IF$_4$BA, 4I$_3$F$_3$BA, 4HBA, 5IF$_4$BA, 5BrF$_4$BA, 5ABA, 6IBA,** and **6ABA** are displayed in Table C.2 and all hydrogen-bond geometries for **4IF$_4$BA, 4I$_3$F$_3$BA, 4HBA, 5IF$_4$BA, 5BrF$_4$BA, 5ABA, 6IBA,** and **6ABA** are listed in Table 3.1.

Table 3.1 Hydrogen-bond geometries for **4IF$_4$BA, 4I$_3$F$_3$BA, 4HBA, 5IF$_4$BA, 5BrF$_4$BA, 5ABA, 6IBA, and 6ABA**

Structure	D-H…A	d(D-H)/Å	d(H…A)/Å	d(D…A)/Å	<(DHA)/°
4 IF$_4$BA	O(11)-H(11)…N(24)	0.84	1.85	2.6470(14)	157.3
4 HBA [i]	O(21)-H(21)…N(14)	0.965(16)	1.756(16)	2.7203(11)	177.0(15)
	O(24)-H(24)…O(11)#1	0.897(16)	1.7563(17)	2.6442(11)	166.8(15)
5 IF$_4$BA [ii]	O(31A)-H(31A)…N(14)	0.84	1.87	2.681)4)	161.2
	O(31B)-H(31B)…N(14)	0.84	1.99	2.715(3)	144.8
	O(31C)-H(31C)…O(11)#1	0.84	1.65	2.485(11)	175.1
5 BrF$_4$BA [iii]	O(31A)-H(31A)…N(14)	0.84	1.90	2.711(5)	161.4
	O(31B)-H(31B)…N(14)	0.84	1.81	2.594(8)	154.2
	O(31C)-H(31C)…O(11)#1	0.84	1.82	2.662(8)	179.6
5 ABA [iv]	N(34)-H(34A)…O(11)	0.885(17)	1.956(17)	2.8220(16)	165.8(15)
	N(44)-H(44A)…N(14)	0.906(15)	2.139(15)	3.0437(14)	177.0(13)
	N(44)-H(44B)…O(32)#1	0.876(15)	2.290(15)	3.0713(14)	148.6(13)
	O(31)-H(31)…O(32)#2	0.895(16)	1,724(16)	2.642(11)	172.4(15)
	O(41)-H(41)…O(42)#3	1.259(16)	1.327(16)	2.5849(12)	176.7(13)
6 IBA	O(31)-H(31)…O(11)	0.84	1.76	2.556(2)	158.0
6 ABA [v]	O(31)-H(31)…N(21)	1.01(2)	1.64(2)	2.6440(19)	175.2(16)

Structure	D-H…A	d(D-H)/Å	d(H…A)/Å	d(D…A)/Å	<(DHA)/°
6 ABA [v]	N(34)-H(34A)…N(34)#1	0.87(2)	2.33(2)	3.183(2)	164.5(17)
	N(34)-H(34B)…O(11)#2	0.89(2)	1.98(2)	2.869(2)	176.5(19)

i) #1 x+2,y-1,z ii) #1 x+1,-y+3/2,z+1/2 iii) #1 x-1,-y+1/2,z-1/2 iv) #1 -x+1,y+1/2,-z+1/2 #2 -x+2,-y+1,-z+1 #3 -x-1,-y,-z v) #1 -x+1/2,y+1/2,-z+3/2 #2 x+1/2,-y+1/2,z+1/2

3.3.1 Molecular Electrostatic Potential Calculations

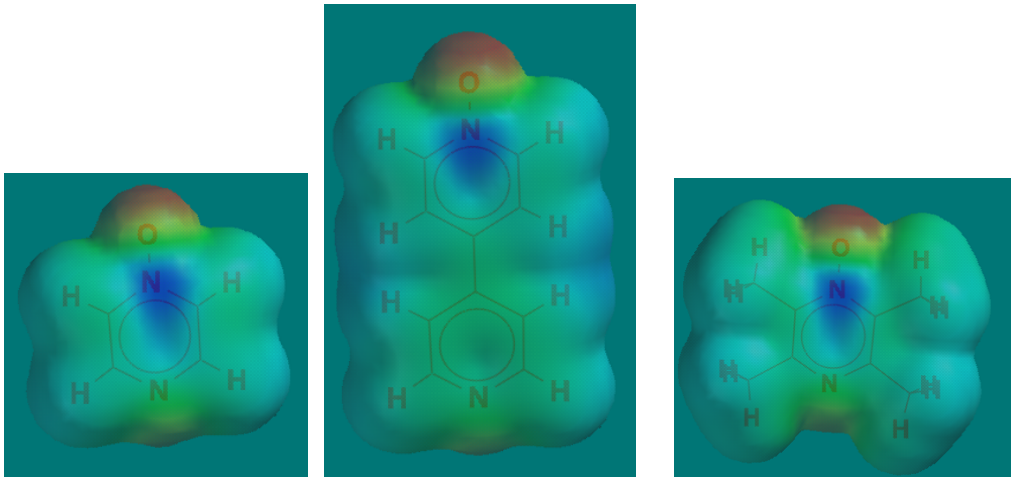

(a) (b) (c)

Figure 3.5 Electrostatic potentials of (a) pyrazine mono N-oxide, (b) 4,4'-bipyridine mono N-oxide, (c) tetramethylpyrazine mono N-oxide.

Table 3.2 shows the results of the electrostatic potentials calculated for the mono N-oxides as well as the donor ligands used in this study, and Figure 3.5 shows the electrostatic potential diagrams for each type of mono N-oxides.

Table 3.2 Electrostatic potentials of all acceptor and donor ligands used in this study

Compounds	E (kJ/mol) (N^+-O^-)	E (kJ/mol) (N)	E (kJ/mol) (COOH)	E (kJ/mol) (OH)	E (kJ/mol) (NH_2)	E (kJ/mol) (IF_4BA)	E (kJ/mol) (IBA)	E (kJ/mol) (BrF_4BA)	E (kJ/mol) (I_3F_3B)
Pyrazine mono N-oxide	-282	-238	-	-	-	-	-	-	-
Tetramethylpyrazine mono N-oxide	-297	-253	-	-	-	-	-	-	-
Bipyridyl mono N-oxide	-300	-253	-	-	-	-	-	-	-
4-Iodotetrafluorobenzoic acid	-	-	143	-	-	219	-	-	-
4-Iodobenzoic acid	-	-	123	-	-	-	130	-	-
4-Bromotetrafluorobenzoic acid	-	-	146	-	-	-	-	160	-
1,3,5-trifluorotriiodobenzene	-	-	-	-	-	-	-	-	191
4-Hydroxybenzoic acid	-	-	111	165	-	-	-	-	-
4-Aminobenzoic acid	-	-	114	-	145	-	-	-	-

3.3.2 Crystal structure of pyrazine mono N-oxide 4-iodotetrafluorobenzoic acid (1:1), $4IF_4BA$

In the crystal structure of **$4IF_4BA$** the asymmetric unit consists of one molecule of **4** and one molecule of **IF_4BA**; forming a hydrogen bond between the carboxylic acid and the pyrazine-N moiety, (O11…N24) 2.6470(14) Å, Figure 3.6. The architecture is further extend into an infinite 1-D chain through the iodine atom and the pyrazine mono N-oxide oxygen with, N^+-O^-…I distance of 2.814 Å, Figure 3.7.

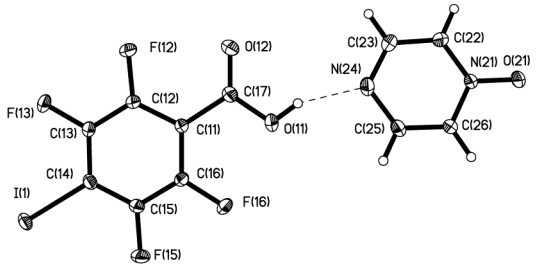

Figure 3.6 Thermal ellipsoids (50%) of the 1:1 binary cocrystal of **$4IF_4BA$**.

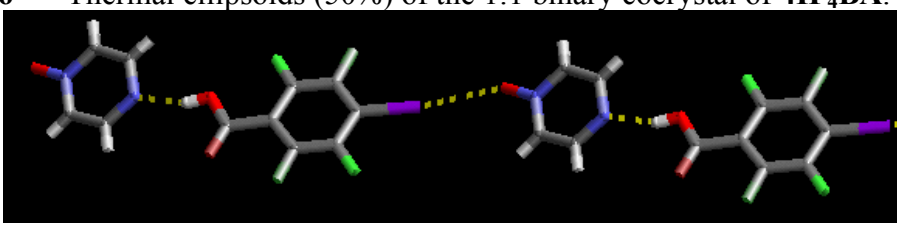

Figure 3.7 1-D chain of **$4IF_4BA$** held together via O-H…N hydrogen bond and N-O…I halogen bond.

3.3.3 Crystal structure of pyrazine mono N-oxide 1,3,5-trifluorotriiodobenzene (1:1), $4I_3F_3B$

The asymmetric unit of **$4I_3F_3B$** contains one molecule of **4** and one molecule of **I_3F_3B**. The supermolecule is constructed through the interaction of one of the iodo-moiety of the **I_3F_3B** and O atom of **4** with a bond distance of 2.69Å, Figure 3.8.

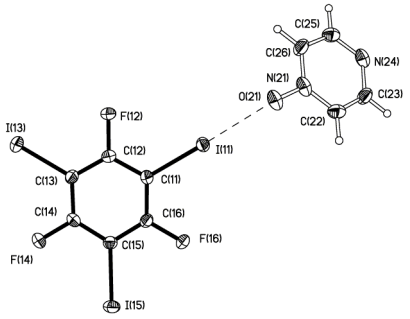

Figure 3.8 Thermal ellipsoids and labeling scheme of **$4I_3F_3B$**.

Furthermore, the structure is extremely disordered making it difficult to observe any short contacts between the pyrazine mono N-oxide nitrogen atom and any of the iodo-moiety. The ideal interaction that should be observed is a halogen bond between the N-oxide oxygen and nitrogen atom as is shown in Figure 3.9, resulting in an infinite 1-D chain.

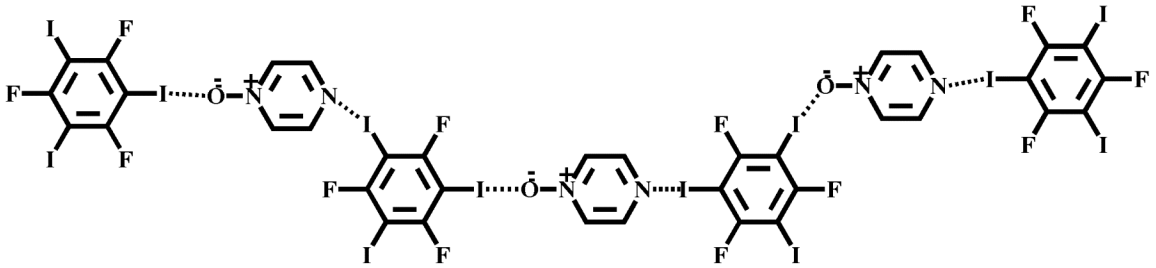

Figure 3.9 1-D chain of **$4I_3F_3B$** as a result of halogen bonding.

Nevertheless, a ring-like system is formed through halogen bonds between the N-oxide oxygen as well as through some short contacts between the iodine groups, with an I-I bond distance of 3.95Å and an angle of 120°, Figure 3.10.

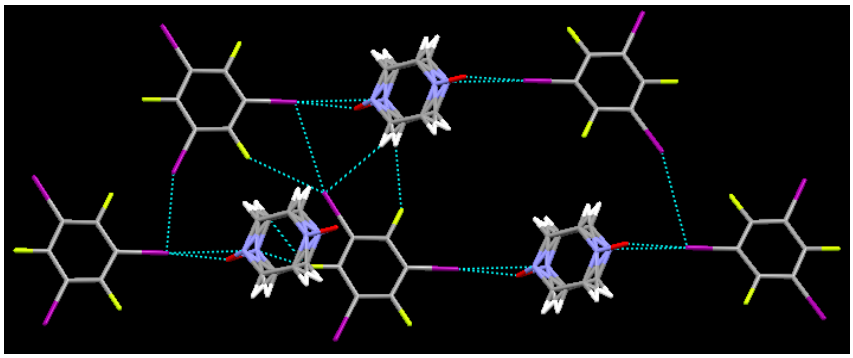

Figure 3.10 Ring-like arrangement in **4I$_3$F$_3$B** formed via N^+-O^-…I and I…I halogen bonds.

3.3.4 Crystal structure of pyrazine mono N-oxide 4-hydroxybenzoic acid (1:1), 4HBA

The crystal structure of **4HBA** has one molecule of **4** and one molecule of **HBA** in the asymmetric unit. This supermolecule is constructed through O-H…N hydrogen bonds between the O-H of the carboxylic acid group and the pyrazine nitrogen atom O21…N14, 2.7203(11) Å, Figure 3.11. The structure is further expanded into an infinite 1-D chain via the phenolic hydroxy group hydrogen bond to the oxygen atom of pyrazine mono N-oxide, O24…O11#1, 2.6442(11) Å, Figure 3.12.

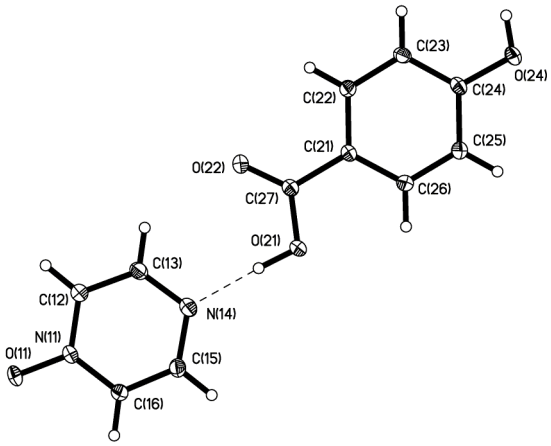

Figure 3.11 Thermal ellipsoids (50%) and labeling scheme of the unique molecules in **4HBA**.

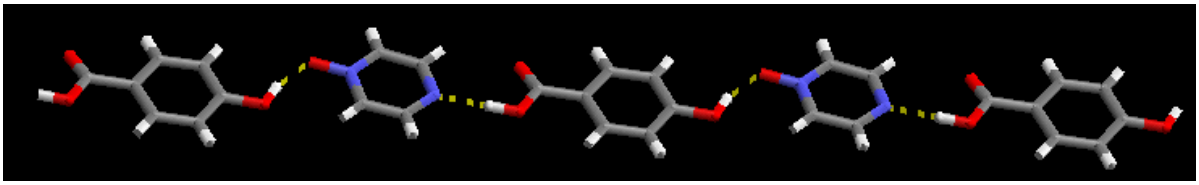

Figure 3.12 1-D chain of **4HBA** held to via O-H…N and O-H…O hydrogen bonds.

3.3.5 Crystal structure of tetramethylpyrazine mono N-oxide 4-iodotetrafluorobenzoic acid (1:1), 5IF$_4$BA

The crystal structure of **5IF$_4$BA** contains one molecule **5** and one molecule of **IF$_4$BA** in the asymmetric unit. The structure exhibits some disorder; nonetheless the supermolecule is constructed through O-H…N hydrogen bonds between the O-H of the acid and the tetramethylpyrazine mono N-oxide nitrogen atom O31A…N14, 2.681(4) Å, Figure 3.13. The structure is further extended into an infinite 1-D chain through the assistance of a halogen bond formed between the N^+-O^- of the tetramethylpyrazine mono N-oxide and the 4-iodotetrafluorobenzoic acid moiety, Figure 3.14.

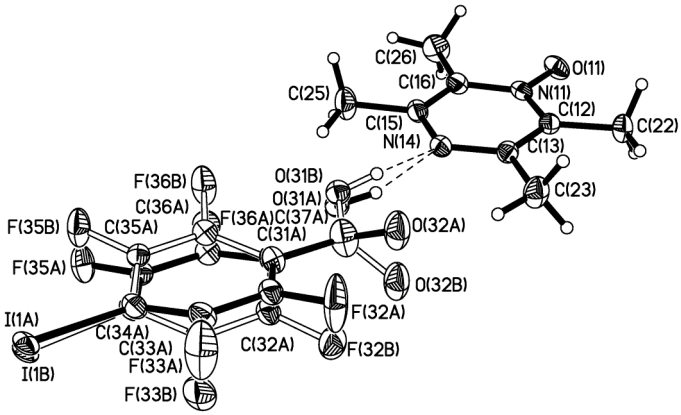

Figure 3.13 Thermal ellipsoids (50%) and labeling scheme of the supramolecule **5IF$_4$BA**.

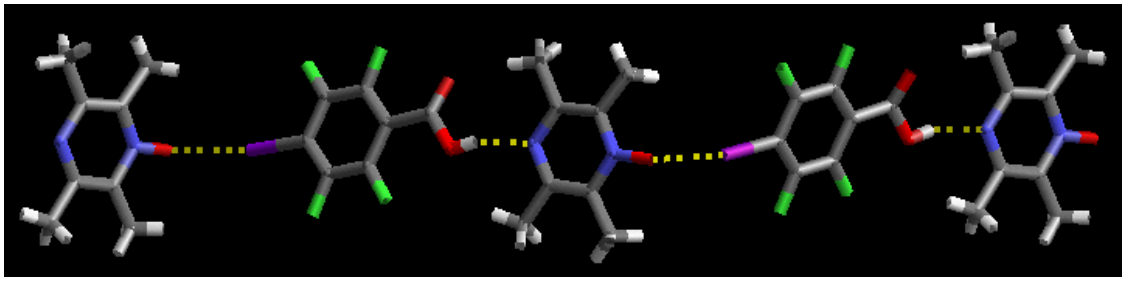

Figure 3.14 1-D chain of **5IF$_4$BA** held together via hydrogen and halogen bonding.

3.3.6 Crystal structure of tetramethylpyrazine mono N-oxide 4-bromotetrafluorobenzoic acid (1:1), 5BrF$_4$BA

The asymmetric unit of **5BrF$_4$BA** contains one molecule of **5** and one molecule of **BrF$_4$BA**; similar to **5IF$_4$BA** the crystal structure of **5BrF$_4$BA** is also disordered. The disorder resulted in the hydroxy group of the acid forming a hydrogen bond with the tetramethylpyrazine mono N-oxide O31A…N14, 2.711(5) Å, Figure 3.15. The architecture is further extended into this 1-D chain with the aid of halogen bonds formed through the bromo-substituent of the acid, Figure 3.16.

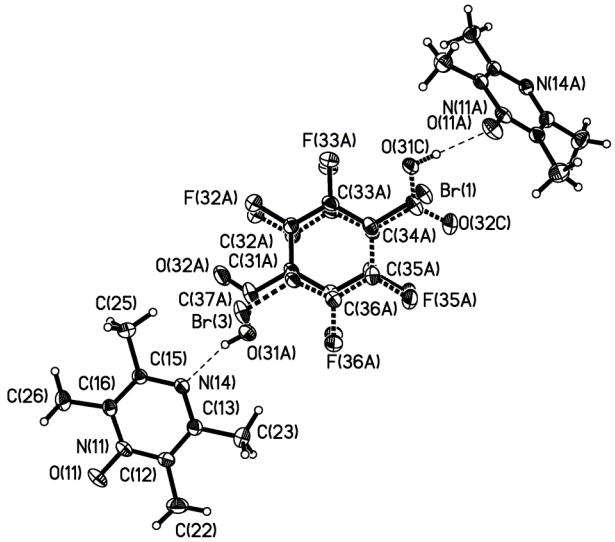

Figure 3.15 Thermal ellipsoids (50%) and labeling scheme of the supramolecule **5BrF$_4$BA**.

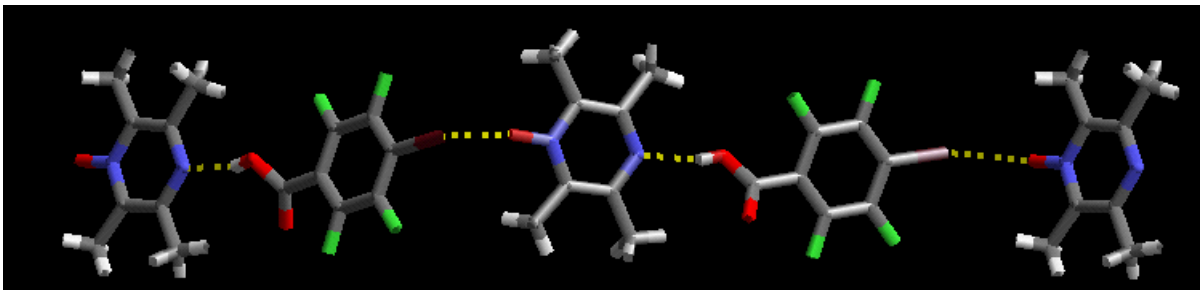

Figure 3.16 Alignment of binaries by O-H…N hydrogen bonds and C-Br…O halogen bonds resulting in infinite 1-D chain in **5BrF$_4$BA**.

3.3.7 Crystal structure of tetramethylpyrazine mono N-oxide 4-aminobenzoic acid (1:2), 5ABA

In the crystal structure of **5ABA**, the main motif comprises of hydrogen-bonding interactions between the amino group and the tetramethylpyrazine mono N-oxide moiety, with bond distances of N34…O34A, 2.8220(16) Å and N44…N14, 3.0437(14) Å respectively, Figure 3.17. The structure is further connected through self-complementary acid-acid dimers, O-H…O hydrogen bonds with bond distances of O31…O(32), 2.642(11) Å and O41…O(42), 2.5849(12) Å respectively, resulting in an infinite 1-D chain, Figure 3.18.

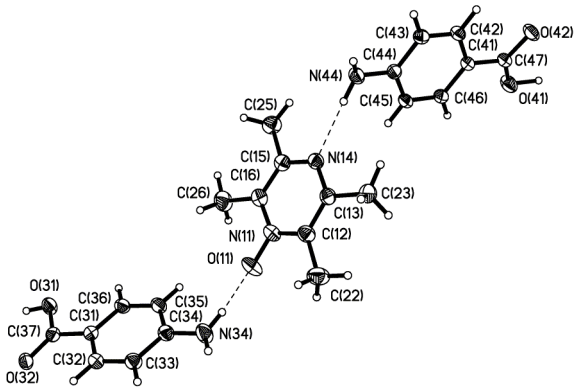

Figure 3.17 Thermal ellipsoids (50%) and labeling scheme of the supramolecule **5ABA**.

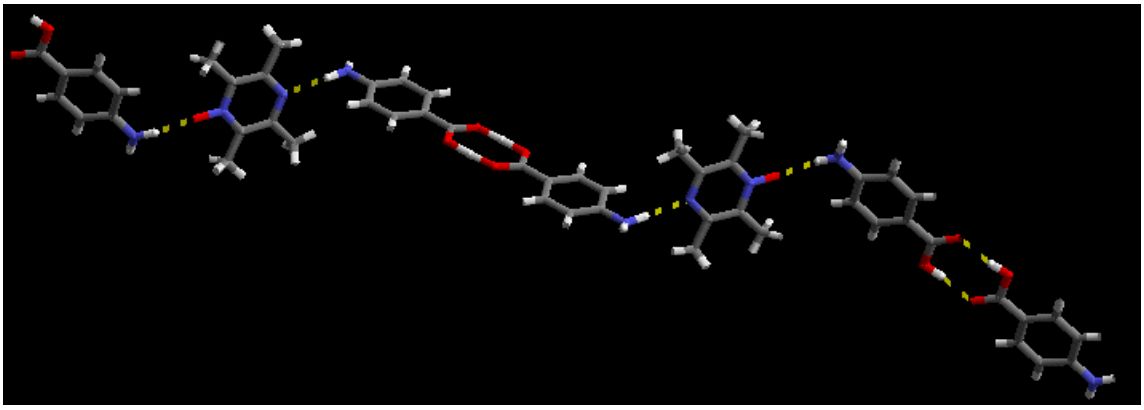

Figure 3.18 1-D chain of **5ABA** held together by N-H…O, N-H…N and an acid-acid dimer hydrogen bond.

3.3.8 Crystal structure of bipyridyl mono N-oxide 4-iodobenzoic acid (1:1), 6IBA

The crystal structure of **6IBA** contains one molecule of **6** and one molecule of **IBA** in the asymmetric unit cell. The supermolecule is constructed from O-H…O hydrogen bonds between the O-H of the acid and the O atom of the N-oxide moiety resulting in bond distance of O31…O11, 2.556(2) Å, Figure 3.19. The architecture is further expanded through interactions between the iodo-moiety and the N atom having the lowest charge resulting in an infinite 1-D chain, Figure 3.20.

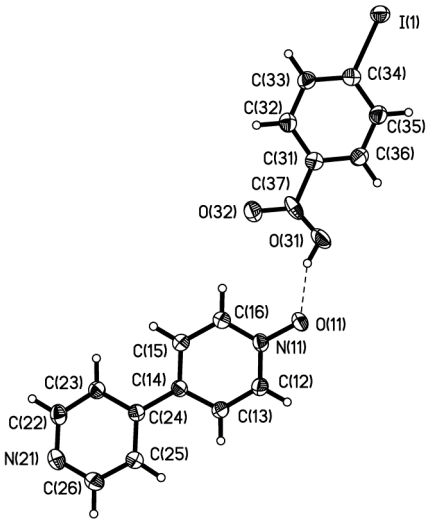

Figure 3.19 Thermal ellipsoids (50%) and labeling scheme of the supermolecule in **6IBA**.

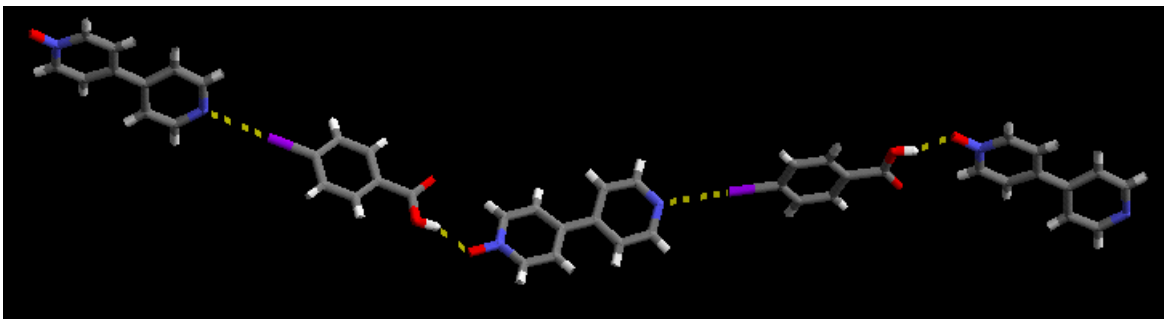

Figure 3.20 1-D chain of **6IBA** held together by O-H…O hydrogen bond and C-Br…N halogen bond.

3.3.9 Crystal structure of bipyridyl mono N-oxide 4-aminobenzoic acid (1:1), 6ABA

The asymmetric unit cell of **6ABA** contains molecule of **6** and one molecule of **ABA**, held together by O-H…N with bond distance of O31…N21, 2.6440(19) Å, Figure 3.21. The structure is further extended into an infinite 1-D chain held together by N-H…N and N-H…O hydrogen bonds with bond distances of N34…N34, 2.869(2) and N34…O11, 3.183(2) Å, respectively, Figure 3.22.

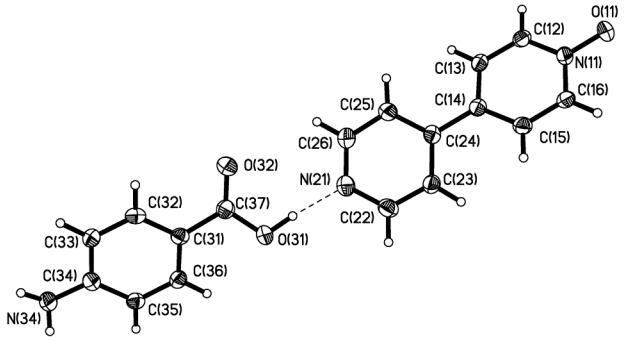

Figure 3.21 Thermal ellipsoids (50%) and labeling scheme of the supramolecule in **6ABA**.

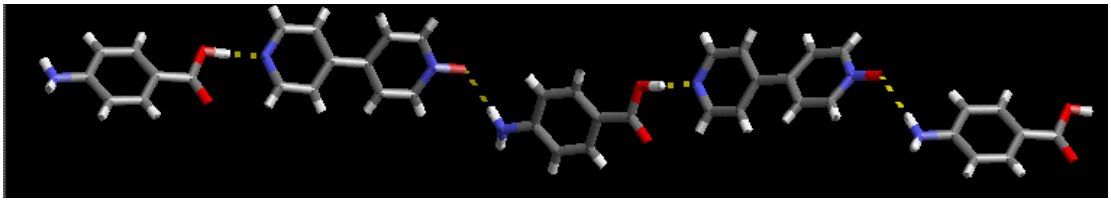

Figure 3.22 Alignment of binaries by N-H…O and O-H…N hydrogen bonds resulting in infinite 1-D chain in **6ABA**.

3.4 Discussion

3.4.1 Characterization of mono N-oxide cocrystals through IR spectroscopy

The results of the co-crystallization reactions were first screened using IR spectroscopy, paying particular attention to the O-H…N hydrogen-bond interactions, shifts in the C-X (X = I or Br) band for conformation of halogen bonding, as well as to any significant shifts in the N^{+}-O^{-} band. In the case of hydrogen bond formation, as

mentioned earlier, two broad stretches near 2450 cm^{-1} and 1900 cm^{-1} are observed. The N^+-O^- stretches for uncomplexed **4**, **5** and **6** are as follows: 1312, 1320 and 1253 cm^{-1} respectively; and upon complexation with the halogenated or non-halogenated benzoic acid the band due to N^+-O^- stretch shifts toward shorter wavenumbers, Table 3.3.

Table 3.3 IR summary of uncomplexed and complexed N^+-O^- and O-H…N interactions for compounds **4-6** and **4IF$_4$BA, 4I$_3$F$_3$B, 4HBA, 5IF$_4$BA, 5BrF$_4$BA, 5ABA, 6IBA, 6ABA.**

Compounds	Uncomplexed N^+-O^- (cm^{-1})	Complexed N^+-O^- (cm^{-1})	O-H…N (cm^{-1})
4	1312	-	-
4 IF$_4$BA	-	1293	2561 & 1931
4 I$_3$F$_3$B	-	1292	-
4 HBA	-	1276	2484 & 1928
5	1320	-	-
5 IF$_4$BA	-	1298	2441 & 1918
5 BrF$_4$BA	-	1301	2448 & 1911
5 ABA	-	1290	2554 & 1900
6	1253	-	-
6 IBA	-	1220	2550 & 1926
6 ABA	-	1225	2448 & 1961

The changes observed in the IR after complexation between the N-oxides and halogenated benzoic acids in **4IF$_4$BA-4I$_3$F$_3$B**, **5IF$_4$BA- 5BrF$_4$BA** could be as a result of the electron withdrawing capabilities of the fluorine atoms on benzoic acid ring, thus resulting in a shift to a lower wavenumber. Similar trends were also observed in **4HBA** with the bands due N^+-O^- stretch shifts towards a lower wavenumber with a difference (of 36 cm^{-1}) when compared to the uncomplexed N-oxide moiety.

These changes along with the principle that pyridine nitrogen and carboxylic acids tend to form strong hydrogen bonds,[12] suggests that in the case of the N-oxide moieties a shift in the N^+-O^- band may indicate a formation of either a halogen-bond or a hydrogen-bond between the oxygen atom of the N-oxide.

3.4.2 Evaluating the capability of mono N-oxide functionality to form predictable assembles through hydrogen and halogen-bonds

Since there are no reported cocrystals of 4,4'-bipyridine or pyrazine mono N-oxide derivatives, it is important to examine the ability of these mono N-oxides to act as a hydrogen or halogen bond acceptors. It is also essential to establish how effective the mono N-oxides are when compared to the 4,4'-bipyridine or pyrazine nitrogen atom in hydrogen or halogen bonding. In the case of pyrazine mono N-oxide for example, two possible interactions could take place, first the acid can form a hydrogen bond with the pyrazine nitrogen leaving the pyrazine mono N-oxide oxygen to interact with either a hydrogen or halogen atom or vice versa, Figure 3.23. The binding interaction demonstrates that the pyrazine N-oxide oxygen is 'active', and can compete successfully with the pyrazine nitrogen atom for the incoming halogen or acid moiety.

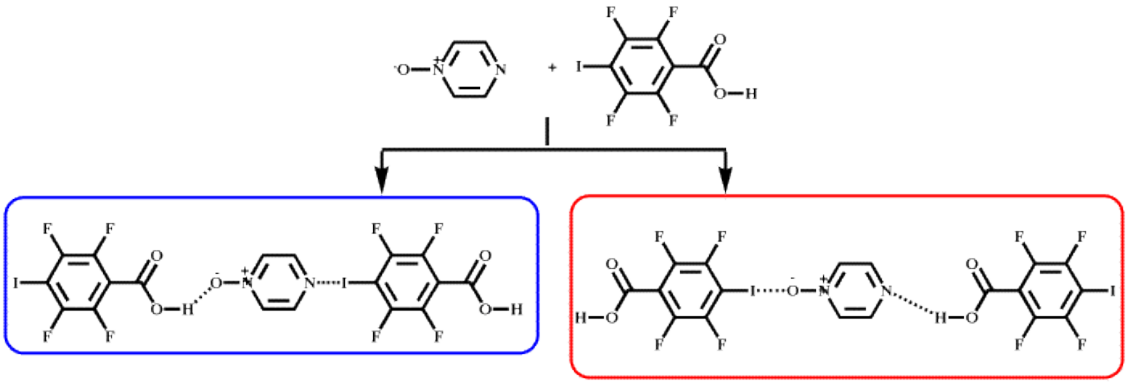

Figure 3.23 Possible binding interactions between pyrazine mono N-oxide and a halogenated species.

Nangia *et al*, have reported a system consisting of both a 4,4'-bipyridine and a 4,4'-bipyridine dioxide, which demonstrate the ability of the oxygen atom of the dioxide to participate in hydrogen bonding with a carboxylic acid, resulting in a zigzag tape structure.[13] This further shows that in a given system containing both nitrogen atom and oxygen atom that the oxygen will participate in some form of non-covalent interaction.

3.4.3 Establishing a balance between hydrogen and halogen bonding

In all the eight cocrystals obtained, seven possess the O-H…N heterosynthon. In five of the eight structures **4IF$_4$BA-4I$_3$F$_3$B**, **5IF$_4$BA- 5BrF$_4$BA** and **6IBA** halogen bonds

i.e. N^+-O^-…I, N^+-O^-…Br or N…I extend the structures into polymeric networks. The halogen bonding patterns and distances for each crystal structure is displayed in Table 3.4.

Table 3.4 Halogen bonding patterns observed in crystal structures **4IF$_4$BA, 4I$_3$F$_3$BA, 5IF$_4$BA, 5BrF$_4$BA, and 6IBA**

Structure #	Donor moieties	Halogen bonds	Type of halogen bonds	Halogen bond distance (Å)
4IF$_4$BA	IF$_4$BA	yes	N^+-O^-…I	2.81
4I$_3$F$_3$B	I$_3$F$_3$B	yes	N^+-O^-…I	2.69
5IF$_4$BA	IF$_4$BA	yes	N^+-O^-…I	2.77
5BrF$_4$BA	BrF$_4$BA	yes	N^+-O^-…Br	2.83
6IBA	IBA	yes	N…I	2.94

A comparison of structures **4IF$_4$BA** and **6IBA** revealed that the halogen bond distance is shorter as a result of fluorination of the aryl ring in **4IF$_4$BA**. The binding interaction observed in **6IBA** is different to that of **4IF$_4$BA**, because the N-oxide oxygen in **4IF$_4$BA** forms a halogen bond with iodine group, whereas in **6IBA** the halogen bond is formed with 4,4'-bipyridine nitrogen and the N-oxide group participates in a hydrogen bond. This connectivity is as a result of the iodine atom in **4IF$_4$BA** being activated by fluorine, subsequently resulting in the formation of a halogen bond between the N-oxide oxygen. Moreover in **5IF$_4$BA** and **5BrF$_4$BA**, connectivity is as a result of aryl ring being fluorinated. Furthermore, in the absence of fluorinated groups on the aryl ring the hydroxy group of the acid forms a hydrogen bond with the N-oxide oxygen leaving the halogen to form a halogen bond with the nitrogen atom. Therefore a combination of hydrogen and halogen bonding provides an additional control on the syntheses and self-assembly of supermolecules, thus creating a versatile strategy for bringing together molecular building blocks.

3.4.4 Hierarchy of hydrogen bond and halogen bond binding preferences based on MEP

PM3 electrostatic potential surfaces were calculated in order to rank the binding preference of **4**, **5** and **6** with a variety of hydrogen and halogen donating compounds.

Each molecule (**4**, **5** and **6**) has two separate charges, pyrazine/4,4'-bipyridine N-oxide oxygen atoms (**A_1**) and pyrazine/4,4'-bipyridine N-oxide nitrogen atoms (**A_2**), Figure 3.24.

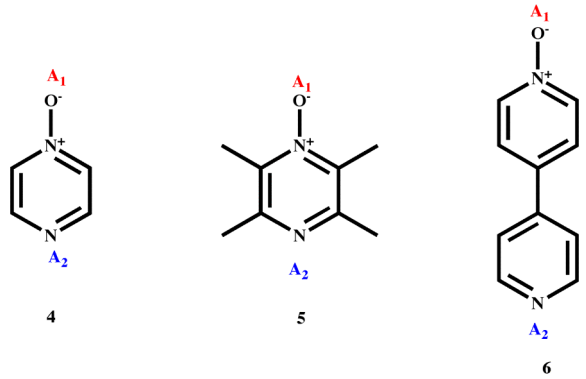

A_1	kJ/mol	-283	-297	-300
A_2	kJ/mol	-238	-253	-253

Figure 3.24 Calculated electrostatic potential surfaces for a variety of mono N-oxide derivatives.

Four of the eight crystal structures obtained in this study contained a combination of hydrogen and halogen bonding moieties, **$4IF_4BA$**, **$5IF_4BA$, $5BrF_4BA$**, and **6IBA**, based on the semi-empirical PM3 calculations carried out our experimental results match the predicted outcome as seen in Figure 3.25.

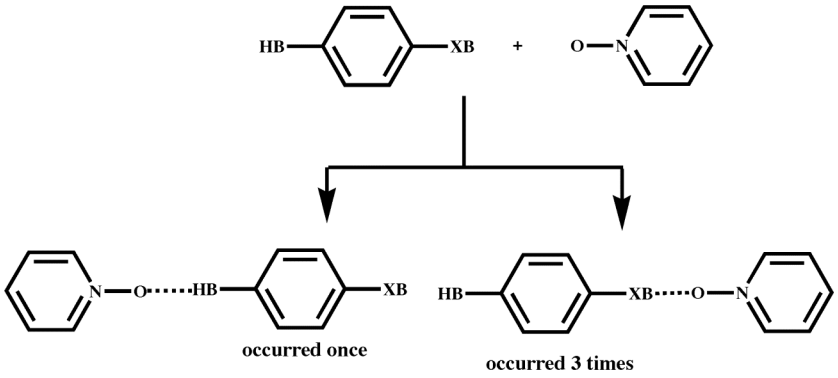

Figure 3.25 Interactions observed in crystal structures between mono N-oxides and a combination of hydrogen bond (HB) and halogen bond (XB) donors.

In the case where the best donor went for the second best acceptor structure **6IBA**, the charges between the carboxyl acid moiety and the halogen differ by 7kJ/mol. This difference may be so small that the two binding sites cannot be distinguished, Table 3.2. Another reason may be due to the geometric match between the bipyridyl mono N-oxide

ring and the carboxylic acid. The aromatic C-H proton may aid this interaction, and hence making this the preferred site for carboxylic acid. From the crystal structure the carbonyl group and the adjacent C-H proton are almost co-planar, further confirming why this interaction may have occurred Figure 3.25.

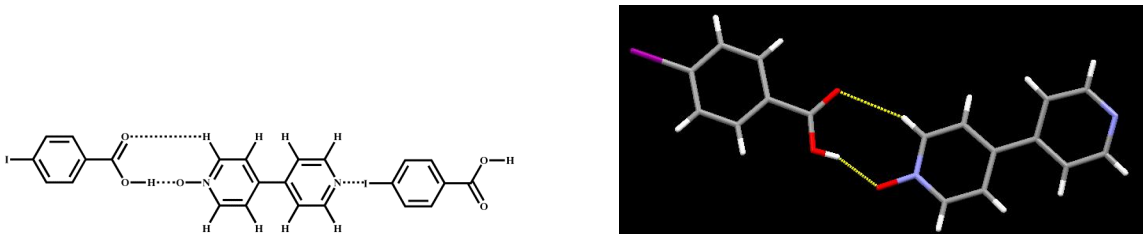

Figure 3.26 Compound **6IBA** showing C-H proton co-planarity to carbonyl group.

The three other structures obtained **4HBA**, **5ABA** and **6ABA** showed similar trends, in that the best donor in all three cases went for the best acceptor leaving the carboxylic acid to interact with the pyrazine/4,4'-bipyridine nitrogen atom. In addition, similar examples of molecules having two different functionality bearing two different MEP charges, displayed comparable interactions; the molecule having the highest charge (i.e. the best donor) formed a hydrogen bond with the best acceptor molecule, again leaving the second best donor to interact with the second best acceptor.[14]

In terms of compound **5ABA** the interaction observed did not totally follow the charges, the amine group being the best donor did form a hydrogen bond with the N-oxide moiety; however instead of the carboxylic acid forming a hydrogen bond with the available tetramethylpyrazine nitrogen atom, an acid-acid dimer homosynthon occurred, Figure 3.26.

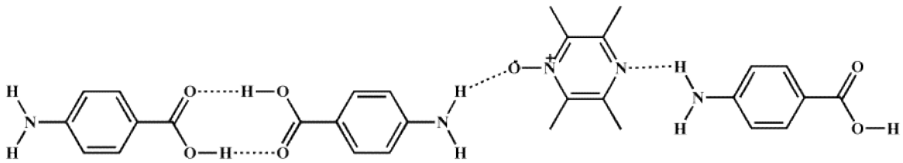

Figure 3.27 Acid-acid homosynthon of **5ABA**.

This could be due to the 1:2 stoichiometry, and it is also possible that a 1:1 cocrystal may have a structure with carboxylic acid tetramethylpyrazine nitrogen synthon on the other side, as there is neither steric hindrance nor intramolecular hydrogen bonding complication in **5ABA**. In fact, crystal structures reported with barbituric acid and

quinoxaline N,N'-dioxide demonstrate similar interactions in that an amide-amide homosynthon was observed despite the availability of the other N-oxide the amide dimer was the preferred interaction.[5]

3.5 Conclusion

This study has demonstrated that a combination of hydrogen and halogen bond can be used to construct predictable assemblies with mono N-oxide derivatives. We were also able to further show that the electron accepting ability of the 4-iodobenzoic acid molecules can be increased upon fluorination when comparing structures **6IBA** and **4IF$_4$BA**. In addition, when given the choice the pyrazine or 4,4'-bipyridine mono N-oxide nitrogen will form a hydrogen bond with incoming acid, thus leaving the halogen to form a halogen atom with the N-oxide oxygen, as demonstrated in **4IF$_4$BA**, and **5IF$_4$BA, 5BrF$_4$BA**.

Finally, semi-empirical PM3 charge calculations can be used as a tool in determining the interaction preferences between different species. The semi-empirical PM3 charge calculations done supported the experimental results that was obtained, in that, seven out of eight time the molecule predicted to be the best donor did interact with other molecule predicted to be the best acceptor. Suggesting a high selectivity of **A$_1$** and **A$_2$** and further confirming that semi-empirical PM3 charge calculations can be used as an aide in ranking binding preferences of a wide variety of molecules.

References

[1] (a) Desiraju, G.R. *Angew. Chem. Int. Ed. Engl*. **1995**, 34, 2311; (b) Babu, J.-N.; Reddy, S.L.; Nangia, A. *Molecular Pharmaceutics*, **2007**, 4, 417; (c) Bailey, M.; Brown, C.J. *Acta Crystallogr*., **1967**, 22, 387; (d) Etter, M.C., *J. Phys. Chem*. **1991**, 95, 4601; (e) Aakeröy, C.B.; Desper, J.; Urbina, J.F. *CrystEngComm*. **2005**, 7, 193.

[2] (a) Shan, N.; Batchelor, E.; Jones, W. *Tetrahedron Lett*. **2002**, 43, 8721; (b) MacGillivray, L.R.; Reid, J.L.; Ripmeester, J.A. *J. Am. Chem*. **2000**, 122, 7817; (c) Kumar, V.S.S.; Nangia, A.; Katz, A.K.; Carrell, H.L. *Cryst. Growth Des*. **2002**, 2, 313; (d) Barnett, A.; Blake, A.J.; Champness, N.R. *CrystEngComm*. **2003**, 5, 134.

[3] (a) Steiner, T. *Acta. Crystallogr*. **2001**, B57, 103; (b) McMahon, J.A.; Bis, J.A.; Vishweshwar, P.; Shattock, T.R.; McLaughlin, O.L.; Zaworotko, M.J. *Z. Kristallogr*. **2005**, 22, 340.

[4] Allen, F.H.; Motherwell, W.D.S.; Raithby, P.R.; Shields, G.P.; Taylor, R. *New J. Chem*. **1999**, 25.

[5] Reference 1b

[6] Allen, F. H. *Acta Crystallogr., Sect. B: Struct. Sci*., **2002**, 58, 380.

[7] Reddy, L.S.; Babu, J.N.; Nangia, A. *Chem. Commun*. **2006**, 1369.

[8] Messina, T.; Metrangolo, P.; Panzer, W.; Pilati, T.; Resnati, G. *Tetrahedron*, **2001**, 57, 8543.

[9] Metrangolo, P.; Resnati, G.; Pilati, T.; Biella, S. *Struct. Bond,* **2008**, 126, 105.

[10] Molecular structures for 4-6 and donor ligands were constructed using Spartan 06 (Wavefunction, Inc. Irvine, CA). All molecules were optimized using PM3, with the maxima and minima in the electrostatic potential surface (0.002 e au^{-1} isosurface) determined using a positive pint charge in the vacuum as a probe.

[11] Koelsch, C.F.; Gumprecht, W.H. *J. Org. Chem*. **1958**, 23, 1603; (b) Prasad, M.-R.; Kamalakar, G.; Madhavi, G.; Kulkarni, S.J.; Raghavan, K.V. *J. Molecular Catalysis A: Chemical*, **2002**, 186, 109.3

[12] (a) Aakeröy, C.B.; Desper, J.; Urbina, J.F. *Cryst. Growth Des*. **2005**, 5, 1283; (b) Aakeröy, C.B.; Beatty, A.M.; Helfrich, B.A.; Nieuwenhuyzen, M. *Cryst. Growth Des*. **2003**, 3, 159; (c) Aakeröy, C.B.; Desper, J.; Helfrich, B.A. *CrystEngComm*. **2004**, 6, 19.

[13] Bhogala, B.R.; Basvoju, S.; Nangia, A. *CrystEngComm*. **2005**, 7, 551.

[14] Aakeröy, C.B.; Desper, J.; Smith, M.M. *ChemComm*. **2007**, 38, 3936.

CHAPTER 4 - Probing halogen bonding interactions in cocrystals of thiophene/thiophane compounds

4.1 Introduction

Hydrogen bonding,[1] is the most frequently used tool for assembling organic molecules in solid, liquid, or gas phases, and it plays an important role in stabilizing supramolecular aggregates even in water. Halogen bonding[2] has also been shown to have similar strength, selectivity, and directionality. For these reasons, halogen bonding provides an additional opportunity for designing functional solid-state architectures.[3]

In Chapter 3 we showed examples of halogen bonding between oxygen atoms in a series of mono N-oxides, which aid in the formation of 1-D chains, Figure 4.1.

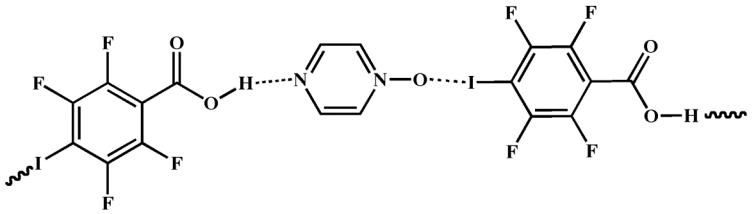

Figure 4.1 Example of an infinite 1-D held together via both hydrogen and halogen bonds.[4]

4.1.1 Theory behind the halogen bond

As mentioned earlier, halogen bonding (XB) is a noncovalent interaction that is in some ways analogous to hydrogen bonding. A puzzling aspect of halogen bonding is that halogen atoms are themselves usually viewed as having partial negative charges. Why then would they interact non-covalently with a heteroatom (N, O, S)? This can be explained either in terms of electrostatic potentials or the hard/soft acid and base (HSAB) principle.

4.1.1.1 Electrostatic potentials and halogen bonding

When atoms combine to form a molecule the accompanying rearrangements of electronic charge normally produce one or more regions of negative charge.[5]

Electrostatic potential calculations on CF_4 reveal that the fluorine hemisphere is negative. However when chlorine is substituted for fluorine, Figure 4.2, a positive

potential develops on the outmost portion of its surface, around its intersection with the C-Cl axis, this positive region, which is centered on the C-X axis is referred to as the "σ-hole".[5] In general, the positive potential along the C-X axis increases on moving from F to I and the electrostatic potential remains negative all round the F atom,[6] Figure 4.2. Therefore, it is these positive regions that are responsible for XB capabilities of CF_3Cl, CF_3Br and CF_3I as well as of other halogen-bonding molecules.

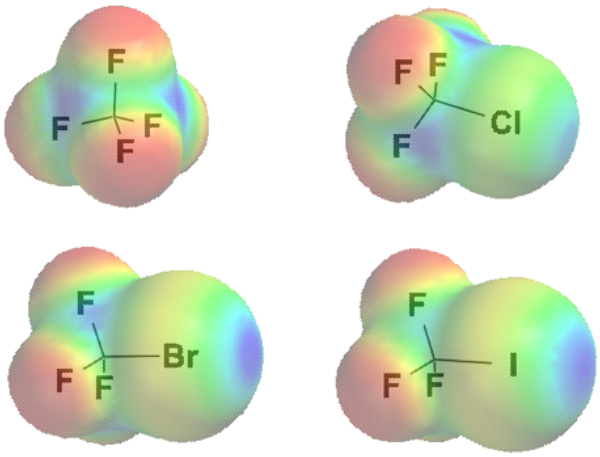

Figure 4.2 Molecular electrostatic potential of: CF_4 (top left), CF_3Cl (top right), CF_3Br (bottom left), CF_3I (bottom right).[5,6]

Additionally, each atom X in the molecules CF_3X, is involve in C-X bonding orbital, σ_{CX}, which also possess three unshared pairs of electrons, two in the p-orbitals perpendicular to the C-X axis and the third in the s-orbital. The electronic configuration $s^2p^2_xp^2_yp^1_z$ is similar to a single atom X in these molecules, with two filled p-orbitals and one half-filled,[5] Figure 4.3.

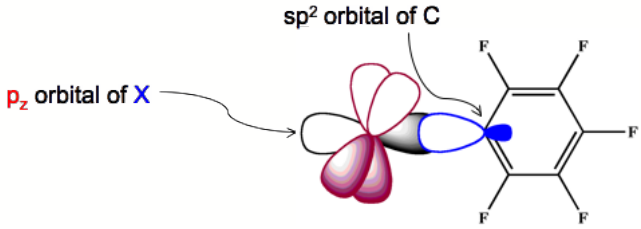

Figure 4.3 Schematic representation of halogen bonding.[5]

4.1.1.2 Hard and soft acid and base interaction and halogen bonding

In 1963, Pearson[7] brought forth a unifying concept by which chemical reactivities, selectivities and stabilities of compounds may be readily rationalized. Chemical entities including atoms, molecules, and ions are categorized as "hard" or "soft" Lewis acids or bases. The "hard" species in general have small atomic radii, and low polarizability, whereas "soft" ones possess the opposite characteristics.

Since the softness of a species is governed by its size, charge and other attached groups, a group having a heavier central atom is the softer base; therefore as anticipated sulfur would be a softer base than oxygen. For example, systems such as 1,4-thioxane (**I**) and thiomorpholine (**II**), Figure 4.4 serve as good models for the consideration of competitive interactions from the standpoint of the HSAB principle.[8]

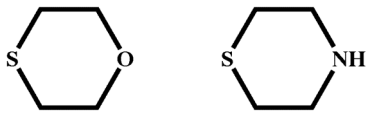

(I) **(II)**

Figure 4.4 Models for competitive interaction based on HSAB principle: (I) thioxane; (II) thiomorpholine.[8]

Compound (**I**) contains atoms belonging to the same group, so that the interaction should be preferentially located at the oxygen atom (hard center) with a hard acid and at the sulfur center in cased interaction with soft acids.[8] Likewise, in compound (**II**) the sulfur having the softer center would be a favorable interaction with a softer acid.

In terms of the halogens, from fluorine, a very hard acid through less hard chlorine, bromine to iodine, a soft acid; reactions are more favorable for 'hard-hard' and 'soft-soft' interactions than for a mix of hard and soft.[9] Therefore, based on the HSAB principles a sulfur…iodine interaction would be more favored over a nitrogen…iodine interaction. Furthermore, in the case of halogens, polarization effects are important for sulfur, which is known to form short directional contacts of the type S…Cl.[10]

Recently there have been reports of S…I interactions in solids based on tetrathiafulavalenes and related compounds.[11] Other examples that have been reported involving halogen bonding between organoiodines and sulfur include the antithyroid

drugs, methylmecaptoimidazole,[12] thiomorpholine,[13] thioxane[13] and most recently a thiourea system, Figure 4.5.[14]

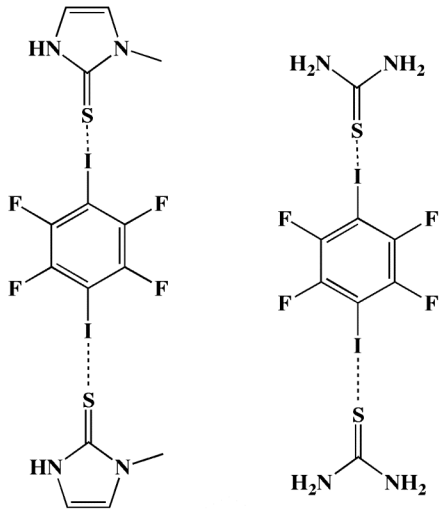

Figure 4.5 Examples of S…I interactions.

4.1.1.3 Understanding the type of interactions in halogen bonding

In order to expand and further understand the interactions taking place in a halogen bonding system, we synthesized a series of thiophene and thiophane compounds; in order to probe whether or not the halogen bond is dominated purely by electrostatic or the HSAB principles. The compounds of interest are seven different thienyl moieties **8**, **9**, **12**, **13**, **16**, **17**, and **19** Figure 4.6, which we react with a variety of hydrogen and halogen bond donors.

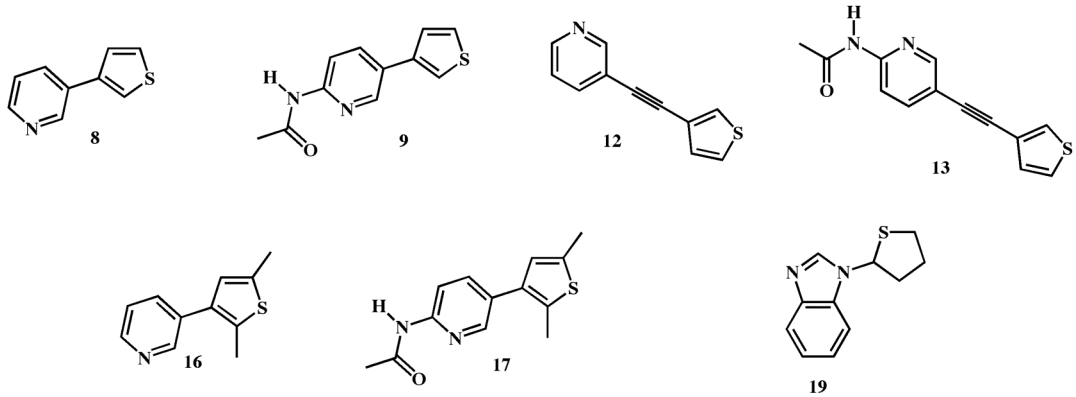

Figure 4.6 Target compounds.

The overall goals of this chapter are:

1. To synthesize a series of thiophene and thiophane compounds.
2. To synthesize a series of cocrystals using different halogen and hydrogen bond donors.
3. To establish whether the halogen bond is primarily an electrostatic or a HSAB interaction.

4.2 Experimental

4.2.1 Synthesis

All chemicals, unless noted, were purchased from Aldrich and used without further purification. Column chromatography was carried out on silica gel (150 Å pore size) from Analtech Inc. Melting points were determined on a GallenKamp melting point apparatus in a capillary tube and are uncorrected. ^{1}H and ^{13}C NMR spectra were recorded on a Varian Unity plus 400 MHz or 200 MHz spectrometers in $CDCl_3$, DMSO-d_6, and CD_3OD-d_4. Compounds were prepared for infrared spectroscopic (IR) analysis as a mixture in KBr or on a ZnSe ATR crystal. Electrospray Ionization – Ion-Trap Mass Spectrometry (ESI-IT-MS) was carried out on a Bruker Daltonics Esquire 3000 Plus.

4.2.2 Synthesis of 3-thienylboronic acid, 7[15]

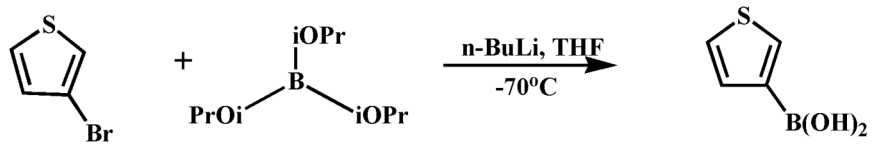

To a dry round bottom flask equipped with a magnetic stirrer and septum toluene (32 mL) and tetrahydrofuran (THF) (8 mL) were added under a nitrogen atmosphere. This was followed b the addition of triisopropylborate (5.1 mL, 22 mmol) and 3-bromothiophene (1.89 mL, 20 mmol). The mixture was cooled to -70°C using a dry ice/acetone bath. n-Butyllithium (1.6M hexane, 9.6 mL) was added dropwise via a syringe pump over 1hr and the reaction mixture was stirred for an additional 30 minutes while maintaining the temperature at -70°C, after which the acetone bath was removed and the reaction was allowed to warm up to -20°C before a 2N hydrochloric acid (20 mL)

was added. When the reaction reached room temperature it was transferred to a separatory funnel. Organic layers were dried over magnesium sulfate and evaporated on a rotary evaporator producing a white solid. **7** was recrystallized from acetonitrile as a white crystalline material, (2.56g, 61%). M.p.: 153-154°C; (Lit. m.p.: 152-154°C).[15] ^{1}H NMR (δ_H; 200 MHz, CD_3OD-d_4): 7.84 (m, 1H), 7.36 (s, 2H).

4.2.3 Synthesis of 3-(thiophen-3-yl)pyridine, 8[16]

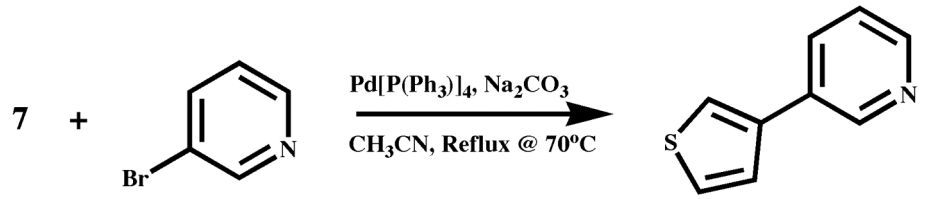

A mixture of 3-bromopyridine (0.99g, 6.4 mmol) and tetrakis(triphenylphosphine)palladium(0) (0.18g, 0.26 mmol) in 20 mL of acetonitrile and 20 mL of water was stirred under nitrogen atmosphere for 10 minutes. To that mixture **7** (1.00g, 7.8 mmol) and sodium carbonate (1.01g, 9.5 mmol) were added and the reaction mixture was allowed to reflux at 70°C and monitored by TLC. After 4 days, water was added and the mixture was extracted with ethyl acetate producing a light brown liquid. The residue was chromatographed on silica using 7:3 hexanes-ethyl acetate as the eluant. **8** was isolated as a light yellow powder and recrystallized from ethanol to produce a crystalline material, (0.85g, 83%). M.p.: 73-76°C; (Lit. m.p.: 76-77°C).[17] ^{1}H NMR (δ_H; 400 MHz, $CDCl_3$): 8.88 (s, 1H), 8.55 (d, 1H, J = 4Hz), 7.87 (d, 1H, J = 8Hz), 7.53 (s, 1H), 7.41 (m, 1H), 7.34 (m, 1H), 7.32 (m, 1H); ^{13}C NMR (δ_C; 400 MHz, $CDCl_3$): 148, 139, 133, 131, 127, 123, 121, 119; IR: 3075, 1576, 1474, 1430, 1321, 1258, 1180, 1018, 860, 782, 700, 640 cm^{-1}.

4.2.4 Synthesis of N-(5-(thiophen-3-yl)pyridin-2-yl)acetamide, 9[18]

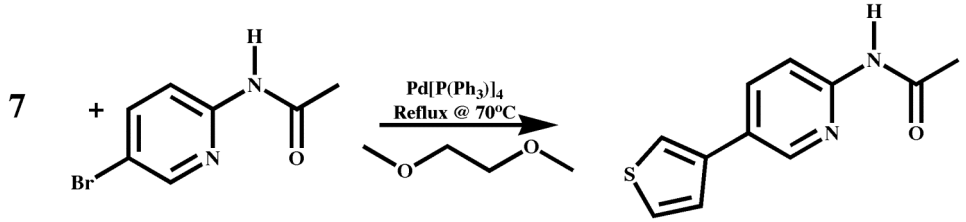

2-Acetamido-5-bromopyridine (1.12g, 5 mmol) and **7** (0.77g, 6 mmol) were dissolved in ethylene glycol dimethylether (20 mL) the mixture was degassed with dinitrogen for 10 minutes, after which 2N sodium carbonate (5 mL) and tetrakis(triphenylphosphine)palladium(0) (0.35g, 0.30 mmol) were added and the reaction was left to reflux at 70°C and monitored by TLC. After 3 days, the reaction mixture was allowed to cool to room temperature. The reaction mixture was filtered and the filtrate extracted with ether. The combined ether layers were washed with saturated aqueous sodium chloride (2 x 100 mL) and water (3 x 100 mL), and dried over magnesium sulfate. The ether was evaporated and the residue was chromatographed on silica with 9:1 hexanes-ethyl acetate as the eluant. **9** was isolated as a light yellow solid, (0.57g, 52%). M.p.: 131-133°C. ^{1}H NMR (δ_H; 400 MHz, $CDCl_3$): 9.10 (s, 1H), 8.52 (d, 1H, J = 4Hz), 8.29 (d, 1H, J = 4Hz), 7.92 (s, 1H), 7.45 (m, 1H), 7.36 (m, 1H), 2.23 (s, 3H); ^{13}C NMR (δ_C; 400 MHz, $CDCl_3$): 169, 150, 141, 138, 136, 128, 127, 125, 120, 114, 24; IR: 2934, 1683, 1586, 1529, 1405, 1302, 1310, 1214, 1000, 848, 758, 735, 697, 652 cm^{-1}.

4.2.5 Synthesis of trimethyl(2-(thiophen-3-yl)ethynyl)silane, 10[19]

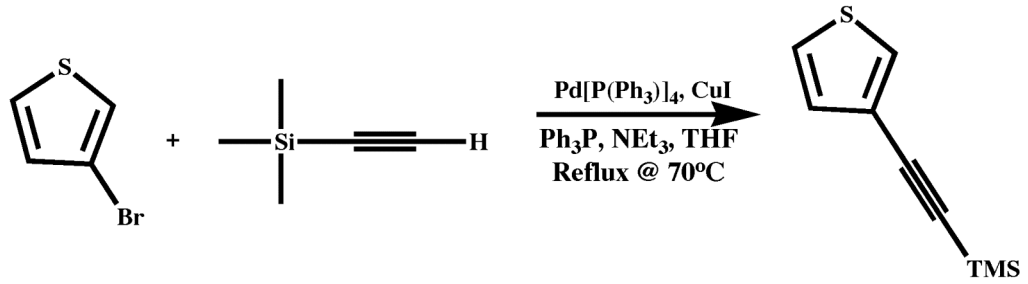

Trimethyl(2-(thiophen-3-yl)ethylnyl)silane was prepared by employing a modification of the previously reported procedure.[19] 3-Bromothiophene (6.15g, 37.7 mmol), trimethylsilylacetylene (4.12g, 41.54 mmol), triphenyl phosphine (0.07g, 0.267 mmol), copper iodide (0.01g, 0.05 mmol), and tetrakis(triphenylphosphine)palladium(0) (0.261g, 0.22 mmol) were added to a dry round bottom flask, to which THF (50 mL) and triethylamine (16 mL) were added followed by degassing with nitrogen for 15 minutes. Reaction mixture was refluxed at 70°C under a N_2 atmosphere and monitored by TLC. After 53 hrs no significant changes were observed in TLC, therefore the reaction was allowed to cool to room temperature. The solution was diluted with 100 mL of hexanes/ethyl acetate (1:1) and washed with water (3 x 100 mL), then washed with

saturated aqueous sodium chloride (1 x 100 mL). The organic layer was dried over sodium sulfate. The solvent was removed on a rotary evaporator and the residue was chromatographed on silica with hexanes-ethyl acetate (10:2) as eluant. **10** was isolated as a red liquid, (6.79g, 81%); ^{1}H NMR (δ_H; 200 MHz, $CDCl_3$): 7.46 (m, 1H), 7.20 (m, 1H), 7.11 (m, 1H), 0.28 (s, 9H).

4.2.6 Synthesis of 3-ethynylthiophene, 11[19]

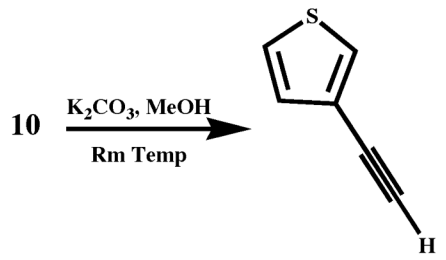

3-Ethylnythiophene was prepared by employing a modification of the previously reported procedure.[19] A mixture of **10** (1.80g, 0.01 mmol) and potassium carbonate (1.04g, 7.5 mmol) was stirred in methanol (30 mL) at room temperature for 2hrs. The reaction mixture was then diluted with dichloromethane (100 mL), washed with water (3 x 50 mL) and dried over magnesium sulfate. The solvent was removed under reduced pressure via a rotary evaporator producing a light brown liquid (0.464g, 52%). ^{1}H NMR (δ_H; 200 MHz, $CDCl_3$): 7.51 (s, 1H), 7.23 (m, 1H), 7.15 (m, 1H), 3.03 (s, 1H).

Note: The compound was used immediately without further purification because it decomposed on silica gel during column chromatography as well as when left at room temperature or in the refrigerator within a 24hr period.

4.2.7 Synthesis of 3-(2-(thiophen-3-yl)ethynyl)pyridine, 12[19]

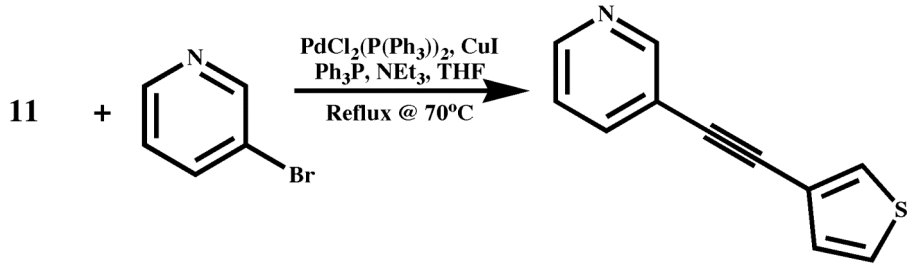

12 was prepared by employing a modification of the previously reported procedure.[19] A mixture of **11** (2.1g, 17 mmol) and 3-bromopyridine (1.47 mL, 15 mmol), copper(I) iodide (0.03g, 0.16 mmol), triphenyl phosphine (0.09g, 0.34 mmol), and

bis(triphenylphosphine)palladium(II) dichloride (0.25g, 0.36 mmol) was added to a dry round bottom flask. THF (60 mL) and triethylamine (15 mL) were added and degassed with dinitrogen for 10 minutes. The reaction mixture was allowed to reflux at 70°C under a nitrogen atmosphere and monitored by TLC. After 36hrs the reaction was allowed to cool to room temperature and diluted with ethyl acetate (100 mL) and washed with water (3 x 100 mL), and saturated aqueous sodium chloride (1 x 100 mL). The organic layer was dried over magnesium sulfate. The solvent was removed on a rotary evaporator and the residue was chromatographed on silica with 9:1 hexanes-ethyl acetate as eluant, to produce **12** as a dark brown powder. **12** dissolved in methanol and subjected to activated carbon wash producing a light brown powder, (1.95g, 70%). M.p.: 60-62°C; ^{1}H NMR (δ_H; 200 MHz, $CDCl_3$): 8.75 (s, 1H), 8.52 (d, 1H, J = 4Hz), 7.75 (d, 1H, J = 4Hz), 7.75 (s, 1H), 7.28 (t, 1H), 7.21 (m, 2H); ^{13}C NMR (δ_C; 400 MHz, $CDCl_3$): 152, 151, 148, 138, 129, 125, 123, 121, 120, 87, 85; IR: 3125, 1552, 1468, 1409, 1182, 1027, 872, 788, 703, 624 cm^{-1}.

4.2.8 Synthesis of N-(5-(2-thiophen-3-yl)ethynyl)pyridin-2-yl)acetamide, 13[19]

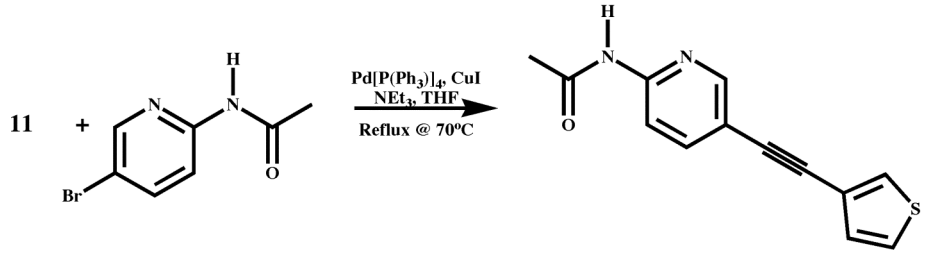

11 was prepared by employing a modification of the previously reported procedure.[19] A mixture of **11** (0.464g, 3.86 mmol) and 2-acetamido-5-bromopyridine (0.430g, 2 mmol), copper(I) iodide (0.004g, 0.021 mmol), triphenyl phosphine (0.03g, 0.11 mmol), and bis(triphenylphosphine)palladium(II) dichloride (0.03g, 0.043 mmol) were added to a dry round bottom flask. THF (10 mL) and triethylamine (5 mL) were added and degassed with dinitrogen for 10 minutes. The reaction mixture was allowed to reflux at 70°C under a nitrogen atmosphere and monitored by TLC. After 36hrs reaction was allowed to cool to room temperature and diluted with ethyl acetate (50 mL) and washed with water (3 x 50 mL) then washed with saturated aqueous sodium chloride (1 x 50 mL). The organic layer was dried over magnesium sulfate. The solvent was removed on a rotary evaporator and the residue was chromatographed on silica with 9:1 hexanes-

ethyl acetate as eluant, producing **13** as a light brown powder, (0.23g, 48%). M.p.: 196-198°C; ^{1}H NMR (δ_H; 200 MHz, $CDCl_3$): 8.75 (s, 1H), 8.52 (d, 1H, J = 4Hz), 7.75 (d, 1H, J = 4Hz), 7.75 (s, 1H), 7.28 (t, 1H), 7.21 (m, 2H); ^{13}C NMR (δ_C; 400 MHz, $CDCl_3$): 169, 150, 148, 141, 129, 125, 121, 116, 115, 114, 87, 85, 24; IR: 2940, 1661, 1672, 1530, 1455, 1367, 1300, 1092, 1002, 828, 778, 704, 623 cm^{-1}.

4.2.9 Synthesis of 3-bromo-2,5-dimethylthiophene, 14[20]

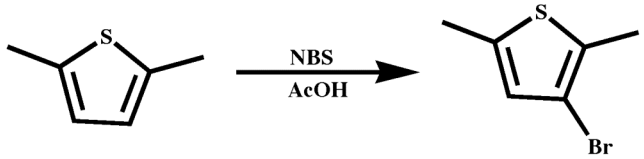

To 50 mL of a glacial acetic acid solution containing 2,5-dimethylthiophene (1.14 mL, 10 mmol), N-bromosuccinimide (NBS) (1.78g, 10 mmol) was slowly added at room temperature. The reaction mixture was stirred for 3hrs, after which it was poured onto excess ice-cold water and extracted with dichloromethane. The organic layer was washed with aqueous sodium carbonate (3 x 50 mL) and water (5 x 50 mL) and dried over magnesium sulfate, and concentrated under reduced pressure via a rotary evaporator. The residue was purified by column chromatography with hexanes as eluant. **14** was isolated as a colorless oil, (1.30g, 68%). ^{1}H NMR (δ_H; 200 MHz, $CDCl_3$): 6.58 (s, 1H), 2.43 (s, 3H), 2.36 (s, 3H).

4.2.10 Synthesis of 2,5-dimethylthiophen-3-yl-boronic acid, 15[21]

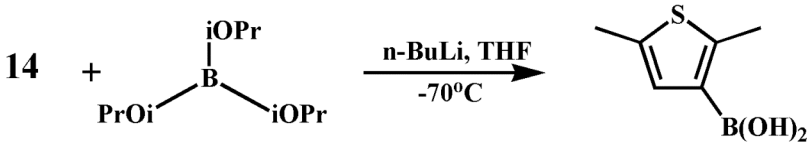

n-Butyllithium (1.6M in hexanes, 9.7 mL, 15.6 mmol) was slowly added to a stirred solution of **14** (2.9g, 14.1 mmol) in anhydrous THF (40 mL) under nitrogen atmosphere at -78°C. The reaction mixture was then stirred at this temperature for 90 minutes. A solution of triisopropyl borate (3.26 mL, 14.2 mmol) was added over 15 minutes. After stirring for 5hrs, 2M aqueous hydrochloric acid solution was added and the reaction mixture was stirred at room temperature for 10 hrs. The reaction mixture was

extracted with diethyl ether and the combined extracts were washed with water (3 x 100 mL). The product was obtained by extracting the ethereal layer with aqueous sodium hydroxide solution (2M, 20 mL) followed by acidification with hydrochloric acid (12M) to commence the precipitation of **15** as a white powder, (1.10g, 68%). M.p.: 180-182°C, (Lit. m.p.: 180-183°C);[22] ^{1}H NMR (δ_H; 200 MHz, DMSO-d_6): 7.75 (s, -OH), 6.85 (s, 1H), 2.37 (s, 3H), 2.33 (s, 3H).

4.2.11 Synthesis of 3-(2,5-dimethylthiophen-3-yl)pyridine, 16[18]

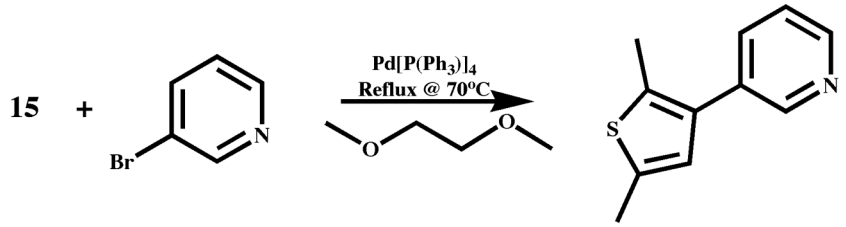

3-Bromopyridine (0.54g, 3.7 mmol) and **15** (0.73g, 4.7 mmol) were dissolved in 20 mL ethylene glycol dimethylether, the reaction mixture was degassed with dinitrogen for 10 minutes, after which 2N sodium carbonate (10 mL) and tetrakis(triphenylphosphine)palladium(0) (0.1g, 0.86 mmol) were added and the reaction mixture was left to reflux at 70°C and monitored by TLC. After 3 days, the reaction was allowed to cool to room temperature. The reaction mixture was filtered and the filtrate extracted with ether. The combined ether layer were washed with a saturated solution of sodium chloride (2 x 50 mL) and water (3 x 100 mL), and dried over magnesium sulfate. The ether was evaporated and the residue was chromatographed on silica with 9:1 hexanes-ethyl acetate as the eluant. **16** was isolated as a light yellow oil, (0.70g, 77%). ^{1}H NMR (δ_H; 200 MHz, $CDCl_3$): 8.63 (s, 1H), 8.52 (d, 1H, J = 4Hz), 7.34 (t, 1H), 7.67 (d, 1H, J = 4Hz), 6.68 (s, 1H), 2.40 (s, 6H); ^{13}C NMR (δ_C; 149, 147, 136, 135, 134, 133, 132, 126, 123, 15, 14; IR: 1556, 1454, 1410, 1300, 1239, 1202, 1008, 840, 762, 680, 620 cm^{-1}.

4.2.12 Synthesis of N-(5-(2,5-dimethylthiophen-3-yl)pyridin-2-yl)acetamide, 17[18]

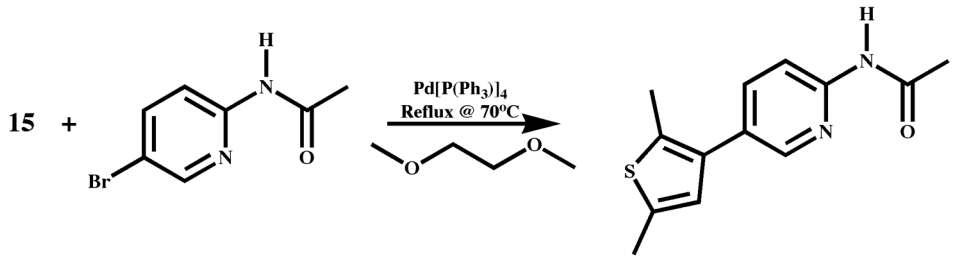

17 was prepared by employing a modification of the previously reported procedure.[18] 2-Acetamido-5-bromopyridine (1.00g, 6.4 mmol) and **15** (1.2g, 5.4 mmol) were dissolved in 30.00 mL ethylene glycol dimethylether, the solution was degassed with dinitrogen for 10 minutes, after which 2N sodium carbonate (15 mL) and tetrakis(triphenylphosphine)palladium(0) (0.2g, 1.7 mmol) were added and the reaction mixture was allowed to reflux at 70°C and monitored by TLC. After 3 days, the reaction mixture was allowed to cool to room temperature, filtered and extracted with ether. The combined ether phases were washed with a saturated solution of sodium chloride (2 x 50 mL) and water (3 x 100 mL), and dried over magnesium sulfate. The ether was evaporated and the residue was chromatographed on silica with 7:3 hexanes-ethyl acetate as the eluant. **17** was isolated as a white solid, (1.33g, 68%). M.p. 141-142°C. ^{1}H NMR (δ_H; 200 MHz, $CDCl_3$): 9.17 (s, 1H), 8.29 (d, 1H, J = 2Hz), 7.73 (d, 1H, J = 2Hz), 6.67 (s, 1H), 2.45 (d, 6H), 2.22 (s, 3H); 13C NMR (δ_C; 400 MHz, CDCl3): 169, 150, 147, 138, 136, 134, 132, 129, 128, 114, 24, 15, 14; IR: 3400, 1684, 1586, 1528, 1435, 1397, 1364, 1312, 1260, 1139, 850, 813, 724, 680 cm^{-1}.

4.2.13 Synthesis of 2-chlorothiophane, 18[23]

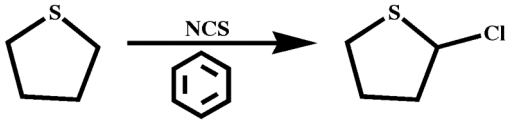

To a stirred solution of thiophane (1.12mL, 10 mmol) in benzene (10.00 mL) was added N-chlorosuccinimide (NCS) (0.75g, 0.06 mmol) in small portions over a period of 5 minutes. Reaction temperature was maintained at 10-20°C using an ice bath. After addition of NCS, stirring was continued for 2 hrs, after which the solution was filtered and the solvent was removed via rotary evaporator to produce **18** as a yellow liquid. **18**

was purified via column chromatography using hexanes as eluant to yield a light yellow liquid, (0.65g, 88%). ^{1}H NMR (δ_H; 200 MHz, $CDCl_3$): 5.98 (s, 1H), 3.29 (t, 2H), 2.89 (m, 2H), 2.11-1.84 (m, 2H).

Note: Compound **18** was immediately used, as it decomposed upon storage at room temperature and in the fridge.

4.2.14 Synthesis of 1-(thiophane)-1H-benzimidazole, 19[24]

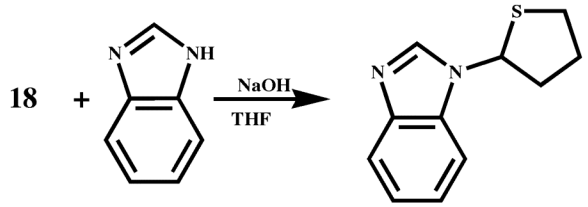

To a round bottom flask, containing benzimidazole (1g, 8 mmol) dissolved in THF (50 mL) was added sodium hydroxide pellets (10g, 250 mmol) and the mixture was stirred at room temperature for 2hrs. This was followed by the addition of **18** (0.49g, 4.00 mmol) in THF (25 mL) and the reaction mixture was stirred at room temperature for 2 days. Upon completion water was added and the layers were separated and dried over magnesium sulfate, and the solvent removed via rotary evaporator resulting in a light yellow solid, (0.4g, 48%). M.p.: 80-82°C. ^{1}H NMR (δ_H; 200 MHz, $CDCl_3$): 8.28 (s, 1H), 7.80 (m, 1H), 7.44 (m, 1H), 7.29 (m, 2H), 6.00 (m, 1H), 3.29 (m, 2H), 2.96 (m, 2H), 2.37 (m, 2H); ^{13}C NMR (δ_C; 400 MHz, $CDCl_3$): 144, 141, 132, 122, 120, 110, 63, 38, 33, 28; ESI-IT-MS m/z 205 [**19**+H]; IR: 1925, 2851, 1456, 1396, 1268, 1244, 1201, 1123, 1004, 877, 767 cm^{-1}.

4.2 Synthesis of cocrystals

The synthesis of a small number of cocrystals is presented here. Co-crystallizations were set up in a 1:1 ratio with halogens/carboxylic acids and thiophene derivatives using a variety of solvents including; ethanol, methanol, nitromethane, acetonitrile as well as a combination of 1:1 methanol-nitromethane, ethanol-nitromethane and ethyl acetate-nitromethane. Only crystals suitable for X-ray crystallography are presented here. All solids obtained were analyzed by IR spectroscopy, results are shown in Table 4.4-4.5.

4.3.1.1 Synthesis of 3-(thiophen-3-yl)pyridine succinic acid (2:1), 8SUC

8 (0.015g, 0.093 mmol) was dissolved in 4 mL of ethanol in a 100 mL beaker. To this a solution of **SUC** (0.011g, 0.093 mmol) in 4 mL ethanol was added. Colorless plates were obtained via slow evaporation after 10 days. M.p.: 109-110°C; IR (KBr pellet): ν 2481 cm^{-1}, 1944 cm^{-1} (O-H…N, br), 1700 cm^{-1} (C=O acid, s).

4.3.1.2 Synthesis of 3-(thiophen-3-yl)pyridine 4-iodobenzoic acid (1:1), 8IBA

8 (0.015g, 0.093 mmol) was dissolved in 2 mL of nitromethane in a 100 mL beaker. To this a solution of **IBA** (0.023g, 0.093 mmol) in 2 mL of nitromethane was added. The solution was left at ambient temperature to undergo slow evaporation. After 5 days colorless plate-like crystals were obtained. M.p.: 195-195°C; IR (ZnSe ATR crystal): ν 2541 cm^{-1}, 1901 cm^{-1} (O-H..N, br), 1670 cm^{-1} (C=O acid, s), 1006 cm^{-1}, 751 cm^{-1} (C-I).

4.3.2 Hartree–Fock 6-31G calculations*

Compounds **8** 3-(thiophen-3-yl)pyridine, **9** N-(5-(thiophen-3-yl)pyridin-2-yl)acetamide**,** **12** 3-(2-(thiophen-3-yl)ethynyl)pyridine, **13** N-(5-(2-thiophen-3-yl)ethynyl)pyridin-2-yl)acetamide, **16** 3-(2,5-dimethylthiophen-3-yl)pyridine, **17** N-(5-(2,5-dimethylthiophen-3-yl)pyridin-2-yl)acetamide, and **19** 1-(thiophane)-1H-benzoimidazole (Figure 4.7) molecular structures were constructed using Spartan ’06 (Wavefunction, Inc. Irvine, CA). All seven molecules were optimized using Hartree-Fock 6-31G*, with the maxima and minima in the electrostatic potential surface (0.002 e/au isosurface) determined using a positive point charge in the vacuum as a probe.

4.4 Results and Discussion

4.4.1 Calculations

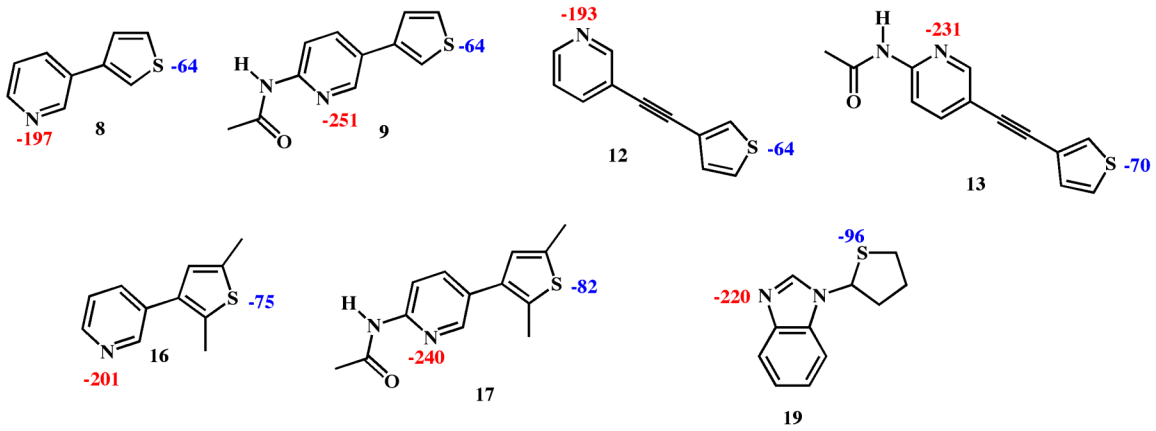

Figure 4.7 Electrostatic potential calculations of **8**, **9**, **12**, **13**, **16**, **17**, **19**, units in ($kJmol^{-1}$).

Table 4.1 shows the results of the electrostatic potentials calculated for the thienyl derivatives used in this study, and Figure 4.7 shows the electrostatic potential surfaces for each acceptor ligands, with A_1 having highest charge thereby being the best acceptor and A_2 the second best acceptor.

Table 4.1 Electrostatic potentials of heterocycles **8**, **9**, **12**, **13**, **16**, **17**, **19**

Heterocycle	MEP A_1/$kJmol^{-1}$	MEP A_2/$kJmol^{-1}$
3-(thiophen-3-yl)pyridine, **8**	-197	-64
N-(5(thiophen-3-yl)pyridin-2-yl)acetamide, **9**	-251	-64
3(2-(thiophen-3-yl)ethynyl)pyridine, **12**	-193	-64
N-(5-(2-thiophen-3-yl)ethynyl)pyridin-2-yl)acetamide, **13**	-231	-70
3-(2,5-dimethylthiophen-3-yl)pyridine, **16**	-201	-75
N-(5-(2,5,-dimethylthiophen-3-yl)pyridin-2-yl)acetamide, **17**	-240	-82
1-(thiophane)-1H-benzoimidazole, **19**	-220	-96

Hartree-Fock 6-31G* electrostatic potential calculations were conducted in order to rank the binding preferences, as well as to establish whether XB interactions of **8, 9, 12, 13, 16, 17, 19** are dominated by electrostatic or HSAB interactions. Each molecule has two separate acceptor sites, the pyridine nitrogen atoms (A_1) and the thienyl sulfur atoms (A_2), Table 4.1. Compounds **16**, **17** and **19** were synthesized in order to increase

the charge on the sulfur atom, therefore increasing the ability of the sulfur atoms to participate in some form of non-covalent interaction. Thus by adding electron-donating groups such as methyl groups we were able to increase the charge on the sulfur atom by approximately 11 $kJmol^{-1}$. Likewise, changing from an aromatic system to an aliphatic system **19**, we were able to increase the charge by approximate 20 $kJmol^{-1}$ on the sulfur atom.

The charges of donor compounds we employed are shown in Table 4.2, with the $\mathbf{D_1}$ being the acidic proton and $\mathbf{D_2}$ the halogen atom in cases where both an acid and halogen atom is present.

Table 4.2 Electrostatic potentials of hydrogen/halogen bonding donor atoms

Donor compounds	MEP D_1/$kJmol^{-1}$	MEP D_2/$kJmol^{-1}$
4-iodobenzoic acid	130	123
4-iodotetrafluorobenzoic acid	219	143
4-bromotetrafluorobenzoic acid	160	146
1,4-diiodobenzene	-	124
1,4-diiodotetrafluorobenzene	-	207
1-bromo-4-iodotetrafluorobenzene	-	202(I) & 142(Br)

Based on the calculated electrostatic potentials and the HSAB theory, the anticipated interactions between the donor and acceptor molecule involving a halogen bond is shown in Figure 4.8-4.9.

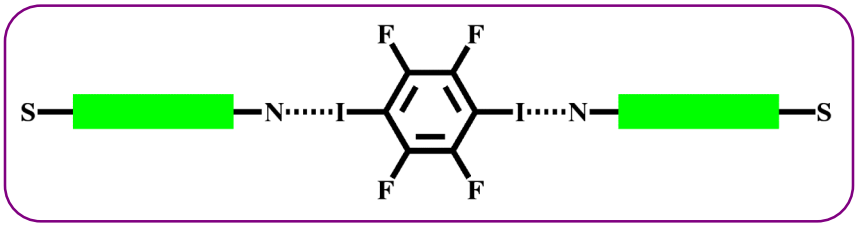

Figure 4.8 Anticipated interaction if electrostatic interaction dominates.

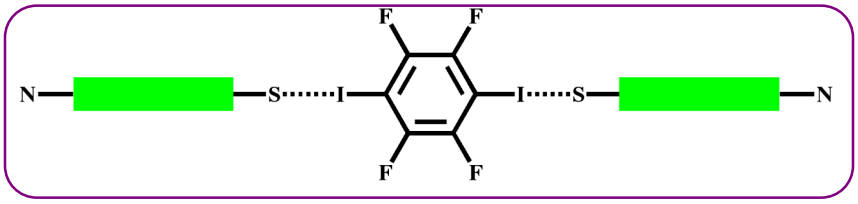

Figure 4.9 Expected intermolecular interactions if HSAB theory dominates

However if the interactions are comparable, then both the sulfur and nitrogen should participate in halogen bonding, Figure 4.10.

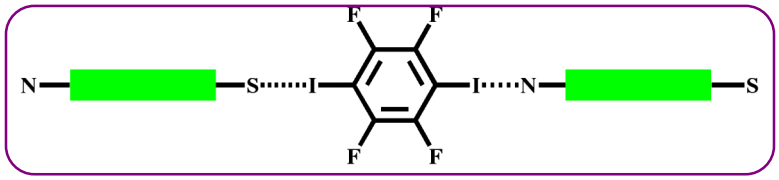

Figure 4.10 Anticipated interaction if sulfur and nitrogen are comparable acceptors.

In the case where we have both a hydrogen bond and halogen bond donor, the anticipated interactions between the acceptors and donors are shown in Figure 4.11.

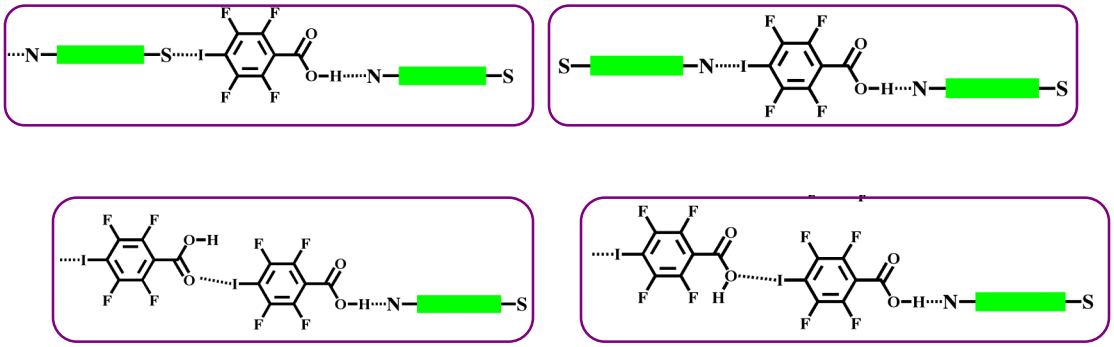

Figure 4.11 Anticipated hydrogen and halogen bonding.

4.4.2 IR spectroscopy

Infrared spectroscopy is an effective tool for investigating hydrogen and halogen bonding interactions[25] through the study of vibrational motions in terms of intensity and shift. The IR spectroscopy data for uncomplexed compounds used in this study are shown in Table 4.3.

Table 4.3 IR stretches of uncomplexed halogen donors

Compounds	C-I/C-Br stretches (cm^{-1})
4-iodobenzoic acid	1007 & 753
4-iodotetrafluorobenzoic acid	1468 & 978
4-bromotetrafluorobenzoic acid	1473 & 983
1.4-diiodobenzene	1066 & 794
1,4-diiodotetrafluorobenzene	1457 & 938
1-bromo-4-iodotetrafluorobenzene	1470 & 947

The data obtained from IR spectroscopy performed on solids from the supramolecular reactions with dicarboxylic acids are shown in Table 4.4.

Table 4.4 IR data (position of O-H...N stretches) from co-crystallization experiments.

Compounds	Dicarboxylic acids	O-H…N band cm^{-1}	Cocrystal formation
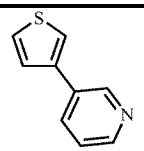 **8**	succinic acid	2481 & 1994	yes
	adipic acid	2530 & 1895	yes
	suberic acid	2530 & 1926	yes
	sebacic acid	2530 & 1905	yes
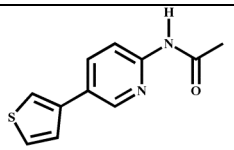 **9**	succinic acid	2501 & 1920	yes
	adipic acid	2487 & 1910	yes
	suberic acid	2340 & 1874	yes
	sebacic acid	2530 & 1926	yes
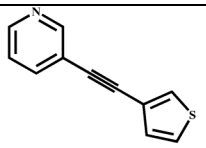 **12**	succinic acid	2550 & 1899	yes
	adipic acid	2668 & 1920	yes
	suberic acid	2509 & 1910	yes
	sebacic acid	2340 & 1874	yes

Based on IR data collected from co-crystallization reactions with aliphatic dicarboxylic acids and **8**, **9** and **12**, twelve out of twelve times the typical stretch at approximately 2500 and 1900 cm^{-1}, indicative of O-H…N heterocycle hydrogen bonds was observed. However, we were unable to tell whether or not sulfur is participating in hydrogen bonding with dicarboxylic acids from the infrared spectra. No significant shifts

in the C-S stretch were observed when the IR of the starting materials was compared with that of the product. Although **8**, **9**, and **12** are able to form cocrystals with dicarboxylic acid based on infrared spectroscopy, we cannot conclude that the sulfur atom is participating in any form of non-covalent interaction.

Similarly, the data obtained from IR spectroscopy performed on solids from the supramolecular reactions with an acid-halogen and halogen bond donors are shown in Table 4.5.

Table 4.5 IR data (position of O-H...N and C-I/Br stretches) from co-crystallization experiments

Compounds	Acid/halogen	O-H…N band cm^{-1}	C-I/Br band cm^{-1}	Formation of C-X…N/S	Cocrystal formation
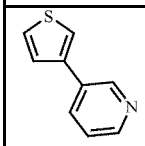 **8**	4-iodobenzoic acid	2541 & 1901	1006 & 751	no	yes
	4-iodotetrafluorobenzoic acid	2500 & 1900	1466 & 938	yes	yes
	4-bromotetrafluorobenzoic acid	2498 & 1952	1470 & 980	no	yes
	1,4-diiodobenzene	-	1066 & 775	yes	yes
	1,4-diiodotetrafluorobenzene	-	1451 & 930	yes	yes
	1-bromo-4-iodotetrafluorobenzene	-	1450 & 931	yes	yes
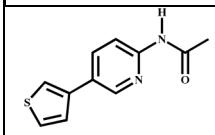 **9**	4-iodobenzoic acid	2533 & 1936	1006 & 752	no	yes
	4-iodotetrafluorobenzoic acid	1903	1462 & 972	yes	yes
	4-bromotetrafluorobenzoic acid	2496 & 1956	1473 & 982	no	yes
	1,4-diiodobenzene	-	1066 & 795	no	no
	1,4-diiodotetrafluorobenzene	-	1451 & 929	yes	yes
	1-bromo-4-iodotetrafluorobenzene	-	1460 & 963	yes	yes
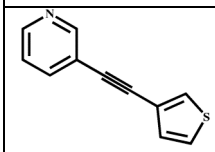 **12**	4-iodobenzoic acid	2549 & 1932	1006 & 752	no	yes
	4-iodotetrafluorobenzoic acid	2459 & 1911	1466 & 935	yes	yes
	4-bromotetrafluorobenzoic acid	2516 & 1948	1461 & 972	yes	yes
	1,4-diiodobenzene	-	1066 & 791	no	no
	1,4-diiodotetrafluorobenzene	-	1449 & 931	yes	yes
	1-bromo-4-iodotetrafluorobenzene	-	1463 & 935	yes	yes

Compounds	Acid/halogen	O-H…N band cm^{-1}	C-I/Br band cm^{-1}	Formation of C-X…N/S	Cocrystal formation
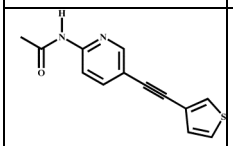 **13**	4-iodobenzoic acid	2498 & 1897	1002 & 750	no	yes
	4-iodotetrafluorobenzoic acid	2381 & 1916	1455 & 974	yes	yes
	4-bromotetrafluorobenzoic acid	2501 & 1952	1473 & 980	no	yes
	1,4-diiodobenzene	-	1066 & 779	yes	yes
	1,4-diiodotetrafluorobenzene	-	1455 & 931	yes	yes
	1-bromo-4-iodotetrafluorobenzene	-	1455 & 972	yes	yes
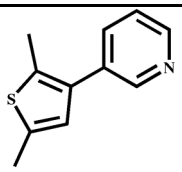 **16**	4-iodobenzoic acid	2498 & 1896	1007 & 752	no	yes
	4-iodotetrafluorobenzoic acid	2500 & 1924	1453 & 970	yes	yes
	4-bromotetrafluorobenzoic acid	2471 & 1912	1468 & 975	yes	yes
	1,4-diiodobenzene	-	1064 & 794	no	no
	1,4-diiodotetrafluorobenzene	-	1449 & 931	yes	yes
	1-bromo-4-iodotetrafluorobenzene	-	1453 & 970	yes	yes
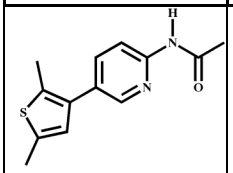 **17**	4-iodobenzoic acid	2553 & 1901	1006 & 751	no	yes
	4-iodotetrafluorobenzoic acid	2498 & 1897	1455 & 973	yes	yes
	4-bromotetrafluorobenzoic acid	2498 & 1944	1471 & 979	no	yes
	1,4-diiodobenzene	-	1066 & 796	no	no
	1,4-diiodotetrafluorobenzene	-	1454 & 929	yes	yes
	1-bromo-4-iodotetrafluorobenzene	-	1458 & 966	yes	yes
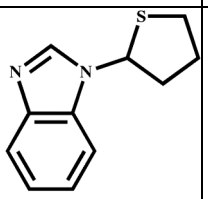 **19**	4-iodobenzoic acid	2569 & 1920	1005 & 738	yes	yes
	4-iodotetrafluorobenzoic acid	2489 & 1944	1455 & 974	yes	yes
	4-bromotetrafluorobenzoic acid	2569 & 1916	1457 & 976	yes	yes
	1,4-diiodobenzene	-	1009 & 736	yes	yes
	1,4-diiodotetrafluorobenzene	-	1448 & 934	yes	yes
	1-bromo-4-iodotetrafluorobenzene	-	1460 & 934	yes	yes

Of the twenty-one co-crystallization reactions with an acid-halogen molecule, twenty-one out of twenty-one times O-H…N (~2500 and 1900 cm^{-1}) interactions were observed in the infrared spectra. However if the halogen atom participated in halogen bonding changes in C-X stretches would undergo a decrease by 7-15 cm^{-1}. Of the twenty-

one reactions 11/21 times a shift in the C-X stretch was observed suggesting that maybe the sulfur atom is participating in halogen bonding.

To further establish whether the sulfur atom in this study is participating in halogen bonding another set of co-crystallization reactions were carried out using only di-halogenated compounds. Of the twenty-one reactions seventeen of those reactions showed a decrease in either the C-I or C-Br stretches indicating that halogen bonding is taking place. Since both nitrogen and sulfur atoms, are present in these complexes it is difficult to establish whether both sulfur and nitrogen is participating in halogen bonding based on the infrared evidence.

Therefore to establish the participation of sulfur atom in halogen bonding we carried out grinding experiments with 2,5-dimethylthiophene and thiophane using **I_2F_4B** as our cocrystal former, Figure 4.12.

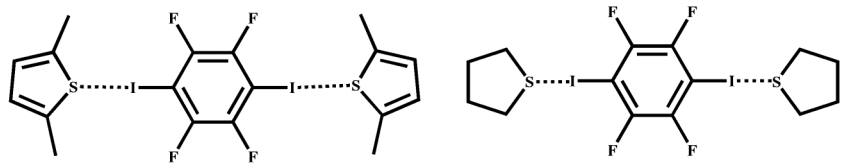

(a) (b)

Figure 4.12 Halogen bonding between: (a) 2,5-dimethylthiophene-I_2F_4B, (b) thiophane-I_2F_4B.

Based on the infrared evidence (Figure 4.13-4.14) no significant changes in the C-I stretch was observed, suggesting that the sulfur atom in these series is not participating in halogen bonding.

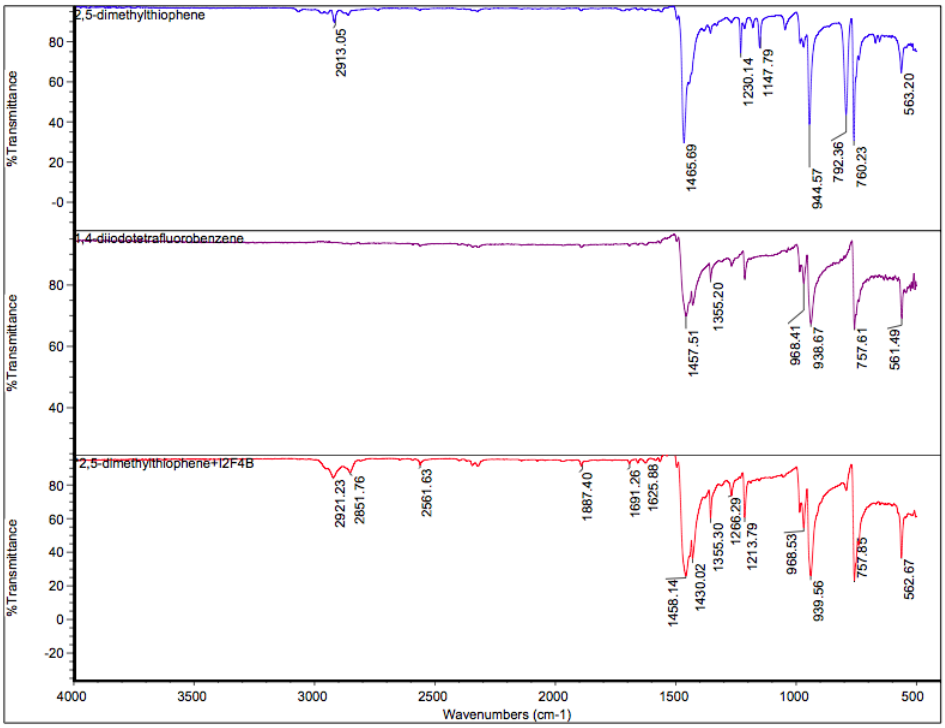

Figure 4.13 IR spectra of grinding experiment with 2,5-dimethylthiophene-I_2F_4B: top (2,5-dimethylthiophene), middle (**I_2F_4B**), bottom (2,5-dimethylthiophene-I_2F_4B).

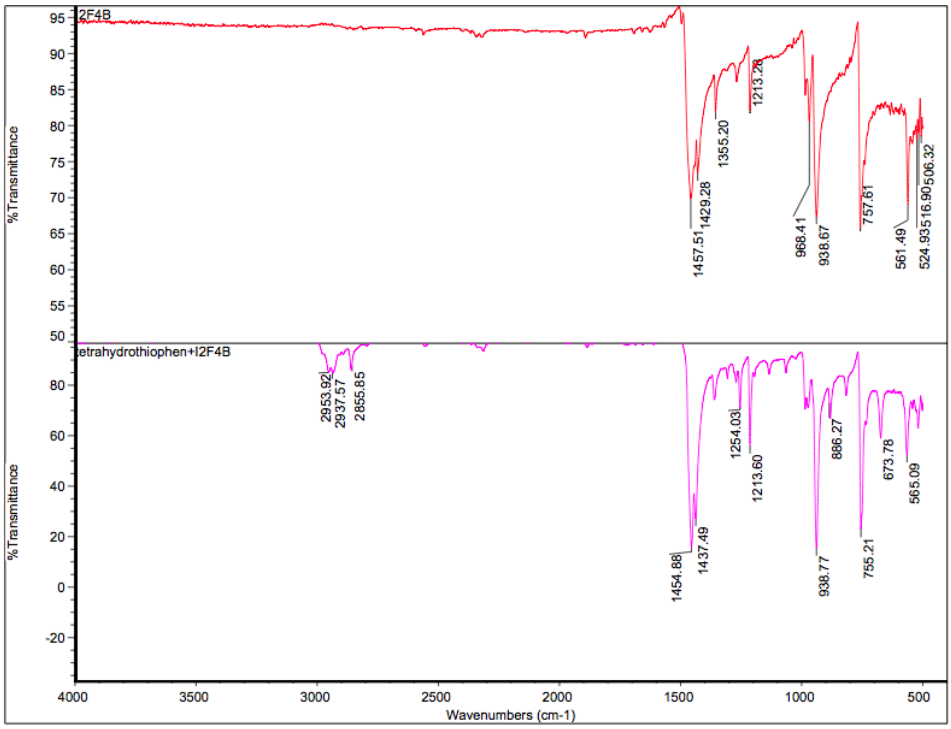

Figure 4.14 IR spectra of grinding experiment with thiophane- I_2F_4B: top (**I_2F_4B**) and bottom (thiophane-I_2F_4B).

4.4.3 Characterization of 9 and 17

9 and **17** were prepared in good yields, crystals suitable for single-crystal X-ray crystallography of **9** and **17** were grown by slow evaporation of saturated ethyl acetate solution at room temperature over 36 hrs, Figure 4.15.

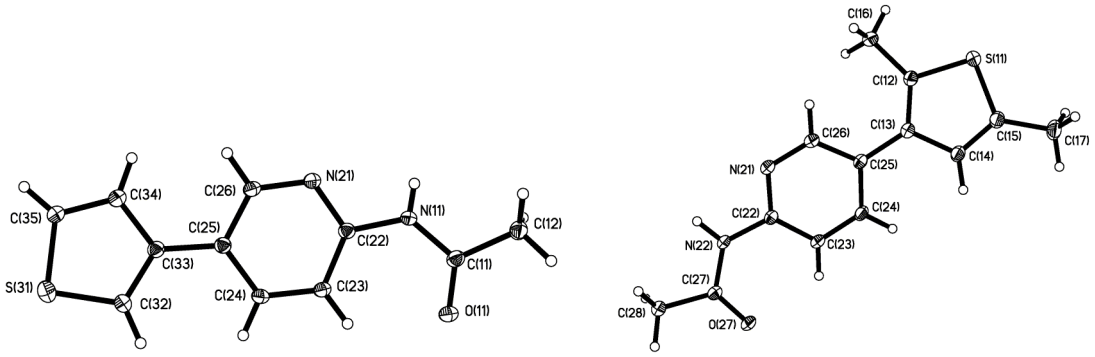

9 **17**

Figure 4.15 Thermal ellipsoids plot (50 % probability level) of **9** and **17**.

The crystal structure determination confirms that both **9** and **17** participate in self-complementary amide-pyridine interaction through N-H…N hydrogen bonds, Figure 4.16.

9 **17**

Figure 4.16 Self-complementary pyridine-amide interaction in **9** and **17**.

Unfortunately, crystals suitable for X-ray diffraction were not obtained for compounds **8**, **12**, **13**, **16** and **19**, however combination of ^{1}H and ^{13}C NMR along with mass spectrometry confirm the identity of the resulting products.

4.4.4 Crystal structure descriptions

A summary of the crystallographic information for **9**, **17**, **8SUC** and **8IBA** is displayed in Table C.3 and all hydrogen-bond geometries for **9**, **17**, **8SUC** and **8IBA** are listed in Table 4.6.

Table 4.6 Hydrogen-bond geometries for **9**, **17**, **8SUC** and **8IBA**

Structure	D-H…A	d(D-H)/Å	d(H…A)/Å	d(D…A)/Å	<(DHA)°
9[i]	N(11)-H(11)…N(21)#1	0.78(2)	2.34(2)	3.1082(17)	170(2)
17[ii]	N(22)-H(22)…N(21)#1	0.885(16)	2.333(16)	3.1984(14)	165.9(14)
8SUC	O(31)-H(31)…N(21)	0.889(16)	1.766(16)	2.6517(10)	174.8(15)
8IBA	O(11)-H(11)…N(21)	0.84	1.89	2.623(4)	144.7

i) #1 -x+2,-y+1,-z ii) #1 -x-1,-y,-z+1

4.4.4.1 Crystal structure of 8SUC

The crystal structure of **8SUC** contains one molecule of **8** and half a molecule of **SUC** in the asymmetric unit; the structure also displays disorder, Figure 4.17. The architecture shows the pyridyl nitrogen hydrogen bonding to the carboxylic acid resulting in a trimer, Figure 4.18. Moreover, the sulfur atom does not participate in any form of non-covalent interactions.

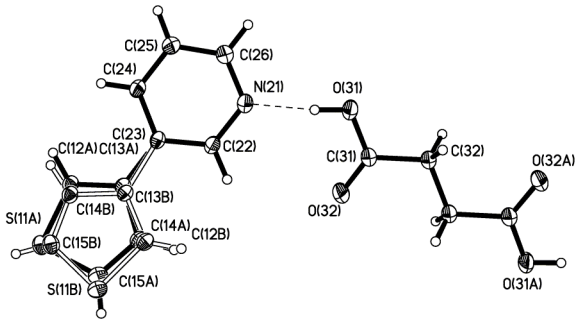

Figure 4.17 Thermal ellipsoid plot (50% probability) of **8SUC**.

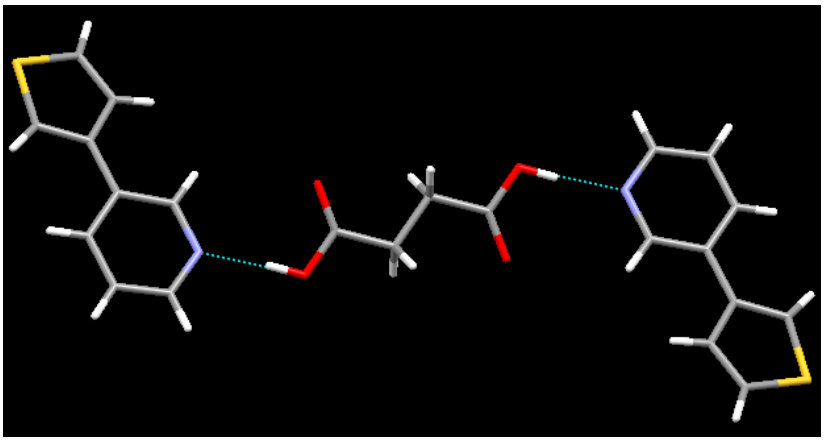

Figure 4.18 Trimer of **8SUC** held together by O-H…N hydrogen bonds.

4.4.4.2 Crystal structure of 8IBA

The asymmetric unit of **8IBA** contains one molecule of **8** and one molecule of **IBA**, Figure 4.19.

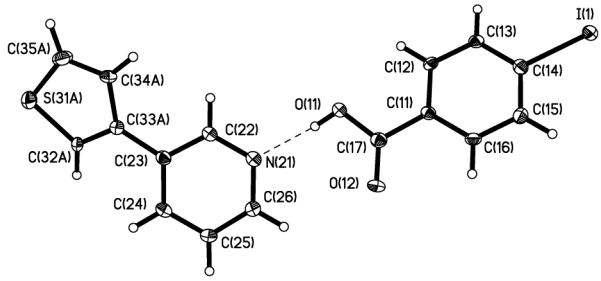

Figure 4.19 Thermal ellipsoid (50% probability) of **8IBA**.

The overall architecture reveals O-H…N hydrogen bonding between the pyridine nitrogen atom and the carboxylic acid, Figure 4.20.

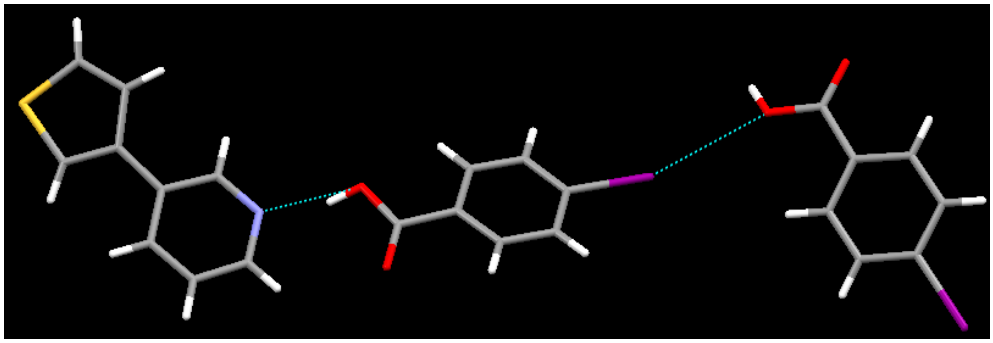

Figure 4.20 1:2 cocrystal of **8IBA** held together by O-H…N and I…O interactions.

Additionally, a halogen bond between the iodine and oxygen atom of the hydroxy group is observed with a bond distance of 3.263Å, and bond angle of 160.75^{o}. The typical bond distance observed for halogen bonding involving an oxygen atom (I…O) normally ranges between 3.04-3.37Å[26] whereas the typical bond angle for contacts with nucleophiles such as oxygens and nitrogen primarily range between 160° and 180°.[27]

As with the previous structures the sulfur atom does not participate in any non-covalent interactions.

4.5 Conclusion

Based on the molecular electrostatic potential calculations conducted the pyridyl and benzimidazole nitrogen having the highest charge formed hydrogen bond with incoming donor molecules 33/33 times (100% success rate).

Additionally, from IR evidence we can conclude that the sulfur atom in 2,5-dimethylthiophene and thiophane did not participate in halogen bonding, therefore in this series the halogen bonding interaction is not dominated by HSAB principles.

Furthermore, from the twenty-one reactions, seventeen of those showed significant shifts in the C-X band, indicating that the formation of halogen bond between the nitrogen or oxygen atom present in the system, thereby confirming that halogen bond is purely electrostatic. This is further demonstrated in **8IBA**, where instead of forming a halogen bond with the sulfur atom, the iodine being the softer acid formed a halogen bond with oxygen a harder base, further confirming that within these series of compounds the dominating interaction is based on electrostatics and not HSAB principles.

References

[1] (a) Jeffrey, G.A. *An Introduction to Hydrogen Bonding*, Oxford University Press, Oxford, **1997**; (b) Ermer, O.; Eling, A. *J. Chem. Soc. Perkin Trans. 2* **1994**, 925; (c) Aakeröy, C.B.; Seddon, K.R. *J. Chem. Soc. Rev*. **1993**, 22, 397.

[2] (a) Metrangolo, P.; Neukirch, H.; Pilati, T.; Resnati, G. *Acc. Chem. Res*. **2005**, 38, 386; (b) Metrangolo, P.; Resnati, G. *Chem. Eur. J*. **2001**, 7, 2511; (c) Legon, A.C. *Chem. Eur. J.* **1998**, 4, 1890.

[3] (a) Metrangolo, P.; Resnati, G.; Pilati, T.; Liantonio, R.; Meyer, F. *J. Pol. Sci. A.* **2007**, 45, 1; (b) Bouchmella, K.; Boury, B.; Dutremez, S.G.; Van der Lee, A. *Chem. Eur. J.* **2007**, 13, 6130; (c) Coradi, E.; Meille, S.V.; Messina, M.T.; Metrangolo, P.; Resnati, G. *Angew. Chem.* **2000**, 112, 1852.

[4] Structure taken from chapter 3.

[5] Clark, T.; Hennemann, M.; Murray, J.S.; Politzer, P. *J. Mol. Model* **2007**, 13, 291.

[6] Metrangolo, P.; Meyer, F.; Pilati, T.; Resnati, G.; Terraneo, G. *Angew. Chem. Int. Ed*. **2008**, 47, 6114.

[7] Pearson, R.G. *J. Am. Chem. Soc*. **1963**, 85, 3533.

[8] (a) Hendra, P.J.; Powell, D.B.; *J. Chem. Soc*. **1960**, 5105; (b) Garnovskii, A.D.; Osipov, O.A.; Bulgarevich, S.B. *Russian Chemical Reviews* **1972**, 41, 341.

[9] Pearson, R.G. *J. Chem. Ed*. **1968**, 45, 581.

[10] (a) Suzuki, T.; Fujii, Y.; Yamashita, C.; Kabuto. S.; Tanaka. M.; Harasawa, T.; Mukai, T.; Miyashi, T. *J. Am. Chem. Soc.* **1992**, 114, 3034; (b) Jøgensen, T.; Hansen, T.H.; Becher, J. *Chem. Soc. Rev*. **1994**, 23, 41.

[11] (a) Herve, K.; Cador, O.; Golhen, S.; Costuas, K.; Halet, J.-F.; Shirahata, T.; Muto, T.; Imakubo, T.; Miyazaki, A.; Ouahab, L. *Chem. Mater*. **2006**, 18, 790; (b) Kosaka, Y.; Yamamoto, H.M.; Nakao, A.; Tamura, M.; Kato, R. *J. Am. Chem. Soc.* **2007**, 129, 3054; (c) Imakubo, T.; Shirahata, T.; Kibune, M.; Yoshino, H. *Eur. J. Inorg. Chem*. **2007**, 4727; (d) Nassimbeni, L.R.; Niven M.L.; Suckling, A.P. *Inorg. Chim. Acta*. **1989**, 159, 209; (e) Imakubo, T.; Sawa, H.; Kato, R. *Chem. Commun*. **1995**, 1097.

[12] Jay, J.I.; Padgett, C.W.; Walsh, R.D.B.; Hanks, T.W.; Pennington, W.T. *Cryst. Growth Des*. **2001**, 1, 501.

[13] Cincic, D.; Friscic, T.; Jones, W. *Chem. Eur. J.* **2008**, 14, 747.

[14] Arman, H.D.; Gieseking, R.L.; Hanks, T.W.; Pennington, W.T. *Chem. Commun*. **2010**, 46, 1854.

[15] Li, W.; Nelson, D.P.; Jensen, M.S.; Hoerrner, R.S.; Cai, D.; Larsen, R.D.; Reider, P.J. *J. Org. Chem*. **2002**, 67, 5394.

[16] Schultheiss, N. **2007**, Dissertation, Kansas State University.

[17] Dawood, K.M.; Kirschning, A. *Tetrahedron* **2005**, 61, 12121.

[18] Gronwitz, S.; Lawitz, K. *Chemica Scripta*, **1984**, 24, 5.

[19] Schultheiss, N.; Barnes, C.L.; Bosch, E. *Cryst. Growth Des*. **2003**, 3, 573.

[20] Lim, J.-S.; An, B.-K.; Park, S.Y. *Macromolecules*, **2005**, 38, 6236.

[21] Ko, C.-C.; Kwok, W.-M.; Yam, V.W.-W.; Phillips, D.L.; *Chem. Eur. J.* **2006**, 12, 5840.

[22] Shorunov, S.V.; Krayushkin, M.M.; Stoyanovich, F.M.; Irie, M. *Russian J. Org. Chem*. **2006**, 42, 1490.

[23] Delaney, P.A.; Johnstone, R.A.W. *Tetrahedron*, **1985**, 41, 3845.

[24] Scott, B. **2008**, Dissertation, Kansas State University.

[25] Messina, M.T.; Metrangolo, P.; Navarrini, W.; Radice, S.; Resnati, G.; Zerbic, G. *J. Mol. Struct*. **2000**, 524, 87.

[26] Metrangolo, P.; Resnati, G. *Chem. Eur. J.* **2001**, 7, 2511.

[27] Politzer, P.; Lane, P.; Concha, M.C.; Ma; Y.; Murray, J.S. *J. Mol Model* **2007**, 13, 305.

CHAPTER 5 - Exploring the co-crystallizing and melting capabilities of pyridylcarboxaldehyde hydrazones

5.1 Introduction

The arrangement of molecules in a crystal determines many fundamental properties such as melting behavior, solubility, hygroscopicity and mechanical strength. These properties can affect the performance of a solid drug. The shape and particle size of the solid drug can influence pharmaceutical operations, such as filtration, washing, drying, milling, mixing, tableting, dissolution, recrystallization of a suspension and lyophilization.[1] Therefore, the ability to control, predict, and change the crystal structure of both known and unknown compounds would contribute significantly to both manufacturers and consumers of solid specialty chemicals.[2]

Current approaches used in changing the physical properties of APIs have drawbacks such as structural changes that may take place upon formation of a new crystalline phase, which can be very drastic (i.e. limiting the fine-tuning of the physical properties) or highly unpredictable. For example, several pharmaceutical crystals such as theophylline,[3] carbamazepine[4] and phenobarbital[5] have been reported to undergo a variety of phase transformations thereby affecting the stability and bioavailability of the drug. As a result, the transformation of a biologically active drug into a viable product is often extremely time consuming, expensive and inefficient.

An alternative approach to over-come this problem is utilizing co-crystallization techniques to form cocrystals[6] of APIs using predesigned, inexpensive and readily available small molecules. This can provide a means for making subtle changes to bulk physical properties without tampering with the pharmacological behavior of the compound at the molecular level and may therefore provide new opportunities for addressing issues related to the dissolution characteristics, hygroscopicity, drug delivery, processability and melting behavior.

A survey of cocrystal formation in the CSD[7] revealed that most cocrystals have been prepared using a combination of functional groups located on a variety of molecules such that they would prefer to bind in a heteromeric fashion, Figure 5.1, rather than in a

homomeric manner.[8,9,10] These particular moieties are ubiquitous in biochemistry as well as in materials science and display favorable geometric and electronic complementarity.

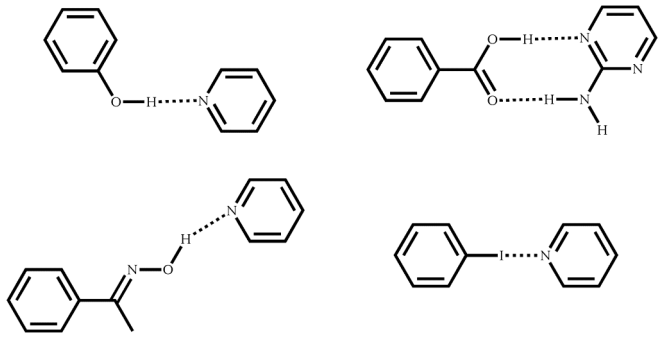

Figure 5.1 Examples of cocrystals constructed via heteromeric intermolecular interactions.

A notable example is isonicotinamide, which has been shown to form cocrystals readily with a variety of carboxylic acids, Figure 5.2.[11] We anticipate that having the isonicotinamide derivative, as part of a scaffold in our molecules can result in the formation of cocrystals with a variety of carboxylic acids.

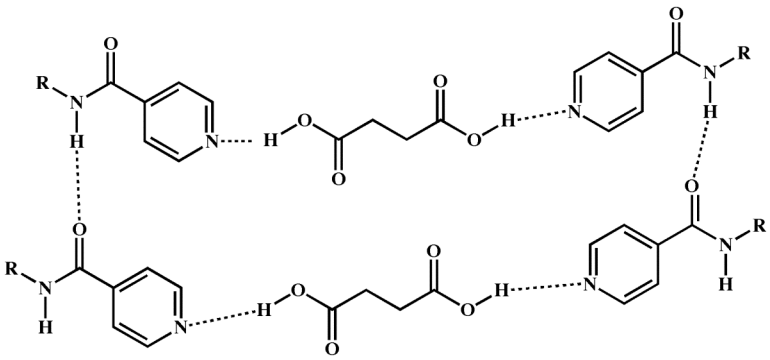

Figure 5.2 Anticipated heteromeric interaction between organic acids and isonicotinamide derivatives.

The compounds of interest to us are a family of hydrazones, which possesses chelating abilities for the treatment of iron-overload disease and acts as agents with considerable anti-tumor activity.[12] Therefore, we designed and synthesized supramolecular architectures with a variety of carboxylic acids using four members of the hydrazone family **20, 21, 23** and **24** Figure 5.3.

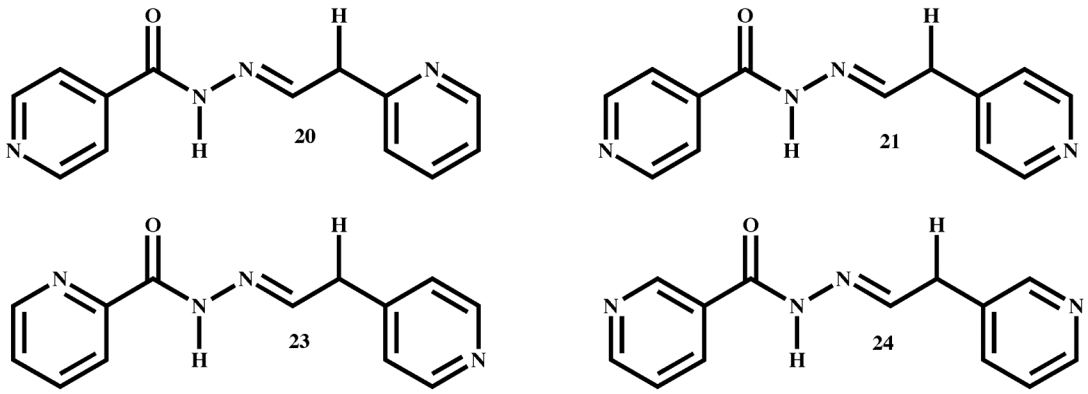

Figure 5.3 Target family of hydrazone compounds.

The overall goals of this chapter are:

1. To synthesize and characterize a series of hydrazones.
2. To determine whether we can synthesize a series of cocrystals with predictable and reliable patterns of behavior.
3. To establish whether the melting point of the cocrystal can be correlated with the nature of the co-crystallizing agent.

5.2 Experimental

5.2.1 Synthesis

All chemicals, unless noted were purchased from Aldrich and used without further purification. Melting points were determined on a GallenKamp melting point apparatus in a capillary tube and are uncorrected. ^{1}H and ^{13}C NMR spectra were recorded on a Varian Unity plus 400 MHz or 200 MHz spectrometers in $CDCl_3$ or DMSO-d_6. Compounds were prepared for infrared spectroscopic (FT-IR) analysis as a mixture in KBr or on a ZnSe ATR crystal. The target compounds were prepared in good yields by Schiff base condensation between the corresponding aldehydes and acid hydrazides.

5.2.1.1 Synthesis of 2-pyridylcarboxaldehyde isonicotinoylhydrazone, 20[13]

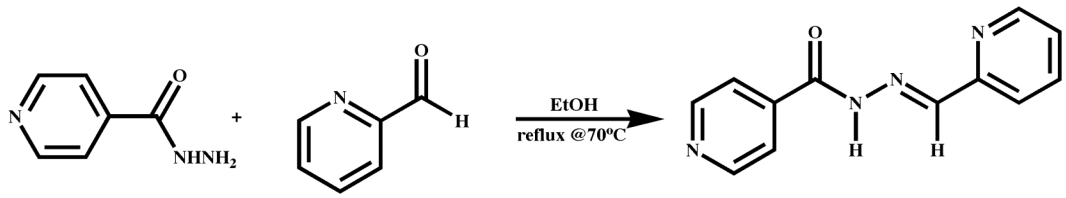

2-Pyridine carboxaldehyde (5.40g, 0.050 mol) and isonicotinic acid hydrazide (6.86g, 0.050 mol) were dissolved in 35 mL of ethanol. Solution was refluxed at 70°C using a Dean Stark apparatus for 2hrs. The refluxed solution was allowed to cool and left standing at room temperature for 24hrs, during which the product precipitated. The product was isolated by filtration then recrystallized from methanol as a white solid, (6.76g, 60%). M.p.: 168-171°C; (Lit m.p. 168-170°C).[14] ^{1}H NMR (δ_H; 400 MHz, DMSO-d_6): 12.29 (s, -CONH-), 8.81 (d, 2H, J = 8Hz), 8.63 (d, 1H, J = 4Hz), 8.49 (s, -N=CH-), 8.00 (d, 1H, J = 8 Hz); 7.91 (d, 1H, J = 8Hz), 7.86 (d, 2H, J = 8Hz), 7.44 (t, 1H, J = 12Hz); ^{13}C NMR (δ_C; 400 MHz, DMSO-d_6): 161, 152, 150, 149, 140, 137, 136, 124, 121, 120; IR (KBr pellet): υ 3288 (N-H), 1667 (C=O), 1544 (C=N), 1463, 1403, 1275(C-O), 1145, 752, 685 cm^{-1}.

5.2.1.2 Synthesis of 4-pyridylcarboxaldehyde isonicotinoylhydrazone, 21[13]

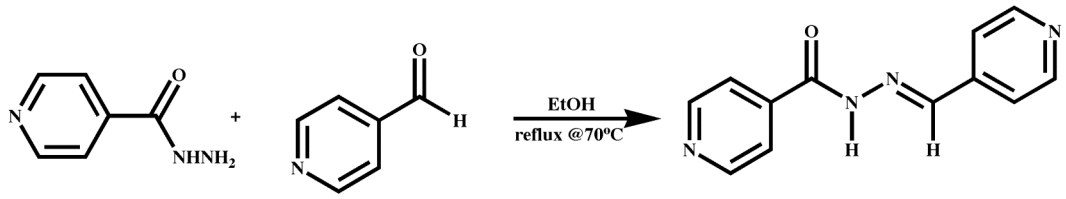

4-Pyridine carboxaldehyde (3.21g. 0.030 mol) and isonicotinic acid hydrazide (4.11g, 0.030 mol) were dissolved in 30 mL of ethanol. The solution was refluxed at 70°C using a Dean Stark apparatus for 2hrs. The refluxed solution was allowed to cool and left standing at room temperature for 24hrs, during which the product precipitated. The product was isolated by filtration then recrystallized from methanol as a white solid, (5.34g, 79%). M.p.: 241-242°C. ^{1}H NMR (δ_H; 400 MHz, DMSO-d_6): 12.35 (s, -CONH), 8.80 (d, 2H, J = 8Hz), 8.64 (d, 2H, J = 4Hz), 8.44 (s, -N=CH-), 7.85 (d, 2H, J = 4 Hz),

7.65 (d, 2H, J = 4Hz); ^{13}C NMR (δ_C; 400 MHz, DMSO-d_6): 162, 150, 146, 141, 140, 121; IR (KBr pellet): υ 3288 (N-H), 1669 (C=O), 1536 (C=N), 1460, 1280 (C-O) cm^{-1}.

5.2.1.3 Synthesis of picolinohydrazide, 22[15]

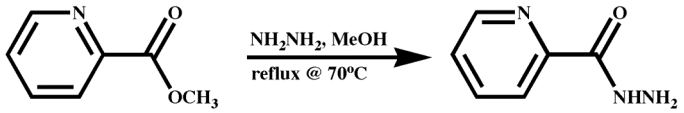

A suspension of methyl picolinate (3.02g, 0.022 mol) and hydrazine (5.00g, 0.156 mol) in 150 mL methanol was refluxed under nitrogen atmosphere for 10 hrs. The reaction was then allowed to cool to room temperature. The solvent was removed on a rotary evaporator and a light pink solid was obtained. Recrystallization from warm ethyl acetate resulted in the product as a white solid, (2.51g, 83%). M.p.: 102-104°C; (Lit m.p. 102-103°C).[15] ^{1}H NMR (δ_H; 400 MHz, $CDCl_3$): 9.06 (s, 1H), 8.53 (d, 1H, J = 5Hz), 8.13 (d, 1H, J = 8Hz), 7.88 (t, 1H), 7.46(t, 1H), 4.11 (s, 2H); IR (KBr pellet): υ 3309, 3206, 1675, 1521, 1000 cm^{-1}.

5.2.1.4 Synthesis of 4-pyridylcarboxaldehyde picolinoylhydrazone, 23[13]

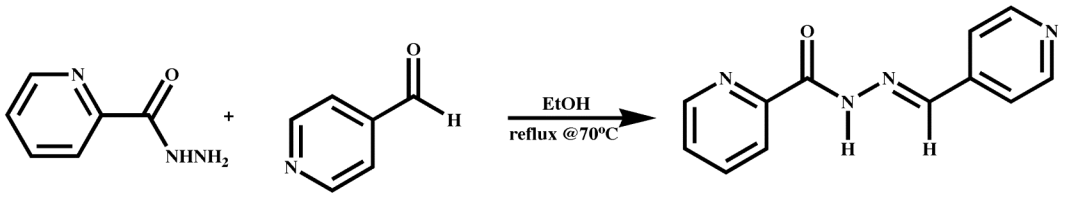

4-Pyridine carboxaldehyde (2.14g 0.020 mol) and **22** (2.74g, 0.020 mol) were dissolved in 25 mL of ethanol. The solution was refluxed at 70°C using a Dean Stark apparatus for 2hrs. The refluxed solution was allowed to cool and left standing at room temperature for 24hrs, during which the product precipitated. The product was isolated by filtration and further purified via recrystallization from methanol to give an off white solid, (2.74g, 61%). M.p. 204-206°C. ^{1}H NMR (δ_H; 400 MHz, DMSO-d_6): 12.45 (s, -CONH-), 8.67 (d, 2H, J = 8Hz), 8.63 (d, 2H, J = 8Hz), 8.16 (d, 1H, J = 8Hz), 8.03 (d, 1H, J = 12 Hz), 7.62 (m, 3H); ^{13}C NMR (δ_C; 400 MHz, DMSO-d_6): 160, 150, 149, 146, 141, 138, 127, 122, 120; IR (KBr pellet): υ 3282 (N-H), 3018, 1684 (C=O), 1510 (C=N), 1355, 1141 cm^{-1}.

5.2.1.5 Synthesis of 3-pyridylcarboxaldehyde nicotinoylhydrazone, 24[13]

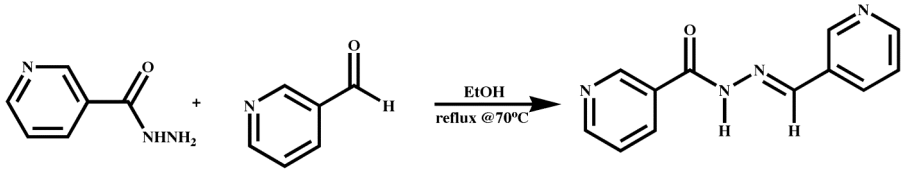

3-Pyridine carboxaldehyde (3.21g 0.030 mol) and nicotinic hydrazide (4.11g, 0.030 mol) were dissolved in 30 mL of ethanol. The solution was refluxed at 70°C using a Dean Stark apparatus for 2hrs. The refluxed solution was allowed to cool and left standing at room temperature for 24hrs, during which the product precipitated. The product was isolated by filtration followed by recrystallized from methanol to give the product as a white solid, (5.28g, 78%). M.p.: 222-224°C. ^{1}H NMR (δ_H; 400 MHz, DMSO-d_6): 12.23 (s, -CONH-), 9.11 (s, 1H), 8.87 (s, -N=CH-), 8.77 (d, 1H, J = 4 Hz), 8.60 (s, 1H), 8.50 (d, 1H, J = 4Hz), 8.28 (d, 1H, J = 4Hz), 8.14 (d 1H, J = 4Hz), 7.56 (t, 1H), 7.46 (t, 1H); ^{13}C NMR (δ_C; 400 MHz, DMSO-d_6): 162, 152, 150, 148, 145, 125, 133, 130, 129, 124, 123; IR (KBr pellet): υ 3232 (N-H), 2824, 1694 (C=O), 1549 (C=N), 1281 (C-O), 1141, 1027, 818 cm^{-1}.

5.2.1.6 Synthesis of 2-pyridinylidene benzoylhydrazine, 25[16]

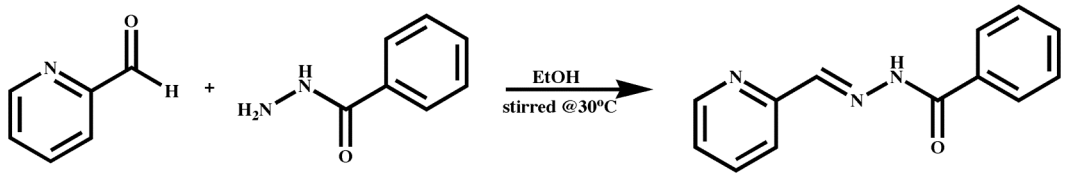

To a solution of benzoic hydrazide (0.110g, 0.830 mmol) in absolute ethanol (7 mL) containing 2 drops of 37% hydrochloric acid was added to 2-pyridine carboxaldehyde (0.093g, 0.870 mmol). The mixture was stirred at 30°C for 24hrs. The reaction mixture was poured into cold water and neutralized with 10% aqueous sodium bicarbonate solution. Using a stirring rod to scratch the beaker resulted in formation of a white precipitate, which was filtered off and dried, (0.131g, 70%). M.p.: 166-168°C; (Lit m.p. 166-168°C).[16] ^{1}H NMR (δ_H; 400 MHz, DMSO-d_6): 12.09 (s, 1H), 8.62 (d, 1H, J = 9.6Hz), 8.49 (s, -N=CH), 7.98 (m, 4H), 7.61 (m, 3H), 7.42 (t, 1H, J = 12.4Hz); IR (ATR ZnSe crystal): υ 3403 (N-H), 2982, 1666 (C=O), 1576 (C=N), 1290 (C-O), 1141, 1076, 776 cm^{-1}.

5.2.2 Synthesis of cocrystals

5.2.2.1 Synthesis of 2-pyridylcarboxaldehyde isonicotinoylhydrazone octanoic acid hydrate (1:1), 20OCT

20 (0.030g, 0.133 mmol) and octanoic acid (0.038g, 0.266 mmol) were added to a beaker along with 4 mL of ethanol. The mixture was heated gently until components were in solution. Colorless plates suitable for X-ray diffraction were obtained after twenty days via slow evaporation of ethanol. M.p.: 72-74°C. IR (KBr pellet): υ 2533 cm^{-1}, 1951 cm^{-1} (O-H···N, br), 1667 cm^{-1} (C=O acid, s).

5.2.2.2 Synthesis of 2-pyridylcarboxaldehyde isonicotinoylhydrazone hexanoic acid hydrate (1:1), 20HEX

20 (0.030g, 0.133 mmol) was dissolved in 4 mL of ethanol and added to beaker containing hexanoic acid (0.031g, 0.266 mmol) in 4 mL of ethanol. The mixture was left at ambient temperature to undergo slow evaporation. After ten days colorless plates were obtained. M.p.: 77-79°C. IR (KBr pellet): υ 2525 cm^{-1}, 1900 cm^{-1} (O-H…N, br), 1675 cm^{-1} (C=O acid, s).

5.2.2.3 Synthesis of 2-pyridylcarboxaldehyde isonicotinoylhydrazone fumaric acid (1:1), 20FUM

20 (0.0565g, 0.245 mmol) was dissolved in 4 mL of ethanol and added to beaker containing fumaric acid (0.029g, 0.245 mmol) in 4 mL of ethanol. The mixture was allowed to slowly evaporate at room temperature. After seven days light orange prism were obtained. M.p.: 208-210°C. IR (KBr pellet): υ 2510 cm^{-1}, 1884 cm^{-1} (O-H…N, br), 1674 cm^{-1} (C=O acid, s).

5.2.2.4 Synthesis of 2-pyridylcarboxaldehyde isonicotinoylhydrazone adipic acid hydrate (1:1), 20ADI

20 (0.029g, 0.130 mmol) was dissolved in 4 mL of nitromethane and added to solution of adipic acid (0.019g, 0.130 mmol) in 4 mL of nitromethane and allowed to slow evaporate at room temperature. After twenty days colorless prism were obtained. M.p.: 112-114°C. IR (KBr pellet): υ 2451 cm^{-1}, 1933 cm^{-1} (O-H…N, br), 1676 cm^{-1} (C=O acid, s).

5.2.2.5 Synthesis of 2-pyridylcarboxaldehyde isonicotinoylhydrazone suberic acid hydrate (1:1), 20SUB

A solution of **20** (0.025g, 0.109 mmol) in 4 mL of ethanol was mixed with a solution of suberic acid (0.019g, 0.109 mmol) in 4 mL of ethanol and allowed to stand at room temperature for slow evaporation. Colorless prisms were obtained after eleven days. M.p.: 134-136°C. IR (KBr pellet): υ 2461 cm^{-1}, 1953 cm^{-1} (O-H…N, br), 1679 cm^{-1} (C=O, s).

5.2.2.6 Synthesis of 2-pyridylcarboxaldehyde isonicotinoylhydrazone sebacic acid dihydrate (1:1), 20SEB

A solution of **20** (0.030g, 0.133 mmol) in 4 mL of nitromethane was mixed with a solution of suberic acid (0.027g, 0.133 mmol) in 4 mL of nitromethane and allowed to stand at room temperature for slow evaporation. Colorless prisms were obtained after five days. M.p.: 105-106°C. IR (KBr pellet): υ 2561 cm^{-1}, 1933 cm^{-1} (O-H…N, br), 1693 cm^{-1} (C=O, s).

5.2.2.7 Synthesis of 2-pyridylcarboxaldehyde isonicotinoylhydrazone 3-fluorobenzoic acid hydrate (1:1) 20FBA

In a test tube containing **20** (0.019g, 0.086 mmol) in 2 mL of ethanol was added to 3-fluorobenzoic acid (0.024g, 0.171 mmol) in 2 mL of ethanol. The solution was placed at room temperature to undergo slow evaporation. After ten days colorless plates were obtained. M.p.: 117-119°C. IR (KBr pellet): υ 2544 cm^{-1}, 1923 cm^{-1} (O-H…N, br), 1669 cm^{-1} (C=O, s).

5.2.2.8 Synthesis of 2-pyridylcarboxaldehyde isonicotinoylhydrazone 4-nitrobenzoic acid hydrate (1:1) 20NBA

A solution of **20** (0.014g, 0.0.059 mmol) in 2 mL of ethanol was added to a solution of 4-nitrobenzoic acid (0.020g, 0.119 mmol) in 2 mL of ethanol and allowed to stand at room temperature for slow evaporation in a test tube. After eleven days colorless prisms were obtained. M.p.: 210-212°C. IR (KBr pellet): υ 2361 cm^{-1}, 1943 cm^{-1} (O-H…N, br), 1669 cm^{-1} (C=O, s).

5.2.2.9 Synthesis of 2-pyridylcarboxaldehyde isonicotinoylhydrazone 2,4-difluorobenzoic acid hydrate (1:1), 20F$_2$BA

In a test tube containing **20** (0.030g, 0.133 mmol) in 2 mL of ethanol was added to 2,4-difluorobenzoic acid (0.084g, 0.531 mmol) in 2 mL of ethanol. The solution was placed at room temperature to undergo slow evaporation. Colorless plate-like crystals were obtained after twenty days. M.p.: 154-156°C. IR (KBr pellet): υ 2498 cm^{-1}, 1900 cm^{-1} (O-H…N, br), 1684 cm^{-1} (C=O, s).

5.2.2.10 Synthesis of 2-pyridylcarboxaldehyde isonicotinoylhydrazone 4-aminobenzoic acid hydrate (1:1) 20ABA

In a beaker containing **20** (0.015g, 0.070 mmol) in 3 mL of ethanol-acetonitrile 4-aminobenzoic acid (0.010g, 0.070 mmol) in 3 mL of ethanol-acetonitrile was added. The solution was placed at room temperature to undergo slow evaporation. Transparent orange block-like crystals were obtained after fifteen days. M.p.: 105-107°C. IR (KBr pellet): υ 2489 cm^{-1}, 1879 cm^{-1} (O-H…N, br), 1684c m^{-1} (C=O acid, s), 3416 cm^{-1} (NH_2 acid, s).

5.2.2.11 Synthesis of 4-pyridylcarboxaldehyde isonicotinoylhydrazone succinic acid dihydrate (1:1), 21SUC

21 (0.030g, 0.133 mmol) was gently heated in 4 mL of ethanol and added to a solution containing succinic acid (0.0157g, 0.133 mmol) in 4 mL of ethanol. The solution was left to stand at room temperature for slow evaporation. After nine days colorless plate-like crystals were obtained. M.p.: 212-214°C. IR (KBr pellet): υ 2431 cm^{-1}, 1948 cm^{-1} (O-H…N, br), 1679 cm^{-1} (C=O acid, s).

5.2.2.12 Synthesis of 4-pyridylcarboxaldehyde isonicotinoylhydrazone adipic acid hydrate (1:1), 21ADI

A solution of **21** (0.030g, 0.133mmol) in 4 mL of ethanol was gently heated and added to a solution of adipic acid (0.019g, 0.133mmol) in 4 mL of ethanol. The mixture was allowed to stand at ambient temperature. After nine days colorless plate-like crystals were obtained. M.p.: 190-192°C. IR (KBr pellet): υ 2476 cm^{-1}, 1903 cm^{-1} (O-H…N, br), 1677 cm^{-1} (C=O acid, s).

5.2.2.13 Synthesis of 4-pyridylcarboxaldehyde isonicotinoylhydrazone suberic acid hydrate (1:1), 21SUB

21 (0.030g, 0.133 mmol) was dissolved in 1 mL methanol-1 mL ethyl acetate and added to a beaker containing suberic acid (0.023g, 0.133 mmol) in 1 mL methanol-1 mL ethyl acetate. The solution was allowed to stand at room temperature for slow evaporation. After twelve days colorless plates were obtained. M.p.: 179-181°C. IR (KBr pellet): υ 2500 cm^{-1}, 1900 cm^{-1} (O-H…N, br), 1678 cm^{-1} (C=O acid, s).

5.2.2.14 Synthesis of 4-pyridylcarboxaldehyde picolinoylhydrazone fumaric acid (1:1), 23FUM

23 (0.030g, 0.133 mmol) was dissolved in 4 mL of ethanol and added to a beaker containing fumaric acid (0.015g, 0.133 mmol) in 4 mL of ethanol. The solution was left to stand at room temperature for slow evaporation. Colorless prisms were obtained ten days later. M.p.: 207-209°C. IR (KBr pellet): υ 2498 cm^{-1}, 1924 cm^{-1} (O-H…N, br), 1695 cm^{-1} (C=O acid, s).

5.2.2.15 Synthesis of 4-pyridylcarboxaldehyde picolinoylhydrazone glutaric acid (1:1), 23GLU

23 (0.030g, 0.133 mmol) was dissolved in 4 mL of ethanol and added to a beaker containing glutaric acid (0.018g, 0.133 mmol) in 4 mL of ethanol. The solution was left to stand at room temperature for slow evaporation. After eight days colorless plate-like crystals were obtained. M.p.: 156-157°C. IR (KBr pellet): υ 2484 cm^{-1}, 1928 cm^{-1} (O-H…N, br), 1715 cm^{-1} (C=O acid, s).

5.2.2.16 Synthesis of 3-pyridylcarboxaldehyde nicotinoylhydrazone adipic acid dihydrate (1:1), 24ADI

A solution of **24** (0.030g, 0.133 mmol) in 4 mL of ethanol was gently heated and added to a solution of adipic acid (0.019g, 0.133 mmol) in 4 mL of ethanol. The solution was allowed to stand at ambient temperature for slow evaporation. After ten days colorless prisms were obtained. M.p.: 139-141°C. IR (KBr pellet): υ 2495 cm^{-1}, 1918 cm^{-1} (O-H…N, br), 1669 cm^{-1} (C=O acid, s).

5.2.2.17 Synthesis of 3-pyridylcarboxaldehyde nicotinoylhydrazone suberic acid hydrate (1:1), 24SUB

24 (0.030g, 0.133 mmol) was dissolved in 4 mL of ethanol by gentle heating and added to beaker containing suberic acid (0.023g, 0.133 mmol) in 4 mL of ethanol. The solution was allowed to stand at room temperature for slow evaporation. Colorless plate-like crystals were obtained twelve days later. M.p.: 152-154°C. IR (KBr pellet): 2475 cm^{-1}, 1924 cm^{-1} (O-H…N, br), 1670 cm^{-1} (C=O acid, s).

5.4 Results

A summary of the crystallographic information for **20OCT, 20HEX, 20FUM, 20ADI, 20SUB, 20SEB, 20FBA, 20NBA, 20F$_2$BA, 20ABA, 21SUC, 21ADI, 21SUB, 23FUM, 23GLU 24ADI** and **24SUB** are displayed in Table C.3 and all the hydrogen-bond geometries are listed in Table 5.1.

Table 5.1 Hydrogen-bond geometries for **20OCT, 20HEX, 20FUM, 20ADI, 20SUB, 20SEB, 20FBA, 20NBA, 20F$_2$BA, 20ABA, 21SUC, 21ADI, 21SUB, 23FUM, 23GLU, 24ADI, 24SUB**

Structure	D-H…A	d(D-H)/Å	d(H…A)/ Å	d(D…A)/ Å	<(DHA)^o
20OCT^i	O(31)-H(31)...N(21)	1.00(4)	1.60(4)	2.597(3)	178(3)
	N(27)-H(27)...O(1S)#1	0.82(3)	2.01(3)	2.815(3)	166(3)
	O(1S)-H(1A)...O(32)	0.81(3)	1.97(3)	2.758(3)	164(3)
	O(1S)-H(1B)...O(27)#2	0.97(4)	1.81(4)	2.767(3)	168(3)
20HEX^{ii}	O(1S)-H(1A)...O(17)#1	0.80(3)	1.98(3)	2.778(3)	177(3)
	O(1S)-H(1B)...O(32)#2	0.94(3)	1.85(3)	2.760(3)	161(3)
	O(31)-H(31)...N(11)	1.04(4)	1.56(4)	2.590(3)	171(3)
	N(17)-H(17)...O(1S)	0.74(3)	2.09(3)	2.815(3)	165(3)
20FUM^{iii}	O(31)-H(31)...N(11)	0.952(18)	1.666(18)	2.6167(15)	176.0(16)
	N(17)-H(17)...O(17)#2	0.870(17)	2.396(17)	3.2462(15)	165.6(15)
20ADI^{iv}	O(31)-H(31)...N(11)	1.01(3)	1.60(3)	2.6035(19)	174(2)
	O(1S)-H(1A)...O(17)#2	0.81(2)	2.00(2)	2.7649(17)	157(2)
	O(1S)-H(1B)...O(32)#3	0.88(3)	1.93(3)	2.7744(19)	161(2)
	N(17)-H(17)...O(1S)	0.84(2)	1.96(2)	2.7928(19)	168(2)
20SUB^v	O(31)-H(31)...N(11)	0.90(4)	1.69(4)	2.593(3)	173(3)
	O(1S)-H(1A)...O(17)	0.88(4)	1.93(4)	2.760(3)	157(3)
	O(1S)-H(1B)...O(32)#2	0.79(4)	1.99(4)	2.753(3)	163(4)
20SEB^{vi}	N171-H171...O(1S)	0.893(15)	1.934(15)	2.8216(15)	172.6(14)
	N172-H172...O(2S)	0.863(14)	1.932(15)	2.7831(14)	168.4(13)
	O(1S)-H(1A)...O171#1	0.866(17)	2.007(18)	2.8318(14)	158.9(15)

Structure	D-H…A	d(D-H)/Å	d(H…A)/ Å	d(D…A)/ Å	<(DHA)°
	O(1S)-H(1B)...O(32)#2	0.856(18)	1.946(18)	2.7946(15)	170.8(16)
20SEB[vi]	O(2S)-H(2A)...O172#3	0.846(18)	1.943(18)	2.7612(13)	162.3(15)
	O(2S)-H(2B)...O(41)#4	0.824(17)	1.975(18)	2.7749(14)	163.2(16)
20FBA[vii]	N(17)-H(17)...O(1S)	0.94(3)	1.90(3)	2.826(4)	167(3)
	O(1S)-H(1A)...O(32)#1	0.94(4)	1.87(4)	2.791(4)	165(3)
	O(1S)-H(1B)...O(17)#2	0.81(4)	2.04(4)	2.817(3)	161(4)
	O(31)-H(31)...N(11)	1.08(4)	1.51(4)	2.552(4)	159(3)
20NBA[viii]	O(1S)-H(1A)...O(17)	0.796(10)	2.138(18)	2.875(3)	154(3)
	O(1S)-H(1B)...O(1S)#1	0.786(10)	2.27(4)	2.904(6)	139(5)
	O(31)-H(31)...N(11)	0.94(5)	1.69(5)	2.624(3)	172(4)
20F$_2$BA[ix]	O(1S)-H(1A)...O(17)	0.84(2)	2.13(2)	2.8653(15)	146(2)
	O(1S)-H(1B)...N(21)#1	0.82(2)	2.34(2)	2.9844(19)	136(2)
	O(31)-H(31)...N(11)	1.11(2)	1.53(2)	2.6337(15)	172.1(18)
	N(17)-H(17)...O(1S)#2	0.88(2)	1.95(2)	2.8264(16)	178(2)
20ABA[x]	O(31)-H(31)...N(11)	0.90(2)	1.73(2)	2.6349(17)	176.7(18)
	N(17)-H(17)...O(1S)	0.915(18)	2.001(18)	2.8570(18)	155.1(15)
	O(1S)-H(1A)...O(17)#1	0.91(2)	2.26(2)	3.0533(19)	145.2(17)
	O(1S)-H(1B)...N(21)#2	1.01(2)	1.82(2)	2.8274(19)	176.8(17)
21SUC[xi]	O(31)-H(31)...N(11)	0.97(2)	1.65(2)	2.612(2)	174(2)
	O(1S)-H(1A)...O(17)	0.92(3)	1.92(3)	2.804(2)	160(2)
	O(2S)-H(2A)...O(32)	0.88(3)	1.86(3)	2.718(2)	166(2)
	N(17)-H(17)...O(2S)#1	0.83(2)	1.98(2)	2.766(2)	157.4(19)
	O(34)-H(34)...N(21)#2	1.11(2)	1.45(2)	2.5566(18)	173.7(18)
	O(1S)-H(1B)...O(35)#3	0.79(3)	1.99(3)	2.775(2)	170(3)
	O(2S)-H(2B)...O(1S)#4	0.86(3)	1.85(3)	2.717(2)	177(2)
21ADI[xii]	N(17)-H(17)...O(1S)	0.860(19)	2.09(2)	2.9376(18)	167.9(17)
	O(31)-H(31)...N(11)	0.87(2)	1.77(2)	2.6269(17)	170(2)
	O(36)-H(36)...N(21)#1	0.94(2)	1.69(2)	2.6269(17)	175.6(19)
	O(1S)-H(1A)...O(32)#2	0.87(2)	1.97(2)	2.7950(19)	158.6(19)

Structure	D-H…A	d(D-H)/Å	d(H…A)/ Å	d(D…A)/ Å	<(DHA)°
	O(1S)-H(1B)...O(17)#3	0.78(2)	2.13(2)	2.8689(16)	156(2)
21SUB[xiii]	O(31)-H(31)...N(11)	0.93(3)	1.74(3)	2.641(3)	166(3)
	O(38)-H(38)...N(21)#1	0.94(3)	1.74(3)	2.666(3)	172(3)
	O(1S)-H(1A)...O(17)	0.86(3)	2.05(3)	2.873(3)	161(3)
	O(1S)-H(1B)...O(32)#2	0.87(3)	1.95(3)	2.795(3)	165(3)
	N(17)-H(17)...O(1S)#3	0.86(3)	2.11(3)	2.942(3)	165(2)
23FUM	O(31)-H(31)...N(21)	1.113(13)	1.472(13)	2.5845(9)	177.8(11)
23GLU[xiv]	O(31)-H(31)...O(17)	0.86(2)	1.84(2)	2.6783(18)	166(2)
	O(35)-H(35)...N(21)#1	1.04(2)	1.62(2)	2.6628(18)	175.5(18)
24ADI[xv]	N(17A)-H(17A)...O(1A)	0.88	2.15	2.993(4)	160.6
	N(27B)-H(27B)...O(1B)#1	0.88	1.95	2.758(11)	152.6
24SUB[xvi]	N(17)-H(17)...O(1S)#1	0.848(16)	2.111(16)	2.9541(14)	172.9(14)
	O(31)-H(31)...N(11)	0.903(17)	1.776(17)	2.6597(13)	165.2(15)
	O(38)-H(38)...N(21)#2	0.902(16)	1.752(17)	2.6447(13)	170.0(15)
	O(1S)-H(1A)...O(17)	0.812(18)	2.147(18)	2.9187(13)	158.8(16)
	O(1S)-H(1B)...O(32)#3	0.864(18)	2.023(18)	2.8728(14)	167.7(15)

i) #1 -x+1,-y,-z+1 #2 -x,-y,-z+1 ii) #1 x+1,y,z #2 -x+1,-y,-z iii) #2 x-1/2,-y+1/2,z-1/2 iv)#1 -x,-y+2,-z+2 #2 x-1,y,z #3 -x,-y+1,-z+1 v) #2 -x+1,-y,-z+1 vi) #1 x-1,y,z #2 -x+2,-y,-z+1 #3 x+1,y,z #4 -x,-y+2,-z vii) #1 -x+2,-y+1,-z+1 #2 x+1,y,z viii) #1 -x+2,-y,-z+1 ix) #1 x+1/2,y+1/2,z #2 -x+1/2,y-1/2,-z+1/2 x) #1 -x+1,-y+1,-z+1 #2 -x,-y+1,-z+1 xi) #1 x-1,y,z #2 x+3/2,-y+3/2,z-1/2 #3 x-1/2,-y+3/2,z+1/2 #4 -x+1,-y+1,-z+1 xii) #1 x-2,y+1,z+1 #2 -x,-y+1,-z #3 x-1,y,z xiii) #1 x-2,y+2,z-1 #2 -x+1,-y+1,-z+1 #3 x-1,y,z xiv) #1 x+1/2,y,-z+1/2 xv) #1 x-1,y,z xvi) #1 x+1,y,z #2 x-2,y-1,z-1 #3 -x+1,-y+1,-z+2

5.4.1 Crystal structure of 20OCT

The crystal structure of **20OCT** contains one molecule of **20**, one molecule of **OCT** and one water molecule with an O-H…N interaction between the carboxylic acid and the pyridine nitrogen atom of **20**, Figure 5.4. The crystal structure is further extended into a 1-D layer through hydrogen bonds between a water molecule and the adjacent carbonyl and amide hydrogen of **20**, Figure 5.5. A water molecule is also hydrogen

bonded to the carbonyl of the acid, with hydrogen bond distances in Table 5.1. No short contacts were observed with the pyridine nitrogen atom in the *ortho* position of **20**.

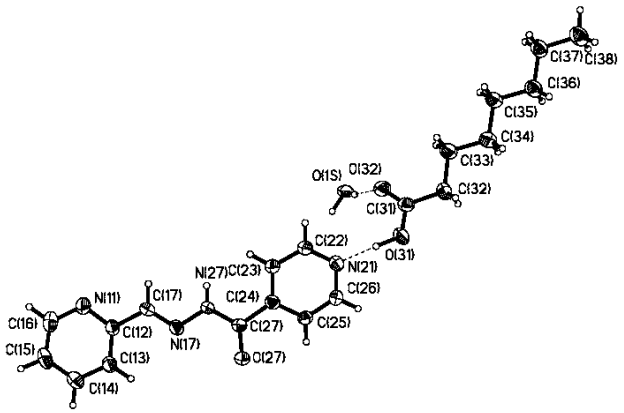

Figure 5.4 Thermal ellipsoids (50%) and labeling scheme of **20OCT**.

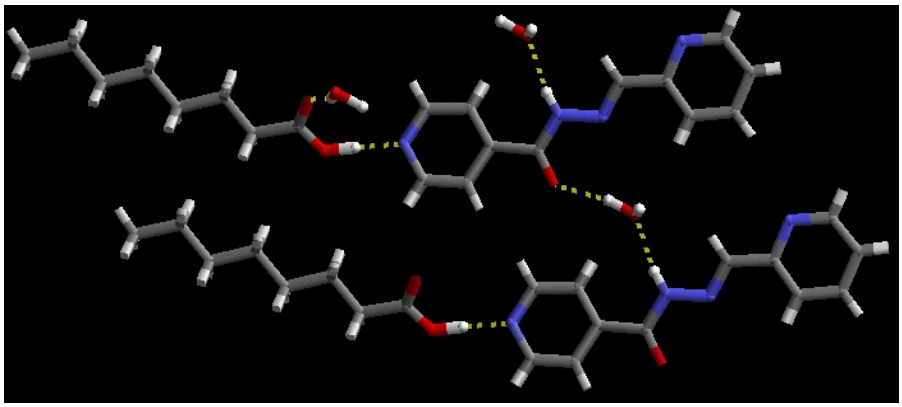

Figure 5.5 Hydrated cocrystal of **20OCT** depicting O-H…N and N-H…O interactions resulting in a 1-D motif.

5.4.2 Crystal structure of 20HEX

The asymmetric unit of **20HEX** contains one molecule of **20**, one molecule of **HEX** and a water molecule, held together by O-H…N hydrogen bonds between the carboxylic acid and the pyridine nitrogen of **20**, Figure 5.6.

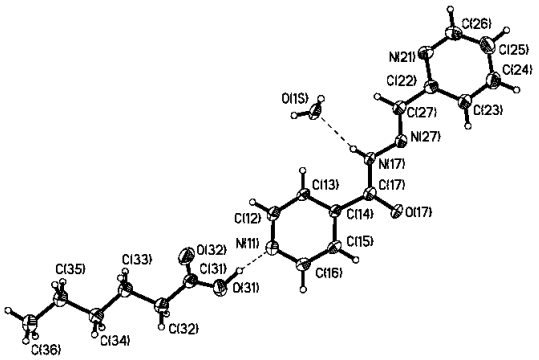

Figure 5.6 Thermal ellipsoids (50%) and labeling of **20HEX**.

The structure is further extended into a 1-D array via the aid of the water molecule hydrogen bonded to the carbonyl and amide of **20**, Figure 5.7. Furthermore, as observed in **20OCT** there were no short contacts observed with the pyridine nitrogen atom in the *ortho* position of **20HEX**. Additionally, as observed in the **20OCT** the water molecule also forms a hydrogen bond with the carbonyl of an acid.

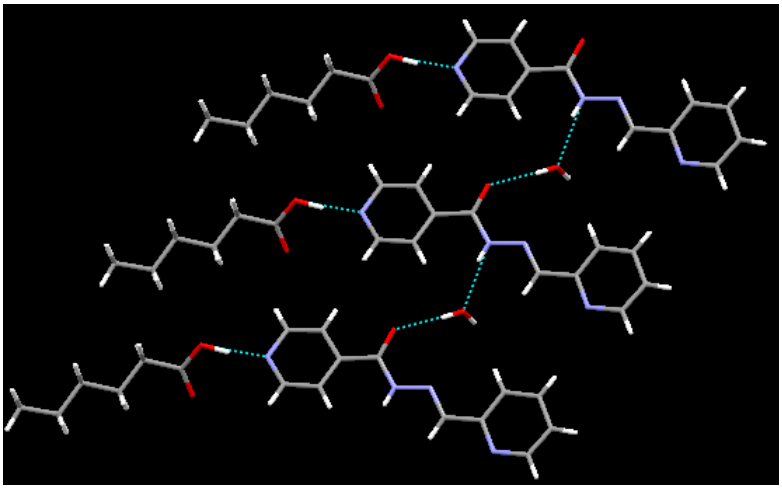

Figure 5.7 1-D layer of **20HEX** held together by both O-H…N and N-H…O hydrogen bonds.

5.4.3 Crystal structure of 20FUM

The asymmetric unit of **20FUM** contains one molecule of **20** and one molecule of **FUM**, held together by O-H…N hydrogen bonds between the pyridine nitrogen in the *para* position and the hydroxy group of acid, Figure 5.8. The structure is further expanded into a trimer via hydrogen bond interactions between the pyridine nitrogen and

carboxylic acid, Figure 5.9. However, as observed in the first two structures the pyridine nitrogen in the *ortho*-position does not participate in any distinct non-covalent interactions. Unlike the two previous structures **20FUM** does not contain a water molecule in the crystalline lattice.

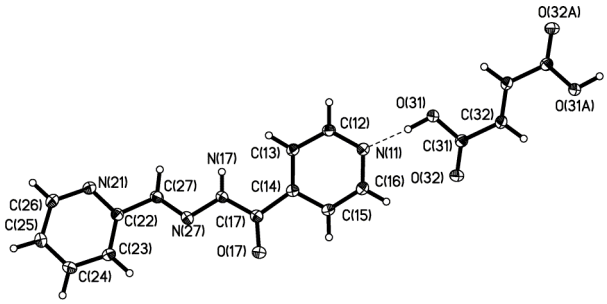

Figure 5.8 Thermal ellipsoids (50%) and labeling scheme of **20FUM**.

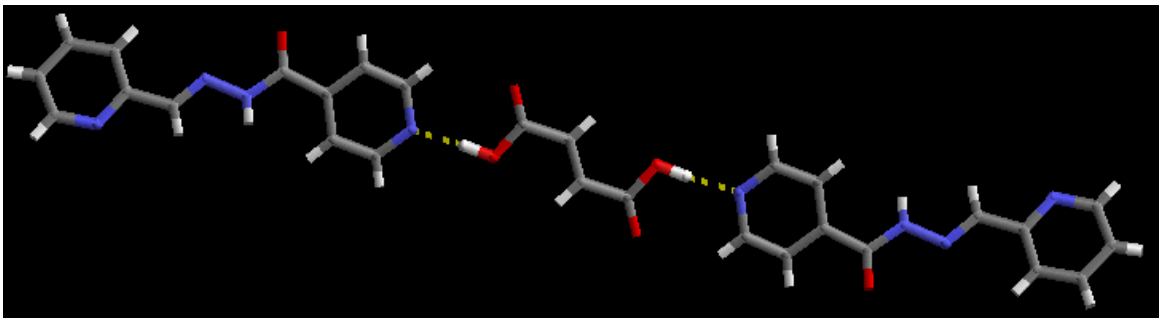

Figure 5.9 Trimer of **20FUM** held together by O-H…N hydrogen bond.

5.4.4 Crystal structure of 20ADI

The crystal structure of **20ADI** contains one molecule of **20**, one molecule of **ADI** and one water molecule in the asymmetric unit. The supermolecule is constructed through O-H…N hydrogen bonds between the carboxylic acid and the *para* position nitrogen atom on **20**, Figure 5.10. A 2-D sheet is formed though hydrogen bonds from the water molecule, to the carbonyl and amide hydrogen, Figure 5.11. No short contacts were observed between the acid and the pyridine nitrogen in the *ortho* position of **20**.

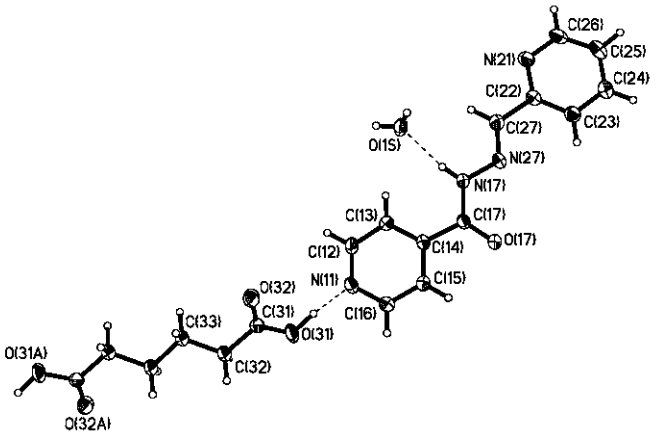

Figure 5.10 Thermal ellipsoids (50%) and labeling of **20ADI**.

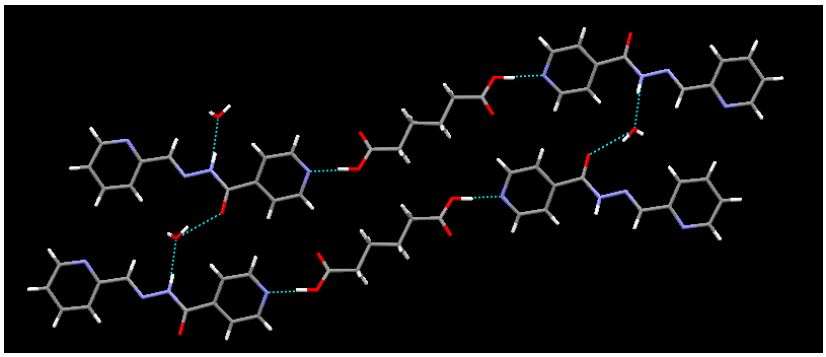

Figure 5.11 2-D sheet of **20ADI** held to together by O-H…N, O…H-O, N-H…O interactions.

5.4.5 Crystal structure of 20SUB

The crystal structure of **20SUB** contains one molecule of **20**, one molecule of **SUB** and one water molecule in the asymmetric unit. The structure display hydrogen bonding interactions between the *para*-position pyridine nitrogen and the carboxylic acid, a water molecule is hydrogen bonded to the carbonyl group of **20**, Figure 5.12, the bond distances is shown in Table 5.1. The structure is further extended into a 2-D sheet via the aid of a hydrogen bond between the water molecule and the carbonyl and amide hydrogen of **20** Figure 5.13, similar to what was observed in **20ADI**. Note that the carbonyl of the acid also forms a hydrogen bond with the water molecule as previously observed.

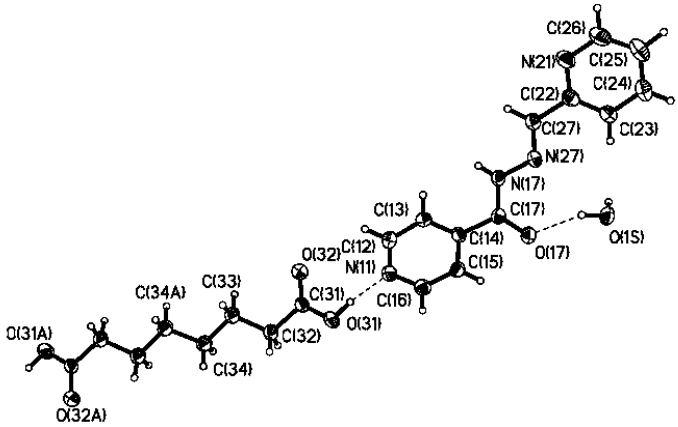

Figure 5.12 Thermal ellipsoids (50%) and labeling scheme of the supermolecule **20SUB**.

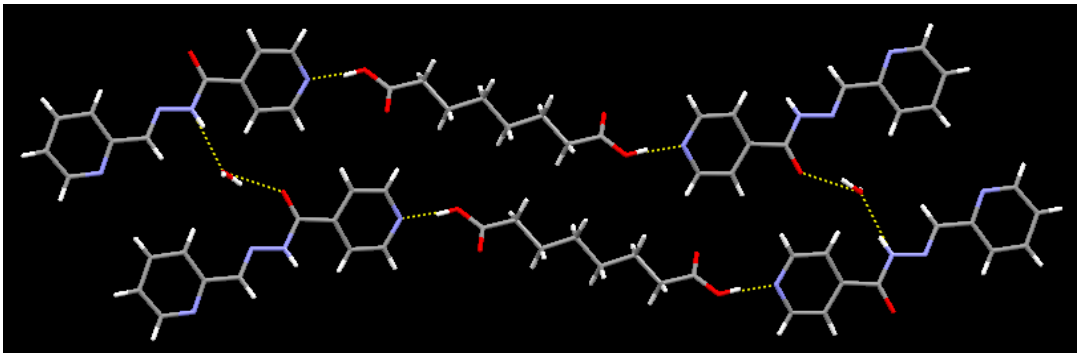

Figure 5.13 2-D sheet of **20SUB** held together via O-H…N, O-H…O and N-H…O hydrogen bonds.

5.4.6 Crystal structure of 20SEB

The asymmetric unit of **20SEB** contains one molecule of **20**, one molecule of **SEB** and one water molecule. As with the two previous structures **20ADI** and **20SUB**, the carboxylic acid forms a hydrogen bond with the *para*-position pyridine nitrogen, Figure 5.14. The water molecule aids in the formation of a 2-D sheet through non-covalent interaction with the carbonyl and amide, Figure 5.15. Again, the ortho-position pyridine nitrogen of **20** shows no distinct non-covalent interaction.

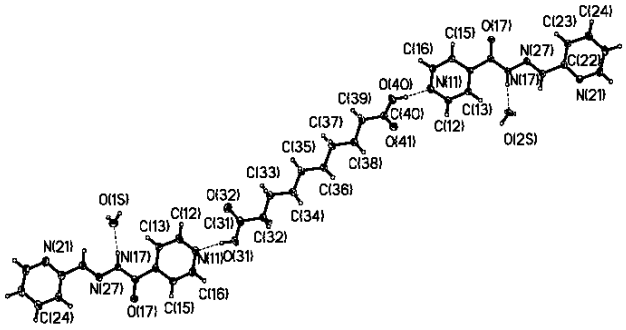

Figure 5.14 Thermal ellipsoids (50%) and labeling scheme of the supermolecule **20SEB**.

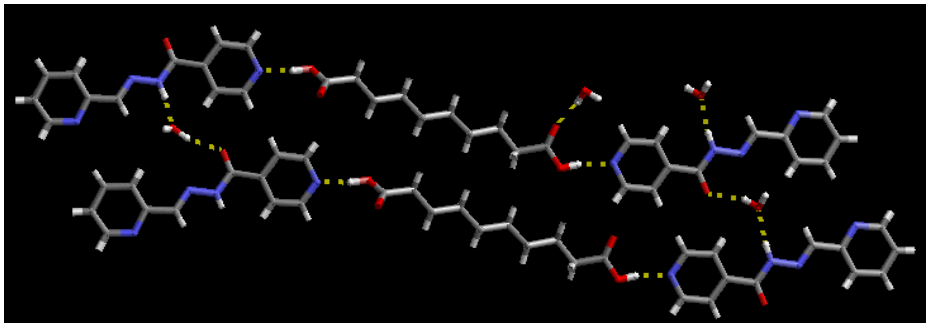

Figure 5.15 2-D sheet of **20SEB** displaying O-H…N, O-H…O and N-H…O non-covalent interactions.

5.4.7 Crystal structure of 20FBA

The crystal structure of **20FBA** consists of one molecule of **20**, one molecule of **FBA** and one water molecule in the asymmetric unit. The supermolecule is constructed through O-H…N hydrogen bonds between the carboxylic acid and the *para*-position pyridine nitrogen atom of **20**, Figure 5.16.

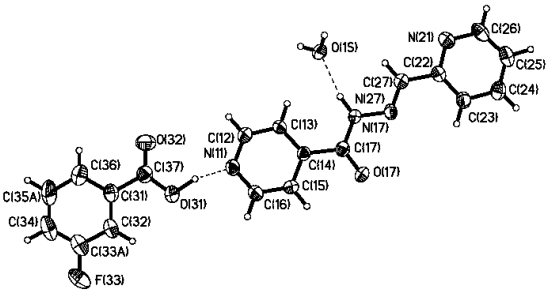

Figure 5.16 Thermal ellipsoids (50%) and labeling scheme of the supermolecule **20FBA**.

The architecture of **20FBA** is similar to **20OCT** and **20HEX**, in that the water molecule helps to extend the structure in 1-D layer by interacting with the carbonyl and amide hydrogen, Figure 5.17.

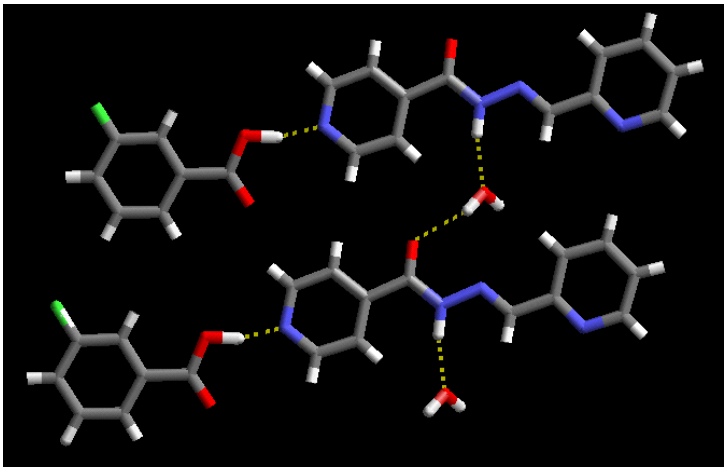

Figure 5.17 1-D layer motif of **20FBA**, held together via O-H…N, N-H…O interactions.

5.4.8 Crystal structure of 20NBA

The asymmetric unit of **20NBA** consists of one molecule of **20**, one molecule of **NBA** and one water molecule, the structure is also disordered. The primary interaction observed in this structure is a hydrogen bond between the pyridine nitrogen in the *para*-position of **20** and the carboxylic acid, Figure 5.18.

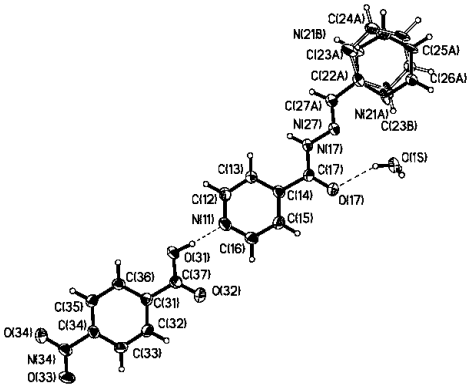

Figure 5.18 Thermal ellipsoids (50%) and labeling scheme of the supermolecule **20NBA**.

The structure is further extended into a 1-D step-like motif, with interactions similar to **20FBA**, in that the disordered water molecule forms a hydrogen bond with the amide hydrogen and carbonyl thus aiding the extension of the structure, Figure 5.19.

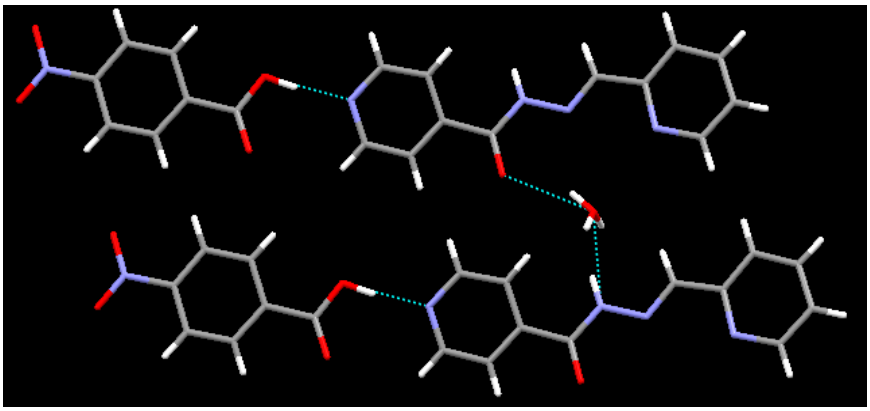

Figure 5.19 1-D step-like motif of **20NBA** displaying O-H…N and N-H…O hydrogen bonds.

5.4.9 Crystal structure of 20F$_2$BA

The asymmetric unit of **20F$_2$BA** contains one molecule of **20**, one molecule of **F$_2$BA** and one water molecule. The structure is held together by hydrogen bonding between the pyridine nitrogen atom *para* to the carbonyl of **20** and the carboxylic acid, resulting in O-H…N interactions, Figure 5.20.

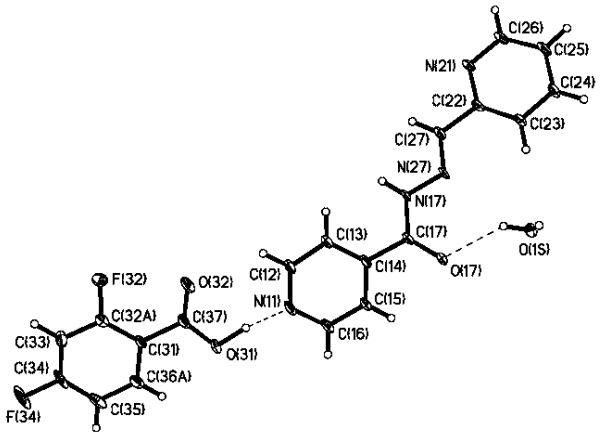

Figure 5.20 Thermal ellipsoids (50%) and labeling scheme of the supermolecule **20F$_2$BA**.

Unlike the previous structures, the water molecule forms a hydrogen bond with the pyridine nitrogen in the *ortho*-position of **20**, and produces a step-like motif via interactions between the amide hydrogen and carbonyl group of **20**, Figure 5.21.

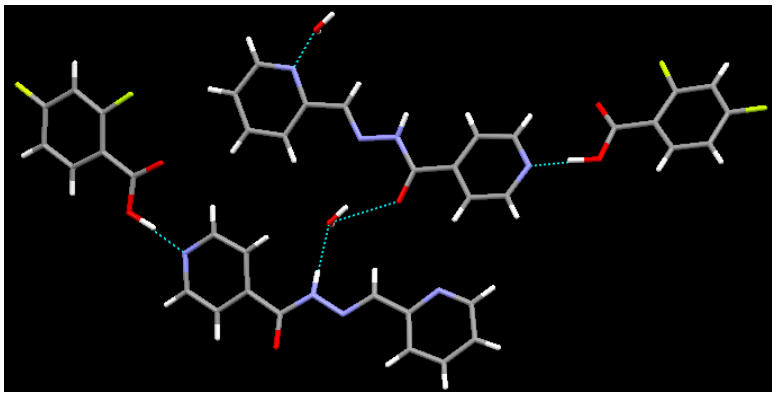

Figure 5.21 Unique hydrogen bond motif of **20F$_2$BA** involving a water molecule.

5.4.10 Crystal structure of 20ABA

In the crystal structure of **20ABA** the asymmetric unit consists of one molecule of **20**, one molecule of **ABA** and one water molecule. Similar to **20FBA**, the carboxylic acid forms a hydrogen bond with the *para*-position pyridine nitrogen of **20**, Figure 5.22.

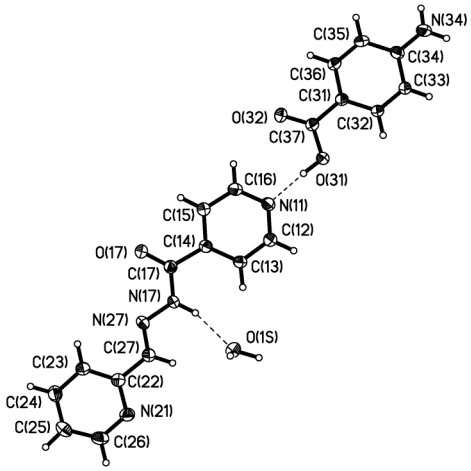

Figure 5.22 Thermal ellipsoids (50%) and labeling scheme of **20ABA**.

Further extension of the architecture of **20ABA**, resulted in an interesting architecture, in that both the pyridine nitrogens participates in some form of hydrogen bond, with bond distances shown in Table 5.1. Moreover, the amide hydrogen of **ABA**

forms a hydrogen bond with the carbonyl of **20**, as well as a amine…acid N-H…O interaction, Figure 5.23.

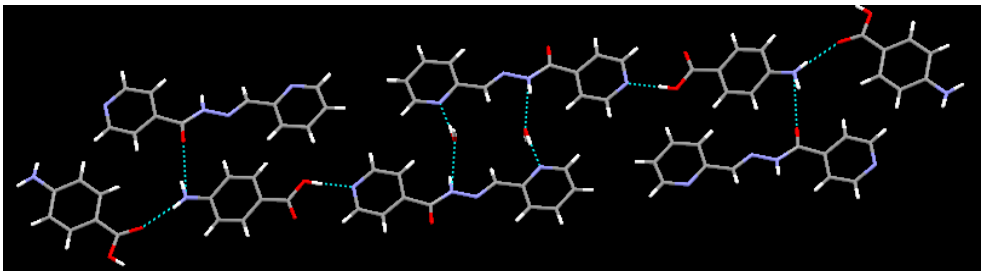

Figure 5.23 Extended architecture of **20ABA**, formed through O-H…N, N-H…O interactions.

5.4.11 Crystal structure of 21SUC

The asymmetric unit of **21SUC** consists of one molecule of **21**, one molecule of **SUC** and two water molecules, with hydrogen bonds between the pyridine nitrogen of **21** and the carboxylic acid, Figure 5.24.

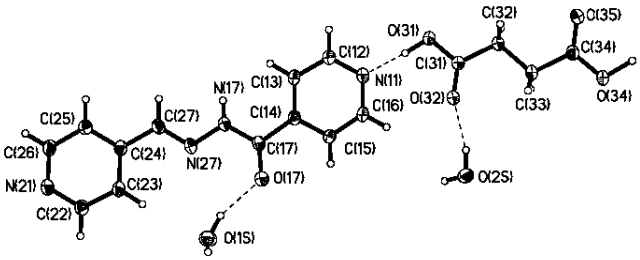

Figure 5.24 Thermal ellipsoids (50%) and labeling scheme of **21SUC**.

A 2-D sheet is produced by hydrogen bonds between the water molecule and the carbonyl and the amide hydrogen of **21**, Figure 5.25.

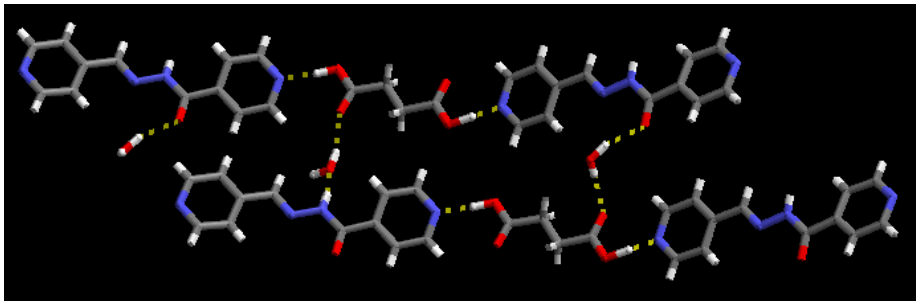

Figure 5.25 2-D motif of **21SUC**, held together by O-H…N, N-H…O and O-H…O hydrogen bonds.

5.4.12 Crystal structure of 21ADI

The asymmetric unit of **21ADI**, contains one molecule of **21**, one molecule of **ADI** and one water molecule, with hydrogen bond formation between the carboxylic acid the pyridine nitrogen of **21**, Figure 5.26.

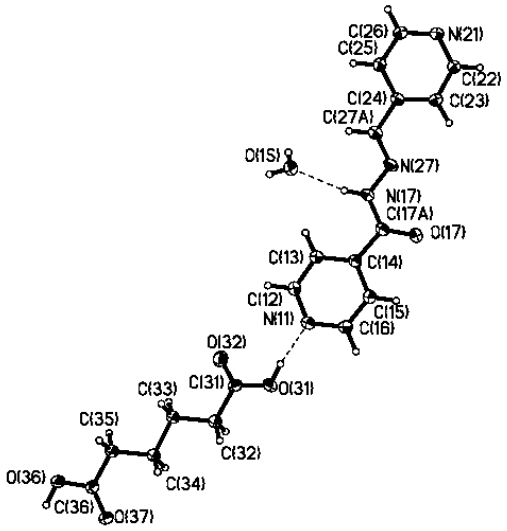

Figure 5.26 Thermal ellipsoids (50%) and labeling scheme of the supermolecule **21ADI**.

21ADI shows similar packing as **21SUC**, with both ends of the acid forming hydrogen bonds with the pyridine nitrogen atoms. Also the structure forms a 2-D sheet via hydrogen bonding between the water and the carbonyl and amide hydrogen of **21**, Figure 5.27.

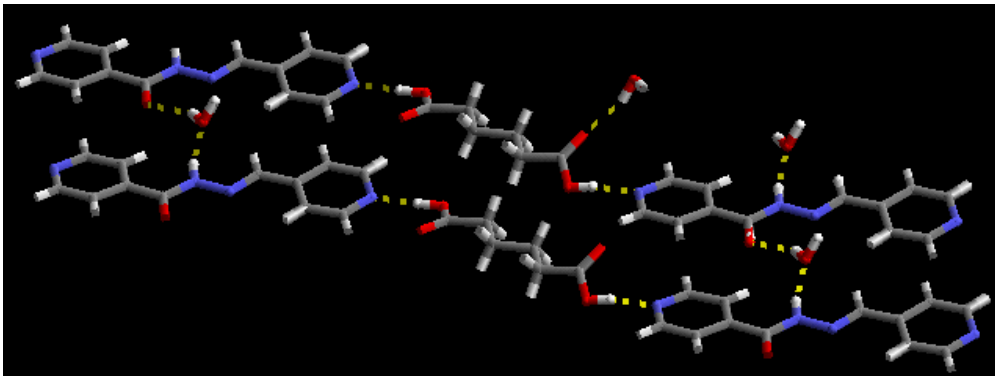

Figure 5.27 2-D architecture **21ADI**, held together by O-H…N, N-H…O and O-H…O hydrogen bonds.

5.4.13 Crystal structure of 21SUB

The asymmetric unit of **21SUB** consists of one molecule of **21**, one molecule of **SUB** and one water molecule. The architecture is similar to that of **21SUC** and **21ADI**, in that the carboxylic acid forms a hydrogen bond with the pyridine nitrogen, Figure 5.28.

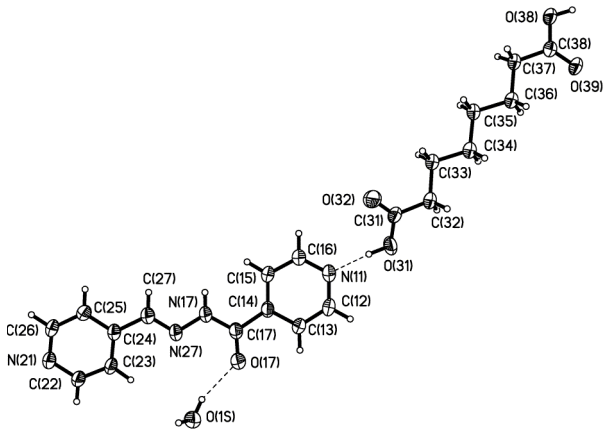

Figure 5.28 Thermal ellipsoids (50%) and labeling scheme of the supermolecule **21SUB**.

The water molecule aids in the formation of the 2-D structure through hydrogen bonding between the amide hydrogen and carbonyl of **21**, Figure 5.29.

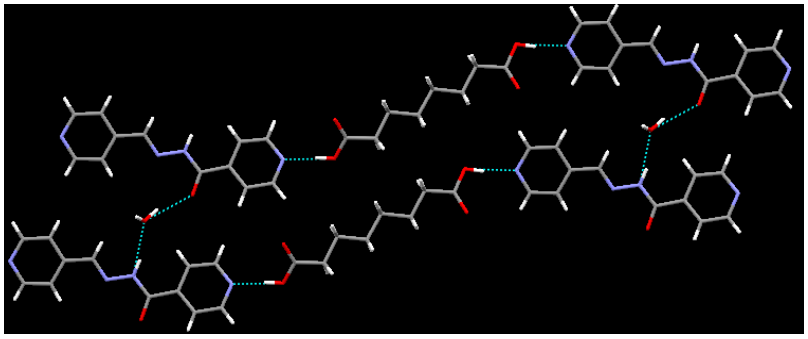

Figure 5.29 2-D sheet in **21SUB** formed via O-H…N, N-H…O and O-H…O hydrogen bonds.

5.4.14 Crystal structure of 23FUM

The crystal structure of **23FUM** has of one molecule of **23** and one molecule of **FUM** in the asymmetric unit. This structure is similar to **20FUM**, in that the acid forms a hydrogen bond with the pyridine nitrogen, Figure 5.30.

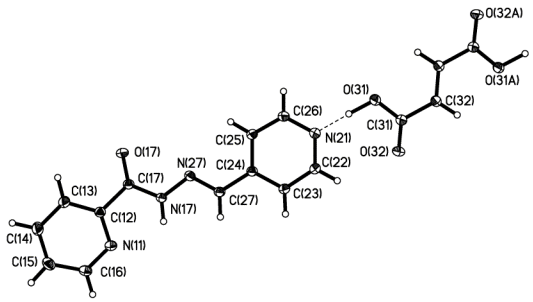

Figure 5.30 Thermal ellipsoids (50%) and labeling scheme of **23FUM**.

The crystal structure does not contain any water molecules but displays a trimer formed through the interaction of both ends of the dicarboxylic acid groups, Figure 5.31. Additionally, no distinct non-covalent interaction was observed with the *ortho*-position nitrogen atom.

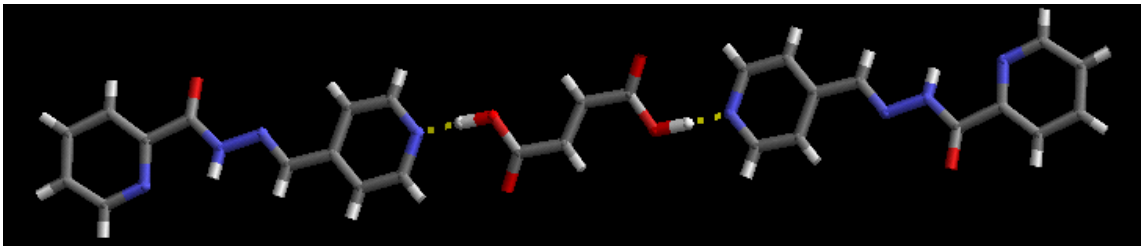

Figure 5.31 Trimer of **23FUM** held together by O-H…N interactions.

5.4.15 Crystal structure of 23GLU

The asymmetric unit of **23GLU** consists of one molecule of **23** and one molecule of **GLU**, held together by hydrogen bonding between the carboxylic acid and the carbonyl of **23**, Figure 5.32.

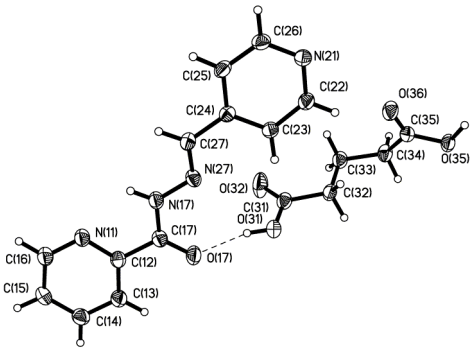

Figure 5.32 Thermal ellipsoids (50%) and labeling scheme of **23GLU**.

The overall 1-D zig-zag motif resulted from the hydrogen bonding interactions at both ends of the dicarboxylic acid and the pyridine nitrogen, Figure 5.33.

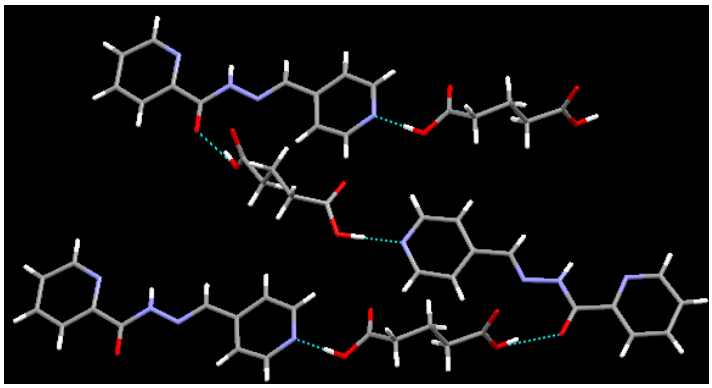

Figure 5.33 1-D zig-zag motif of **23GLU** held together via O-H…N and O-H…O hydrogen bonds.

5.4.16 Crystal structure of 24ADI

The crystal structure of **24ADI** consists of one molecule of **24**, one molecule of **ADI** and two water molecules in the asymmetric unit, however the structure also exhibits some disorder. The structure is held together via hydrogen bonds between the carboxylic acid and pyridine nitrogen, Figure 5.34.

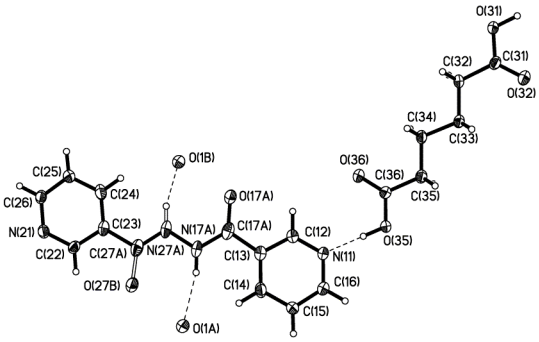

Figure 5.34 Thermal ellipsoids (50%) and labeling of **24ADI**.

A 2-D sheet-like array results from the water molecules hydrogen bonded to both the adjacent carbonyl and amide hydrogen of **24**, Figure 5.35.

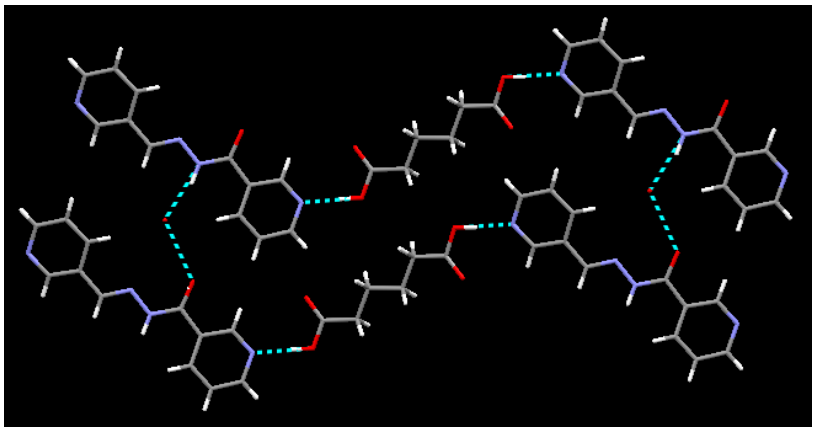

Figure 5.35 2-D array in **24ADI** held together by O-H…N, N-H…O and O-H…O hydrogen bonds.

5.4.17 Crystal structure of 24SUB

The asymmetric unit cell of **24SUB** consists of one molecule of **24**, one molecule of **SUB** and one water molecule. The structure is held together by O-H…N hydrogen-bond interactions between the acid and the pyridine nitrogen, Figure 5.36.

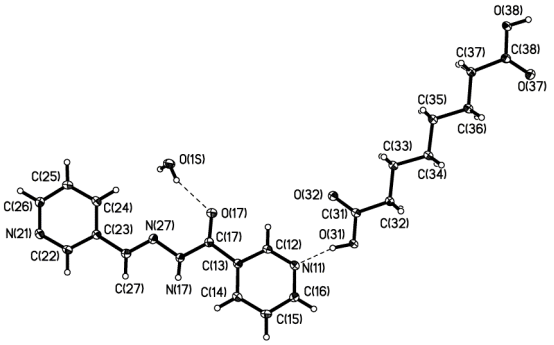

Figure 5.36 Thermal ellipsoids (50%) and labeling of the supermolecule **24SUB**.

A 2-D array similar to that of **24ADI** is formed through hydrogen bonds between the water molecules the carbonyl and amide hydrogen of **24**, Figure 5.37. The water molecule also forms a hydrogen bond with the carbonyl of the acid, with bond distances listed in Table 5.1.

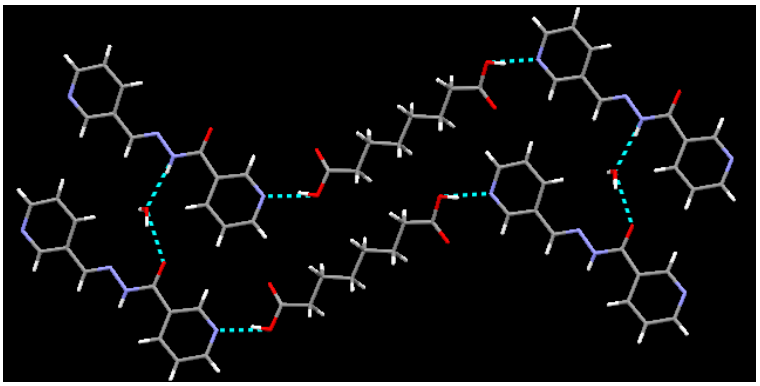

Figure 5.37 2-D array in **24SUB** formed through O-H…N, N-H…O and O-H…O hydrogen bond interactions.

5.5 Discussion

5.5.1 Analyzing compounds via infrared spectroscopy

The infrared spectra of the seventeen compounds prepared in this study indicate the formation of cocrystals in all cases. Broad stretches near 2450 and 1900 cm^{-1} were observed, which are characteristic of intermolecular O-H…N hydrogen bonds that can only come about if the two reactants form heteromeric supramolecular synthons. The vibrational spectra also suggest that the resulting products, in each case exist as molecular cocrystals and not as organic salts. All seventeen compounds, displayed a strong band around 1680 cm^{-1} and a weak band near 1275 cm^{-1} corresponding to C=O and C-O stretches of the carboxylic acid moiety.

Single crystal X-ray data further supported the assignments made on the basis of vibrational spectroscopy. Each carboxylic acid contains two distinctly different C-O bond distances corresponding to the C=O and C-O(H) covalent bonds, and the C-N-C endocyclic bond angle of the heterocyclic moieties fall in the narrow range of 117.1-119.1^{o}, which is indicative of a non-ionized pyridine unit, Table 5.2.[17] In contrast, the C-N-C endocyclic bond angle of a pyridinium cation is 121.1^{o}.[17]

Table 5.2 Distribution of C-O bond lengths for carboxylic acid moieties and C-N-C bond angles for **20OCT, 20HEX, 20FUM, 20ADI, 20SUB, 20SEB, 20FBA, 20NBA, 20F$_2$BA, 20ABA, 21SUC, 21ADI, 21SUB, 23FUM, 23GLU, 24ADI, 24SUB**

Compound	d(C=O) Å	d(C-O) Å	<(C-N-C) ^{o}
20OCT	1.228(3)	1.303(3)	117.8(2)
20HEX	1.229(3)	1.301(3)	116.8(2)
20FUM	1.2295(16)	1.3184(15)	118.19(12)
20ADI	1.210(2)	1.306(2)	118.13(14)
20SUB	1.210(3)	1.297(3)	118.1(2)
20SEB	1.2158(15)	1.3110(15)	117.87(11)
20FBA	1.220(4)	1.291(4)	117.4(3)
20NBA	1.213(4)	1.300(4)	117.8(3)
20F$_2$BA	1.2163(17)	1.3183(18)	117.98(12)
20ABA	1.2217(18)	1.3104(18)	117.54(13)
21SUC	1.203(2)	1.310(2)	118.18(14)
21ADI	1.2112(19)	1.3044(19)	117.52(13)
21SUB	1.215(3)	1.297(3)	117.58(19)
23FUM	1.2228(9)	1.2922(9)	116.98(7)
23GLU	1.204(2)	1.322(2)	116.79(15)
24ADI	1.212(3)	1.325(3)	118.6(3)
24SUB	1.2199(4)	1.3191(13)	118.62(10)

5.5.2 Assessing the co-crystallizing ability of the hydrazones

To better understand the co-crystallizing ability of the series of hydrazones in this study, it is important to look at the possible supramolecular synthons[18] that is taking place when these molecules assemble into supermolecules. From the literature we know that pyridines and carboxylic acids tend to form robust synthons;[19] therefore, the initial assembly of cocrystals should be achieved from interaction between the incoming acid and the pyridyl moiety on the hydrazone fragments. However, each hydrazone has four possible acceptor sites and one donor site Figure 5.38.

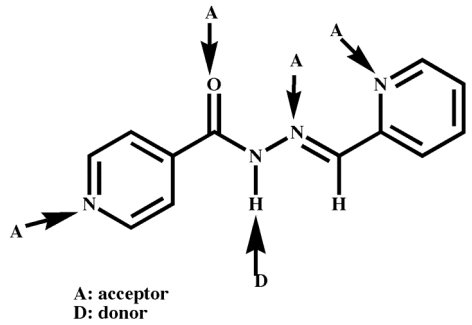

Figure 5.38 Example of a hydrazone depicting the possible acceptor and donor sites.

Therefore, the presence of so many acceptor sites creates some difficulty in accessing the competition of the incoming acid; however the seven possible synthons that can result from their interactions are shown in Figure 5.39.

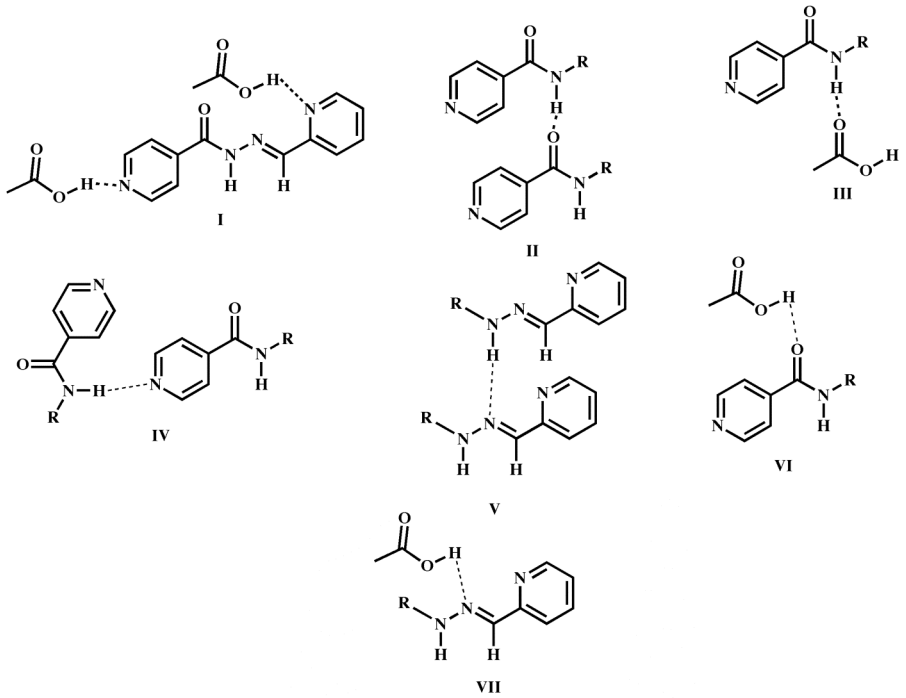

Figure 5.39 Expected acid…pyridine synthon (**I**). Four possible interactions involving N-H hydrogen bond donor: with the amide carbonyl (**II**), with acid carbonyl (**III**), with the pyridine nitrogen (**IV**), with imine nitrogen (**V**) and the carboxylic acid with the amide carbonyl (**VI**), and the imine nitrogen (**VII**).

5.5.2.1 Formation of hydrazones/carboxylic acid cocrystals

In every one of the seventeen cocrystals containing **20**, **21**, **23** and **24** and a carboxylic acid that we have obtained, the intermolecular interaction responsible for the

construction of the main supramolecular assembly is the O-H…N motif between the carboxylic acid and the hydrazone pyridine moieties, Figure 5.40.

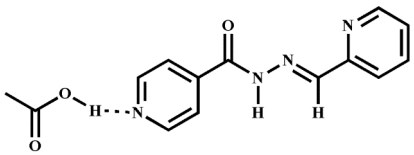

cocrystals	17
primary synthon	hydrazone pyridine/carboxylic acid
# of occurrences	17/17
supramolecular yield	100%

Figure 5.40 Summary of primary hydrogen bonding between **20**, **21**, **23**, **24** and various carboxylic acids.

It is worth emphasizing that the carboxylic acid…pyridine interaction is very effective tool for the assembly of molecular cocrystals,[20] and a search of the CSD[7] reveals forty-nine cocrystals having similar functionality as **20**, **21**, **23** and **24** all assembled via complementary carboxylic acid…pyridine interactions. Undoubtedly, this synthon is a suitable supramolecular tool, capable of bringing together a variety of discrete molecular building blocks into heteromeric molecular cocrystals.

5.5.2.2 Secondary molecular interactions

Other than the primary interaction that takes place between the carboxylic acid and the pyridine moieties, only synthon **VI** from the possible synthons Figure 5.39 was observed in **23GLU**. However we were able to identify two other types of motifs in this series of compounds, Figure 5.41. For simplicity only the carboxylic acid/**20** synthon will be shown.

From the seventeen cocrystals obtained with **20, 21, 23, 24** and carboxylic acids, fourteen of those structures were hydrates, of the fourteen motif **VIII** was observed in twelve of the structures, whereas motif **IX** was only observed in **20F$_2$BA** and **20ABA**. In these two examples water plays an important role in forming a hydrogen bond with the *ortho*-position nitrogen, suggesting that the nitrogen atom is active and should be able to participate in non-covalent interactions.

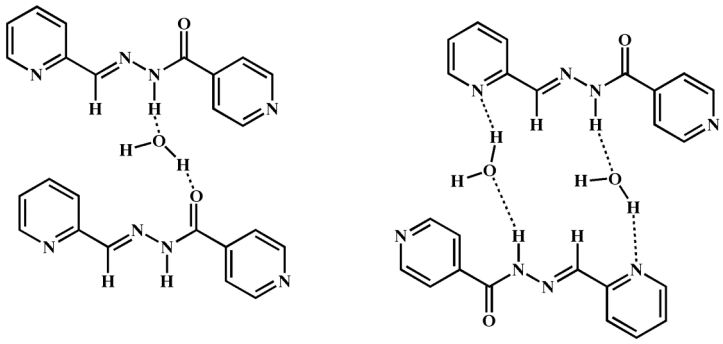

VIII **IX**

# of occurrences	12/14	2/14
percentage	86%	14%

Figure 5.41 Observed motifs between water molecule and cocrystal of **20, 21, 23, 24** and carboxylic acids.

Therefore cocrystals of **20** and **23** offer an excellent comparison of how altering the position of the nitrogen on the aryl ring affects co-crystallization outcome, as well as hydrogen-bond interactions. In **20** the carbonyl group is *para* to the pyridine nitrogen atom, whereas in **23** the carbonyl group is *ortho* to the pyridine nitrogen. However, in the two structures obtained with **23**, not only was there no interaction at the *ortho*-position nitrogen atom, but there was no water molecule present in the structures. Therefore instead of a 2-D layered structure a trimer was observed in one case (**23FUM**) and a 1-D zigzag array in the other case (**23GLU**), Figure 5.42.

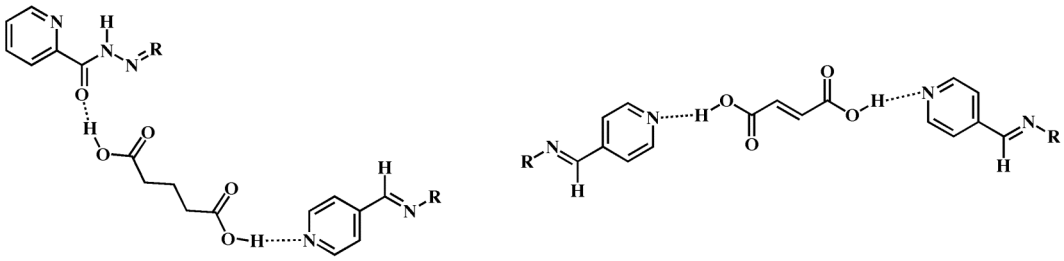

23GLU **23FUM**

Figure 5.42 Binding interactions in the absence of a water molecule.

It is evident that water plays an important role in co-crystallization reactions with **20**, **21**, **23** and **24**. In each case where a water molecule is present in a 2-D layered

structure or step-like motif is formed, whereas in the absence of water the packing is either a 1-D chain or a trimer. These results suggest that the water molecule aids in the formation of the most favorable packing required for this series, a summary of all the observed interactions is shown in Table 5.3.

Table 5.3 Molecular interaction of **20OCT, 20HEX, 20FBA, 20NBA, 20F$_2$BA, 20ABA, 20FUM**, **20ADI**, **20SUB**, **20SEB, 21SUC, 21ADI**, **21SUB, 23FUM**, **23GLU, 24ADI** and **24SUB**

Compounds	*Para*-position nitrogen atom	*Ortho*-position nitrogen atom	Acid carbonyl	API carbonyl	Amide N-H	Structural motif
20OCT	W	X	Y	Y	Y	**I, VIII**
20HEX	W	X	Y	Y	Y	**I, VIII**
20FBA	W	X	Y	Y	Y	**I, VIII**
20NBA	W	X	Y	Y	Y	**I, VIII**
20F$_2$BA	W	Y	Y	Y	Y	**I, IX**
20ABA	W	Y	Z	Z	Y	**I, IX**
20FUM	W	X	X	X	X	**I**
20ADI	W	X	Y	Y	Y	**I, VIII**
20SUB	W	X	Y	Y	Y	**I, VIII**
20SEB	W	X	Y	Y	Y	**I, VIII**
21SUC	W	-	Y	Y	Y	**I, VIII**
21ADI	W	-	Y	Y	Y	**I, VIII**
21SUB	W	-	Y	Y	Y	**I, VIII**
23FUM	W	X	X	X	X	**I**
23GLU	W	X	X	W	V	**I, VI**
24ADI	-	W	Y	Y	Y	**I, VIII**
24SUB	-	W	Y	Y	Y	**I, VIII**

V = hydroxyl oxygen of acid; **W** = hydroxyl group of acid binds; **X** = no interactions; **Y** = water molecule binds; **Z** = binds with the N-H proton from the acid.

5.5.3 Structural consistency of hydrazones

The hydrazones we have studied have proven to be selective in their binding preferences, with only three out of the seventeen cases exhibiting the absence of a water molecule in the lattice of the structure. From the twelve cocrystals of **20** and **23** only two

times does the *ortho*-position nitrogen atom form a hydrogen bond. A summary of the binding between pyridine nitrogen and the carboxylic acids of the four APIs in the study is shown in Figure 5.43.

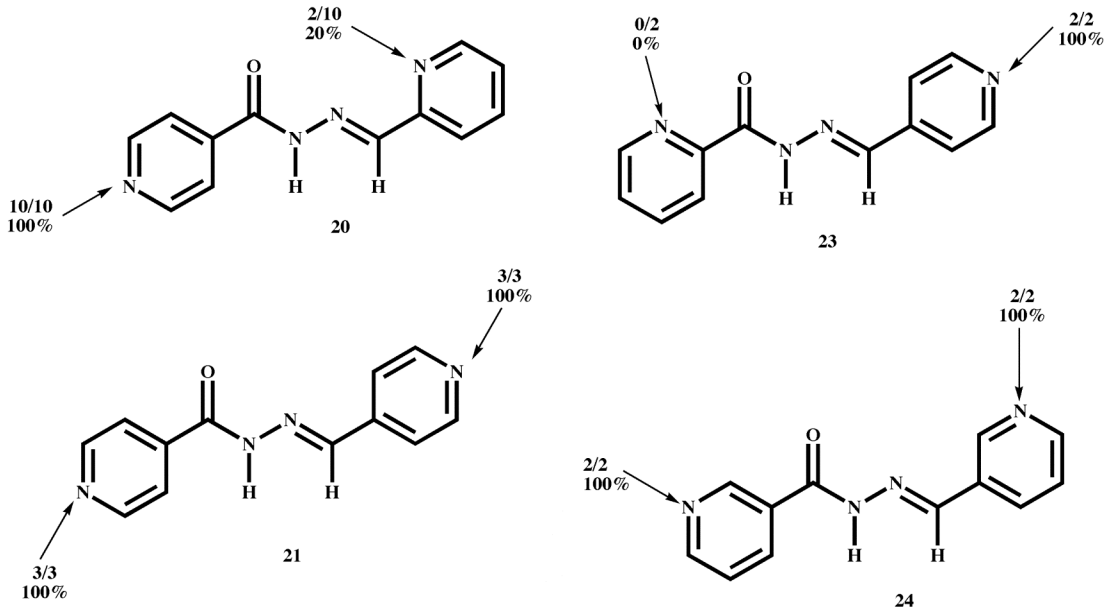

Figure 5.43 Binding preferences of API with carboxylic acids.

The cocrystals present in this study exemplify remarkable structural consistency, in that hydrates were observed fourteen out of seventeen times. The water molecule also formed hydrogen bonds thirteen out of seventeen times with both the API carbonyl as well as with the acid carbonyl, Figure 5.44.

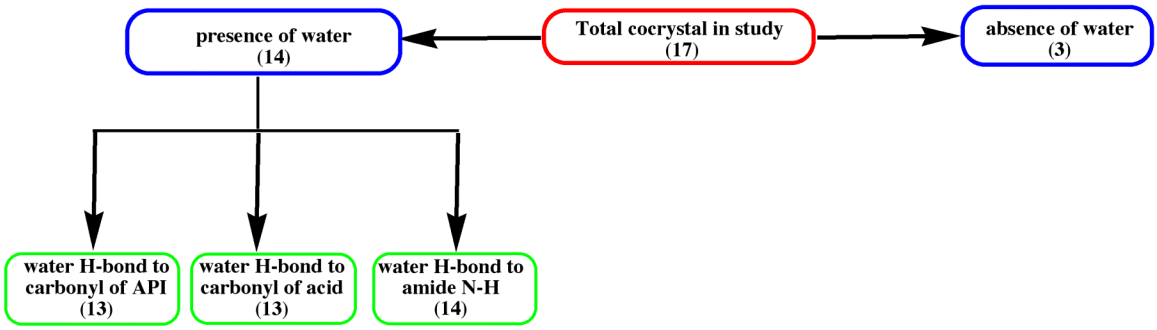

Figure 5.44 Classification of crystal structures obtained from supramolecular reactions between APIs and a variety of acids. The numbers obtained in each case are in brackets.

Although only two of the possible synthons were observed in this study, the hydrazone family of compounds tends to form cocrystals readily. Additionally, the water molecule demonstrates great selectively towards both the carbonyl of the API and acid as well as the N-H amide.

5.5.4 Probing the ortho-position nitrogen in the formation of cocrystal

Based on the cocrystals obtained for both **20** and **23**, it begs the question, what would happen if the nitrogen atom *para* to the carbonyl was not present in the ring? Would that force the *ortho*-position nitrogen to participate in hydrogen bonding with incoming acids? Thus to answer these questions compound **25** was synthesized Figure 5.45 and setup with the same series of acids used with **20** and **23**.

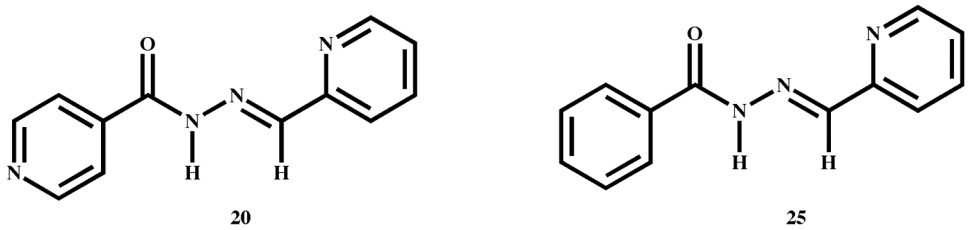

Figure 5.45 Comparison between **20** and **25**.

Cocrystal screening was carried out using FT-IR with particular attention focused to the 1900 and 2500 cm^{-1} region of the IR spectra, which is indicative of the formation of O-H…N hydrogen bonding. Based on the FT-IR obtained eleven out of eleven times no O-H…N stretches were observed in the FT-IR; examples are shown in Figure 5.46 (**25NBA**) and Figure 5.47 (**25FUM**).

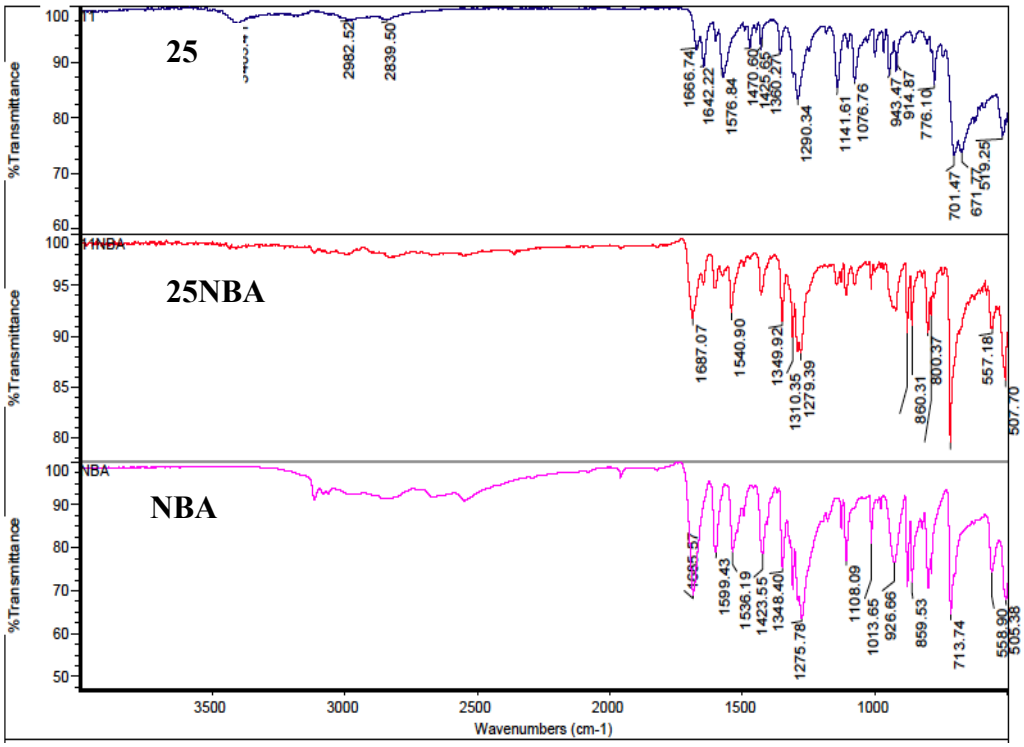

Figure 5.46 FT-IR of **25NBA**: **25**(dark blue), **25NBA** (red) and **NBA** (pink).

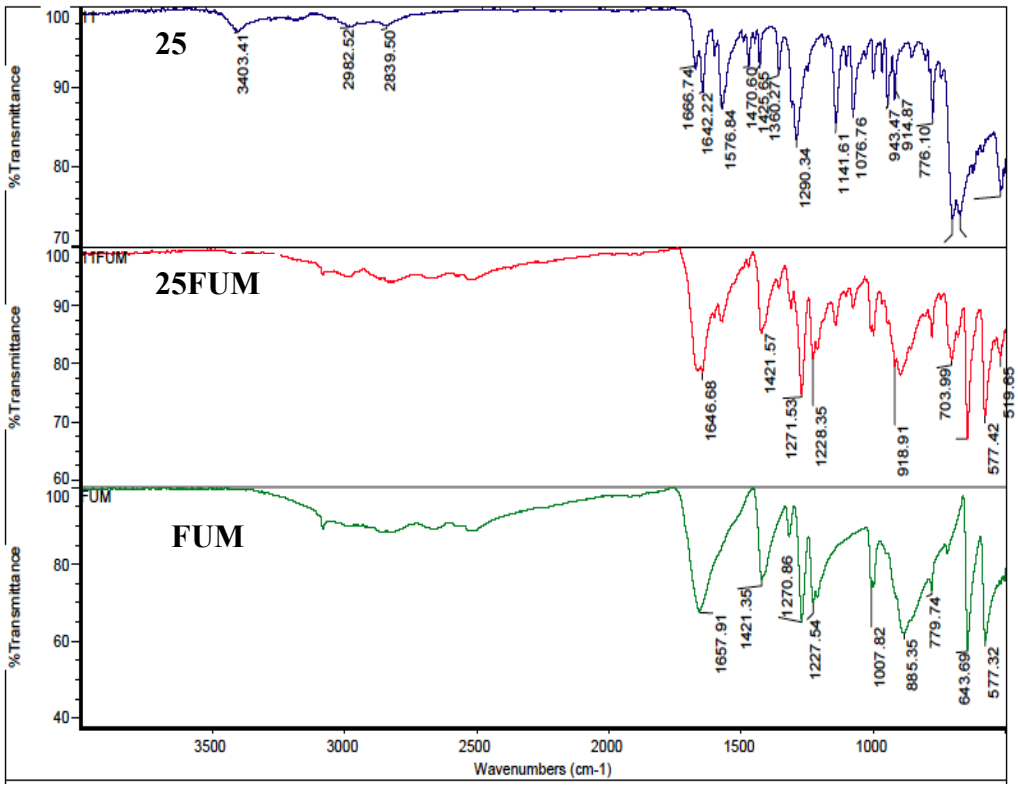

Figure 5.47 FT-IR of **25FUM**: **25**(dark blue), **25FUM** (red) and **FUM** (green).

From the two figures not only are the two prominent stretches missing but there are also no significant shifts of the carbonyl stretches in **25** or any of the acids observed in the **25NBA** or **25FUM**. Even though a water molecule is able to bind to the *ortho*-position nitrogen, the incoming acid is unable to bind. This may be as a result of the type of packing preferred by the molecule making it difficult for larger molecules to come in and interact with the *ortho*-position nitrogen atom.

5.5.4 Probing the melting behavior of cocrystals of 20

Melting point is a fundamental physical property and since we obtain structural consistency we decided to examine the melting behavior of cocrystals obtained with **20OCT**, **20NBA**, **20FBA**, **20F$_2$BA**, **20SUC**, **20ADI**, **20SUB**, **20SEB**.

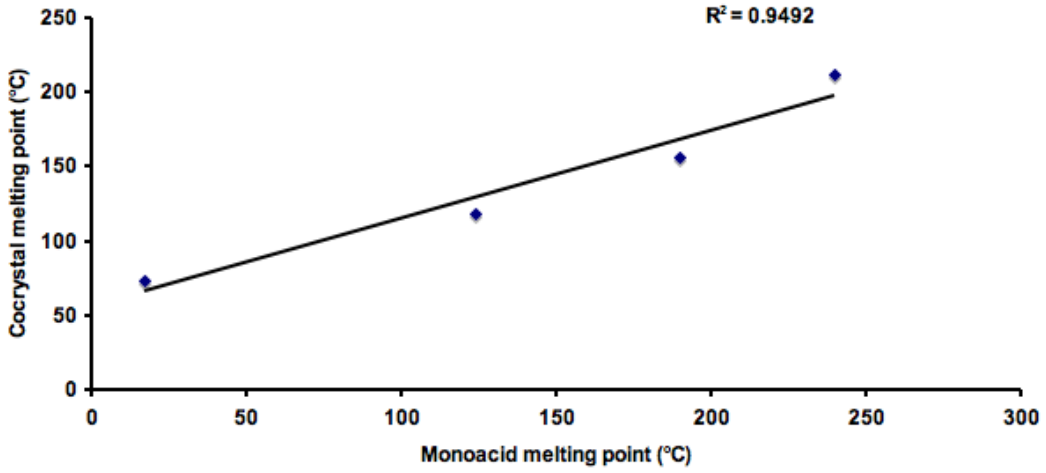

Figure 5.48 Melting point correlation profile of **20OCT, 20NBA, 20FBA** and **20F$_2$BA**.

The melting points of the five cocrystals are plotted against the melting points of the corresponding monoacids. Melting point of **20** is 168-171°C and from the graph upon co-crystallization with **F$_2$BA** and **NBA** an increase in melting point is observed, whereas the opposite is observed with cocrystal formed with **OCT** and **FBA**. This resulted in a positive correlation between the melting point of the acid and that of the corresponding cocrystal, Figure 5.48.

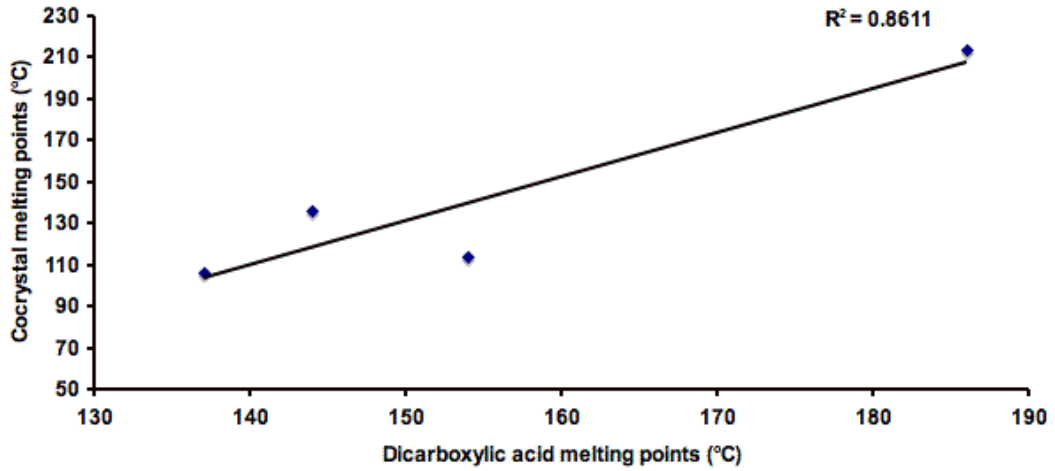

Figure 5.49 Melting point correlation for **20SUC**, **20ADI**, **20SUB** and **20SEB**.

Likewise cocrystals with **20** and dicarboxylic acids also displayed similar trends, (Figure 5.49) as carbon chain length of the acids increases the melting point of the cocrystals decreases. Using linear regression, a correlation coefficient of 0.8611 was found, indicating that 86% of the variability in cocrystal melting points can be explained by variability in the melting point of the co-crystallizing agent.

These findings suggest that the melting behavior of these crystalline solids are directly related to the melting points in the carboxylic acids. The highest-melting cocrystal contains the dicarboxylic acid with the highest melting point, and the lowest-melting acid produces the lowest melting cocrystal; suggesting that the melting behavior of the solid forms of this API can be modified over a considerable range (74-212°C) and (106-214°C), with mono-and di-carboxylic acids respectively. Moreover, the relationship between cocrystal and cocrystal former melting points has previously been reported for a series of 2-acetaminopyridine cocrystals with various acids.[8]

5.6 Conclusion

Four APIs were synthesized and seventeen cocrystals were obtained, resulting in fourteen hydrates. In **20** two of the ten crystal structures had the nitrogen atom *ortho* to the carbonyl participating in hydrogen bonding from a water molecule.

The absence of nitrogen atom from the aryl ring **25** resulted in no cocrystal formation, suggesting that maybe these types of compounds prefer to pack in a certain manner. Thus, in each case a water molecule is present in the crystalline lattice to satisfy or counter balance the acceptor to donor ratio present in the compounds.

Nevertheless, this study highlighted the structural consistency as well as the capability of the hydrazones to form cocrystals. It also highlights the difficulty in predicting the possible molecular interactions with any given acid.

In addition, the results demonstrated that melting point behavior can be correlated to the molecular properties of the co-crystallizing agent, thus providing more insight into how we can fine-tune the melting behavior of a particular API without making or breaking of covalent bonds.

References

[1] (a) Hancock, B.C.; Zografi, G. *J. Pharm. Sci*., **1997**, 86, 1; (b) Datta, S.; Grant, D.J.W. *Nature Rev. Drug Discovery*, **2004**, 3, 42; (c) Huang, L.F.; Tong, W.Q. Adv. *Drug Delivery Rev*. **2004**, 56, 321.

[2] Bryn, S.E.; Pfeiffer, R.R.; Stowell, J.G. *Solid State Chemistry of Drugs*; SSCI, Inc.: West Lafayette, 1999.

[3] Phadnis, N.V.; Suryanarayanan, R. J. Pharm. Sci. 1997, 86, 1256.

[4] (a) Otsuka, M.; Hasegawa, H.; Matsuda, Y. *Chem. Pharm. Bull*. **1997**, 45, 894; (b) Otsuka, M.; Hasegawa, H.; Matsuda, Y. *Chem. Pharm. Bull.* **1999**, 47, 852.

[5] Otsuka, M.; Nakanishi, M.; Matsuda, Y. *Drug Dev. Ind. Pharm*. **1999**, 25, 205.

[6] (a) Aakeröy, C.B.; Desper, J.; Helfrich, B.A. *Cryst. Eng. Comm.* **2004**, 6, 19; (b) Aakeröy, C.B.; Beatty, A.M.; Nieuwenhuyzen, M.; Zou, M. *J. Mater. Chem*. **1998**, 8, 1385; (c) Shan, S.; Batchelor, E.; Jones, W. *Tetrahedron Lett*. **2002**, 43, 8721; (d) Bailey Walsh, R.D.; Bradner, M.W.; Fleischman, S.; Morales, L.A.; Moulton, B.; Rodriguez-Hornedo, N.; Zaworotko, J.L.; Ripmeester, J.A. *J. Am. Chem. Soc.* **2000**, 122, 7817; (e) Vishweshwar, P.; Thaimattam, R.; Jaskolski, M.; Desiraju, G.R. *Chem. Commun*. **2002**, 1830; (f) Lehn, J.M.; Mascal, M.; DeCian, A.; Fischer, J. *J. Chem. Soc. Chem. Commun*. **1990**, 479.

[7] Allen, F.A. *Acta Crystallogr*. **2002**, B58, 380.

[8] Aakeröy, C.B.; Hussain, I.; Desper, J. *Crystal Growth Des*. **2006**, 6, 474.

[9] Aakeröy, C.B.; Hussain, I.; Forbes, S.; Desper, J. *CrystEngComm*. **2007**, 9, 46.

[10] Childs, S.L.; Hardcastle, K.I. *Cryst. Growth Des*. **2007**, 7, 1291.

[11] (a) Aakeröy, C.B.; Beatty, A.M.; Helfrich, B.A. *J. Am. Chem. Soc*. **2002**, 124, 14425; (b) Vishweshwar, P.; Nangia, A.; Lynch, V.M. *Cryst. Growth Des*. **2003**, 3, 783.

[12] (a) Richardson, D.R.; Becker, E.; Bernhardt, P.V. *Acta Cryst*. **1999**, C55, 2102; (b) Richardson, D.R. *Expert Opin. Investig. Drugs* **2003**, 12, 235; (c) Becker, E.; Lovejoy, D.B.; Greer, J.M.; Watts, R.; Richard, D.R. *British J. Pharm*. **2003**, 138, 819; (d) Armstrong, C.M.; Bernhardt, P.V.; Chin, P.; Richardson, D.R. *Eur. J. Inorg. Chem.* **2003**, 1145; (e) Bernhardt, P.V.; Chin, P.; Sharpe P.C.; Wang, J.-Y.C.; Richardson, D.R. *J. Biol. Inorg. Chem*. **2005**, 10, 761.

[13] (a) Johnson, D.K.; Murphy, T.B.; Rose, N.J. *Inorganica Chimica Acta*, **1982**, 67, 159; (b) Richard, D.R.; Becker, E.; Bernhardt, P.V.; *Acta Crystallographica. Section C* **1999**, 55, 2102.

[14] Xu, C.; Mao, H.; Shen, X.; Zhang, H.; Liu, H.; Wu, Q.; Zhu, Y. *J. Coordination Chemistry*, **2007**, 60, 193.

[15] Zhao, X.; Wang, X.-Z.; Jiang, X.-K.; Chen, Y.-Q.; Li, Z.-T.; Chen, G.-J. *J. Am. Chem. Soc*. **2003**, 125, 15128.

[16] Lima, P.C.; Lima, L.M.; da Silva, K.C.M.; Leda, P.H.-O.; de Miranda, A.L.P.; Fraga, C.A.M.; Barreiro, E.J. *Eur. J. Med. Chem*. **2000**, 35, 187.

[17] (a) Boenigk, D.; Mootz, D. *J. Am. Chem. Soc*. **1988**, 110, 2135; (b) Cowan, J.A.; Howard, J.A.K.; McIntyre, G.J.; Lo, S.; M.-F.; Williams, I.D. *Acta Crystallogr*. **2003**, B59, 794.

[18] Desiraju, G.R. *Angew. Chem. Int. Ed. Engl*. **1995**, 34, 2311.

[19] (a) Kane, J. J.; Liao, R.-F.; Lauher, J.W. and Fowler, F.W. *J. Am. Chem. Soc*. **1995**, 117, 12003; (b) Grunert, M.; Howie, R.A.; Kaeding, A.; Imrie, C.T. *J. Mater. Chem*. **1997**, 7, 211; (c) Vishweshwar, P.; Nangia, A.; Lynch, V.M. *J. Org. Chem*. **2002**, 67, 556; (d) Palmore, G.T.R.; Luo, T.-J.M.; McBride-Wieser, M.T.; Picciotto, E.A.; Reynoso-Paz, C.M. *Chem. Mater*. **1999**, 11, 3315; (e) Aakeröy, C.B.; Beatty, A.M.; Tremayne, M.; Rowe, D. *Cryst. Growth Des*. **2001**, 1, 377; (f) Sharma, C.V.K.; Zaworotko, M. J. *Chem. Commun*. **1996**, 2655, (g) Pedireddi, V.R.; Chatterjee, S. and Ranganathan, A. *Tetrahedron* **1998**, 54, 9457, (h) Amai, M.; Endo, T.; Nagase, H.; Ueda, H.; Nakagaki, M. *Acta Crystallogr*. **1998**, C54, 1367.

[20] (a) Shan, N.; Bond, A. D.; Jones, W. *New J. Chem*. **2003**, *2*, 365; (b) Arora, K. K.; Pedireddi, V. R. *J. Org. Chem*. **2003**, *67*, 556; (c) Sugiyama, T.; Meng, J.; Matsuura, T. *J. Mol. Struct*. **2002**, *611*, 53; (d) Shan, N.; Batchelor, E.; Jones, W. *Tetrahedron Lett*. **2002**, *43*, 8721; (e) Bhogala, B. R.; Nangia, A. *Cryst. Growth Des*. **2002**, *2*, 325; (f) Zaworotko, M. J. *Chem. Commun*. **2001**, 1.

CHAPTER 6 - Using cocrystal to systematically modulate aqueous solubility and melting behavior of neoplasm inhibitors containing alkyenebisamides

6.1 Introduction

During development and formulation of any active pharmaceutical ingredient (API) that is to be delivered in a solid form, a wide range of stringent performance parameters such as solubility, dissolution rate, bioavailability, thermal stability, and hygroscopicity *etc.* needs to be carefully considered.[1] It is therefore not surprising that poor biopharmaceutical properties (as opposed to toxicity or lack of efficacy) [2] is the main reason that less than one percent of active compounds eventually make it onto the market place.[3] Poor solubility remains a key issue,[4] and a number of approaches for addressing this issue have been pursued such as micronization which can increase surface area,[5] the use of salt forms with enhanced dissolution profiles,[6] solubilization of drugs in co-solvents[7] and micellar solutions.[8,9,10] Although these techniques can be effective, there is still a great need for a broader range of solid forms from which to choose a particular API in order to optimize physico-chemical properties without tampering with the intrinsic biological activity.

Recent advances in crystal engineering[11] have enabled the design of cocrystals where two or more molecular compounds are incorporated within the same crystalline lattices in specific stoichiometric amounts.[12] Cocrystal synthesis does not involve making/breaking of covalent bonds, and it may therefore be possible to fine-tune physical properties by exercising precise control over the supramolecular assembly since the crystal structure determines the resulting physical properties of the compound.

There have been several examples in literature where co-crystallization has been used as a tool for improving the physical properties of a given API.[13] One notable example is 2-[4-(4-chloro-2-fluorophenoxy)phenyl]pyrimidine-4-carboxamide co-crystallized with glutaric acid, which showed an increase in the aqueous dissolution rate of eighteen times as compared to the homomeric crystalline form of the drug.[14] Additionally, single dose dog exposure studies confirmed that the cocrystal increased the

area under the plasma concentration-time curve (AUC) values by three times at two different dose levels.[14] These results and others demonstrate the importance of cocrystals as an additional class of crystalline solid forms with desired physical properties.

Furthermore, structural and physical properties have been shown to be directly correlated in a series of even-chained aliphatic dicarboxylic acids, where the melting point decreases monotonically with increasing number of methylene groups in the chain. The structural consistency among these five compounds, Figure 6.1, translates to a predictable relationship between molecular structure (number of carbon atoms in the chain) and the melting point.[15]

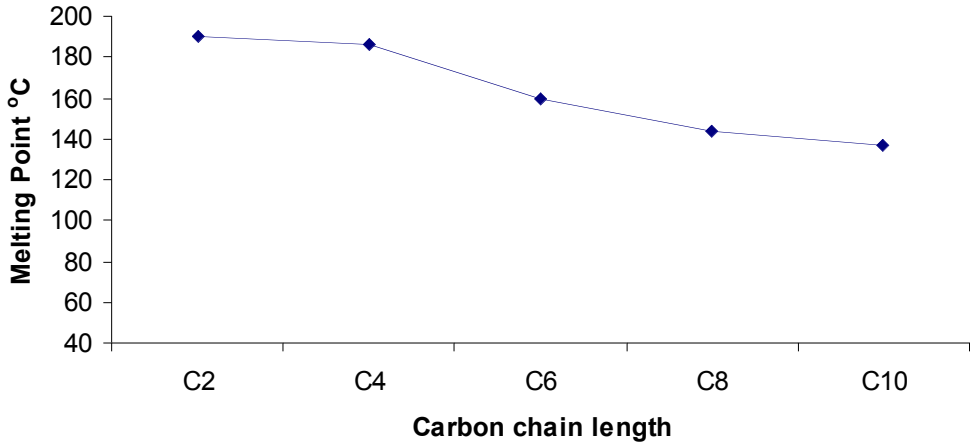

Figure 6.1 The melting points of even chain aliphatic acids as a function of carbon chain length.

However, the melting point of odd-chain dicarboxylic acid is significantly lower than their even-numbered analogues as a result of significant differences in crystal structure/packing.[15]

Consequently, we hypothesize that if we can incorporate an API within a series of crystalline solids characterized by considerable structural consistency, we may be able to fine-tune melting behavior and aqueous solubility. Changes to the physical properties could be achieved by varying the co-crystallizing agents in a systematic fashion without altering the precise nature of the molecular recognition events that drive the supramolecular assembly.

In this study we present a systematic structure-property study of a series of cocrystals with neoplasm inhibitors containing alkylenebisamide, which are capable of inhibiting the proliferation of lung cancer cells.[16] Our strategy was to synthesize infinite API…acid…API…acid chains using the well-known carboxylic acid…pyridine hydrogen bond based synthon,[17] Figure 6.2 (top), and these chains will subsequently be arranged into 2-D layers as a result of API-based self-complementary amide…amide hydrogen bonds,[18] Figure 6.2(bottom). The FDA generally regards all the acids used in this study as safe.[19]

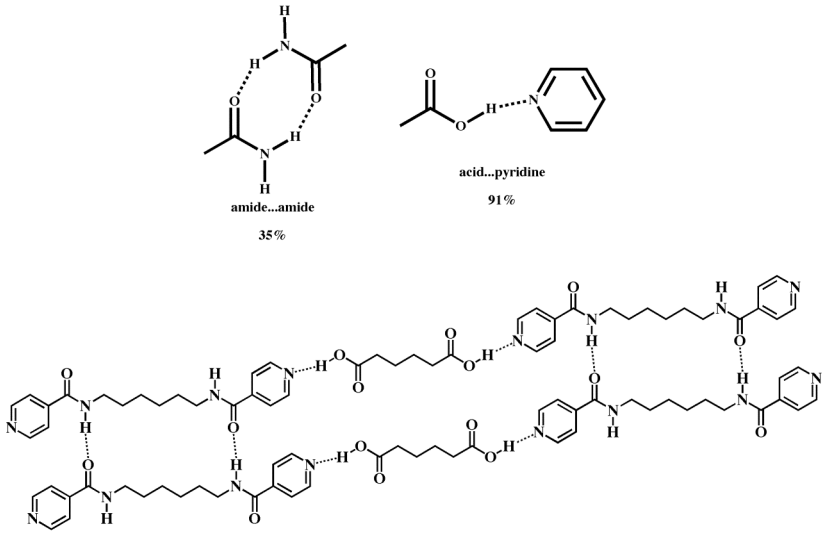

Figure 6.2 Example of the robust and well-known acid…pyridine heterosynthon and amide…amide homosynthon as well as anticipated 2-D layer.

Therefore with the above in mind we synthesized the target alkylene-pyridinecarboxamide compounds **26-33**, Figure 6.3.

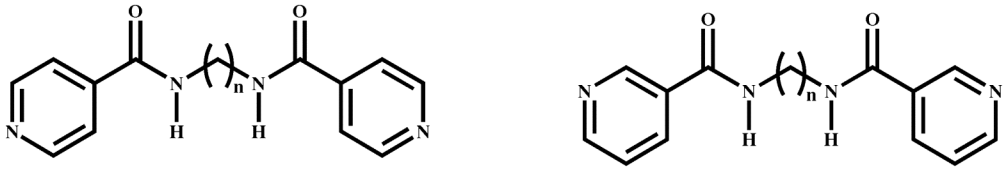

26	n = 0	**30**	n = 0
27	n = 4	**31**	n = 4
28	n = 6	**32**	n = 6
29	n = 8	**33**	n = 8

Figure 6.3 Target APIs

The main objectives of this study are:

1. To determine whether we can synthesize a series of cocrystals with the desired structural consistency.
2. To establish how well the melting point of the cocrystal can be correlated with the nature of the co-crystallizing agent.
3. To establish whether the solubility can be modulated.

6.2 Experimental

6.2.1 Synthesis

All chemicals, unless noted were purchased from Aldrich and Alfa Aesar and used without further purification. Column chromatography was carried out on silica gel (150 Å pore size) from Analtech Inc. Melting points were determined on a GallenKamp melting point apparatus in a capillary tube and are uncorrected. ^{1}H and ^{13}C NMR spectra were recorded on a Varian Unity plus 400 MHz or 200 MHz spectrometers in $CDCl_3$ or DMSO-d_6. Compounds were prepared for infrared spectroscopic (FT-IR) analysis as a mixture in KBr or on a ZnSe ATR crystal.

6.2.1.1 Synthesis of N,N'-Bis(isonicotinic acid)hydrazide, 26[20]

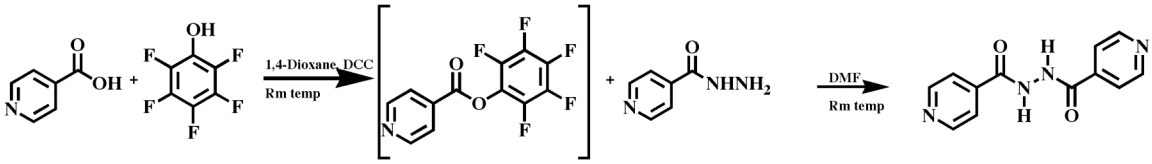

Isonicotinic acid (1.23g, 0.010 mol), pentafluorophenol (2.02g, 0.011 mol) and dicyclohexylcarbodimide (DCC) (2.06g, 0.010 mol) was dissolved in 40 mL of dry 1,4-dioxane and allowed to stir at room temperature for 24 hrs, after which a white precipitate of dicyclohexylurea was observed, filtered off and discarded. The filtrate was evaporated to give a yellow oil of pentafluorophenol isonicotinate, which was not purified. To the oil 30 mL of dimethylformamide (DMF) and isoniazid (1.51g, 0.011 mol) were added and left to stir at room temperature for 36 hrs. The solvent was then evaporated on a rotary

evaporator to produce the crude compound as a light brown solid, which was purified via column chromatography on silica with ethyl acetate as the eluant. The product **26** was isolated as a light yellow powder and recrystallization from ethanol gave microcrystalline particles, (1.98g, 66%). M.p.: 260-261°C; (Lit. m.p.: 267-268°C);[21] ^{1}H NMR (δ_H; 200 MHz, DMSO-d_6): 10.97 (s, 2H), 8.82 (d, 4H, J = 4.8Hz) 7.83 (d, 4H, J = 4.8Hz); IR (KBr pellet): υ 3168, 1639, 1514, 1241, 1121, 997 cm^{-1}.

6.2.1.2 Synthesis of N,N'-1,4-butanediylbis-4-pyridinecarboxamide, 27[22]

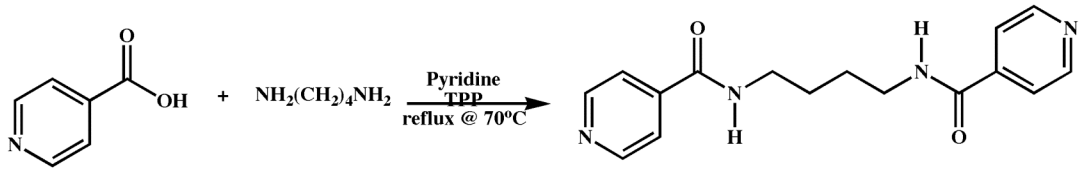

1,4-Diaminobutane (1.21g, 0.012 mol) was slowly added to a pyridine solution (50 mL) of isonicotinic acid (2.95g, 0.024 mol). The mixture was stirred for 15 minutes and triphenyl phosphite (TPP) (6.29 mL, 0.024 mol) was slowly added with a dropping funnel over a period of 15 minutes. The mixture was refluxed for 6 hrs at 70°C and the volume was reduced to 10 mL under vacuum. The solution was left to stand at room temperature for 24 hrs. After 24 hrs a light peach precipitate was observed and the solid was filtered off and washed numerous time with cold water. The solid obtained was recrystallized in ethanol to produce white microcrystalline particles (3.15g, 88%). M.p.: 230-232°C, (Lit. m.p.: 230-232°C).[23] ^{1}H NMR (δ_H; 200 MHz, DMSO-d_6): 8.79 (s, 2H), 8.73 (d, 2H, J = 4.8Hz), 7.76 (d, 2H, J = 4.8Hz), 3.33 (4H, m); IR (KBr pellet): υ 3301, 3055, 2832, 1638, 1531, 1415, 1291, 1115, 997 cm^{-1}.

6.2.1.3 Synthesis of N,N'-1,6-hexanediylbis-4-pyridinecarboxamide, 28[22]

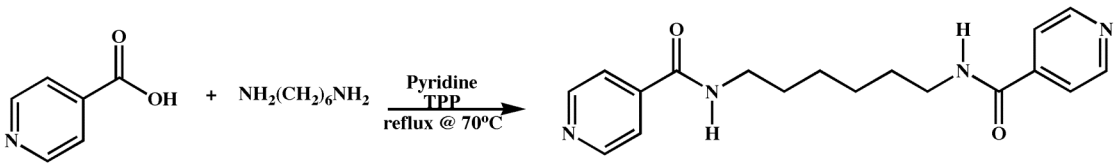

1,6-Diaminohexane (1.98g, 0.017 mol) was slowly added to a pyridine solution (50 mL) of isonicotinic acid (4.20g, 0.034 mol). The mixture was stirred for 15 minutes

and TPP (9 mL, 0.034 mol) was slowly added with a dropping funnel over a period of 15 minutes. The mixture was refluxed for 6 hrs at 70°C and the volume was reduced to 10 mL under vacuum. The solution was left to stand at room temperature for 24 hrs after which a light peach precipitate was observed and the solid was filtered off and washed numerous times with cold water. The solid obtained was recrystallized in ethanol to produce white crystalline particles (2.717g, 50%). M.p.: 181-182°C, (Lit. m.p.: 178-180°C).[23] ^{1}H NMR (δ_H; 400 MHz, DMSO-d_6): 8.72 (d, *J* =5.49Hz, 4H), 7.74 (d, *J* = 5.49Hz, 4H), 3.26 (m, 4H), 1.53 (m, 4H), 1.34 (m, 4H); ^{13}C NMR (δ_C; 200 MHz, DMSO-d_6): 163, 149, 140, 120, 28, 25; IR (KBr pellet): υ 3305, 2937, 2872, 1630, 1529, 1466, 1409, 1293, 1070, 992 cm^{-1}.

6.2.1.4 Synthesis of N,N'-1,8-octanediylbis-4-pyridinecarboxamide, 29[22]

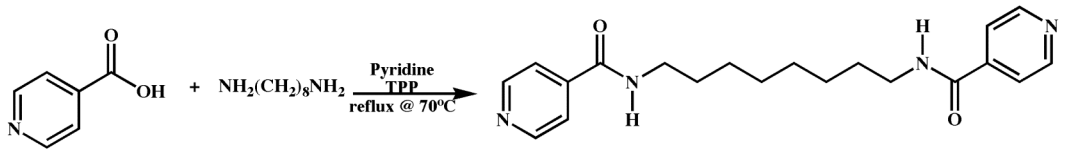

1,8-Diaminooctane (2.73g, 0.012 mol) was slowly added to a pyridine solution (50 mL) of isonicotinic acid (2.95g, 0.024 mol). The mixture was stirred for 15 minutes and triphenyl phosphite (TPP) (6.29 mL, 0.024 mol) was slowly added with a dropping funnel over a period of 15 minutes. The mixture was refluxed for 6 hrs at 70°C and the volume was reduced to 10 mL under vacuum. The solution was left to stand at room temperature for 24 hrs after a creamy precipitate was observed the solid was filtered off and washed with cold water (5 x 100 mL). The solid obtained was recrystallized in ethanol to produce off-white crystalline particles (2.41g, 57%). M.p.: 168-170°C, (Lit. m.p.: 165-166°C).[23] ^{1}H NMR (δ_H; 400 MHz, DMSO-d_6): 8.72 (d, 2H, J = 5.8Hz), 7.75 (d, 2H, J = 5.8Hz), 3.27 (m, 4H), 1.51 (m, 4H); ^{13}C NMR (δ_C; 400 MHz, D_6-DMSO): 164, 150, 141, 121, 28, 26; IR (KBr pellet): υ 3316, 2929, 1633, 1589, 1526, 1477, 1290, 1183, 937 cm^{-1}.

6.2.1.5 Synthesis of N,N'-Bis(nicotinic acid)hydrazide, 30[20]

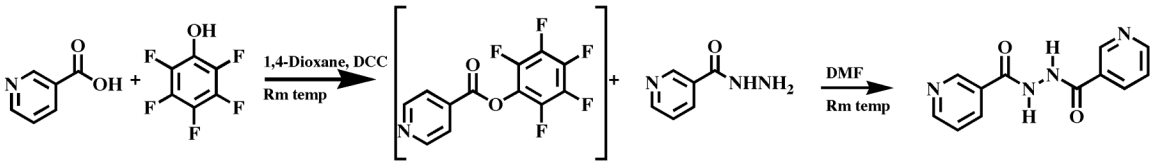

Nicotinic acid (1.23g, 0.010 mol), pentafluorophenol (2.02g, 0.011 mol) and dicyclohexylcarbodimide (DCC) (2.06g, 0.010 mol) was dissolved in 40 mL of dry 1,4-dioxane and allowed to stir at room temperature for 24 hrs after which a white precipitate of dicyclohexylurea was observed and filtered off and discarded. The filtrate was evaporated to give a yellow oil of pentafluorophenol isonicotinate, which was not purified. To this oil, 30 mL of dimethylformamide (DMF) and nicotinic hydrazide (1.4g, 0.01 mol) were added and left to stir at room temperature for 36 hrs. The solvent was then evaporated on a rotary evaporator to produce the crude compound as a light yellow solid. Product **30** was recrystallization from ethyl acetate as light yellow crystalline particles, (2.60g, 87%). M.p. 230-232°C; (Lit. m.p.: 229-232°C);[24] ^{1}H NMR (δ_H; 200 MHz, DMSO-d_6): 10.85 (s, 2H), 9.0 3(s, 2H) 8.81 (d, 2H, J = 4.8Hz), 8.29 (d, 2H, J = 6.2Hz), 7.62 (m, 2H); IR (KBr pellet): υ 3160, 2996, 1634, 1511, 1295, 1121, 997 cm^{-1}.

6.2.1.6 Synthesis of N,N'-1,4-butanediylbis-3-pyridinecarboxamide, 31[22]

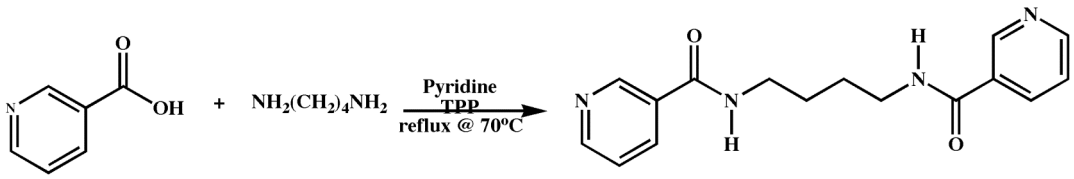

1,4-Diaminobutane (1.21g, 0.012 mol) was slowly added to a pyridine solution (50 mL) of nicotinic acid (2.95g, 0.024 mol). The mixture was stirred for 15 minutes and TPP (6.29 mL, 0.024 mol) was slowly added with a dropping funnel over a period of 15 minutes. The mixture was refluxed for 6 hrs at 70°C and the volume was reduced to 10 mL by vacuum evaporation. Solution was left to stand at room temperature for 24 hrs, at which time an off-white precipitate was observed and the solid was filtered off and washed with cold water (5 x 100 mL). The solid obtained was recrystallized in ethanol to produce off-white crystalline particles (1.00g, 28%). M.p.: 199-202°C, (Lit. m.p.: 199-204°C).[23] ^{1}H NMR (δ_H; 200 MHz, DMSO-d_6): 8.99 (s, 1H), 8.69 (d, 2H, J = 4.8Hz), 8.19

(d, 2H, J = 8Hz), 7.52(m, 4H), 1.58 (m, 3H); IR (KBr pellet): υ 3297, 3074, 2952, 1633, 1592, 1551, 1490, 1429, 1310, 1240, 989S cm^{-1}.

6.2.1.7 Synthesis of N,N'-1,6-hexanediylbis-3-pyridinecarboxamide, 32[22]

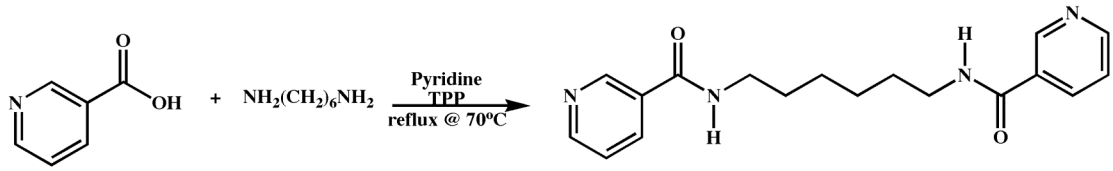

1,6-Diaminohexane (1.98g, 0.017 mol) was slowly added to a pyridine solution (50 mL) of nicotinic acid (4.20g, 0.034 mol). The mixture was stirred for 15 minutes and TPP (9 mL, 0.034 mol) was slowly added with a dropping funnel over a period of 15 minutes. The mixture was refluxed for 6 hrs at 70°C and the volume was reduced to 10 mL by vacuum evaporation. The solution was left to stand at room temperature for 24 hrs, producing a light peach precipitate, which was filtered and washed with cold water (5 x 100 mL). The solid obtained was recrystallized in ethanol to produce white crystalline material (2.71g, 50%). M.p.: 167-170°C, (Lit. m.p. 168-170°C).[25] ^{1}H NMR (δ_H; 200 MHz, DMSO-d_6): 13.47 (s, 1H), 9.07 (s, 2H), 8.97 (d, 2H, J = 2Hz), 8.30 (d, 2H, J = 7.6Hz), 7.59 (m, 2H), 3.3 (m, 2H), 2.09 (m, 2H); ^{13}C NMR (δ_C; 400 MHz, DMSO-d_6): 164, 151, 148, 134, 123, 29, 26; IR (KBr pellet): υ 3315, 1631, 1590, 1533, 1478, 1294, 1193, 989 cm^{-1}.

6.2.1.8 Synthesis of N,N'-1,8-octanediylbis-3-pyridinecarboxamide, 33[22]

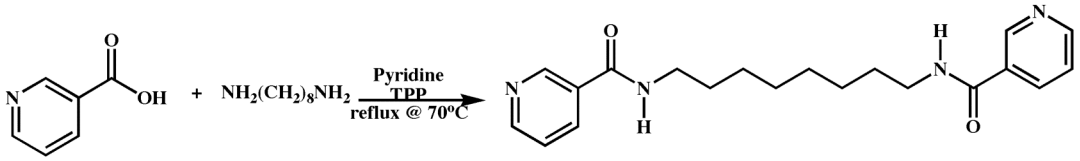

1,8-Diaminooctane (2.73g, 0.012 mol) was slowly added to a pyridine solution (50 mL) of nicotinic acid (2.95g, 0.024 mol). The mixture was stirred for 15 minutes and TPP (6.29 mL, 0.024 mol) was slowly added with a dropping funnel over a period of 15 minutes. The mixture was refluxed for 6 hrs at 70°C and the volume was reduced to 10 mL by vacuum evaporation. The solution was left to stand at room temperature for 24 hrs, producing a creamy precipitate, which was filtered and washed with cold water (5 x 100 mL). The solid obtained was recrystallized in ethanol to produce off-white crystalline

particles (4.42g, 73%). M.p.: 154-156°C, (Lit. m.p.: 150-154 & 154-158°C).[23,25] ^{1}H NMR (δ_H; 200 MHz, DMSO-d_6): 8.99 (s, 1H), 8.69 (d, 2H, J = 3Hz), 8,19 (d, 1H, J = 8Hz), 7.52(m, 1H), 3.30 (m, 3H) 1.51 (m, 5H); ^{13}C NMR (δ_C; 400 MHz, D_6-DMSO): 164, 151, 148, 134, 130, 123, 29, 26; IR (KBr pellet): υ 3316, 2929, 1630, 1585, 1533, 1476, 1287, 1180, 934 cm^{-1}.

6.2.2 Synthesis of cocrystals

6.2.2.1 Synthesis of 4-(4-pyridinylcarbonyl)hydrazide succinic acid hydrate (1:1), 26SUC

26 (0.015g, 0.062 mmol) was dissolved in 4 mL of nitromethane and added to a beaker containing **SUC** (0.007g, 0.062 mmol) in 2 mL of nitromethane. The mixture was allowed to stand at ambient temperature for slow evaporation. After five days, colorless needles were obtained. M.p.: 234-236°C. IR (ZnSe ATR crystal): υ 2402 cm^{-1}, 1956 cm^{-1} (O-H…N, br), 3415 cm^{-1} (N-H amide), 1687 cm^{-1} (C=O acid, s), 1638 cm^{-1} (C=O amide, s).

6.2.2.2 Synthesis of 4-(4-pyridinylcarbonyl)hydrazide adipic acid (1:1), 26ADI

26 (0.015g, 0.062 mmol) was dissolved in 4 mL of nitromethane and added to a beaker containing **ADI** (0.009g, 0.062 mmol) in 2 mL of nitromethane. The mixture was allowed to stand at ambient temperature for slow evaporation. After ten days, orange plates were obtained. M.p.: 213-215°C. IR (ZnSe ATR crystal): υ 2533 cm^{-1}, 1891 cm^{-1} (O-H…N, br), 3400 cm-^{1} (N-H amide), 1706 cm^{-1} (C=O acid, s), 1634 cm^{-1} (C=O amide, s).

6.2.2.3 Synthesis of 4-(4-pyridinylcarbonyl)hydrazide dodecanedioic acid (1:1), 26DOD

26 (0.015g, 0.062 mmol) was dissolved in 4 mL of nitromethane and added to a beaker containing **DOD** (0.029g, 0.062 mmol) in 2 mL of nitromethane. The mixture was allowed to stand at ambient temperature for slow evaporation. After five days, colorless plates were obtained. M.p.: 224-226°C. IR (ZnSe ATR crystal): υ 2516 cm^{-1}, 1944 cm^{-1} (O-H…N, br), 3166 cm^{-1} (N-H amide), 1699 cm^{-1} (C=O acid, s).

6.2.2.4 N,N'-1,4-butanediylbis-4-pyridinecarboxamide succinic acid hydrate (1:2), 27SUC

27 (0.015g, 0.053 mmol) was dissolved in 4 mL of ethanol-nitromethane (1:1) to which **SUC** (0.006g, 0.053 mmol) in 4 mL of ethanol-nitromethane (1:1) was added and allowed to stand at room temperature to slowly evaporate. Colorless needles were obtained after five days. Mp 227-229°C; (ZnSe ATR crystal) υ 2504 cm^{-1}, 1973 cm^{-1} (O-H…N, br), 3382 cm^{-1} (N-H amide), 1699 cm^{-1} (C=O, acid, s), 1625 cm^{-1} (C=O, amide, s).

6.2.2.5 N,N'-1,4-butanediylbis-4-pyridinecarboxamide adipic acid (1:1), 27ADI

27 (0.015g, 0.053 mmol) was dissolved in 4 mL of ethanol-nitromethane (1:1) to which **ADI** (0.007g, 0.053 mmol) in 4 mL of ethanol-nitromethane (1:1) was added and allowed to stand at room temperature to slowly evaporate. Colorless needles were obtained after five days. Mp 201-203°C; (ZnSe ATR crystal) ν 2537 cm^{-1}, 1871 cm^{-1} (O-H…N, br), 3382 cm^{-1} (N-H amide), 1699 cm^{-1} (C=O, acid, s), 1622 cm^{-1} (C=O, amide, s).

6.2.2.6 N,N'-1,4-butanediylbis-4-pyridinecarboxamide suberic acid (1:1), 27SUB

27 (0.015g, 0.053 mmol) was dissolved in 4 mL of ethanol-nitromethane (1:1) to which **SUB** (0.009g, 0.053 mmol) in 4 mL of ethanol-nitromethane (1:1) was added and allowed to stand at room temperature to slowly evaporate. Colorless needles were obtained after ten days. Mp 196-198°C; (ZnSe ATR crystal) ν 2500 cm^{-1}, 1875 cm^{-1} (O-H…N, br), 3313 cm^{-1} (N-H amide), 1703 cm^{-1} (C=O, acid, s), 1629 cm^{-1} (C=O, amide, s).

6.2.2.7 Synthesis of N,N'-1,6-hexanediylbis-4-pyridinecarboxamide succinic acid (1:1), 28SUC

28 (0.03g, 0.092 mmol) was dissolved in 5 mL of ethanol and ethyl acetate (1:1). To this solution was added **SUC** (0.011g, 0.092 mmol) in 5 mL of ethanol-ethyl acetate (1:1). The resulting solution was heated and allowed to stand at room temperature to slowly evaporate. Light pink plate-like crystals were obtained after ten days. M.p.: 186-188°C; IR (ZnSe ATR crystal) ν 2488 cm^{-1}, 1871 cm^{-1} (O-H…N, br), 3317 cm^{-1} (NH amide), 1702 cm^{-1} (C=O acid, s), 1636 cm^{-1} (C=O amide, s).

6.2.2.8 Synthesis of N,N'-1,6-hexanediylbis-4-pyridinecarboxamide adipic acid (1:1), 28ADI

28 (0.03g, 0.092 mmol) was dissolved in 5 mL of ethanol. To this solution was added **ADI** (0.013g, 0.092 mmol) in 5 mL of ethanol. The resulting solution was heated and allowed to stand at room temperature to slowly evaporate. After 8 days, transparent needles were obtained. M.p.: 165-167°C; IR (ZnSe ATR crystal) ν 2512 cm^{-1}, 1858 cm^{-1} (O-H…N, br), 3309 cm^{-1} (NH amide), 1699 cm^{-1} (C=O acid, s), 1631 cm^{-1} (C=O amide, s).

6.2.2.9 Synthesis of N,N'-1,6-hexanediylbis-4-pyridinecarboxamide suberic acid (1:1), 28SUB

28 (0.03g, 0.092 mmol) was dissolved in 7 mL methanol and mixed with a solution of **SUB** (0.016g, 0.092 mmol) in 5 mL of methanol. The resulting solution was heated and allowed to stand at room temperature to slowly evaporate. Colorless prisms were obtained after fifteen days. M.p.: 158-160°C; (ZnSe ATR crystal) ν 2504 cm^{-1}, 1879 cm^{-1} (O-H…N, br), 3317 cm^{-1} (NH amide), 1707 cm^{-1} (C=O acid, s), 1632 cm^{-1} (C=O amide, s).

6.2.2.10 Synthesis of N,N'-1,6-hexanediylbis-4-pyridinecarboxamide sebacic acid (1:1), 28SEB

28 (0.03g, 0.092 mmol) was dissolved in 5 mL methanol and mixed with a solution of **SEB** (0.019g, 0.092 mmol) in 5 mL of methanol. The resulting solution was heated and allowed to stand at room temperature to slowly evaporate. Transparent needles were observed after 8 days. M.p.: 148-150°C; (ZnSe ATR crystal) ν 2520 cm^{-1}, 1862 cm^{-1} (O-H…N, br), 3321 cm^{-1} (NH amide), 1707 cm^{-1} (C=O acid, s), 1632 cm^{-1} (C=O amide, s).

6.2.2.11 Synthesis of N,N'-1,6-hexanediylbis-4-pyridinecarboxamide dodecanedioic acid (1:1), 28DOD

28 (0.03g, 0.092 mmol) was dissolved in 5 mL ethanol and mixed with a solution of **DOD** (0.022g, 0.092 mmol) in 5 mL of methanol. The resulting solution was heated and allowed to stand at room temperature to slowly evaporate. After fifteen days

transparent needles were obtained. M.p.: 146-148°C; (ZnSe ATR crystal) ν 2508 cm^{-1}, 1866 cm^{-1} (O-H…N, br), 3325 cm^{-1} (NH amide), 1707 cm^{-1} (C=O acid, s), 1632 cm^{-1} (C=O amide, s).

6.2.2.12 Synthesis of N,N'-1,6-hexanediylbis-4-pyridinecarboxamide oxalic acid (1:1), 28OXA

28 (0.03g, 0.092 mmol) was dissolved in 5 mL of ethanol-nitromethane (1:1) and mixed with a solution of **OXA** (0.008g, 0.092 mmol) in 5 mL of ethanol-nitromethane (1:1). The mixture was gently heated and allowed to stand at ambient temperature to slowly evaporate. After two days, colorless needles were obtained. M.p.: 188-190°C; (ZnSe ATR crystal) ν 2402 cm^{-1}, 1862 cm^{-1} (O-H…N, br), 3305 cm-^{1} (NH amide), 1679 cm^{-1} (C=O acid, s), 1633 cm^{-1} (C=O amide, s).

6.2.2.13 Synthesis of N,N'-1,6-hexanediylbis-4-pyridinecarboxamide pimelic acid (1:1), 28PIM

28 (0.03g, 0.092 mmol) was dissolved in 5 mL of ethanol-nitromethane (1:1) and mixed with a solution of **PIM** (0.015g, 0.092 mmol) in 5 mL of ethanol-nitromethane (1:1). The mixture was gently heated and allowed to stand at ambient temperature to slowly evaporate. After six days colorless needles were obtained. M.p.: 173-175°C; (ZnSe ATR crystal) ν 2500 cm^{-1}, 1928 cm^{-1} (O-H…N, br), 3297 cm^{-1} (NH amide), 1699 cm^{-1} (C=O acid, s), 1634 cm^{-1} (C=O amide, s).

6.2.2.14 Synthesis of N,N'-1,8-octanediylbis-4-pyridinecarboxamide succinic acid (1:1), 29SUC

A solution of **29** (0.02g, 0.056 mmol) in 5 mL ethanol was mixed with a solution of **SUC** (0.007g, 0.056 mmol) in 5 mL of ethanol and was allowed to stand to slowly evaporate. Colorless plates were obtained at ten days. M.p.: 166-168°C; (KBr pellet) ν 2495 cm^{-1}, 1920 cm^{-1} (O-H...N, br), 3309 cm^{-1} (NH amide), 1704 cm^{-1} (C=O acid, s), 1630 cm^{-1} (C=O amide, s).

6.2.2.15 Synthesis of N,N'-1,8-octanediylbis-4-pyridinecarboxamide adipic acid (1:1), 29ADI

A solution of **29** (0.02g, 0.056 mmol) in 5 mL ethanol was mixed with a solution of adipic **ADI** (0.008g, 0.056 mmol) in 5 mL of ethanol and was allowed to stand to slowly evaporate. Light pink prisms were obtained after fifteen days. M.p.: 185-187°C; (KBr pellet) ν 2500 cm^{-1}, 1926 cm^{-1} (O-H...N, br), 3320 cm^{-1} (NH amide), 1710 cm^{-1} (C=O acid, s), 1638 cm^{-1} (C=O amide, s).

6.2.2.16 Synthesis of N,N'-1,8-octanediylbis-4-pyridinecarboxamide suberic acid (1:1), 29SUB

29 (0.02g, 0.056 mmol) was dissolved in 5 mL of ethanol. To this solution was added **SUB** (0.009, 0.056 mmol) in 5 mL of ethanol. The resulting solution was allowed to stand at room temperature to slowly evaporate. Colorless needles were obtained after twenty days. M.p.: 163-165°C; (KBr pellet) ν 2501 cm^{-1}, 1892 cm^{-1} (O-H...N, br), 3317 cm^{-1} (NH amide), 1706 cm^{-1} (C=O acid, s), 1635 cm^{-1} (C=O amide, s).

6.2.2.17 Synthesis of N,N'-1,8-octanediylbis-4-pyridinecarboxamide sebacic acid (1:1), 29SEB

29 (0.015g, 0.0423 mmol) was dissolved in 4 mL of ethanol-nitromethane (1:1) to which **SEB** (0.009g, 0.0423 mmol) in 4 mL of ethanol-nitromethane (1:1) was added and allowed to stand at room temperature to slowly evaporate. Colorless needles were obtained after thirteen days. M.p.: 162-164°C; (ZnSe ATR crystal) ν 2520 cm^{-1}, 1871 cm^{-1} (O-H…N, br), 3322 cm^{-1} (N-H amide), 1699 cm^{-1} (C=O acid, s), 1631cm^{-1} (C=O amide, s).

6.2.2.18 Synthesis of N,N'-1,8-octanediylbis-4-pyridinecarboxamide malonic acid (1:1), 29MAL

29 (0.030g, 0.0847 mmol) was dissolved in 5 mL of ethanol-nitromethane (1:1) to which **MAL** (0.009g, 0.0847 mmol) in 5 mL of ethanol-nitromethane (1:1) was added and allowed to stand at ambient temperature to slowly evaporate. After ten days light pink plate-like crystals were obtained. M.p.: 146-148°C; (ZnSe ATR crystal) ν 2501 cm^{-1},

1971 cm^{-1} (O-H…N, br), 3317 cm^{-1} (N-H amide), 1690 cm^{-1} (C=O acid, s), 1635 cm^{-1} (C=O amide, s).

6.2.2.19 Synthesis of 3-(3-pyridinylcarbonyl)hydrazide sebacic acid (1:1), 30SEB

30 (0.030g, 0.10 mmol) was dissolved in 4 mL ethanol to which **SEB** (0.020g, 0.10 mmol) in 4 mL of ethanol was added and mixture was allowed to stand at room temperature to slowly evaporate. After ten days, orange plates were obtained. M.p.: 209-210°C; (KBr pellet) ν 2496 cm^{-1}, 1913 cm^{-1} (O-H…N, br), 3188 cm^{-1} (N-H amide), 1697 cm^{-1} (C=O acid, s), 1605 cm^{-1} (C=O amide, s).

6.2.2.20 Synthesis of N,N'-1,4-butanediylbis-3-pyridinecarboxamide succinic acid (1:1), 31SUC

A solution of **31** (0.015g, 0.050 mmol) in 2 mL ethanol-nitromethane (1:1) was mixed with a solution of **SUC** (0.006g, 0.050 mmol) in 2 mL of ethanol-nitromethane (1:1) and allowed to stand for slow evaporation. Colorless needles were obtained after ten days. M.p.: 168-170°C; (ZnSe ATR crystal) ν 2467 cm^{-1}, 1916 cm^{-1} (O-H...N, br), 3301 cm^{-1} (NH amide), 1700 cm^{-1} (C=O acid, s), 1630 cm^{-1} (C=O amide, s).

6.2.2.21 Synthesis of N,N'-1,4-butanediylbis-3-pyridinecarboxamide suberic acid (1:1), 31SUB

31 (0.015g, 050 mmol) was dissolved in 2 mL of ethanol-nitromethane (1:1) and **SUB** (0.009g, 0.050 mmol) in 2 mL ethanol-nitromethane (1:1) was added and allowed to stand at room temperature to slowly evaporate. After five days prism-like crystals were obtained. M.p.: 166-168°C; (ZnSe ATR crystal) ν 2496 cm^{-1}, 1887 cm^{-1} (O-H…N, br), 3329 cm^{-1} (N-H, amide), 1697 cm^{-1} (C=O acid, s), 1628 cm^{-1} (C=O amide, s).

6.2.2.22 Synthesis of N,N'-1,4-butanediylbis-3-pyridinecarboxamide dodecanedioic acid (1:1), 31DOD

31 (0.015g, 050 mmol) was dissolved in 2 mL of ethanol-nitromethane (1:1) and **DOD** (0.023g, 0.050 mmol) in 2 mL ethanol-nitromethane (1:1) was added and left at room temperature for slow evaporation. After seven days plate-like crystals were obtained. M.p.: 144-146°C; (ZnSe ATR crystal) ν 2500 cm^{-1}, 1875 cm^{-1} (O-H…N, br), 3305 cm^{-1} (N-H, amide), 1710 cm^{-1} (C=O acid, s), 1626 cm^{-1} (C=O amide, s).

6.2.2.23 N,N'-1,6-hexanediylbis-3-pyridinecarboxamide succinic acid (1:1), 32SUC

A solution of **32** (0.02g, 0.061 mmol) in 8 mL acetonitrile-ethyl acetate (1:1) was mixed with a solution of **SUC** (0.007g, 0.061 mmol) in 2 mL acetonitrile-ethyl acetate (1:1) and allowed to slowly evaporate at room temperature. Colorless plate-like crystals were obtained after ten days. M.p.: 147-148°C; IR (KBr pellet) ν 2481 cm^{-1}, 1924 cm^{-1} (O-H…N, br), 3309 cm^{-1} (N-H amide), 1690 cm^{-1} (C=O acid, s), 1637 cm^{-1} (C=O amide, s).

6.2.2.24 Synthesis of N,N'-1,6-hexanediylbis-3-pyridinecarboxamide adipic acid (1:1), 32ADI

32 (0.015g, 0.046 mmol) was dissolved in 2 mL of ethanol-nitromethane (1:1) and **ADI** (0.007g, 0.046 mmol) in 2 mL ethanol-nitromethane (1:1). The resulting solution was gently heated and left at room temperature for slow evaporation. After twenty days, colorless needles were obtained. M.p.: 166-168°C; (ZnSe ATR crystal) ν 2516 cm^{-1}, 1895 cm^{-1} (O-H…N, br), 3309 cm^{-1} (N-H, amide), 1695 cm^{-1} (C=O acid, s), 1629 cm^{-1} (C=O amide, s).

6.2.2.25 Synthesis of N,N'-1,6-hexanediylbis-3-pyridinecarboxamide suberic acid (1:1), 32SUB

32 (0.015g, 0.046 mmol) was dissolved in 10 mL nitromethane-ethyl acetate (1:1) and mixed with a solution of **SUB** (0.008g, 0.046 mmol) in 5 mL of nitromethane-ethyl acetate (1:1). The resulting solution was heated and allowed to stand at ambient temperature for slow evaporation. Colorless prisms were obtained after four days. M.p.: 182-184°C; (ZnSe ATR crystal) ν 2496 cm^{-1}, 1896 cm^{-1} (O-H…N, br), 3329 cm^{-1} (NH amide), 1701 cm^{-1} (C=O acid, s), 1627 cm^{-1} (C=O amide, s).

6.2.2.26 Synthesis of N,N'-1,6-hexanediylbis-3-pyridinecarboxamide sebacic acid (1:1), 32SEB

32 (0.05g, 0.140 mmol) was dissolved in 10 mL nitromethane-ethyl acetate (1:1) and mixed with a solution of **SEB** (0.028g, 0.140 mmol) in 5 mL of nitromethane- ethyl acetate (1:1). The resulting solution was heated and allowed to stand at ambient

temperature for slow evaporation. Colorless needles were obtained after ten days. M.p.: 180-181°C; (KBr pellet) ν 2508 cm^{-1}, 1905 cm^{-1} (O-H…N, br), 3305 cm^{-1} (NH amide), 1700 cm^{-1} (C=O acid, s), 1637 cm^{-1} (C=O amide, s).

6.2.2.27 Synthesis of N,N'-1,6-hexanediylbis-3-pyridinecarboxamide dodecanedioic acid (1:1), 32DOD

32 (0.015g, 0.046 mmol) was dissolved in 10 mL nitromethane-ethyl acetate (1:1) and mixed with a solution of **DOD** (0.011g, 0.046 mmol) in 5 mL of nitromethane-ethyl acetate (1:1). The resulting solution was heated and allowed to stand at ambient temperature for slow evaporation. Colorless prisms were obtained after five days. M.p.: 160-162°C; (ZnSe ATR crystal) ν 2500 cm^{-1}, 1901 cm^{-1} (O-H…N, br), 3302 cm^{-1} (N-H amide), 1708 cm^{-1} (C=O acid, s), 1625 cm^{-1} (C=O amide, s).

6.2.2.28 Synthesis of N,N'-1,6-hexanediylbis-3-pyridinecarboxamide oxalic acid (1:1), 32OXA

A solution of **32** (0.030g, 0.092 mmol) in 5 mL ethanol-nitromethane (1:1) was mixed with a solution of **OXA** (0.008g, 0.092 mmol) in 5 mL ethanol-nitromethane (1:1) and allowed to stand at room temperature for slow evaporation. Colorless needles were obtained after five days. M.p.: 179-181°C; IR (ZnSe ATR crystal) ν 2501 cm^{-1}, 1928 cm^{-1} (O-H…N, br), 3299 cm^{-1} (N-H amide), 1695 cm^{-1} (C=O acid, s), 1639 cm^{-1} (C=O amide, s).

6.2.2.29 Synthesis of N,N'-1,6-hexanediylbis-3-pyridinecarboxamide glutaric acid (1:2), 32GLU

A solution of **32** (0.023g, 0.070 mmol) in 5 mL ethanol was mixed with a solution of **GLU** (0.009g, 0.070 mmol) in 5 mL ethanol and allowed to stand at room temperature for slow evaporation. Colorless needles were obtained after five days. M.p.: 142-144°C; IR (KBr pellet) ν 2474 cm^{-1}, 1918 cm^{-1} (O-H…N, br), 3345 cm^{-1} (N-H amide), 1705 cm^{-1} (C=O acid, s), 1630 cm^{-1} (C=O amide, s).

6.2.2.30 Synthesis of N,N'-1,6-hexanediylbis-3-pyridinecarboxamide heptanoic acid (1:1), 32HEP

A solution of **32** (0.030g, 0.092 mmol) in 5 mL acetonitrile-nitromethane (1:1) was mixed with a solution of **HEP** (0.024g, 0.184 mmol) in 5 mL acetonitrile-nitromethane (1:1) and allowed to stand at room temperature for slow evaporation. Colorless plates were obtained after five days. M.p.: 135-137°C; IR (KBr pellet) ν 2534 cm^{-1}, 1938 cm^{-1} (O-H…N, br), 3317 cm^{-1} (N-H amide), 1714 cm^{-1} (C=O acid, s), 1628 cm^{-1} (C=O amide, s).

6.2.2.31 Synthesis of N,N'-1,6-hexanediylbis-3-pyridinecarboxamide octanoic acid (1:1), 32OCT

A solution of **32** (0.030g, 0.092 mmol) in 5 mL acetonitrile-nitromethane (1:1) was mixed a solution of **OCT** (0.027g, 0.184 mmol) in 5 mL acetonitrile-nitromethane (1:1) and allowed to stand at room temperature for slow evaporation. Colorless plates were obtained after three days. M.p.: 136-138°C; IR (KBr pellet) ν 2509 cm^{-1}, 1909 cm^{-1} (O-H…N, br), 3328 cm^{-1} (N-H amide), 1707 cm^{-1} (C=O acid, s), 1629 cm^{-1} (C=O amide, s).

6.2.2.32 Synthesis of N,N'-1,6-hexanediylbis-3-pyridinecarboxamide lauric acid (1:1), 32LAU

32 (0.030g, 0.092 mmol) was dissolved in 5 mL acetonitrile-nitromethane (1:1) and mixed with a solution of **LAU** (0.0369g, 0.184 mmol) in 5 mL of acetonitrile-nitromethane (1:1). The resulting solution was heated and allowed to stand at ambient temperature for slow evaporation. Colorless plates were obtained after fifteen days. M.p.: 172-174°C; (KBr pellet) ν 2528 cm^{-1}, 1904 cm^{-1} (O-H…N, br), 3306 cm^{-1} (N-H amide), 1700 cm^{-1} (C=O acid, s), 1637 cm^{-1} (C=O amide, s).

6.2.2.33 Synthesis of N,N'-1,8-octanediylbis-3-pyridinecarboxamide succinic acid (1:1), 33SUC

33 (0.015g, 0.042 mmol) was dissolved in 2 mL ethanol-nitromethane (1:1) and mixed with a solution of **SUC** (0.005g, 0.042 mmol) in 2 mL of ethanol-nitromethane (1:1). The resulting solution was heated and allowed to stand at ambient temperature for

slow evaporation. Colorless plates were obtained after four days. M.p.: 160-162°C; (ZnSe ATR crystal) ν 2516 cm^{-1}, 1891 cm^{-1} (O-H…N, br), 3301 cm^{-1} (N-H amide), 1694 cm^{-1} (C=O acid, s), 1626 cm^{-1} (C=O amide, s).

6.2.2.34 Synthesis of N,N'-1,8-octanediylbis-3-pyridinecarboxamide suberic acid (1:1), 33SUB

33 (0.015g, 0.042 mmol) was dissolved in 2 mL ethanol-nitromethane (1:1) and mixed with a solution of **SUB** (0.007g, 0.042 mmol) in 2 mL of ethanol-nitromethane (1:1). The resulting solution was heated and allowed to stand at ambient temperature for slow evaporation. Colorless needles were obtained after ten days. M.p.: 152-154°C; (ZnSe ATR crystal) ν 2496 cm^{-1}, 1891 cm^{-1} (O-H…N, br), 3329 cm^{-1} (N-H amide), 1699 cm^{-1} (C=O acid, s), 1629 cm^{-1} (C=O amide, s).

6.2.2.35 Synthesis of N,N'-1,8-octanediylbis-3-pyridinecarboxamide pimelic (1:2), 33PIM

33 (0.030g, 0.085 mmol) was dissolved in 5 mL ethanol-nitromethane (1:1) and mixed with a solution of **PIM** (0.014g, 0.085 mmol) in 5 mL of ethanol-nitromethane (1:1). The resulting solution was heated and allowed to stand at ambient temperature for slow evaporation. Colorless needles were obtained after fifteen days. M.p.: 147-149°C; (ZnSe ATR crystal) ν 2508 cm^{-1}, 1903 cm^{-1} (O-H…N, br), 3333 cm^{-1} (N-H amide), 1691 cm^{-1} (C=O acid, s), 1625 cm^{-1} (C=O amide, s).

6.3 Solubility studies

6.3.1 Preparation of cocrystals for solubility studies

Cocrystals of **28, 29** and dicarboxylic acid (1:1 molar ratio) were prepared via a solvothermal method.[26] Supersaturation of **28** and **SUC** were created by cooling a solution of **28** (0.5112g, 1.566 mmol) and **SUC** (0.1849, 1.566 mmol) in 25.00 mL of ethanol from 40 to 25°C. The solid phase was harvested by vacuum filtration and dried at room temperature (22-23°C) on a Fisherbrand filter paper for 40 min to remove loosely bound solvent. The solid obtained was confirmed to be a cocrystal by FT-IR spectroscopy; also the IR obtained matched the previous IR of crystals submitted for X-ray analysis. Cocrystals were stored in a desiccator over anhydrous calcium sulfate.

The remaining cocrystals in this study were made and analyzed following the same procedure.

6.3.1.2 Aqueous solubility of APIs and cocrystals

The solubility of **28, 29** and their respective cocrystals in water was determined from undersaturation by adding excess cocrystal solid phase in water.[26] The suspensions were stirred with magnetic stirrers in a sealed 500 mL flask at constant temperature (25 ± 0.5^{o}C) maintained with a water bath. Samples were drawn at various time intervals over 72hrs and filtered. Samples were diluted with the same solvent in which the solubility analysis was performed. The solutions equilibrated within 48hrs and average sample concentration differed by <3% at 24hrs and 48hrs. Concentrations of samples were obtained measuring the absorbance of **28, 29** and their respective cocrystals at λ_{max} = 236.4, and 234.8nm respectively. All UV-Visible measurements were carried out on a Shimadzu UV-1650 PC.

6.4 Results and Discussion

6.4.1 Crystal structure descriptions

Summaries of the crystallographic information are displayed in Table C.5 and all hydrogen-bond geometries are listed in Table 6.1.

Table 6.1 Hydrogen-bond geometries for **26SUC, 26ADI, 26DOD, 27SUC, 27ADI, 27SUB, 28SUC, 28ADI, 28SUB, 28SEB, 28DOD, 28OXA, 28PIM, 29SUC, 29ADI, 29SUB, 29SEB, 29MAL, 30SEB, 31SUC, 31SUB, 31DOD, 32SUC, 32ADI, 32SUB, 32SEB, 32DOD, 32OXA, 32GLU, 32HEP, 32OCT, 32LAU** and **33UC, 33SUB, 33PIM**

Structure	D-H…A	d(D-H)/Å	d(H…A)/ Å	d(D…A)/ Å	<(DHA)^{o}
26SUC[i]	N(17)-H(17)...O(1W)	0.90(4)	1.86(4)	2.756(4)	173(4)
	O(21)-H(21)...N(11)	1.04(4)	1.55(4)	2.588(3)	172(3)
	O(1W)-H(1A)...O(22)#3	0.95(4)	1.83(4)	2.776(3)	172(3)
	O(1W)-H(1B)...O(17)#4	0.79(5)	2.05(5)	2.828(3)	168(4)
26ADI[ii]	O(21)-H(21)...N(11)	0.90(3)	1.82(3)	2.707(2)	166(2)
	N(17)-H(17)...O(17)#3	0.82(3)	2.14(3)	2.949(2)	168(2)
26DOD[iii]	O(21)-H(21)...N(11)	1.00(2)	1.71(2)	2.6746(16)	162.1(17)
	N(17)-H(17)...O(17)#3	0.885(17)	1.986(17)	2.8121(16)	154.9(15)
27SUC[iv]	O(31)-H(31)...N(11)	1.064(16)	1.518(16)	2.5768(13)	173.0(14)
	O(41)-H(41)...O(1W)	0.912(18)	1.676(18)	2.5832(13)	172.7(17)
	O(1W)-H(1A)...O(32)	0.909(19)	1.91(2)	2.8067(15)	170.5(16)
	O(1W)-H(1B)...O(17)#4	0.82(2)	1.93(2)	2.7422(14)	172.7(17)
	N(17)-H(17)...O(42)#5	0.876(17)	2.030(17)	2.8625(15)	158.2(14)
27ADI[v]	O(31)-H(31)...N(11)	0.908(14)	1.788(14)	2.6940(9)	175.0(13)
	N(17)-H(17)...O(17)#3	0.864(13)	2.139(13)	2.9876(9)	167.1(12)
27SUB[vi]	O(31)-H(31)...N(11)	0.938(15)	1.756(16)	2.6942(11)	178.7(14)
	N(17)-H(17)...O(17)#3	0.880(14)	2.130(14)	2.9920(11)	166.1(12)
28SUC[vii]	O(31)-H(31)...N(11)	0.98(2)	1.73(2)	2.7094(19)	176(2)
	N(17)-H(17)...O(17)#3	0.92(2)	2.11(2)	2.9902(19)	161.6(17)
28ADI[viii]	O(31)-H(31)...N(11)	0.929(16)	1.780(17)	2.7079(13)	177.6(15)

Structure	D-H…A	d(D-H)/Å	d(H…A)/ Å	d(D…A)/ Å	<(DHA)°
	N(17)-H(17)...O(17)#3	0.902(15)	2.127(15)	3.0072(13)	165.0(13)
28SUB[ix]	O(31)-H(31)...N(11)	0.977(13)	1.723(13)	2.6998(9)	179.8(13)
	N(17)-H(17)...O(17)#3	0.898(12)	2.122(12)	3.0025(10)	166.5(11)
28SEB[x]	O(31)-H(31)...N(11)	0.962(14)	1.738(14)	2.6990(11)	177.2(13)
	N(17)-H(17)...O(17)#3	0.926(15)	2.102(15)	3.0127(14)	167.4(11)
28DOD[xi]	O(31)-H(31)...N(11)	0.92(2)	1.79(2)	2.7085(18)	177.6(19)
	N(17)-H(17)...O(17)#3	0.836(18)	2.207(19)	3.0222(17)	165.3(18)
28OXA[xii]	O(31)-H(31)...N(11)	0.95(2)	1.71(2)	2.6521(10)	177.0(19)
	N(17)-H(17)...O(17)#3	0.881(14)	2.102(14)	2.9509(10)	161.5(12)
28PIM[xiii]	O(51)-H(51)...N(11)	0.974(14)	1.743(14)	2.7138(10)	173.7(12)
	O(57)-H(57)...N(21)	0.930(14)	1.761(14)	2.6756(11)	167.0(12)
	N(17)-H(17)...O(17)#3	0.882(12)	2.044(12)	2.9193(10)	171.3(11)
	N(27)-H(27)...O(27)#3	0.844(12)	2.253(12)	3.0922(10)	172.4(11)
29SUC[xiv]	O(31)-H(31)...N(11)	0.896(19)	1.817(19)	2.7128(15)	178.3(18)
	N(17)-H(17)...O(17)#3	0.844(16)	2.150(16)	2.9834(14)	169.5(15)
29ADI[xv]	O(31)-H(31)...N(11)	0.925(15)	1.782(15)	2.7056(11)	176.3(13)
	N(17)-H(17)...O(17)#3	0.848(14)	2.170(14)	3.0039(12)	167.9(13)
29SUB[xvi]	O(31)-H(31)...N(11)	0.905(18)	1.798(18)	2.7026(14)	177.2(17)
	N(17)-H(17)...O(17)#3	0.853(17)	2.173(17)	3.0067(14)	165.5(15)
29SEB[xvii]	O(31)-H(31)...N(11)	0.96(2)	1.73(2)	2.6912(17)	178.6(18)
	N(17)-H(17)...O(17)#3	0.899(19)	2.125(19)	2.9984(16)	163.5(16)
29MAL[xviii]	N(17)-H(17)...O(17)#1	0.884(14)	2.115(15)	2.9904(13)	170.4(12)
	N(27)-H(27)...O(27)#2	0.825(15)	2.168(15)	2.9401(14)	155.7(13)
	O(41)-H(41)...N(11)	0.919(15)	1.801(15)	2.7079(13)	169.0(13)
	O(43)-H(43)...N(21)#3	1.024(14)	1.613(14)	2.6353(12)	175.3(13)
30SEB[xix]	O(21)-H(21)...N(11)	0.84	1.83	2.663(2)	173.2
	N(17)-H(17)...O(17)#3	0.88	2.08	2.8234(19)	141.5

Structure	D-H…A	d(D-H)/Å	d(H…A)/ Å	d(D…A)/ Å	<(DHA)°
31SUC[xx]	N(17)-H(17)...O(27)#3	0.889(14)	2.068(14)	2.9333(11)	164.3(12)
	N(27)-H(27)...O(17)#4	0.908(14)	2.046(14)	2.9359(10)	166.3(12)
	O(41)-H(41)...N(11)	0.836(17)	1.829(17)	2.6593(12)	172.2(15)
	O(51)-H(51)...N(21)	0.878(16)	1.852(17)	2.7113(11)	165.4(14)
31SUB[xxi]	O(31)-H(31)...N(11)	0.974(17)	1.735(17)	2.7074(13)	175.9(14)
	N(17)-H(17)...O(17)#3	0.891(15)	2.105(15)	2.9814(12)	167.4(13)
31DOD[xxii]	O(31)-H(31)...N(11)	0.84	1.85	2.684(8)	171.4
	N(17)-H(17A)...O(17)#3	0.88	2.09	2.935(10)	161.6
32SUC[xxiii]	O(31A)-H(31A)...N(11)	0.84	1.81	2.6488(10)	176.8
	O(31B)-H(31B)...N(11)	0.84	2.06	2.894(7)	173.6
	N(17)-H(17)...O(17)#3	0.852(12)	2.089(12)	2.9244(9)	166.8(11)
32ADI[xxiv]	O(31)-H(31)...N(11)	1.010(17)	1.704(17)	2.7137(15)	177.2(15)
	N(17)-H(17)...O(17)#3	0.835(17)	2.110(18)	2.9394(14)	172.1(15)
32SUB[xxv]	O(31)-H(31)...N(11)	1.00(3)	1.73(3)	2.728(2)	175(2)
	N(17)-H(17)...O(17)#3	0.80(2)	2.24(2)	3.021(2)	165.6(19)
32SEB[xxvi]	O(31)-H(31)...N(11)	0.935(19)	1.748(19)	2.6802(13)	175.0(15)
	N(17)-H(17)...O(17)#3	0.913(16)	1.997(16)	2.8953(12)	167.6(13)
32DOD[xxvii]	O(31)-H(31)...N(11)	0.862(19)	1.826(19)	2.6839(15)	173.7(17)
	N(17)-H(17)...O(17)#3	0.851(18)	2.060(18)	2.8993(14)	169.1(15)
32OXA[xxviii]	N(17)-H(17)...O(17)#1	0.914(13)	2.033(13)	2.9172(11)	162.2(11)
	N(27)-H(27)...O(27)#2	0.838(14)	2.138(14)	2.9656(11)	169.1(12)
	O(41)-H(41)...N(11)	0.959(16)	1.645(16)	2.6021(11)	176.1(13)
	O(43)-H(43)...N(21)#3	0.935(15)	1.674(15)	2.6030(12)	172.0(14)
32GLU[xxix]	N(17)-H(17)...O(17)#2	0.830(13)	2.292(13)	3.1019(10)	165.4(11)
	O(31)-H(31)...N(11)	0.955(15)	1.726(15)	2.6731(10)	171.2(13)
	O(35)-H(35)...O(36)#3	0.894(14)	1.725(14)	2.6154(9)	173.6(13)
32HEP[xxx]	O(31)-H(31)...N(11)	0.882(18)	1.836(19)	2.7123(14)	171.9(16)
	N(17)-H(17)...O(17)#2	0.858(15)	2.124(16)	2.9674(12)	167.2(14)

Structure	D-H…A	d(D-H)/Å	d(H…A)/ Å	d(D…A)/ Å	<(DHA)°
32OCT[xxxi]	N(17)-H(17)...O(17)#2	0.893(16)	2.118(16)	2.9903(13)	165.5(13)
	O(31)-H(31)...N(11)	0.934(18)	1.785(18)	2.7188(13)	177.5(16)
32LAU[xxxii]	O(31)-H(31)...N(11)	0.86(3)	1.82(3)	2.671(2)	170(2)
	N(17)-H(17)...O(17)#2	0.88(3)	2.02(3)	2.881(2)	168.8(19)
33SUC[xxxiii]	O(31)-H(31)...N(11)	0.94(3)	1.78(3)	2.717(2)	172(3)
	N(17)-H(17)...O(17)#3	0.844(19)	2.12(2)	2.9555(17)	168.9(18)
33SUB[xxxiv]	N(17)-H(17)...O(17)#3	0.898(18)	2.016(18)	2.9012(17)	168.4(15)
	O(31)-H(31)...N(11)	0.981(19)	1.69(2)	2.6694(16)	172.8(16)
33PIM[xxxv]	O(31)-H(31)...N(11)	0.939(16)	1.760(17)	2.6923(12)	171.6(14)
	N(17)-H(17)...O(17)#2	0.834(14)	2.229(14)	3.0546(12)	170.6(13)
	O(38)-H(38)...O(37)#3	0.907(16)	1.717(16)	2.6207(11)	174.3(14)

i) #3 x-1/2,y+1/2,z #4 -x,y-1,-z+1/2 ii) #3 x+1,y,z iii) #3 x+1,y,z iv) #4 x-2,y+1,z #5 x+1,y,z v) #3 x-1,y,z vi) #3 x-1,y,z vii) #3 x-1,y,z viii) #3 x-1,y,z ix) #3 x+1,y,z x) #3 x-1,y,z xi) #3 x-1,y,z xii) #3 x-1,y,z xiii) #3 x+1,y,z xiv) #3 x,y-1,z xv) #3 x-1,y,z xvi) #3 x+1,y,z xvii) #3 x+1,y,z xviii) #1 x,y-1,z #2 x,y+1,z #3 x+1/2,-y+1/2,z-1/2 xix) #3 x-1,y,z xx) #3 -x+1,-y+1,-z+1 #4 -x+1,-y+2,-z+1 xxi) #3 x-1,y,z xxii) #3 x+1,y,z xxiii) #3 x-1,y,z xxiv) #3 x+1,y,z xxv) #3 x+1,y,z xxvi) #3 x+1,y,z xxvii) #3 x-1,y,z xxviii) #1 x-1,y,z #2 x+1,y,z #3 x-1,y+1,z-1 xxix) #2 x-1,y,z #3 -x+1,-y,-z-1 xxx) #2 x+1,y,z xxxi) #2 x+1,y,z xxxii) #2 x+1,y,z xxxiii) #3 x,y-1,z xxxiv) #3 x+1,y,z xxxv) #2 x-1,y,z #3 -x+3,-y+1,-z-1

6.4.1.1 Crystal structure of 26SUC

The primary motif in the crystal structure of **26SUC** is composed of half a molecule of **26**, half a molecule of **SUC** and one water molecule with interactions between the acid and the pyridyl moiety, as well as between the water molecule and amide moiety. The primary synthon is an acid…pyridine hydrogen bond, Figure 6.4. Instead of the typical amide…amide interaction, which is often observed the water molecule disrupts the architecture of the structure resulting in N-H…O and O-H…O interaction, Figure 6.5.

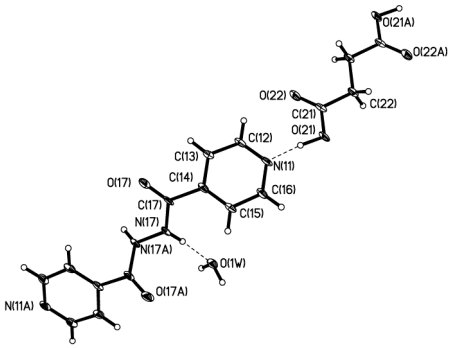

Figure 6.4 Thermal ellipsoid (50%) and labeling scheme of **26SUC**.

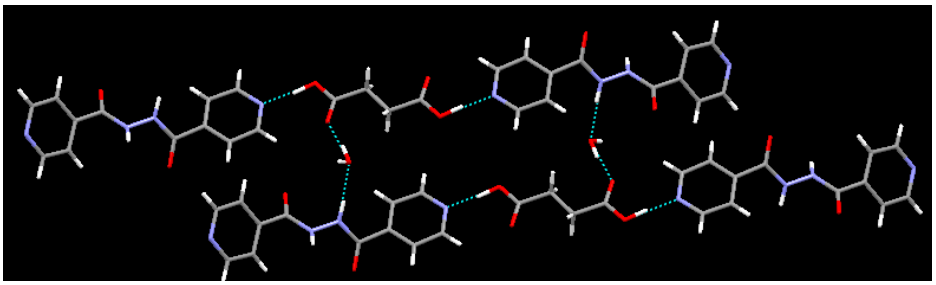

Figure 6.5 2-D sheet of **26SUC** with N-H…O, O-H…N, and O-H…O hydrogen bonds.

6.4.1.2 Crystal structures of 26ADI and 26DOD

Unlike **26SUC**, the crystal structure of **26ADI** and **26DOD** contain half a molecule of **26** and half a molecule of **ADI** and **DOD** respectively, with no water molecule observed in the crystalline lattice. The robust synthon of N-H…O is observed between the acid and the pyridine nitrogen in both cases Figure 6.6.

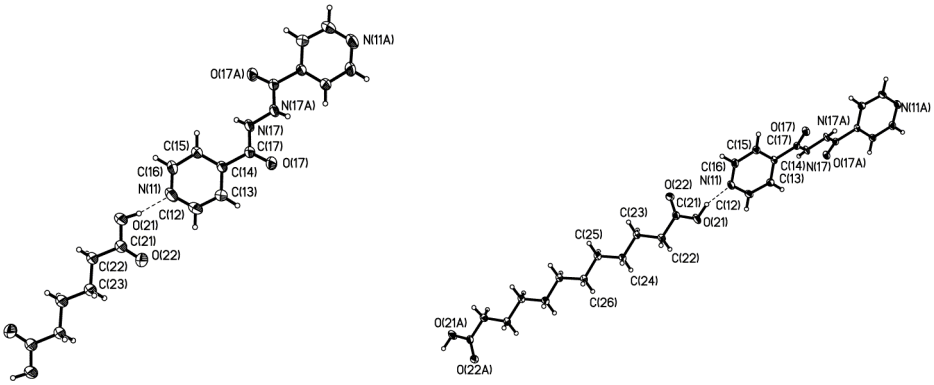

26ADI **26DOD**

Figure 6.6 Thermal ellipsoids (50%) and labeling scheme of the supermolecules in **26ADI** and **26DOD**.

Furthermore, **26ADI** contains amide…amide homosynthons, resulting in a 2-D sheet, Figure 6.7. However the overall architecture of **26DOD**, displayed a slight twist in the structure resulting in a ribbon-like 2-D structure, via the amide…amide homosynthon, Figure 6.8.

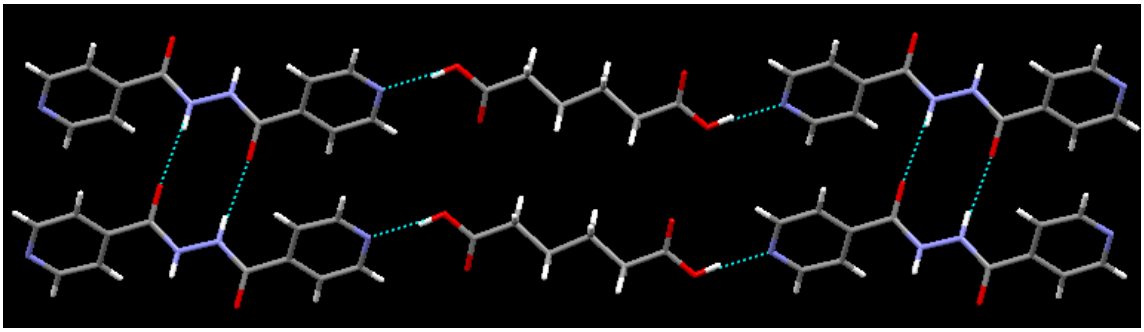

Figure 6.7 2-D sheet in **26ADI** with both O-H…N and N-H…O hydrogen bonds.

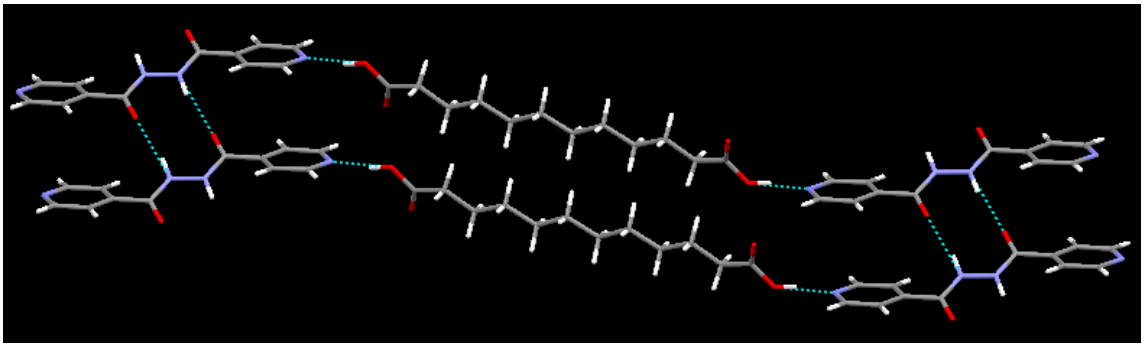

Figure 6.8 Slightly twisted 2-D architecture in **26DOD**.

6.4.1.3 Crystal structure of 27SUC

Similar to **26SUC**, the asymmetric unit of **27SUC** contains one water molecule as well as one molecule of **27**, however instead of one molecule of **SUC** the lattice contains two molecules of **SUC**. Furthermore, as with **26SUC** the acid…pyridine heterosynthon is observed, along with the water molecule forming hydrogen bonds with the carbonyl of the API, as well as with the carbonyl of the acid and the hydroxy group of the other acid, Figure 6.9. The interesting thing about this structure is its unique packing resulting from the water molecule, which aids in the formation of 2-D layered structure, Figure 6.10.

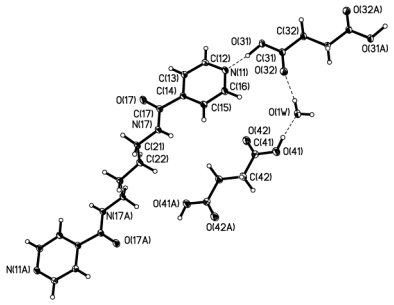

Figure 6.9 Thermal ellipsoid (50%) and labeling of **27SUC**.

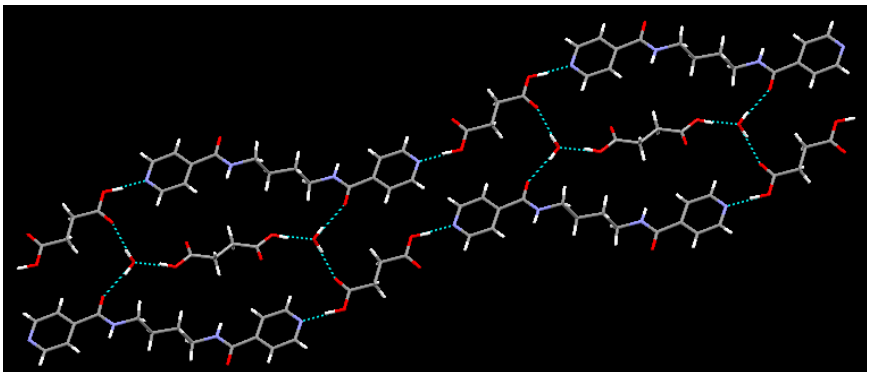

Figure 6.10 Unique packing of **27SUC** resulting in O-H…N and O-H…O hydrogen bonding.

6.4.1.4 Crystal structures of 27ADI and 27SUB

The asymmetric unit of **27ADI** and **27SUB** contains half a molecule of **27** and half a molecule of **ADI,** and **DOD** respectively, with hydrogen bonds between the pyridine nitrogen and the dicarboxylic acid in both structures, Figure 6.11.

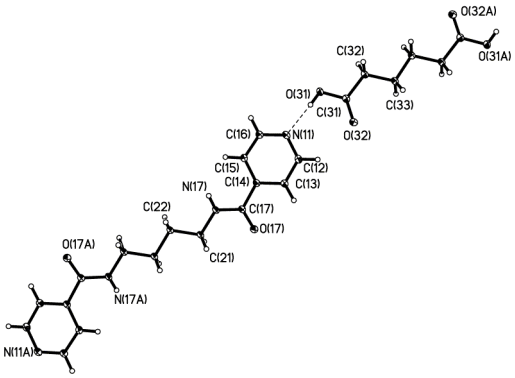

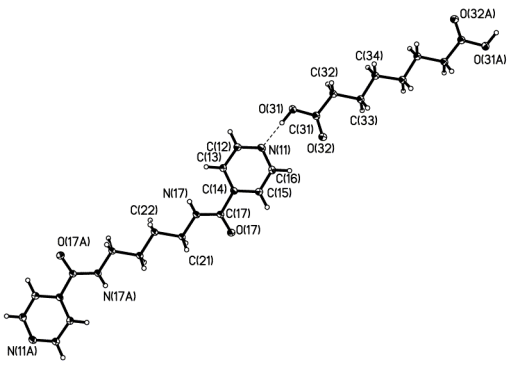

27ADI **27SUB**

Figure 6.11 Thermal ellipsoids (50%) and labeling scheme of **27ADI** and **27SUB**.

The N-H…O interactions result in a 1-D chain, which is expanded into a 2-D sheet via the aide of amide…amide (N-H…O) interactions, Figure 6.12 and Figure 6.13, respectively.

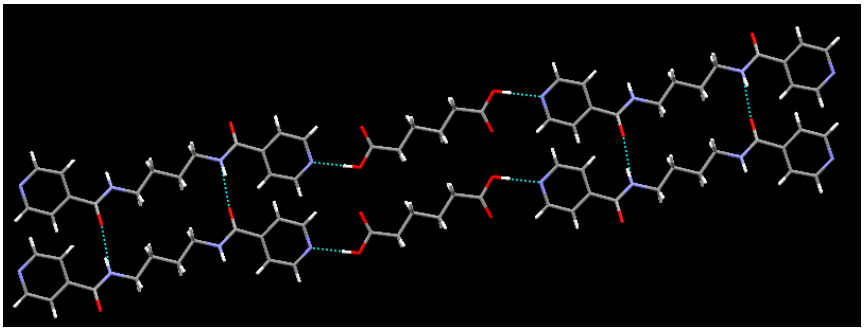

Figure 6.12 2-D sheet in **27ADI**, held together by O-H…N and N-H…O interactions.

Figure 6.13 2-D sheet in **27SUB** held together by O-H…N and N-H…O interactions.

6.4.1.5 Crystal structures of 28SUC, 28ADI, 28SUB, 28SEB, 28DOD, 28OXA and 28PIM

The crystal structures of **28SUC, 28ADI**, **28SUB**, **28SEB**, **28DOD**, **28OXA** and **28PIM** are all similar in that they are 1:1 cocrystals of **28** and the given dicarboxylic acids, all displaying the robust O-H…N heterosynthon between the pyridine nitrogen and the carboxylic acid, Figure 6.14.

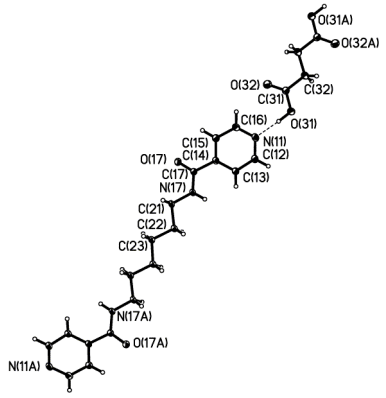

28SUC

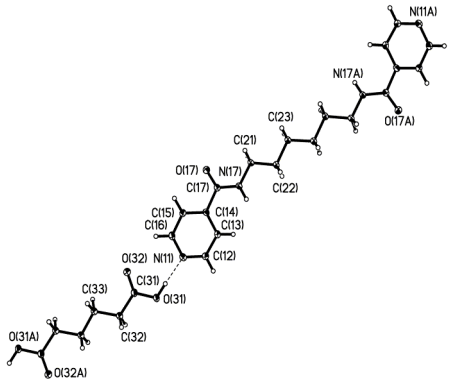

28ADI

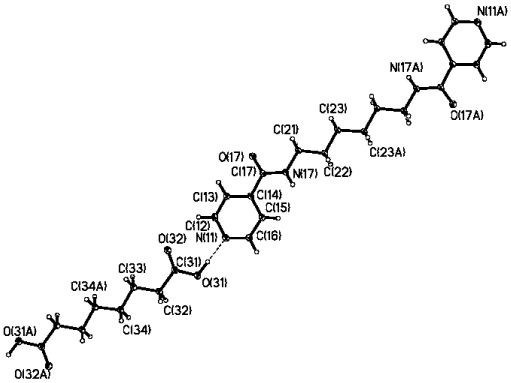

28SUB

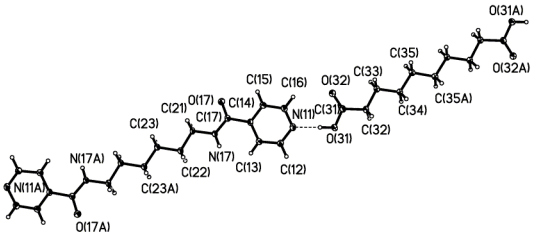

28SEB

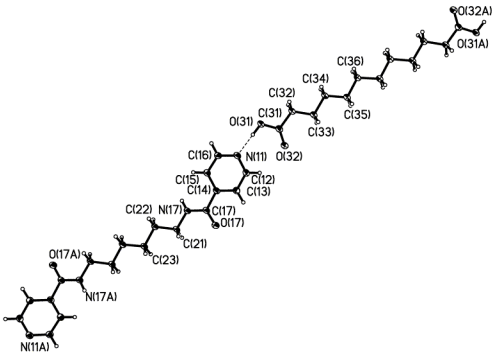

28DOD

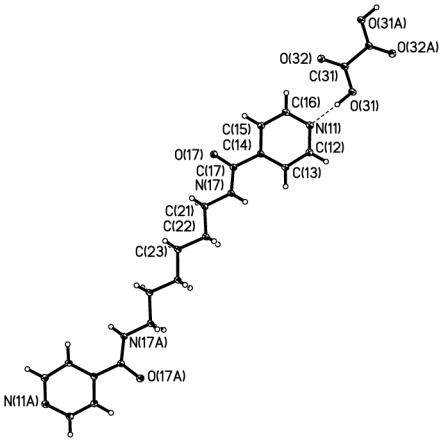

28OXA

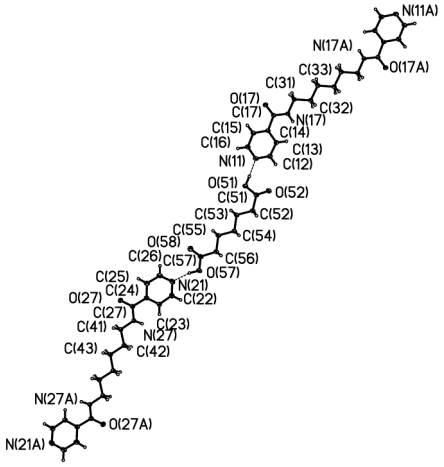

28PIM

Figure 6.14 Thermal ellipsoids (50%) and labeling scheme of the 1:1 supermolecule of **28SUC**, **28ADI**, **28SUB**, **28SEB**, **28DOD**, **28OXA** and **28PIM**.

These interactions result in the formation of 1-D chains Figures 6.15-6.21 respectively, which in turn are organized into layers via inter-chain N-H…O hydrogen bonds; bond distances are shown in Table 6.1. Although the packing of the **28PIM** is slightly different from the others in that the structure form this twisted 2-D layer instead of the linear array that was observed in the other structures.

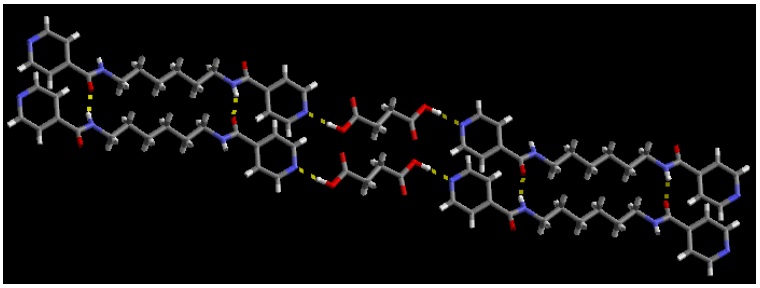

Figure 6.15 2-D sheet in **28SUC** held together via O-H…N and N-H…O hydrogen bonds.

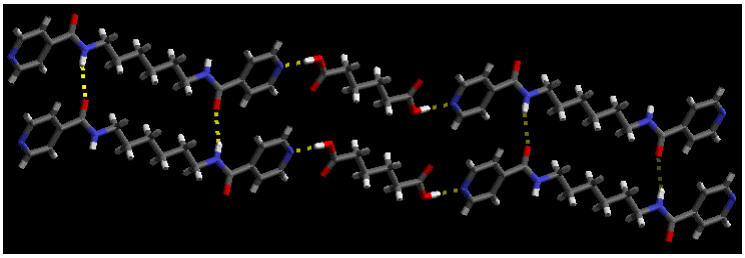

Figure 6.16 2-D sheet in **28ADI** held together via O-H…N and N-H…O hydrogen bonds.

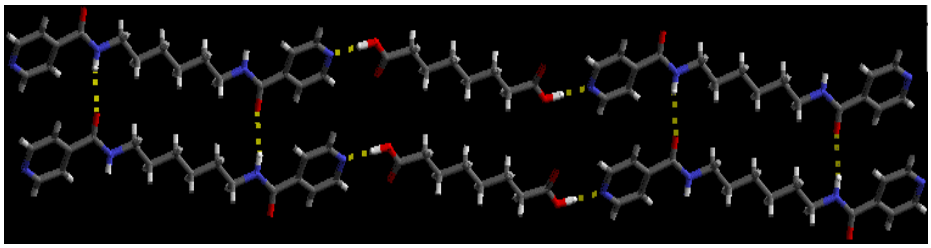

Figure 6.17 2-D sheet in **28SUB** held together via O-H…N and N-H…O hydrogen bonds.

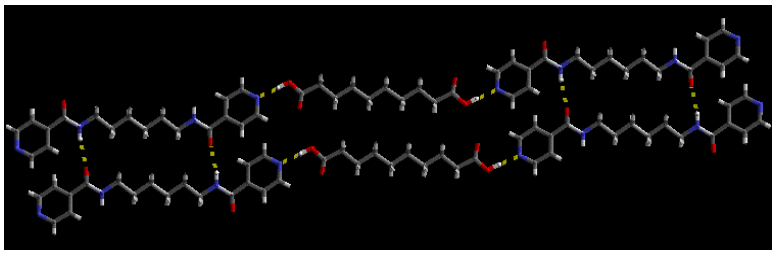

Figure 6.18 2-D sheet in **28SEB**.

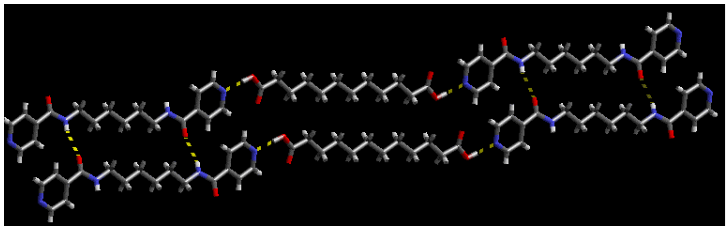

Figure 6.19 2-D sheet in **28DOD**.

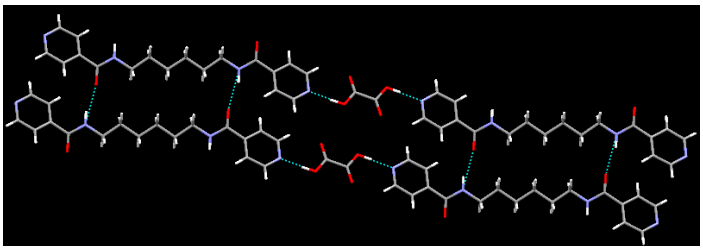

Figure 6.20 2-D sheet in **28OXA** held together through O-H…N and N-H…O hydrogen bonds.

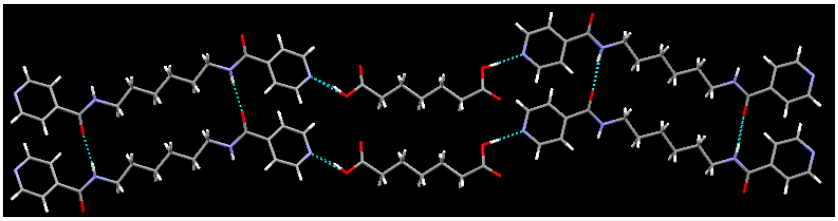

Figure 6.21 Slightly twisted 2-D sheet in **28PIM**.

6.4.1.6 Crystal structures of 29SUC, 29SUC, 29ADI, 29SUB, 29SEB and 29MAL

The crystal structures of **29** are very similar in that each asymmetric unit consists of one molecule of **29** and one molecule of the corresponding dicarboxylic acid. Again the acid…pyridine supramolecular synthon is observed, Figure 6.22.

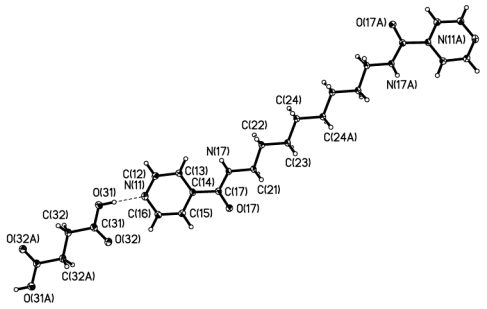

29SUC

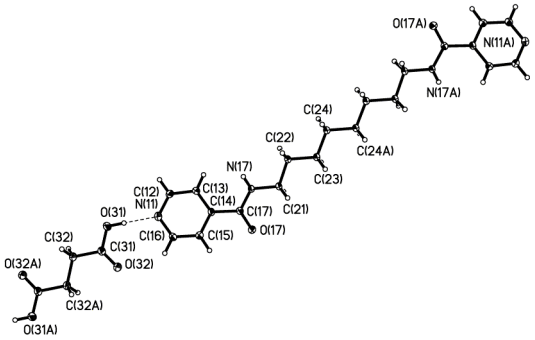

29ADI

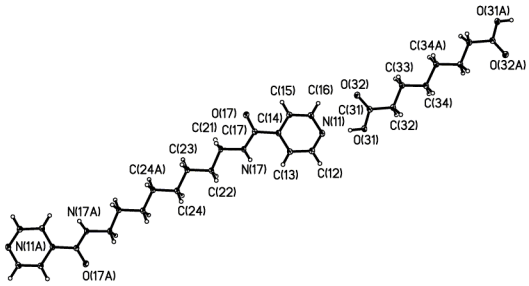

29SUB

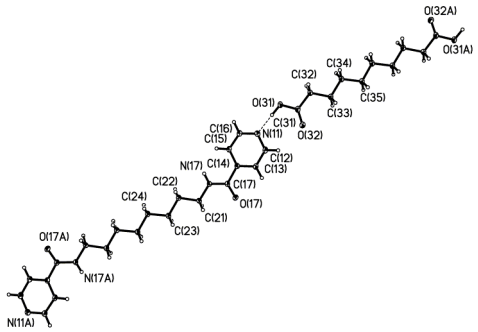

29SEB

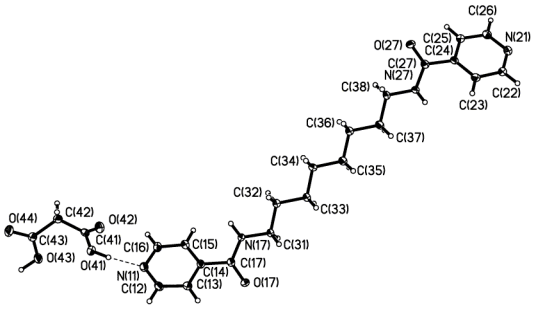

29MAL

Figure 6.22 The thermal ellipsoids (50%) and labeling scheme of **29SUC**, **29ADI**, **29SUB**, **29SEB** and **29MAL**.

The overall architecture in each case is a 2-D sheet-like structure via intermolecular interactions between the adjacent amides, Figures 6.23-27. In addition, even though the binding interactions are similar in all the structures with **29**, the packing of **29MAL** is different in that it formed a 2-D zig-zag array.

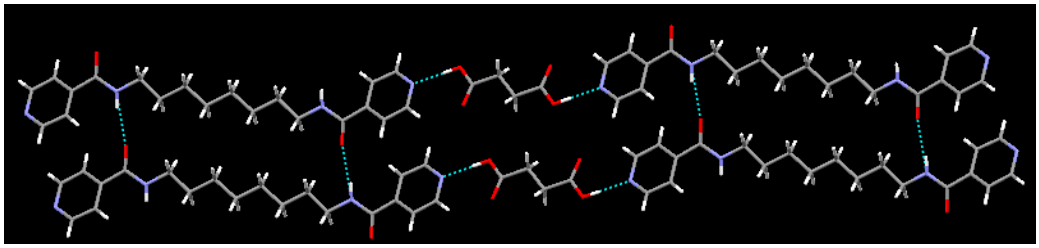

Figure 6.23 2-D sheet-like structure in **29SUC**.

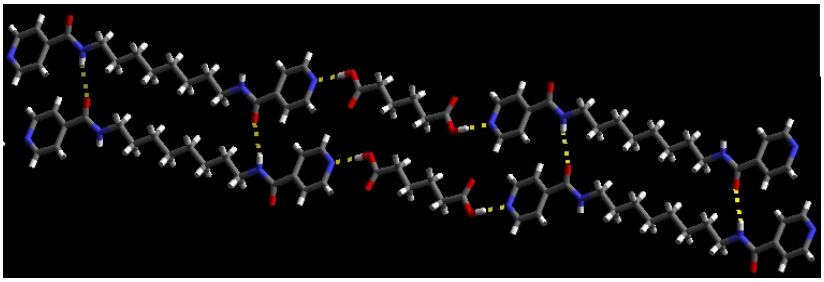

Figure 6.24 2-D sheet observed in **29ADI**.

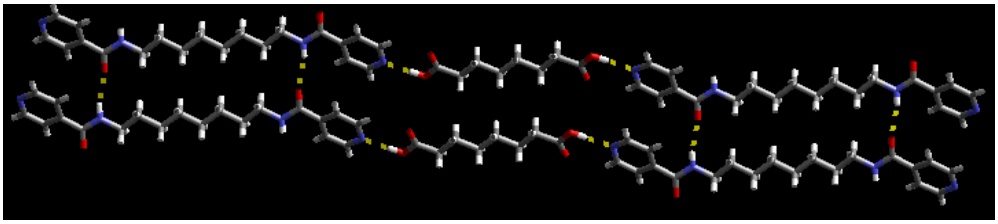

Figure 6.25 2-D sheet-like structure in **29SUB**.

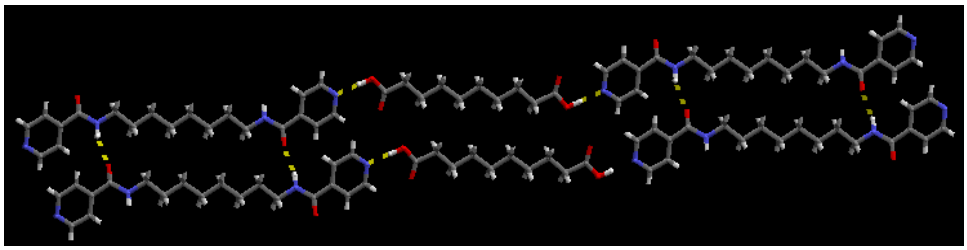

Figure 6.26 2-D sheet-like structure in **29SEB**.

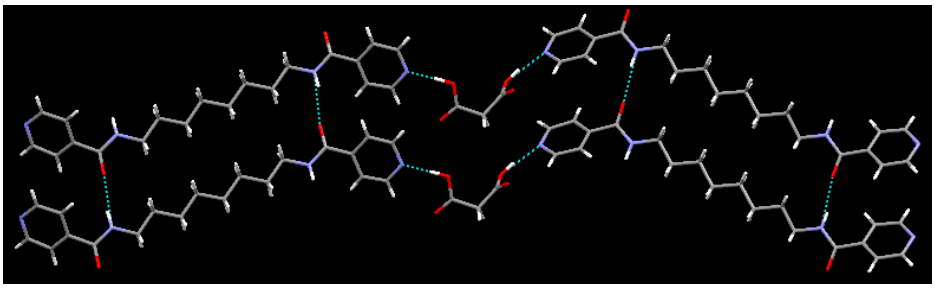

Figure 6.27 2-D zig-zag array in **29MAL** formed through O-H…N and N-H…O hydrogen bonds.

6.4.1.7 Crystal structure of 30SEB

The crystal structure of **30SEB** consists of one molecule of **30** and one molecule of **SEB** in the asymmetric unit. The primary O-H…N supramolecule synthon is observed, resulting from the interaction between the pyridine nitrogen and the dicarboxylic acid, Figure 6.28.

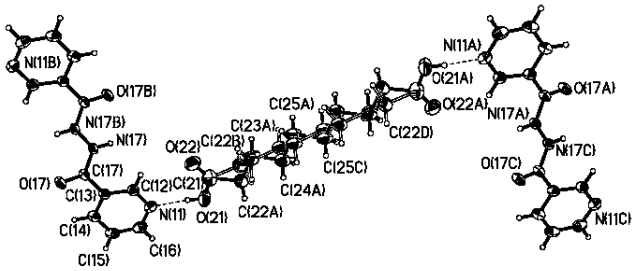

Figure 6.28 Thermal ellipsoids and labeling scheme for the supermolecule of **30SEB**.

The overall architecture is a 2-D zig-zag array via intermolecular interactions between the adjacent amides, Figure 6.29.

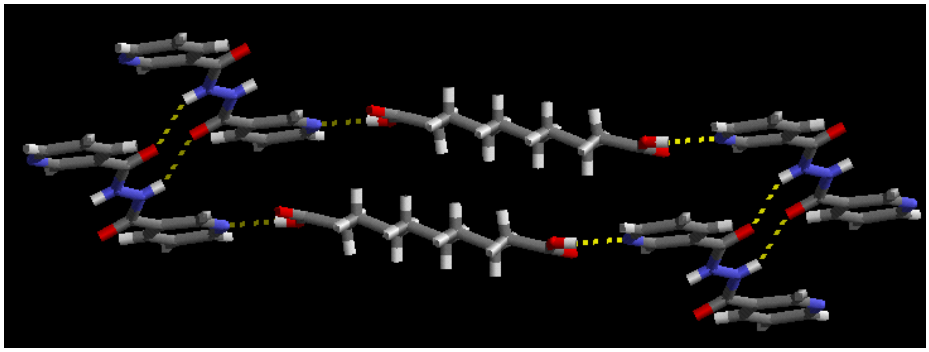

Figure 6.29 2-D zig-zag array in **30SEB**.

6.4.1.8 Crystal structures of 31SUC, 31SUB, 31DOD

The crystal structures of **31** are very similar in that each asymmetric unit consists of half a molecule of **31** and half a molecule of the corresponding dicarboxylic acid. The structures are held together via acid…pyridine (O-H…N) Figure 6.30, bond distances, Table 6.1.

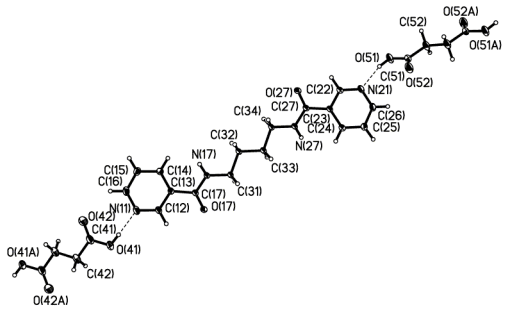

31SUC

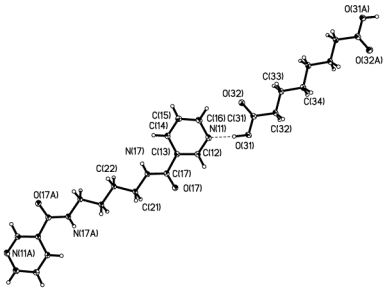

31SUB

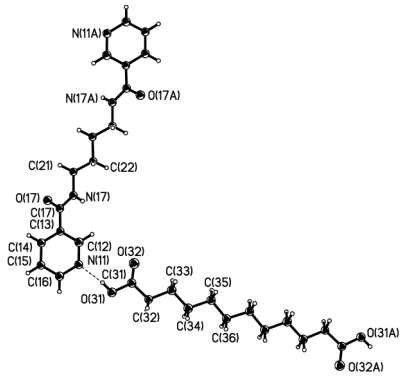

31DOD

Figure 6.30 Thermal ellipsoids (50%) and labeling scheme for the supermolecules of **31SUC**, **31SUB** and **31DOD**.

The 2-D array observed is held together via intermolecular interactions between the adjacent amides, Figures 6.31-6.33. The crystal packing in **31DOD** was different from the other two structures, it formed a zig-zag array compare to the planar packing observed in both **31SUC** and **31SUB**.

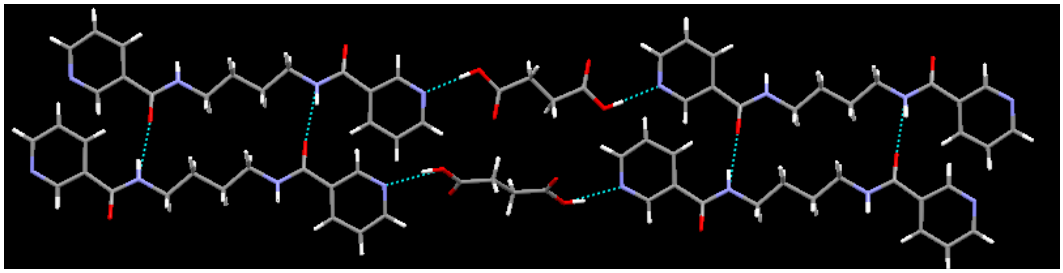

Figure 6.31 2-D sheet-like structure in **31SUC**.

Figure 6.32 2-D array in **31SUB** held together by both O-H…N and N-H…O hydrogen bonds.

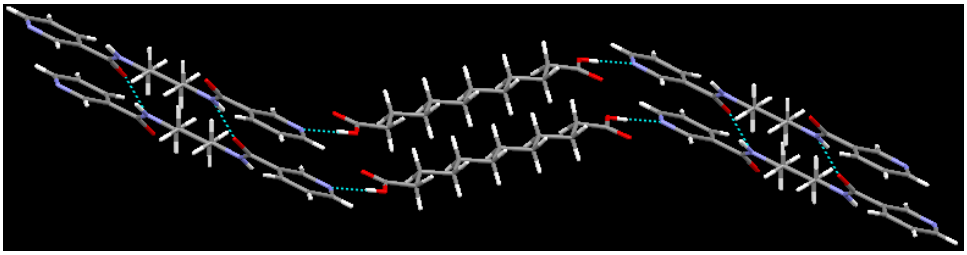

Figure 6.33 Zig-zag array in **31DOD** held together via O-H…N and N-H…O hydrogen bonds.

6.4.1.9 Crystal structures of 32SUC, 32ADI, 32SUB, 32SEB, 32DOD, 32OXA, 32GLU, 32HEP, 32OCT, 32LAU

The crystal structures of **32** consist of half a molecule of **32** and half a molecule of the corresponding mono or dicarboxylic acid in the asymmetric unit. The primary O-H…N supramolecule synthon is observed, resulting from the interaction between the pyridine nitrogen and the dicarboxylic acid, Figure 6.34. In addition, the crystal structure of **32SUC** is somewhat disordered.

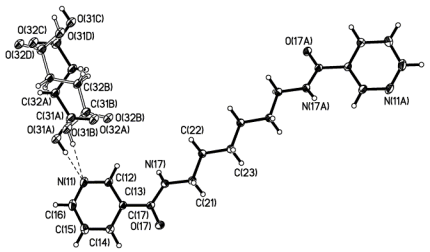

32SUC

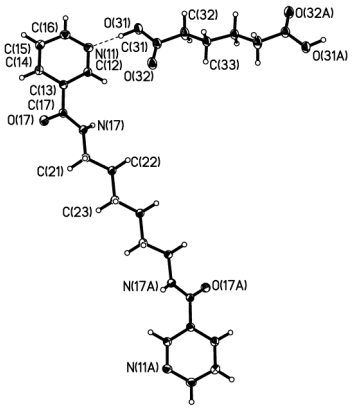

32ADI

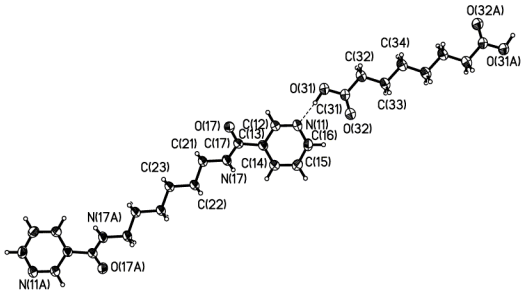

32SUB

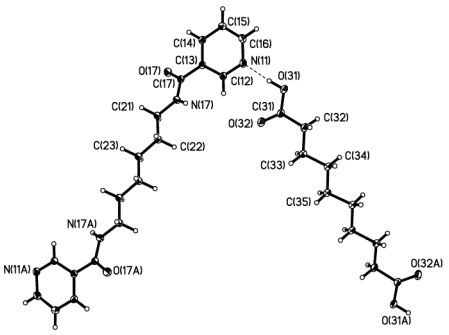

32SEB

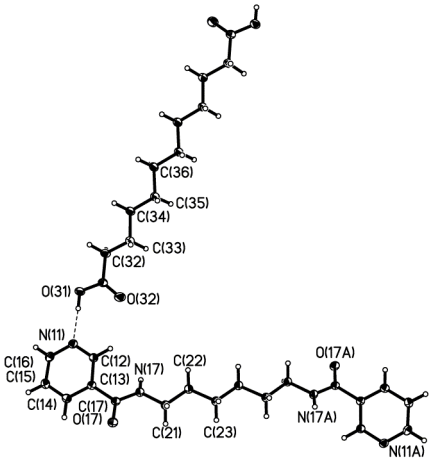

32DOD

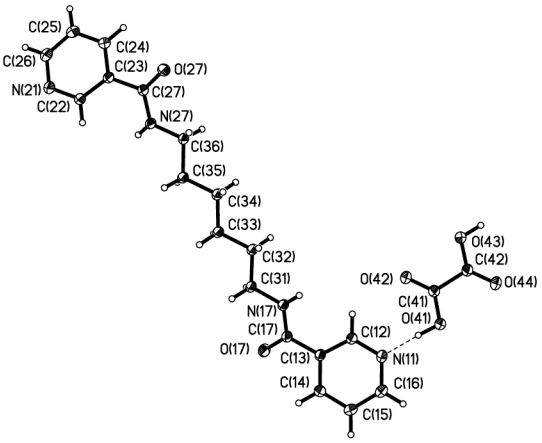

32OXA

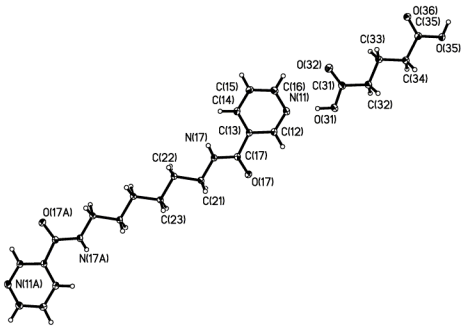

32GLU

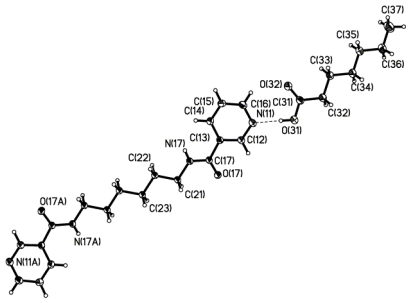

32HEP

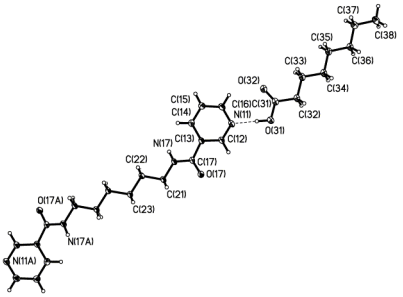

32OCT

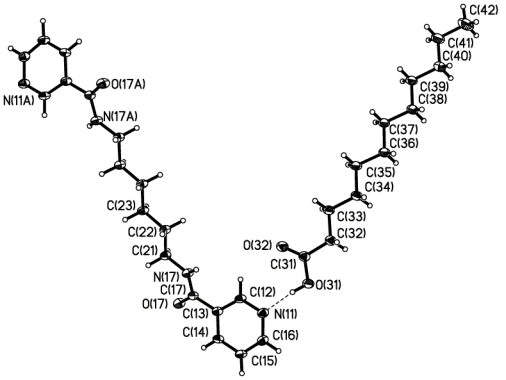

32LAU

Figure 6.34 Thermal ellipsoids (50%) and labeling scheme for the supermolecules of **32SUC**, **32ADI**, **32SUB**, **32SEB**, **32DOD**, **32OXA**, **32GLU**, **32HEP**, **32OCT** and **32LAU**.

The 2-D layer in these structures are held together via intermolecular interactions between the adjacent amides, Figures 6.35-6.44. Although the connections in each of the molecules are the same, the packing is different, in that crystal structures **32SUC**, **32ADI**, **32SEB**, **32DOD**, and **32OXA** all packed in a zig-zag array, whereas the other crystal structures of **32** are packed in a planar fashion. Interestingly, although **32HEP**, **32OCT** and **32LAU** are formed with monoacids they still result in the same intermolecular interactions, Figures 6.42-6.44. Additionally, of all the dicarboxylic acids, **32GLU** packed in an exceptional fashion, not only is the robust O-H…N synthon observed, but the structure also forms an acid…acid dimer which aids in the extension of the linear 2-D sheet, Figure 6.41.

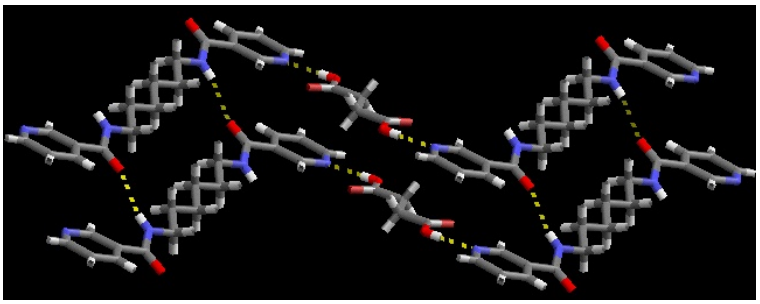

Figure 6.35 2-D zig-zag array in **32SUC** held together via O-H…N and N-H…O hydrogen bonds.

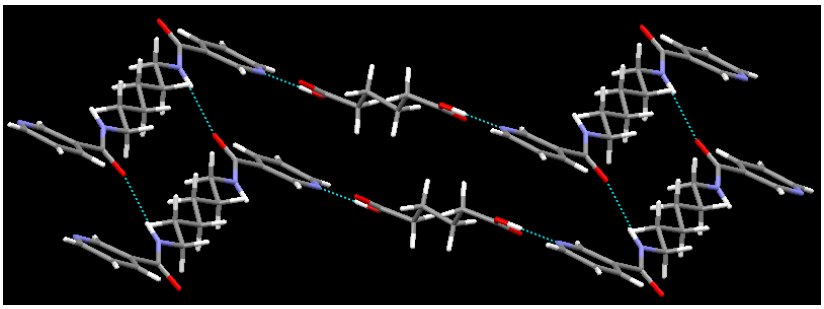

Figure 6.36 2-D zig-zag array in **32ADI** held together by O-H…N and N-H…O hydrogen bonds.

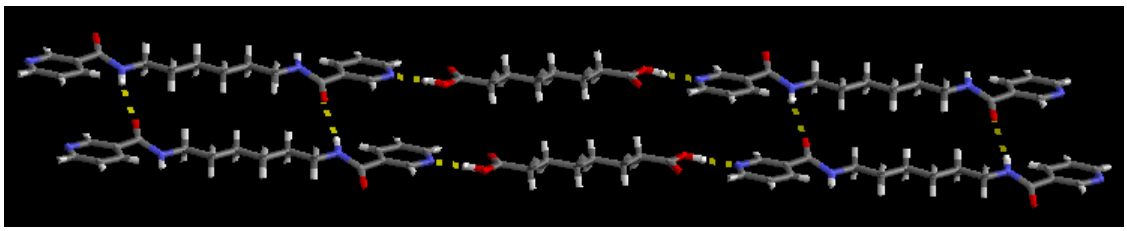

Figure 6.37 2-D sheet-like structure in **32SUB**, formed through O-H…N and N-H…O hydrogen bonds.

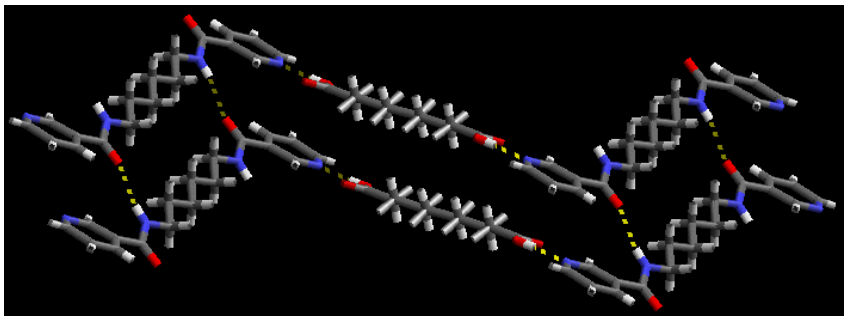

Figure 6.38 Zig-zag array of **32SEB** formed through O-H…N and N-H…O hydrogen bonds.

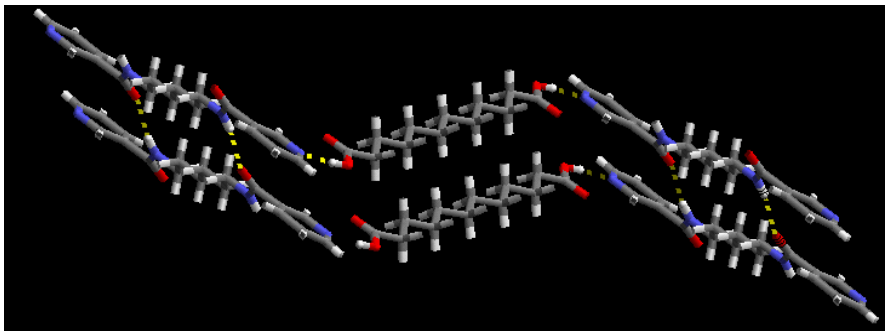

Figure 6.39 2-D zig-zag array in **32DOD** formed through O-H…N and N-H…O hydrogen bonds.

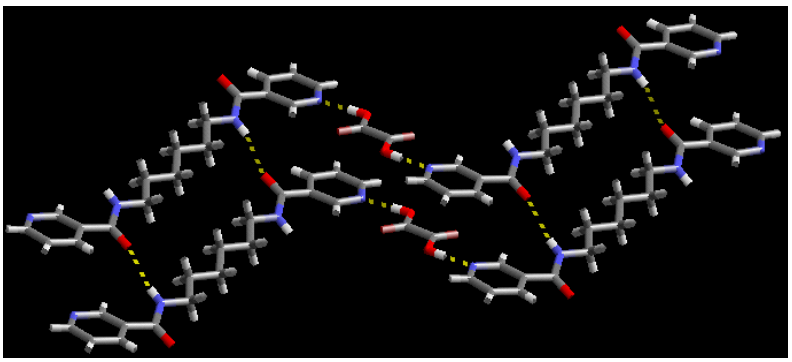

Figure 6.40 Zig-zag array in **32OXA**, formed through O-H…N and N-H…O hydrogen bonds.

Figure 6.41 Unique 2-D array in **32GLU** held together via O-H…N, N-H…O and O-H…O hydrogen bonds.

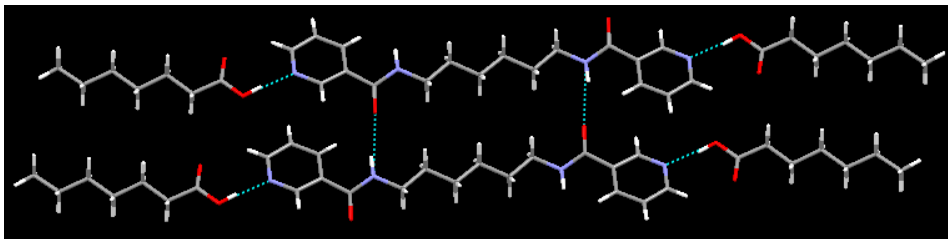

Figure 6.42 1:1 cocrystal in **32HEP** formed through O-H…N and N-H…O hydrogen bonds.

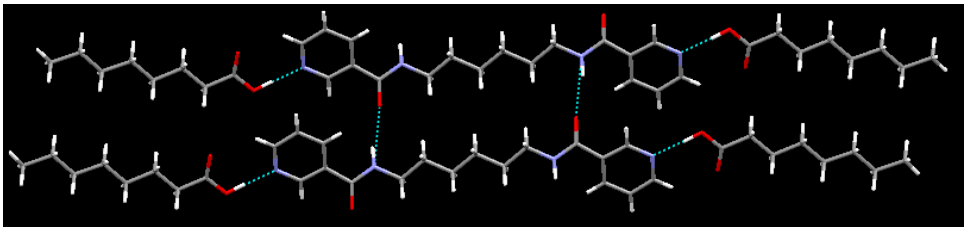

Figure 6.43 1:1 cocrystal in **32OCT** formed via O-H…N and N-H…O hydrogen bonds.

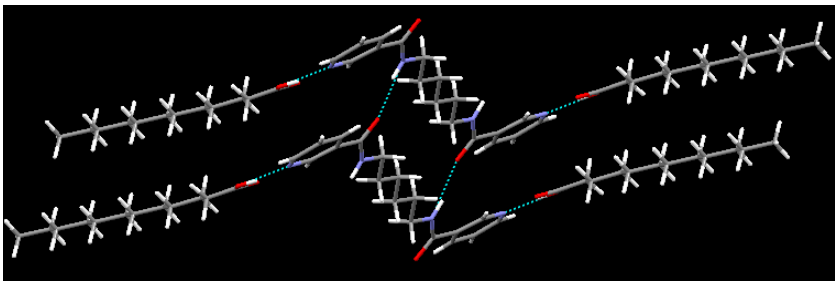

Figure 6.44 1:1 cocrystal in **32LAU** forming a 2-D zig-zag array through O-H…N and N-H…O hydrogen bonds.

6.4.1.10 Crystal structures of 33SUC, 33SUB, 33PIM

The crystal structures of **33** consist of half a molecule of **33** and half a molecule of the corresponding dicarboxylic acid in the asymmetric unit. The primary O-H…N supramolecule synthon is observed, resulting from the interaction between the pyridine nitrogen and the dicarboxylic acid, Figure 6.45.

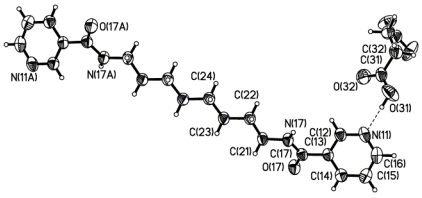

33SUC

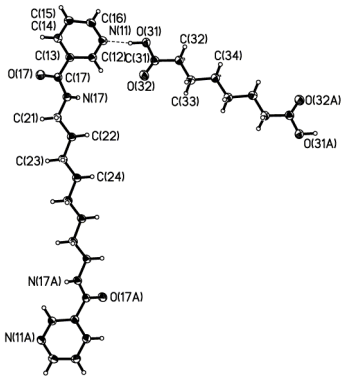

33SUB

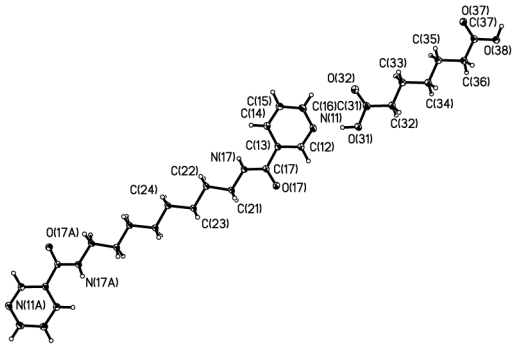

33PIM

Figure 6.45 Thermal ellipsoids (50%) and labeling scheme for the supermolecules of **33SUC**, **33SUB**, and **33PIM.**

A 2-D array is formed via interactions between adjacent amides, Figures 6.46-6.48. Although the connections in each structure are the same, the packing is different. Crystal structures **33SUC** and **33SUB** both packed in a zig-zag array. Whereas, **33PIM** not only packed in a planar fashion, but instead of a 1:1 structure, it is a 1:2 structure, which is similar to **32GLU**, because it also forms an acid…acid dimer, resulting in a linear packing of the overall structure, Figure 6.48.

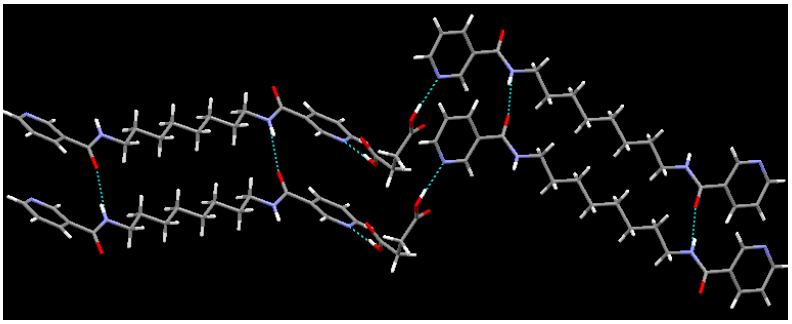

Figure 6.46 2-D zig-zag array in **33SUC**, formed through O-H…N and N-H…O hydrogen bonds.

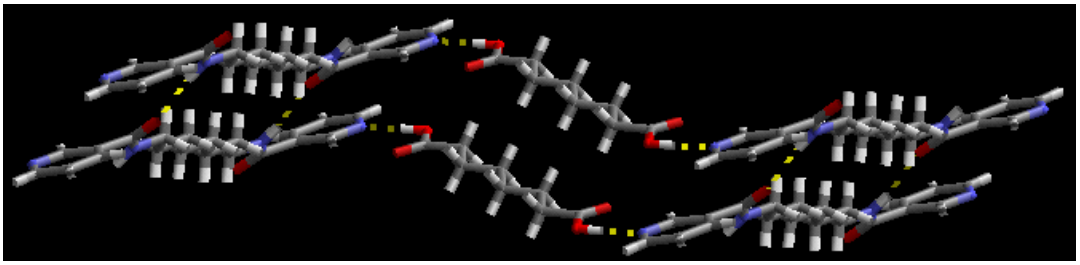

Figure 6.47 Zig-zag array in **33SUB** formed through intermolecular interactions of O-H…N and N-H…O hydrogen bonds.

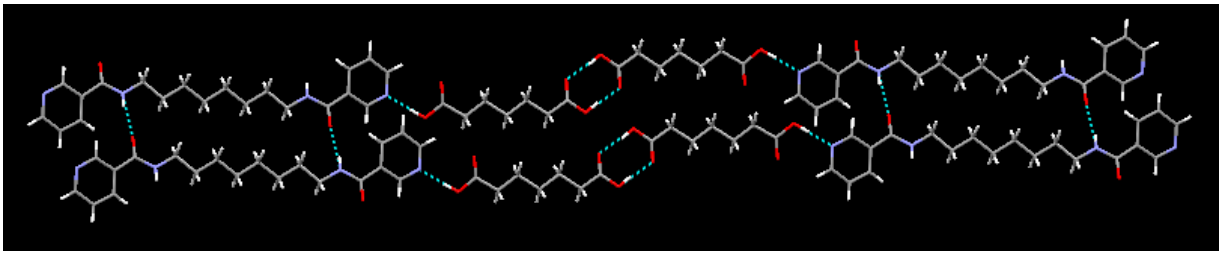

Figure 6.48 Unique 2-D array in **33PIM** formed through O-H…N, N-H…O and O-H…O hydrogen bonds.

6.4.2 IR spectroscopy

IR spectroscopy was used to screen all co-crystallization reactions in order to determine the formation of cocrystal. The solids obtained from co-crystallization reactions showed very similar stretches, at approximately 2450 cm^{-1} and 1900 cm^{-1} the formation of O-H…N(py) hydrogen bonds. Moreover, each cocrystal obtained showed a carbonyl stretch above 1670 cm^{-1} which further confirms cocrystal formation, not a salt, which would have a carbonyl shift below 1660 cm^{-1} suggesting the presence of COO^- anions. Table 6.2 summarizes the vibrational stretch observed for each structure and Figure 6.49 depicts an example of cocrystal formed with **28**; the remaining spectrum are shown in Table D.1 (Appendix D).

Table 6.2 Summary of IR data for compounds **26SUC, 26ADI, 26DOD, 27SUC, 27ADI, 27SUB, 28SUC, 28ADI, 28SUB, 28SEB, 28DOD, 28OXA, 28PIM, 29SUC, 29ADI, 29SUB, 29SEB, 29MAL, 30SEB, 31SUC, 31SUB, 31DOD, 32SUC, 32ADI, 32SUB, 32SEB, 32DOD, 32OXA, 32GLU, 32HEP, 32OCT, 32LAU** and **33SUC, 33SUB, 33PIM**

Compounds	Observed stretch (O-H..N) cm^{-1}	Observe COOH cm^{-1}	Product
26SUC	2402 & 1956	1687	cocrystal
26ADI	2533 & 1891	1706	cocrystal
26DOD	2516 & 1944	1699	cocrystal
27SUC	2504 & 1973	1699	cocrystal
27ADI	2537 & 1871	1699	cocrystal
27SUB	2500 & 1875	1703	cocrystal
28SUC	2488 & 1871	1702	cocrystal
28ADI	2512 & 1858	1699	cocrystal
28SUB	2504 & 1879	1707	cocrystal
28SEB	2520 & 1862	1707	cocrystal
28DOD	2508 & 1866	1707	cocrystal
28OXA	2402 & 1862	1679	cocrystal
28PIM	2500 & 1928	1699	cocrystal
29SUC	2495 & 1920	1704	cocrystal
29ADI	2500 & 1926	1710	cocrystal
29SUB	2501 & 1892	1706	cocrystal
29SEB	2520 & 1871	1699	cocrystal
29MAL	2501 & 1971	1690	cocrystal
20SEB	2496 & 1913	1697	cocrystal
31SUC	2467 & 1916	1700	cocrystal
31SUB	2496 & 1887	1697	cocrystal
31DOD	2500 & 1875	1710	cocrystal
32SUC	2481 & 1924	1690	cocrystal
32ADI	2516 & 1895	1695	cocrystal
32SUB	2496 & 1896	1701	cocrystal
32SEB	2508 & 1905	1700	cocrystal
32DOD	2500 & 1901	1708	cocrystal
32OXA	2501 & 1928	1695	cocrystal
32GLU	2474 & 1918	1705	cocrystal
32HEP	2534 & 1938	1714	cocrystal
32OCT	2509 & 1909	1707	cocrystal
32LAU	2528 & 1904	1700	cocrystal
33SUC	2516 & 1891	1694	cocrystal
33SUB	2496 & 1891	1699	cocrystal
33PIM	2508 & 1903	1691	cocrystal

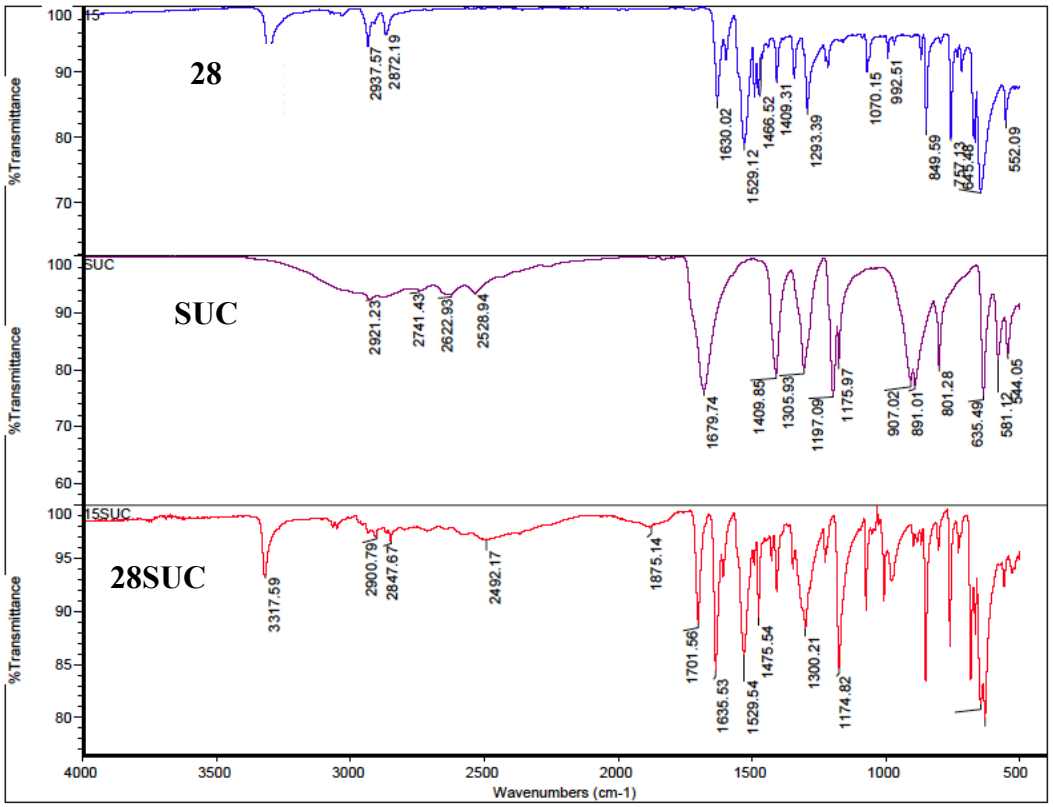

Figure 6.49 IR spectra depicting cocrystal formation in **28SUC**; **28** (blue), **SUC** (purple), **28SUC** (red).

The APIs formed cocrystals thirty-five out of thirty-five cases, given a supramolecular yield of 100%. In each case a broad stretch at approximately 2500 and 1900 cm^{-1} was observed, which as previously mentioned is indicative of O-H…N (heterocyclic) hydrogen bonds. The formation of cocrystal in each case is driven by O-H…N interactions. However, even though each compound was able to form a cocrystal, the structural consistency of each cocrystal can only be obtained from single crystal X-ray crystallography data.

6.4.3 Addressing structural consistency

The intermolecular interactions observed in the series of cocrystals are remarkably consistent. In all thirty-five cases the pyridine nitrogen…acid heterosynthon was observed both in the IR spectra and X-ray structures. However, the amide…amide homosynthon was observed thirty-three out of thirty-five times with a 94% success rate. In the two exceptions **26SUC** and **27SUC**, this was due to disruption of the architecture

by a water molecule. A summary of the unit cell parameters for the crystal structures of **28SUC, 28ADI, 28SUB, 28SEB, 28DOD** are given in Table 6.3.

Table 6.3 Comparison of structural data of cocrystals of **28**

	28SUC	**28ADI**	**28SUB**	**28SEB**	**28DOD**
a (Å)	5.1754(4)	5.1412(4)	5.1392(5)	5.1506(4)	5.1519(4)
b (Å)	10.9294(8)	5.2394(4)	5.2412(5)	5.2481(4)	5.2778(5)
c (Å)	10.9423(8)	21.396(2)	23.145(2)	24.521(2)	26.148(3)
α (deg)	118.826(4)	95.094(5)	94.959(3)	89.647(4)	86.023(6)
β (deg)	91.381(5)	95.603(4)	95.222(2)	87.252(4)	89.386(6)
γ (deg)	99.872(4)	91.076(5)	91.277(2)	88.505(5)	88.496(6)
V ($Å^3$)	530.11(7)	571.10(8)	619.0(1)	661.82(8)	709.0(1)

As shown by the structural parameters, the five cocrystals of **28** are isostructural, and the increase in unit cell volume is a reflection of an increase in the size of the co-crystallizing agent. Likewise, with the other structures obtained with **27**, **29-33**, they all are isostructural displaying similar increases in unit cell volume, Tables 6.4-6.5.

Table 6.4 Comparison of structural data of cocrystals of **27** and **29**

	27ADI	**27SUB**	**29SUC**	**29ADI**	**29SUB**	**29SEB**
a	5.1160(4)	5.1072(4)	5.1072(4)	5.1403(3)	5.1420(4)	5.1264(6)
b	5.1957(4)	5.2045(4)	5.1171(4)	5.2489(3)	5.2541(4)	5.2432(6)
c	19.5042(16)	21.5019(14)	22.119(2)	22.9829(15)	24.624(2)	26.127(3)
α	90.704(2)	94.963(2)	96.134(6)	93.859(4)	89.785(4)	85.874(4)
β	93.362(2)	95.404(2)	94.037(6)	95.267(4)	87.095(4)	89.354(4)
γ	91.346(2)	91.630(2)	91.340(6)	91.289(4)	88.590(4)	88.356(4)
V	517.36(7)	568.12(7)	573.05(8)	615.82(6)	664.209(9)	700.11(14)

Table 6.5 Comparison of structural data of cocrystals of **31** and **32**

	31SUC	**31SUB**	**31DOD**	**32SUC**	**32ADI**	**32SEB**	**32SUB**	**32DOD**
a	10.0264(7)	5.0982(5)	5.097(3)	5.0275(6)	5.0282(6)	5.1671(13)	4.9817(4)	4.9821(4)
b	10.1248(7)	11.4639(10)	5.486(3)	6.9253(9)	6.7877(8)	11.646(3)	6.8634(6)	6.8797(6)
c	11.0782(8)	11.4873(11)	23.823(13)	16.058(2)	17.522(2)	11.779(4)	20.0493(16)	21.4410(17)
α	91.733(2)	115.707(3)	86.020(18)	89.749(6)	98.124(3)	67.873(11)	90.233(4)	87.936(6)
β	107.922(2)	98.696(4)	86.521(18)	81.536(5)	97.604(3)	80.585(12)	90.233(4)	86.223(6)
γ	110.922(2)	100.874(4)	87.553(18)	80.93(6)	94.605	79.827(12)	98.285(4)	81.469(5)
V	493.555(12)	573.10(9)	662.8(6)	545.92(12)	583.82(12)	642.6(3)	677.32(10)	724.93(10)

Additionally, the crystal structures **32GLU** and **33PIM** both formed an acid…acid dimer along with the other excepted supramolecular synthons. This unique intermolecular interaction could be as a result of the structure wanting to form a linear network instead of a zigzag off-stack motif that was observed in the structures of **32** and **33**.

6.4.4 Correlating melting behavior with the nature of the co-crystallizing agent

It has been demonstrated that co-crystallization can be used as a tool for improving the thermal stability[27] as well as other physicochemical properties[12,13] of variety of APIs. With this in mind and having achieved the required structural consistency, we subsequently examined whether the thermal behavior of cocrystals formed with **27**, **28** and **29** could be correlated with any molecular feature of the five even numbered dicarboxylic acids. Melting point were recorded for the resulting cocrystals, and in the case of **27**, **28** and **29** cocrystals, a graph of dicarboxylic acid melting point versus cocrystal melting point was plotted, Figure 6.50. The data clearly shows that the melting points of these five crystalline solids are directly related to the melting point of dicarboxylic acids.

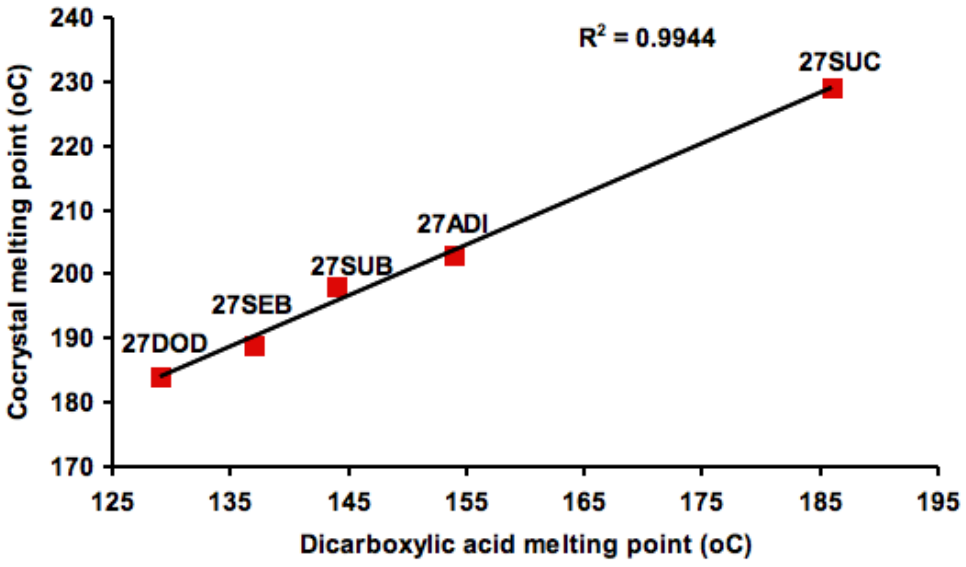

(a)

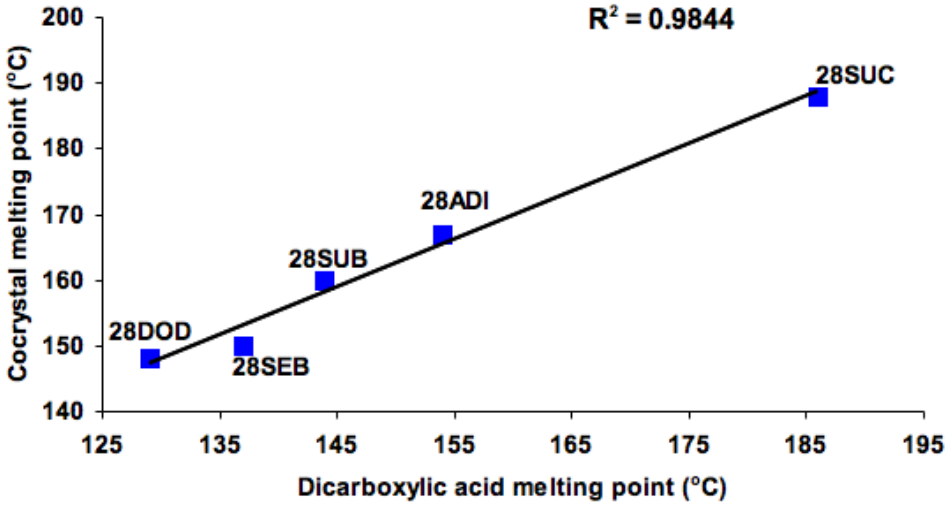

(**b**)

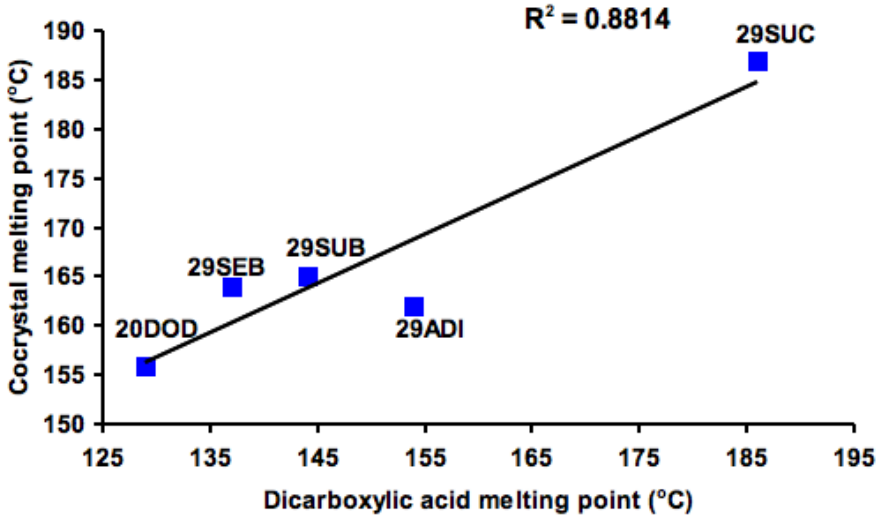

(**c**)

Figure 6.50 Melting points of cocrystals plotted vs. the melting point for the corresponding diacids; (a) **27SUC-27DOD**; (b) **28SUC-28DOD**; (c) **29SUC-29DOD**.

The cocrystals in each series displayed higher melting points than the corresponding pure diacids (Table 6.6); this is because of the strong hydrogen bonds and the efficient close packing, which stabilize the structures of the molecular complexes.

Table 6.6 Melting point of aliphatic dicarboxylic acids and their 1:1 cocrystals of **27**, **28**, and **29**.

	Dicarboxylic acids	M.p. of diacid	M.p. of cocrystal of 27	M.p. of cocrystal of 28	M.p. of cocrystal of 29
	SUC	186	229	188	187
	ADI	154	203	167	162
	SUB	144	198	160	165
	SEB	137	189	150	163
	DOD	129	184	148	156
R^2			0.9944	0.9844	0.8814
Equation of line			y = 0.79x + 82	y = 0.72x + 54	y = 0.50x + 92

Thus in each case the highest-melting cocrystal contains the dicarboxylic acid with the highest melting point, and the lowest-melting acid produces the lowest melting point cocrystal; demonstrating that the melting behavior of a given API can be modulated in a predictable and controlled manner. Additionally, the melting point alteration in this co-crystalline series constitutes a readily explainable change in the physical properties of a pure component series as a consequence of cocrystal formation.

6.4.5 Modulating aqueous solubility

Although thermal properties are important; aqueous solubility is one of the key physicochemical parameters of a drug substance that needs to be assessed early on in the drug discovery and drug candidate selection process. Therefore the aqueous solubility of cocrystals of **28** and **29** (Figure 6.51 and Table E.1 Appendix E) were determined.

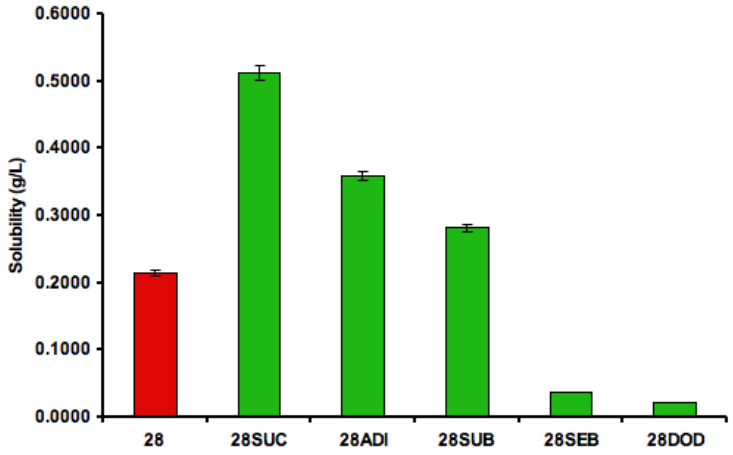

(a)

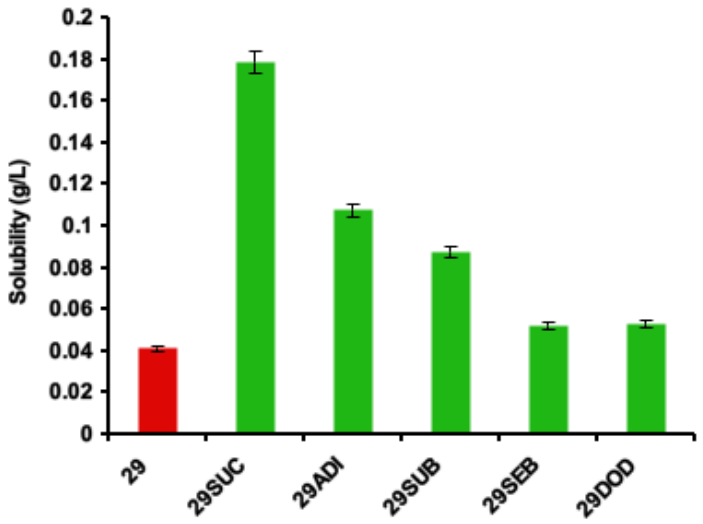

(b)

Figure 6.51 Aqueous solubility of: (a) **28** and **28SUC-28DOD** (b) **29** and **29SUC-29DOD**.

The results show that the aqueous solubility of **28** and **29** can in fact be improved by a factor of 2.5 and 4.5 respectively, without altering the molecular structure of the API itself. Although the solubility of the cocrystals of **28** and **29** did not produce a linear correlation with the aliphatic even chain dicarboxylic acids, as did the melting points, the trend in physicochemical properties of the cocrystals can certainly be rationalized in terms of the aqueous solubility of the dicarboxylic acids. The cocrystals of the longer-chain diacids, which are less polar and more hydrophobic in nature, show a decrease in aqueous solubility relative to that of the API itself. Even though a decrease in solubility is normally not desired within the pharmaceutical industry, a decreased solubility is preferred in some applications of specialty chemicals such as in the agrochemical industry.

6.5 Conclusion

Although it is obvious that not every cocrystal will deliver an improvement in physicochemical properties relative to that of the active ingredient, we have shown that systematic changes to the molecular nature of the co-crystallizing agent combined with control over the way that the individual building blocks are organized within crystalline lattice makes it possible to establish predictable links between molecular structure and

macroscopic physical properties. In this context, cocrystals may therefore offer unique opportunities for developing new solid forms in which a variety of desired physical properties can be tuned in a predictable manner.

References

[1] (a) Kerns, E.H.; Di, L. Drug-like Properties: Concepts, Structure Design and Methods: from ADME to Toxicity Optimization, Elsevier, 2008, p7-9; (b) Basavoju, S.; Boström, D.; Velaga, S.P. *Pharm. Res.*, **2008**, 25(3), 530.

[2] Lipper, R.B. *Modern Drug Discovery*, 1999, 2(1), 55.

[3] (a) Pharmaceutical Research and Manufacturers of America, Pharmaceutical Industry Profile 2006 (Washington, DC: PhRMA, March 2006); (b) Ramanathan, R., ed. Mass Spectrometry in Drug Metabolism and Pharmacokinetics, Wiley, 2009, p1-4.

[4] Blagden, N.; de Matas, M.; Gavan, P.T.; York, P. *Adv. Drug Del. Rev.*, **2007**, 59, 617.

[5] Chaumeil, J.C. *Exp. Clin. Pharmacol.*, **1998**, 20(3), 211.

[6] Agharkar, S.; Lindenbaum, S.; Higuchi, T. *J. Pharm. Sci.*, **1976**, 65(5), 747.

[7] Aim, K.; Dannenfelser, R.-M.; Zielinski, J.; Wang, B. *J. Pharm. Sci.*, **2004**, 93(9), 2244.

[8] Torchillin, V.P. *Pharm. Res.*, **2007**, 24(1), 1.

[9] Rajewski, R.A.; Stella, V.J. *J. Pharm. Sci.*, **1996**, 85(11), 1142.

[10] Humberstone, A.J.; Charman, W.N. *Adv. Drug Deliv. Rev.*, **1997**, 25(1), 103.

[11] (a) Goldberg I. *CrystEngComm*, **2008**, 10, 637-645; (b) Aakeröy, C.B; Desper J.; Levin, B. *CrystEngComm*, **2005**, 7, 102; (c) Banerjee, R.; Saha, B.K.; Desiraju, G. *CrystEngComm.*, **2006**, 8, 680; (d) Saha, B.K.;. Nangia, A.; (e) Jaskólski, M. *CrystEngComm.*, **2005**, 7, 355; (f) Aakeröy, C.B. *Acta Cryst.*, **1997**, B53, 569; (g) Reddy, C.M.; Reddy, L.S.; Artipamula, S.; Nangia, A.; Lam, C.-K.; Mak, T.C.W. *CrystEngComm.*, **2005**, 7, 44; (h) Braga, D.; Brammer, L.; Champness, N.R. *CrystEngComm.*, **2005**, 7, 1; (i) Nangia, A. *CrystEngComm.*, **2002**, 4, 93.

[12] (a) McNamara, D.P.; Childs, S.L.; Giordano, J.; Iarriccio, A.; Cassidy, J.; Shet, M.S.; Mannion, R.; O'Donnell, E.; Park, A. *Pharm. Res.*, **2006**, 23(8), 1888; (b) Childs, S.L.; Chyall, L.J.; Dunlap, J.T.; Smolenskaya, V.N.; Stahly, B.C.; Stahly, P.G. *J .Am. Chem. Soc.*, **2004**, 126, 13335; (c) Jayasankar, A.; Reddy, S.L.; Bethune, S..J.; Rodríguez-Hornedo, N. *Cryst. Growth and Des.*, **2009**, 9(2), 889; (d) Trask, A.V.; Motherwell, W.D.S.; Jones. W. *Int. J. Pharm.*, **2006**, 320, 114.

[13] (a) Basavoju, S.; Boström, D.; Velaga, S.P. *Pharm. Res.* **2008**, 25, 530; (b) Childs, S.L.; Rodríguez-Hornedo, N.; Reddy, S.-L.; Jayasankar, A.; Maheswari, C.; McCausland, L.; Shipplett, R.; Stahly, B.C. *CrystEngComm.* **2008**, 10, 856; (c) Remenar, J.F.; Morissette, S.L.; Peterson, M.L.; Moulton, B.; MacPhee, J.M.; Guzmán, H.R.; Almarsson, Ö. *J. Am. Chem. Soc.* **2003**, 125, 8456; (d) Hickey, M.B.; Peterson, M.L.; Scoppettuolo, L.A.; Morrisette, S.L.; Vetter, A.; Guzmán, H.; Remenar, J.F.; Zhang, Z.; Tawa, M.D.; Haley S.; Zaworotko, M.J.; Almarsson, Ö. *Eur. J. Pharm. Biopharm.* **2007**, 67, 112; (e) Fleischman, S.G.; Kuduva, S.S.; McMahon, J.A.; Moulton, B.; Walsh, -B.R.D.; Rodríguez-Hornedo, N.; Zaworotko, M.J. *Cryst. Growth Des.* **2003**, 3, 909.

[14] Reference 13a

[15] (a) Thalladi, V.R.; Nüsse, M.; Boese, R. *J. Am. Chem. Soc*., **2000**, 122, 9227; (b) Vishweshwar, P.; Nangia, A.; Lynch, V.M. *Cryst. Growth and Des*., **2003**, 3(5), 783; (c) Morrison, J.D.; Robertson, J.M. *J. Chem. Soc*., **1949**, 2, 980; (d) Verweel, H.J.; MacGillavry, C.H. *Nature*, **1938**, 142, 161.

[16] (a) Ao, E.; Tanaka, H.; Nakao, R.; Yamagami, K.; Fujii, A. Jpn. Patent 03081222, 1991; (b) Liu, Q.; Zhang, W.; Wei, Y.G.; Shao, M.-C. *Acta Cryst*. **1996**, C52, 2260.

[17] (a) Shan, N.; Zaworotko, M.J. *Drug Discovery Today* **2008**, 11, 440; (b) Aakeröy, C.B.; Beatty, A.M.; Helfrich, B.A.; Nieuwenhuyzen, M. *Cryst. Growth Des*. **2003**, 3, 159; (c) Aakeröy, C.B.; Desper, J.; Helfrich, B.A. *CrystEngComm*. **2004**, 6, 19; (d) Aakeröy, C.B.; Desper, J.; Urbina, J.F. *Cryst. Growth Des*. **2005**, 5, 1283.

[18] (a) Lauher, J.W.; Fowler, F.W.; Goroff, N.S. *Acc. Chem. Res*. **2008**, 41, 1215; (b) Bailey, M. *Acta Cryst*. **1955**, 8, 575.

[19] (a) FDA Select Committee on GRAS Substances (SCOGS) Database Overview. http://www.cfsan.fda.gov/opascogs.html

[20] Bernhardt, P.V.; Chin, P.; Richardson, D.R. *J. Biol. Inorg. Chem*. **2001**, 6, 801.

[21] Quiroga, J.; Portilla, J.; Abonia, R.; Insuasty, B.; Nogueras, M.; Cobo, J. *Tetrahedron Letters*, **2008**, 49, 5943.

[22] Muthu, S.; Yip, J. Vittal, J. *J. Chem. Soc., Dalton Trans*. **2002**, 4561.

[23] Sarkar, M.; Biradha, K. *Cryst. Growth Des*. **2006**, 6, 202.

[24] Du, M.; Zhang, Z.-H.; Wang, Z.-G.; Wu, H.-F.; Wang, Q. *Cryst. Growth Des*. **2006**, 6, 1867.

[25] Murakami, Y.; Aoyama, Y.; Kikuchi, J.; Nishida, K. *J. Am. Chem. Soc*. **1982**, 104, 5189.

[26] Nehm, S.J.; Rodríguez-Spong, B.; Roderíguez-Hornedo, N. *Cryst. Growth Des*. **2006**, 6, 592.

[27] (a) Variankaval, N.; Wenslow, R.; Murry, J.; Hartman, R.; Helmy, R.; Kwong, E.; Clas, S.-D.; Dalton, C.; Santos, I. *Cryst. Growth Des.* **2006**, 6, 690; (b) Seefeldt, K.; Miller, J.; Alvarez-Núñez, F.; Rodríguez-Hornedo, N. J. *Pharm. Sci.* **2007**, 96, 1147.

CHAPTER 7 - Summary & Future Works

7.1 Summary

Supramolecular chemistry has come a long way, in providing chemist with a wide variety of reliable complementary interactions such as hydrogen and halogen bonds, allowing for the design and synthesis of supermolecules. The ability to synthesize supermolecules with predictable connectivities and stiochiometries can be accomplished by relying on established hierarchy of reliable intermolecular interactions.

We designed and synthesized three supramolecular reactants (SR's) containing two distinct hydrogen bonding acceptor sites and one donor site (acetamidopyridine) in order to map out the behavior of the hydrogen-bonded sites during co-crystallization. These SR's were allowed to react with various aliphatic and aromatic carboxylic acids producing both 1:1 molecular cocrystals as well as 1:2 ionic salts through O-H…N or charge-assisted $N\text{-}H^{+}\ldots O^{-}$ hydrogen bonds with the acetamidopyridine binding site, Figure 7.1.

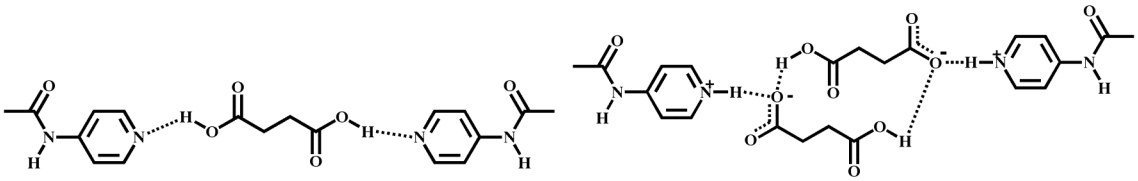

Figure 7.1 Summary of primary hydrogen bonding motifs between 4-acetamidopyridine and aliphatic carboxylic acids.

The intermolecular interaction of pyridine…carboxylic acid observed in this study can be employed in subsequent supramolecular synthetic strategies, thus providing important information on the molecular recognition processes of small molecules, thereby allowing us to use this information in understanding larger and more complicated molecules.

The ability to incorporate both a hydrogen and halogen-bonding moiety into the same crystalline lattice has provided supramolecular chemist with opportunity of designing new solid-state architectures. Therefore we design a system having two different acceptor sites and the molecular interaction preferences both a hydrogen and halogen bond is present as the donor molecules, Figure 7.2.

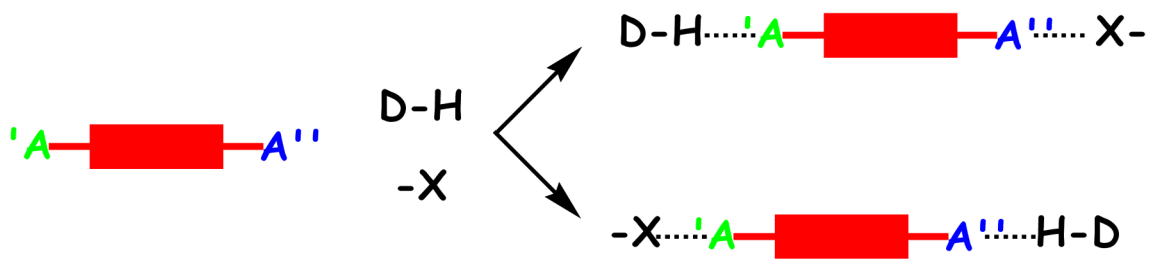

Figure 7.2 Possible interaction between two different acceptor moieties and a hydrogen and halogen bond donor, where **A'** is the best acceptor and **A''** is second best acceptor; **-X** is the halogen bond donor and **D-H** is the hydrogen bond donor.

In the attempt to determine the strength of the acceptor moieties, semi-empirical PM3 molecular electrostatic potential calculations were carried on the acceptor sites in mono N-oxide derivatives, Figure 7.3.

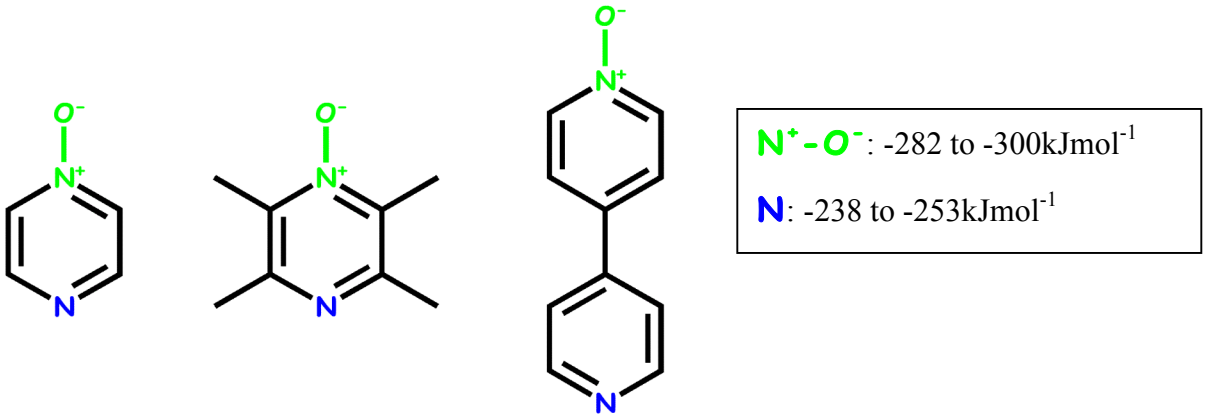

Figure 7.3 Electrostatic potentials for acceptor moieties.

Based on the electrostatic potential calculations of the two binding sites, the N-O moiety is the superior acceptor site for an incoming halogen or acid in comparison with the N atom. The ranking in binding sites strength was further supported by crystal structures that we obtained, in which of the eight structures obtained with the N-oxide moieties seven out of those structures had the best acceptor interaction with the best donor (88% supramolecular yield).

Moreover, when halogenated benzoic acids were present in the same system 3/4 times (75% supramolecular yield) halogen bonds the best donor (N…I or N…Br) aid in extending the architecture into polymeric networks, Figure 7.4

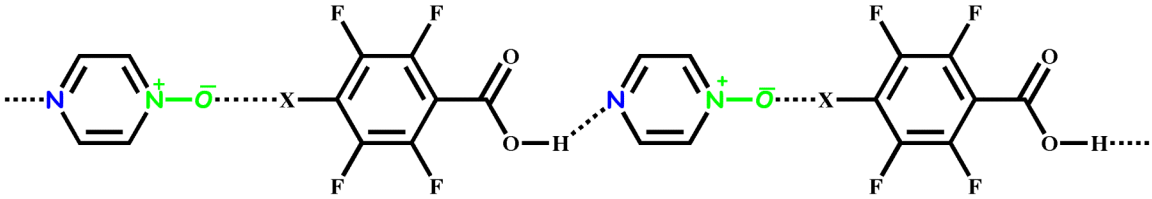

Figure 7.4 Polymeric network formed through hydrogen and halogen bonds (X = I, Br).

This study has allowed us design new solid-state architectures incorporating both hydrogen and halogen bonds, furthering our understanding of molecular recognition. In addition, we have also learned that semi-empirical calculations can be use as a guide in determining the binding preferences of a variety of molecules as long as the charges on the molecules are significantly different.

With our success in designing supermolecules with predictable connectivities using reliable intermolecular interactions as well as semi-empirical calculations; we can then use this knowledge in synthesizing pharmaceutical cocrystal, with the ultimate goal of fine-tuning both physical and chemical properties such as melting point, solubility, *etc*.

Finally, we used our understanding of molecular recognition to construct pharmaceutical cocrystals. Consequently, we were able to incorporate an active pharmaceutical ingredient (API) within a new crystalline lattice in a controllable manner without make or breaking covalent bonds. The series of pharmaceutical cocrystals synthesized exhibit tremendous structural consistency, Figure 7.5.

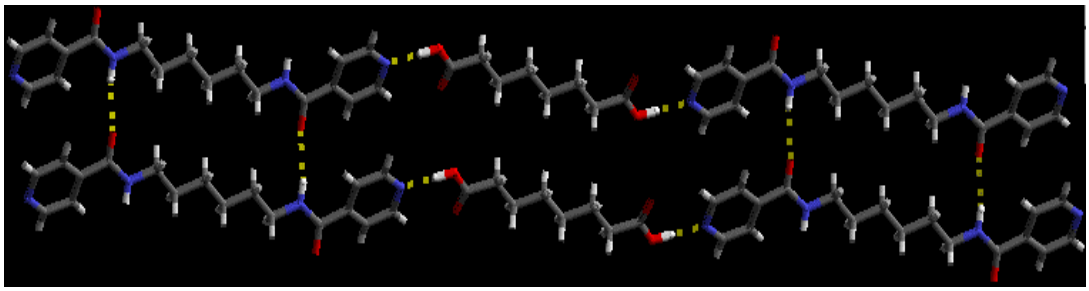

Figure 7.5 Example of a pharmaceutical cocrystal held together by hydrogen bonds.

We were also able to show that both the melting behavior and solubility of a given API can be modulated in a controllable fashion. Moreover, form both the solubility

and melting behavior studies we can great a library of co-crystallizing agents that can be used to obtained the desire melting point or solubility of a given compound.

Furthermore, we can also use our understanding to improve the poor biopharmaceutical properties of other drugs that did not make it onto the market or even drugs that are currently on the market. Instead of administrating a drug intravenously, we can move to orally administration and eventually transdermal patches.

Additionally, molecular recognition can also be used in the agrochemical industry, in which a low soluble pesticide or herbicide is desired. So we can go back to the library of compounds that we have synthesized and use that knowledge to modulate the solubility of a variety of agrochemicals thereby creating longer lasting and more environmentally friendly chemicals.

7.2 Future works

Although our understanding of molecular recognition and intermolecular interactions has led us in designing new solid-state architectures with improved physical and chemical properties, there is still more work to be done, in order take each system to the next level.

First, halogen bonding has aided in the expansion of molecular architectures. Therefore, we can use aliphatic dihalogenated species, analogous to the aliphatic dicarboxylic acids used in the studies herein and probe whether this type of non-covalent interactions can be use to form structurally consistent cocrystals, Figure 7.6.

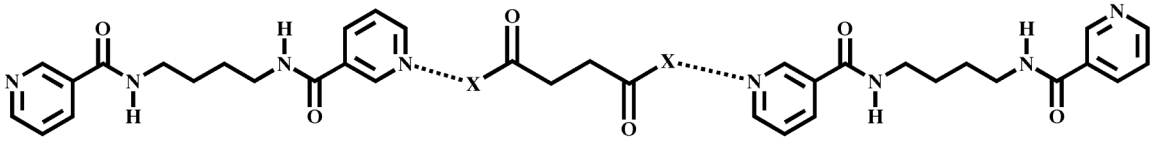

Figure 7.6 Proposed network formed through halogen bonds (X = I, Br).

Consequently similar melting behavior and solubility studies can be carried and compared with the studies done with aliphatic dicarboxylic acids. This will then allow us to push this system further by incorporating both hydrogen and halogen bonded moieties into the same crystalline lattice and test which one of the three possible non-covalent interactions give us the optimal results in terms of fine-tuning the physical and chemical properties.

Furthermore, to establish whether the bioactivity of APIs in this study is still in tact, biological studies will be carried out on both the pure API as well as the pharmaceutical cocrystal using both breast and lung cancer cell lines. First *in vitro* studies will be carried out, followed by *in vivo* studies to establish the lethal dose 50 of pharmaceutical cocrystals were synthesized.

Finally, we can implement our understanding of molecular recognition on the poorly soluble drugs from top 300 drugs list. Thereby, providing a library of suitable co-crystallizing agents to be used in modulating the physical and chemical properties.

Appendix A - Crystallographic Experimental Data

Chapter 2 Cocrystal and salt

X-ray data for **2SEB** was collected on a SMART APEX CCD diffractometer at 100 K or a Bruker SMART 1000 four circle CCD diffractometer at 173 K (**2HG**) using a fine-focus molybdenum K*a* tube. Data were collected using SMART.[1] Initial cell constants were found by small widely separated ‘‘matrix’’ runs. Generally, an entire hemisphere of reciprocal space was collected regardless of Laue´ symmetry. Scan speed and scan width were chosen based on scattering power and peak rocking curves.

Unit cell constants and orientation matrix were improved by least-squares refinement of reflections threshold from the entire dataset. Integration was performed with SAINT,[2] using this improved unit cell as a starting point. Precise unit cell constants were calculated in SAINT from the final merged dataset. Lorenz and polarization corrections were applied. Laue´ symmetry, space group, and unit cell contents were found with XPREP.

Data were reduced with SHELXTL.[3] The structures were solved in all cases by direct methods without incident. In general, hydrogen atoms were assigned to idealized positions and were allowed to ride. Where possible, the coordinates of the amide hydrogen atoms were allowed to refine. Heavy atoms were refined with anisotropic thermal parameters. Unless otherwise noted, data were corrected for absorption.

Compound **2SEB**. The unique amide sits on a general position. The dicarboxylic acid sits on a crystallographic inversion center. Positional coordinates for the amide hydrogen (H17) and the carboxylic acid hydrogen (H21) were allowed to refine.

Compound **2HG**. The unique amide and unique carboxylic acid both sit on general positions. Positional coordinates for the pyridinium hydrogen H11, amide hydrogen H14, and carboxylic acid hydrogen H25 were allowed to refine.

Chapter 2 Metal Complexes

X-ray data were collected on a Bruker SMART 1000 four circle charge coupled device (CCD) diffractometer (**1b, 2a**), Bruker Kappa APEX II (**5**), or Bruker SMART APEX CCD diffractometer (**1a**) using, in each case, a fine-focus molybdenum Kα tube. Data were collected using *SMART* (**1b, 2a**)[1] or *APEX2* (**1a**)[4] software. Initial cell

constants were found by small widely separated 'matrix' runs. Generally, an entire hemisphere of reciprocal space was collected regardless of Laué symmetry. Scan speed and scan width were chosen based on scattering power and peak rocking curves.

Unit cell constants and orientation matrix were improved by least-squares refinement of reflections threshold from the entire dataset. Integration was performed with *SAINT*,[2] using this improved unit cell as a starting point. Precise unit cell constants were calculated in *SAINT* from the final merged dataset. Lorenz and polarization corrections were applied. Laué symmetry, space group, and unit cell contents were found with *XPREP*.

Data were reduced with *SHELXTL*.[5] The structures were solved in all cases by direct methods without incident. In general, hydrogen atoms were assigned to idealized positions and were allowed to ride. Where possible, the coordinates of the amide hydrogen atoms were allowed to be refined. Heavy atoms were refined with anisotropic thermal parameters. Absorption correction was performed with *SADABS* where possible.

Compound 1a: Data were corrected for absorption using *SADABS*. The position of the amide proton was allowed to be refined; all other hydrogen atoms were included in calculated positions and allowed to ride.

Compound 1b: Data were corrected for absorption using *SADABS*. The asymmetric unit contains three species: a nickel complex, an ordered dichloromethane solvent molecule, and a disordered dichloromethane solvent molecule. Geometry of all three dichloromethane fragments was restrained with SAME commands. All non-hydrogen atoms were given anisotropic thermal parameters. Thermal parameters for the two (closely located) disordered dichloromethane species were pair wise constrained using EADP commands. The position of the two-amide protons (H13 and H23) was allowed to be refined; all other hydrogen atoms were included in calculated positions and allowed to ride.

Compound 2a: Data were corrected for absorption using *SADABS*. The asymmetric unit contains five species: a complete copper(II) complex on a general position, a half-complex (sitting on an inversion centre), and three ordered dichloromethane molecules. Five of the six $-CF_3$ groups were disordered. Four were modeled with two species, and the fifth was modeled with three species. Geometry of all

–CF3 fragments was restrained to be similar to the first fragment (C41A, F41A-F41C) by the SAME command. The geometry of the first fragment (C41A, etc.) was idealized to tetrahedral by using DFIX restraints on the C–F bond distances and F–F distances. Thermal parameters for the set of three fluorine atoms on each species having occupancy <50% were constrained with EADP commands. The fluorine atoms having occupancy >60% were given isotropic thermal parameters (anisotropic refinement of other fluorine atoms was unstable). All hydrogen atoms were included in calculated positions and were allowed to ride.

Chapter 6

Data sets for **28SUC, 28ADI, 28SUB, 28SEB** and **28DOD** were collected on Bruker Kappa APEX II systems using MoKα radiation. Data were collected using APEX2 software.[6] Initial cell constants were found by small widely separated "matrix" runs. Data collection strategies were determined using COSMO.[7] Scan speed and scan width were chosen based on scattering power and peak rocking curves. All datasets were collected at – 153 °C using an Oxford Croystream low-temperature device.

Unit cell constants and orientation matrix were improved by least-squares refinement of reflections threshold from the entire dataset. Integration was performed with SAINT,[8] using this improved unit cell as a starting point. Precise unit cell constants were calculated in SAINT from the final merged dataset. Lorenz and polarization corrections were applied. A multi-scan absorption correction was performed with SADABS[9] for **28SUB**; absorption corrections were not applied for the other structures (μ ≤ 0.1 mm-1 in each case).

Data were reduced with SHELXTL.[10] The structures were solved in all cases by direct methods without incident. In each case, both di-acid and di-pyridine molecules sit on inversion centers in space group P-1 to give one formula unit per unit cell. For each structure, the coordinates for the unique amide and carboxylic acid hydrogens were allowed to refine; all other hydrogen atoms were located in idealized positions and were treated with a riding model. All structures were fully ordered and none contained solvent or water of hydration.

References

[1] SMART v5.060, Bruker Analytical X-ray Systems, Madison, WI, 1997–1999.

[2] SAINT v6.02, Bruker Analytical X-ray Systems, Madison, WI, 1997–1999.

[3] SHELXTL v5.10, Bruker Analytical X-ray Systems, Madison, WI, 1997.

[4] *APEX2* v2.2.0 2005–2007 (Bruker Analytical X-ray Systems, Madison, WI).

[5] *SHELXTL* v6.10, 2001 (Bruker Analytical X-ray Systems, Madison, WI).

[6] APEXII v2009. 5-1, © 2009, Bruker Analytical X-ray Systems, Madison, WI.

[7] COSMO v1. 60, © 1999 - 2009, Bruker Analytical X-ray Systems, Madison, WI.

[8] SAINT v7. 60a, © 1997 - 2008, Bruker Analytical X-ray Systems, Madison, WI.

[9] SADABS v2008/1, © 2008, Bruker Analytical X-ray Systems, Madison, WI.

[10] SHELXTL v2008/4, © 20080, Bruker Analytical X-ray Systems, Madison, WI.

Appendix B - ^{1}H and ^{13}C NMR

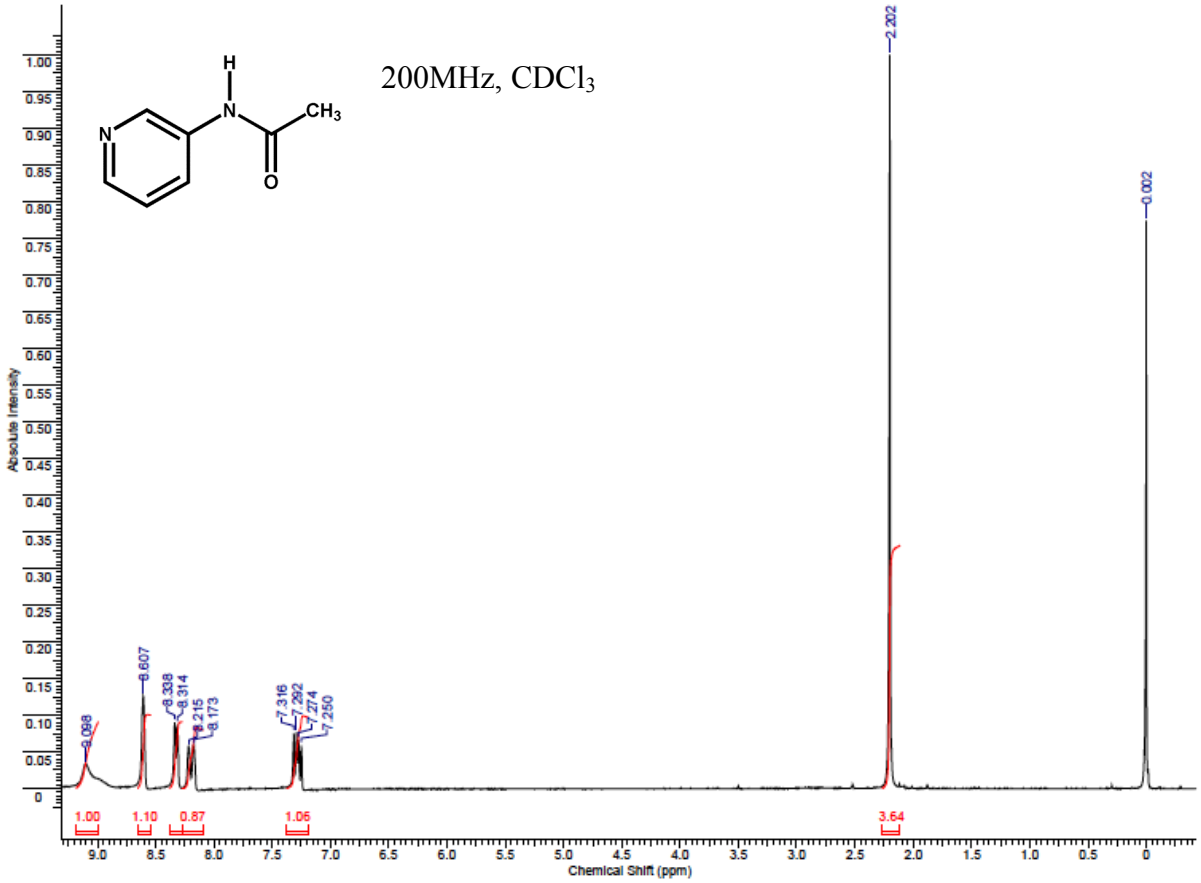

Figure B.1 ^{1}H NMR of **1**

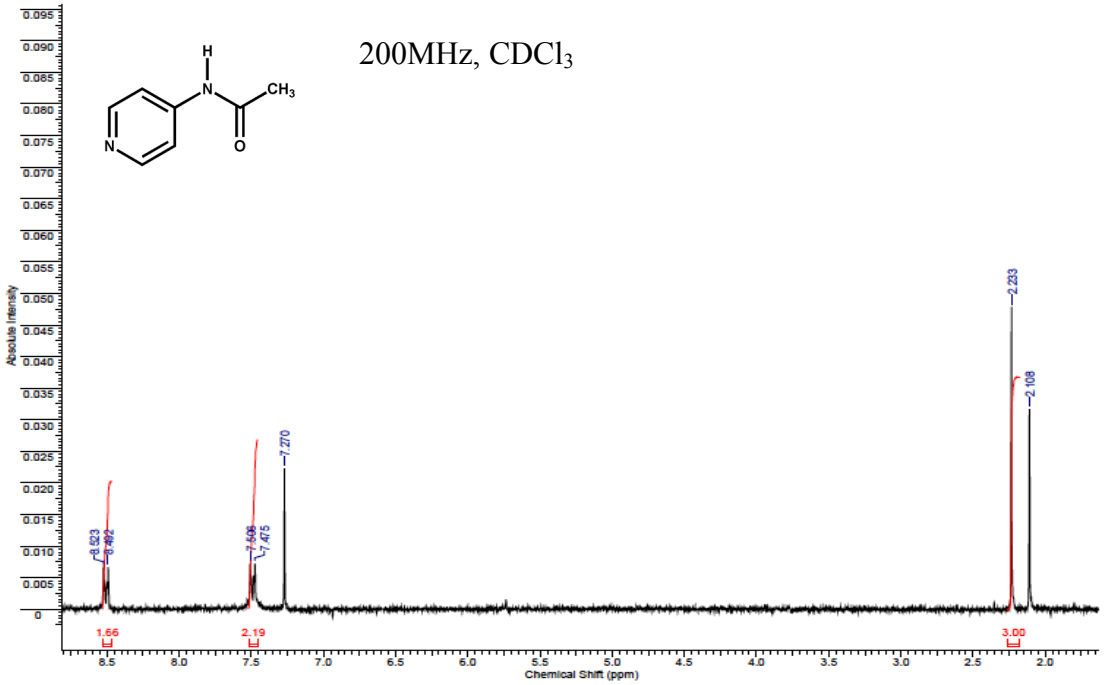

Figure B.2 ^{1}H NMR of **2**

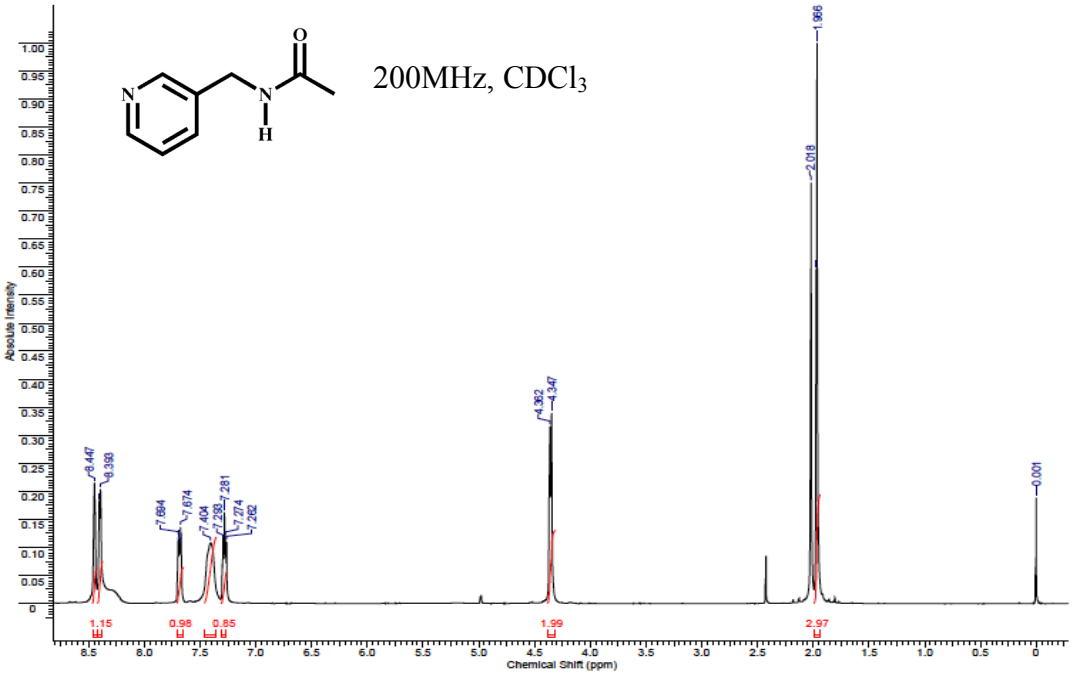

Figure B.3 ^{1}H NMR of **3**

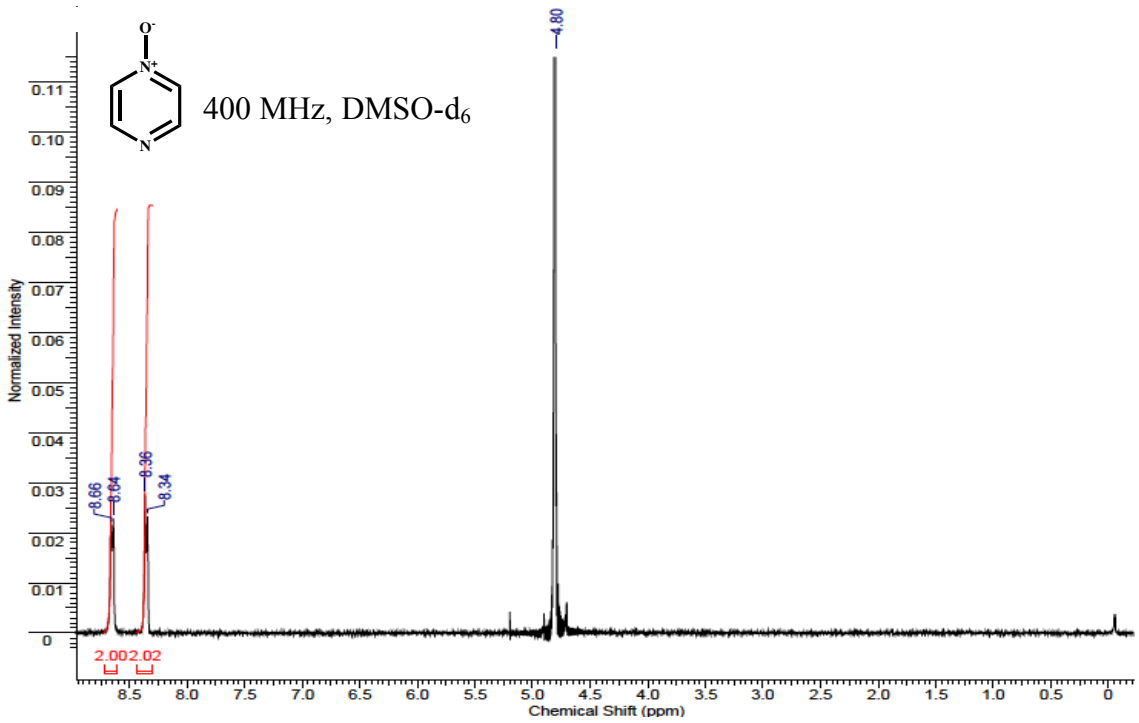

(a)

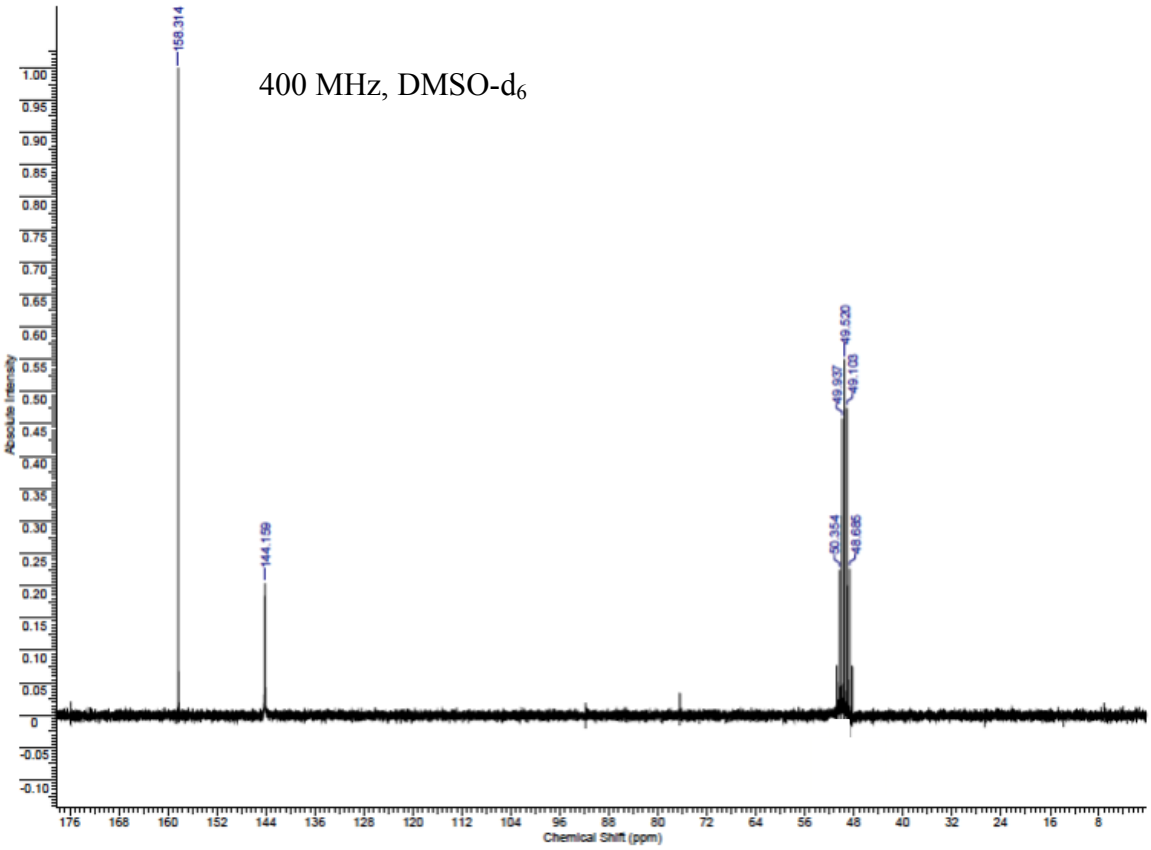

(b)

Figure B.4 (a) ^{1}H and (b) ^{13}C NMR of **4**

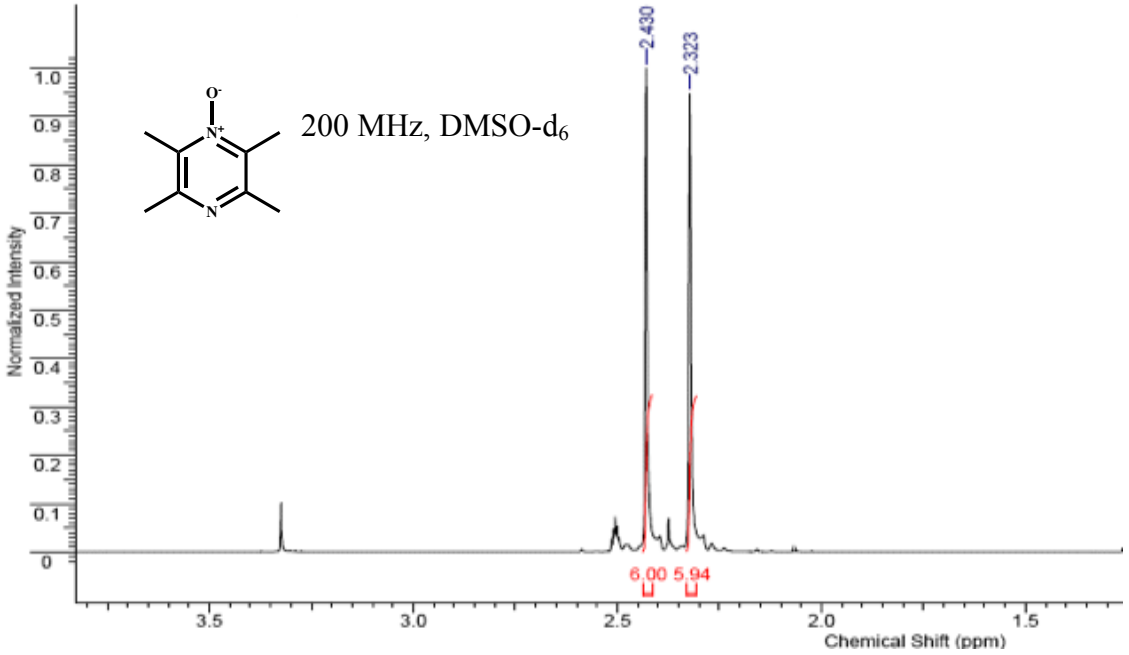

(a)

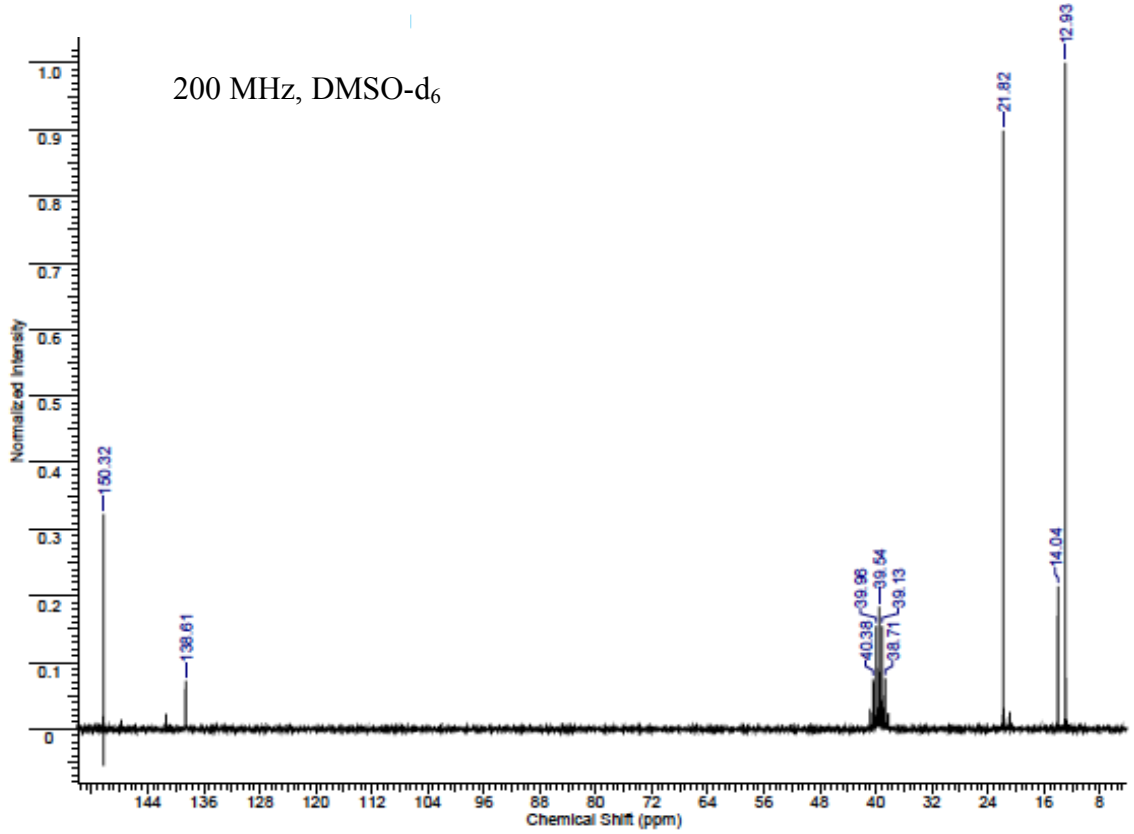

(b)

Figure B.5 (a) ^{1}H and (b) ^{13}C NMR of **5**

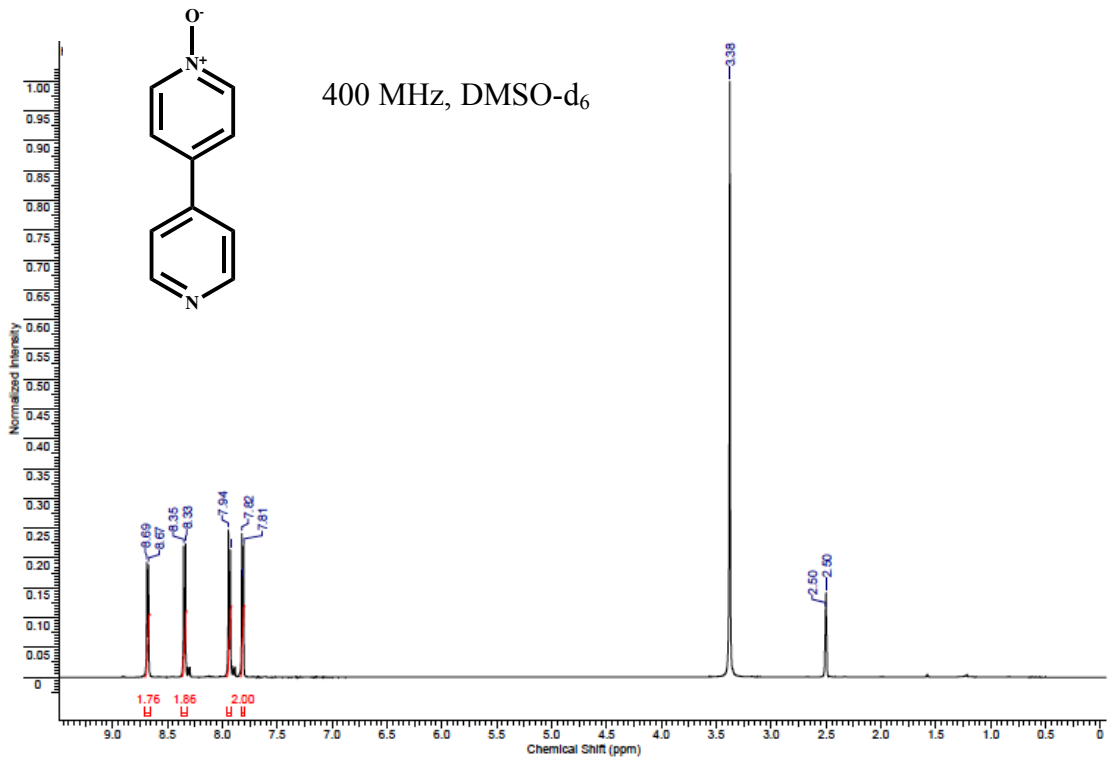

(a)

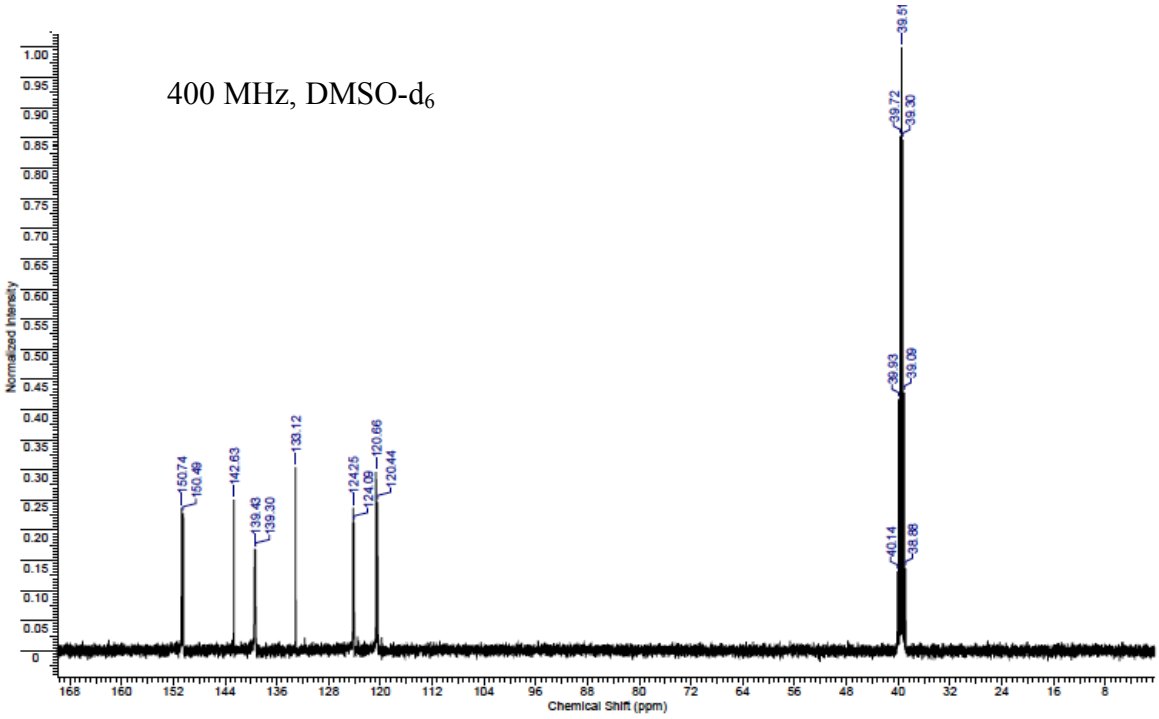

(b)

Figure B.6 (a) ^{1}H and (b) ^{13}C NMR of **6**

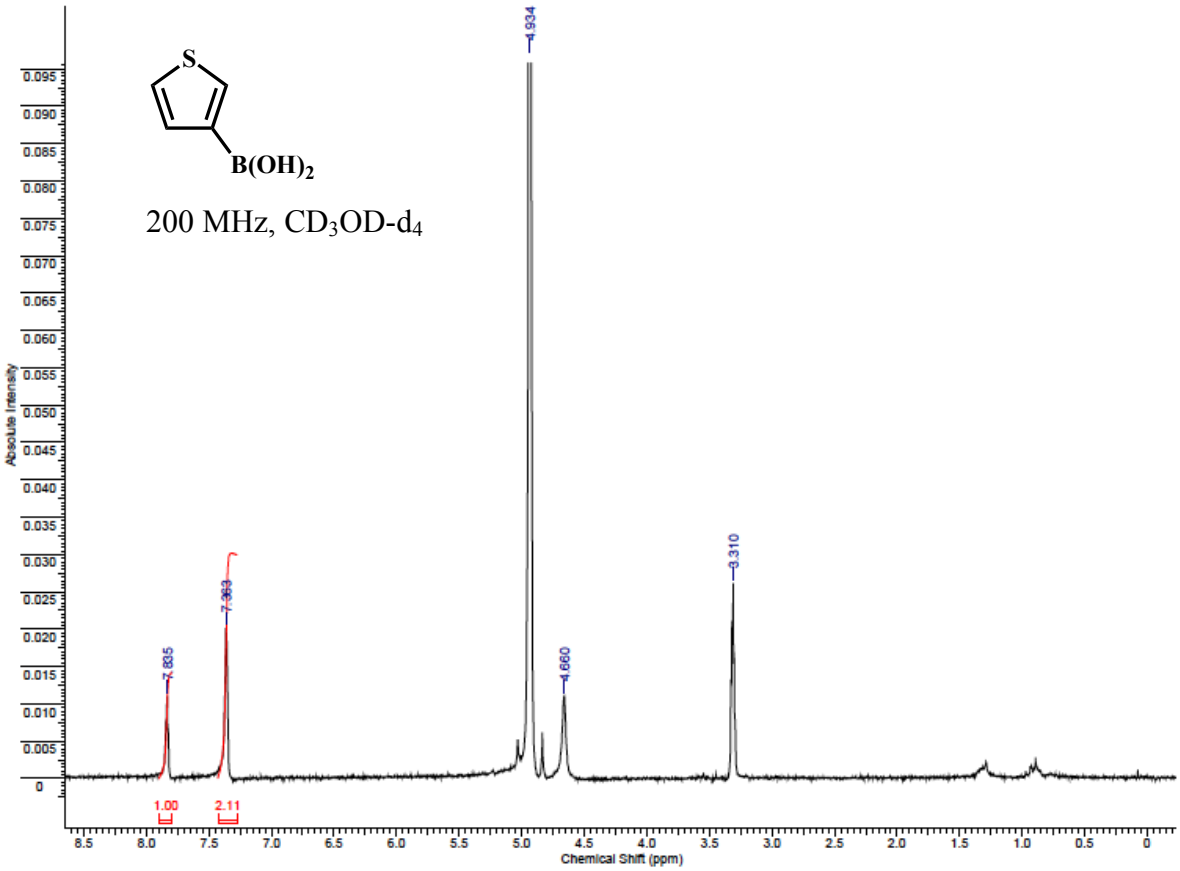

Figure B.7 ^{1}H NMR of **7**

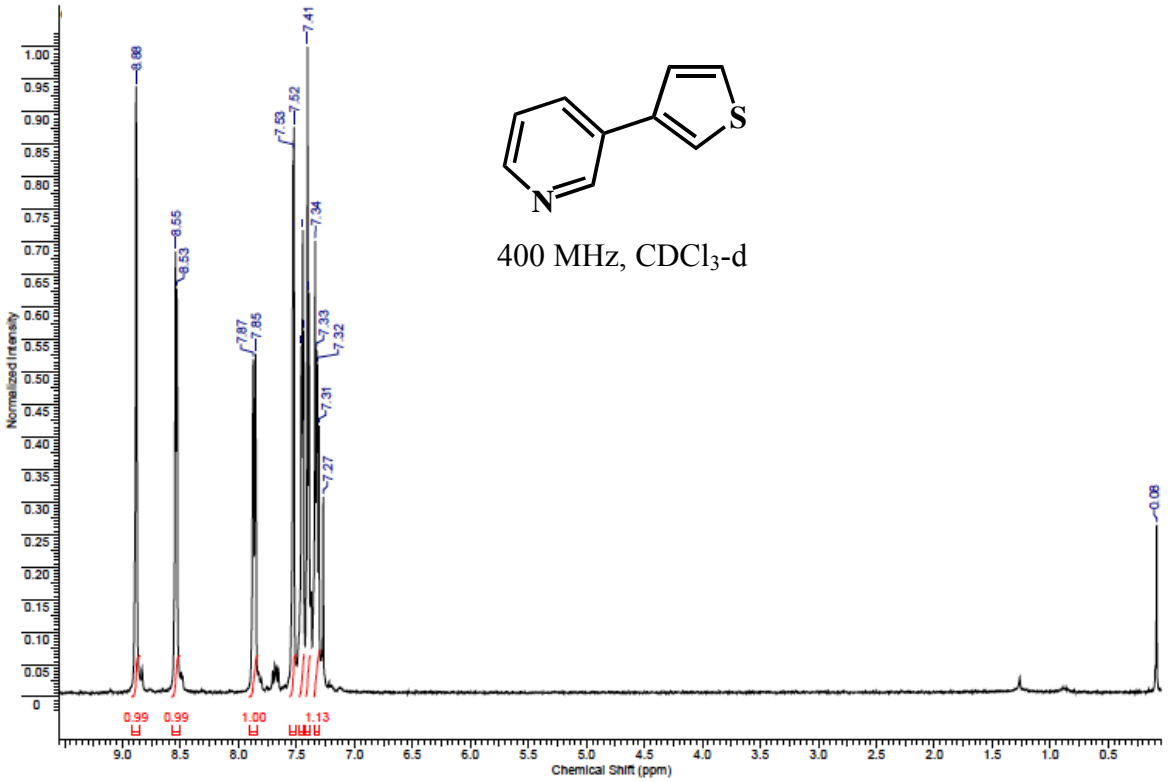

(a)

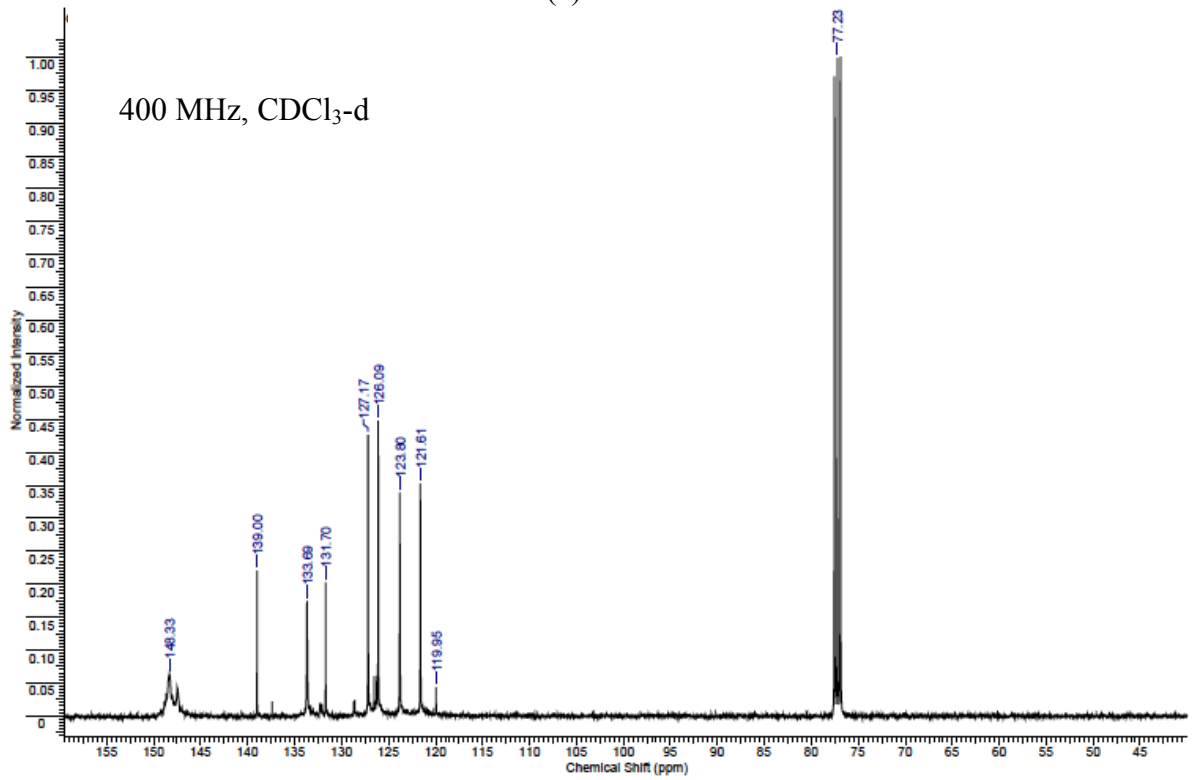

(b)

Figure B.8 (a) ^{1}H and (b) ^{13}C NMR of **8**

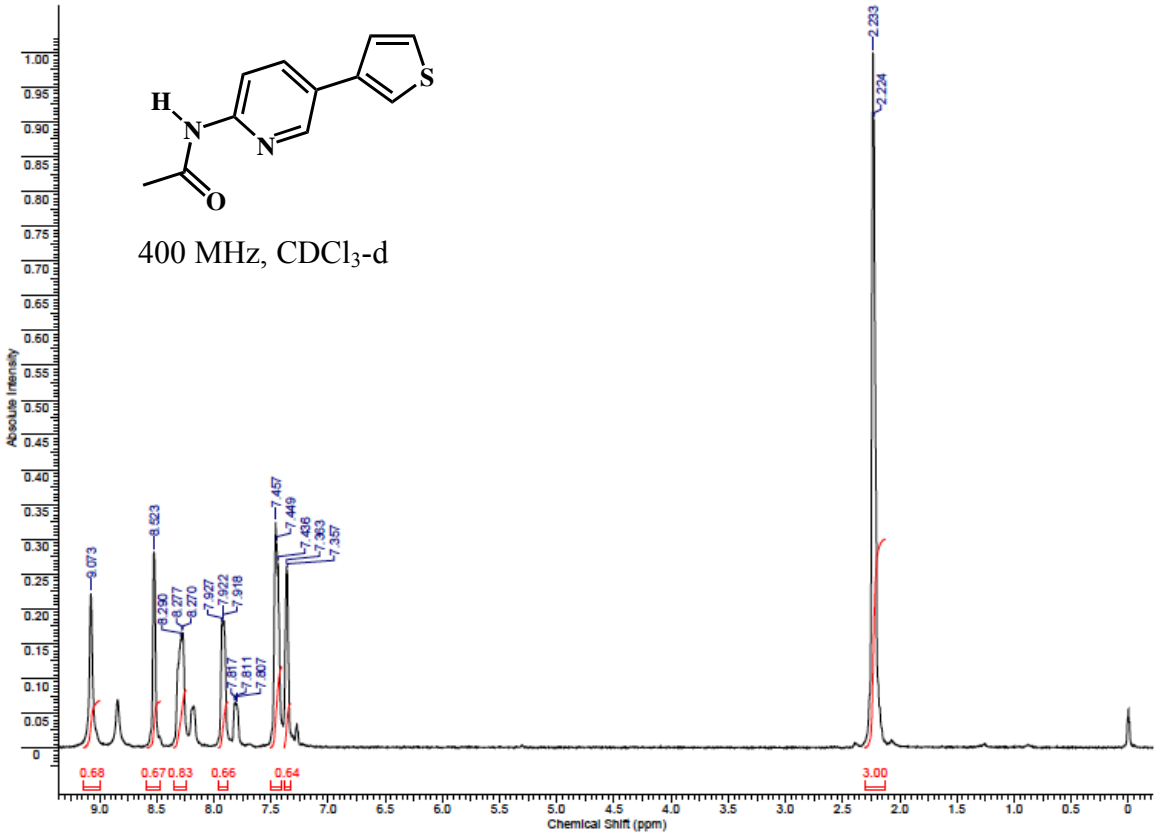

(a)

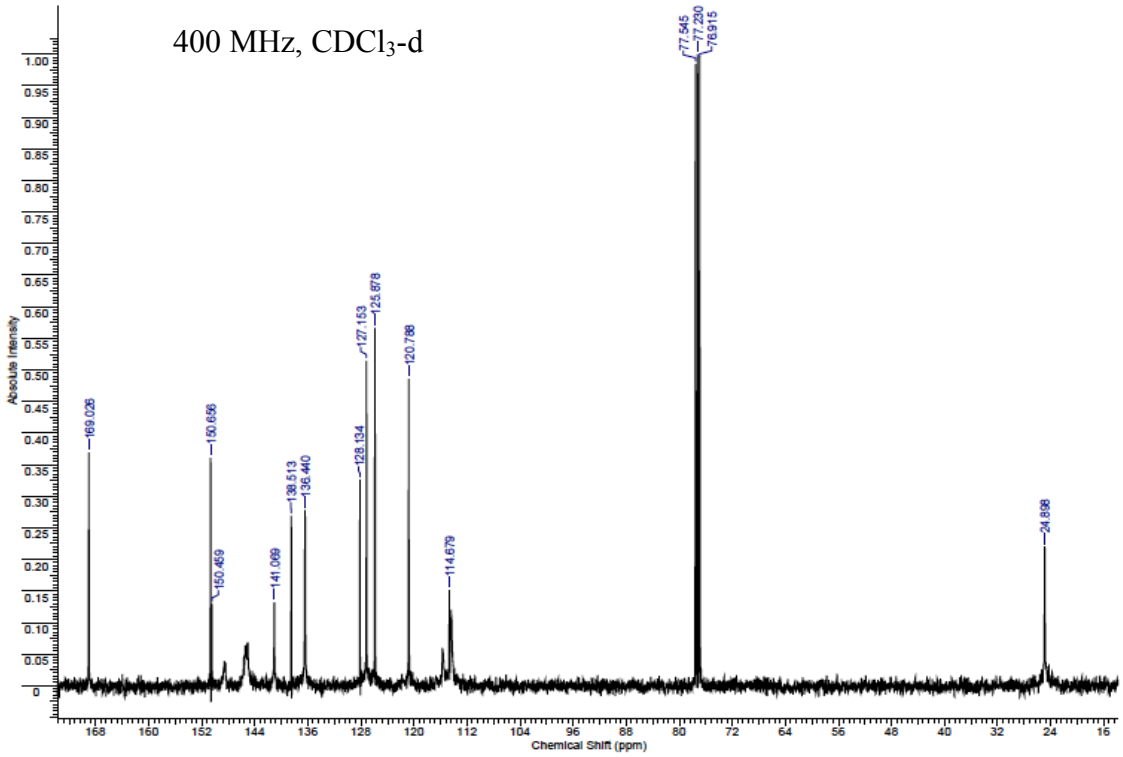

(b)

Figure B.9 (a) ^{1}H and (b) ^{13}C NMR of **9**

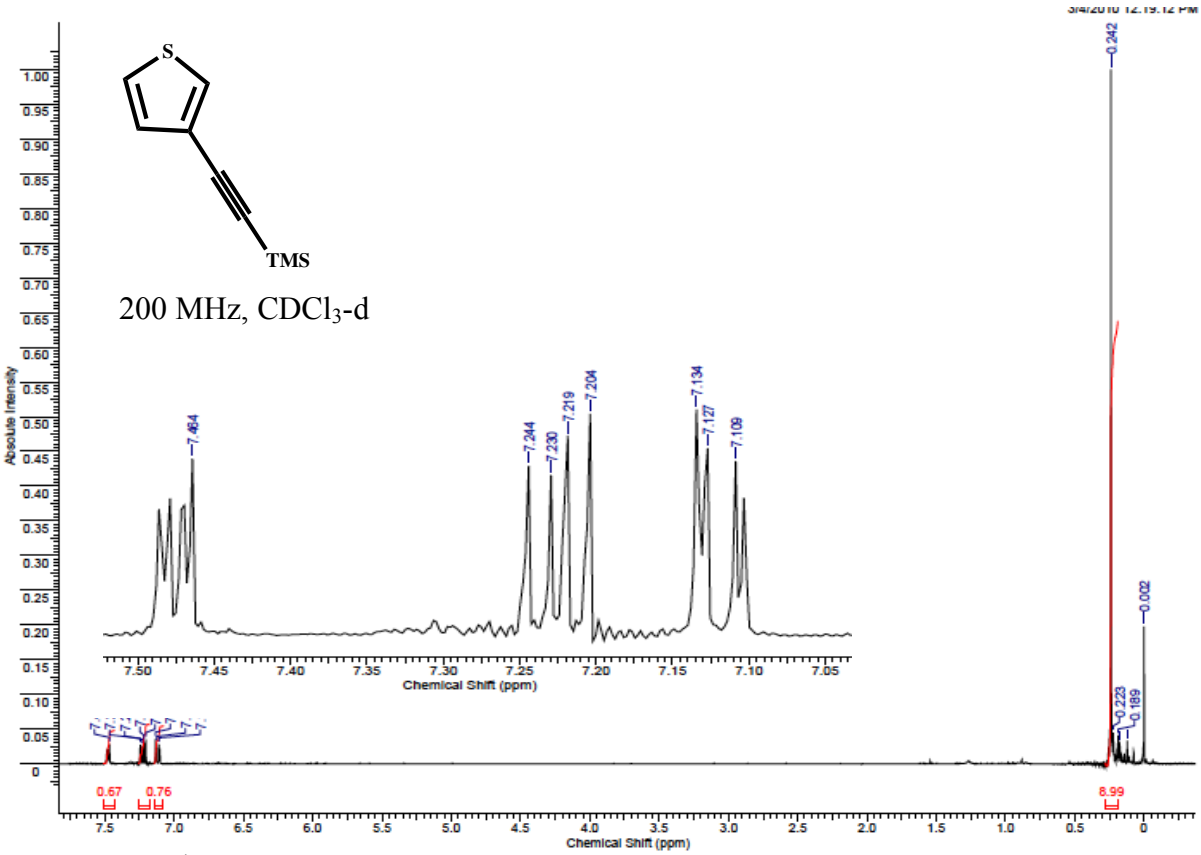

Figure B.10 ^{1}H NMR of **10**

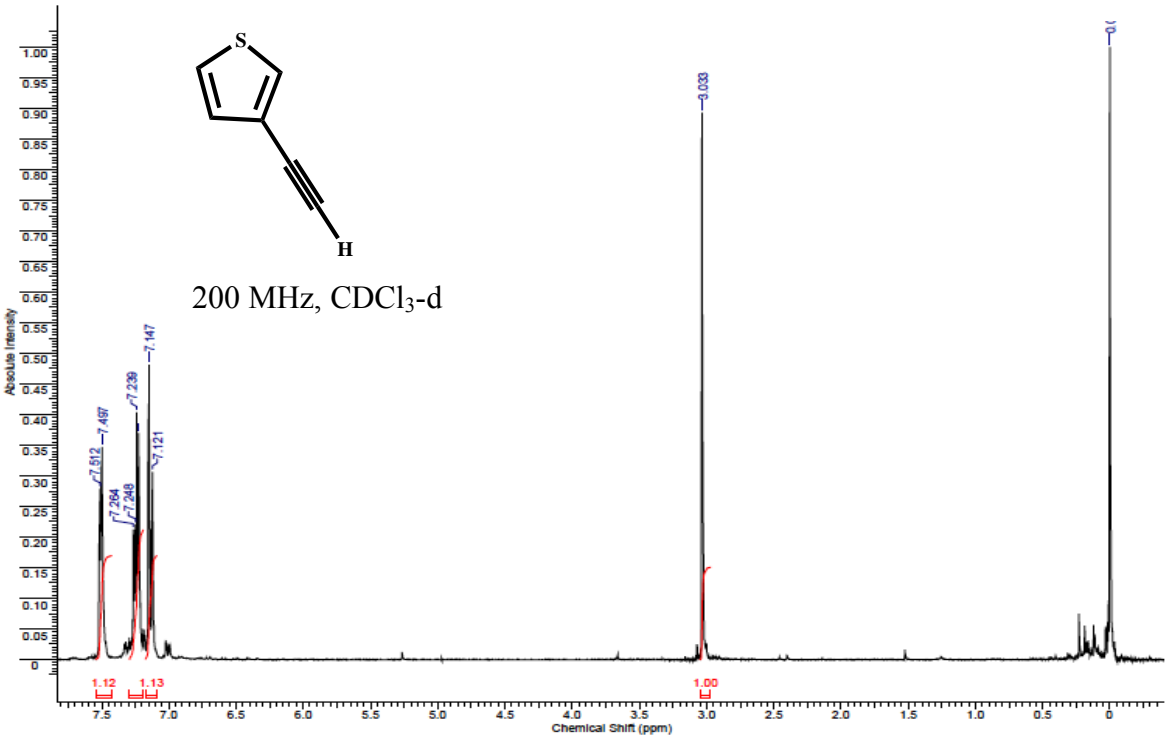

Figure B.11 ^{1}H NMR of **11**

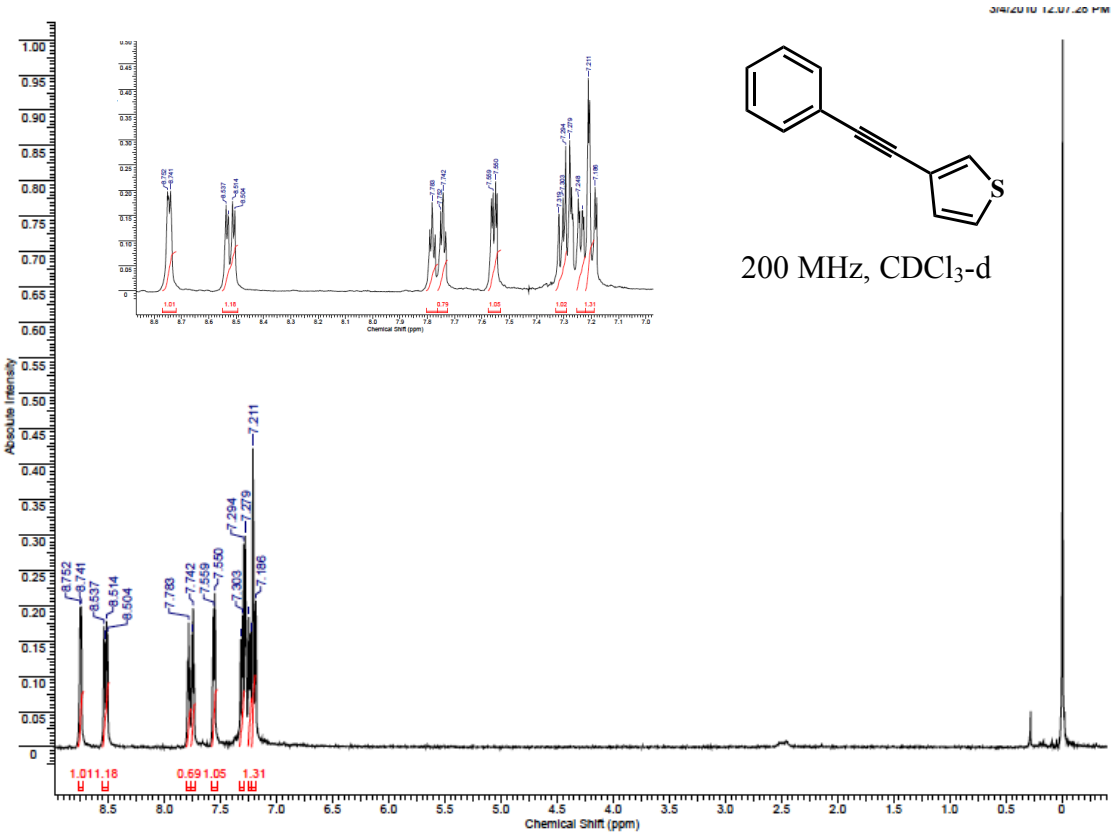

(a)

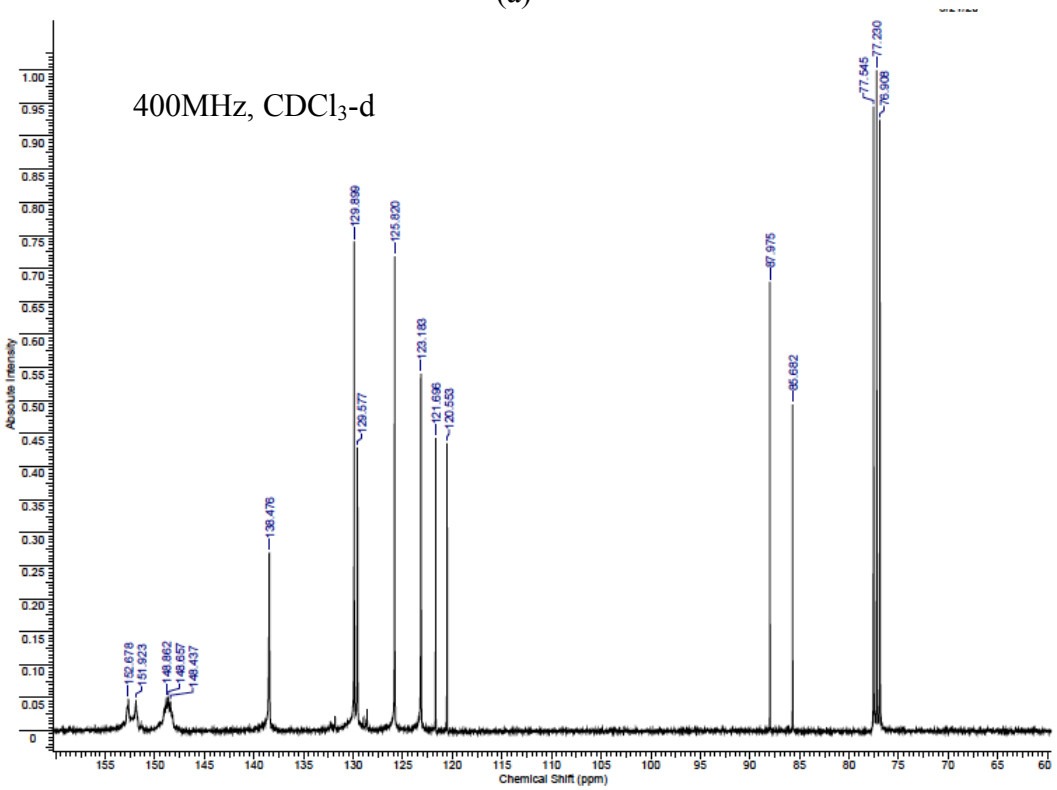

(b)

Figure B.12 (a) ^{1}H and (b) ^{13}C NMR of **12**

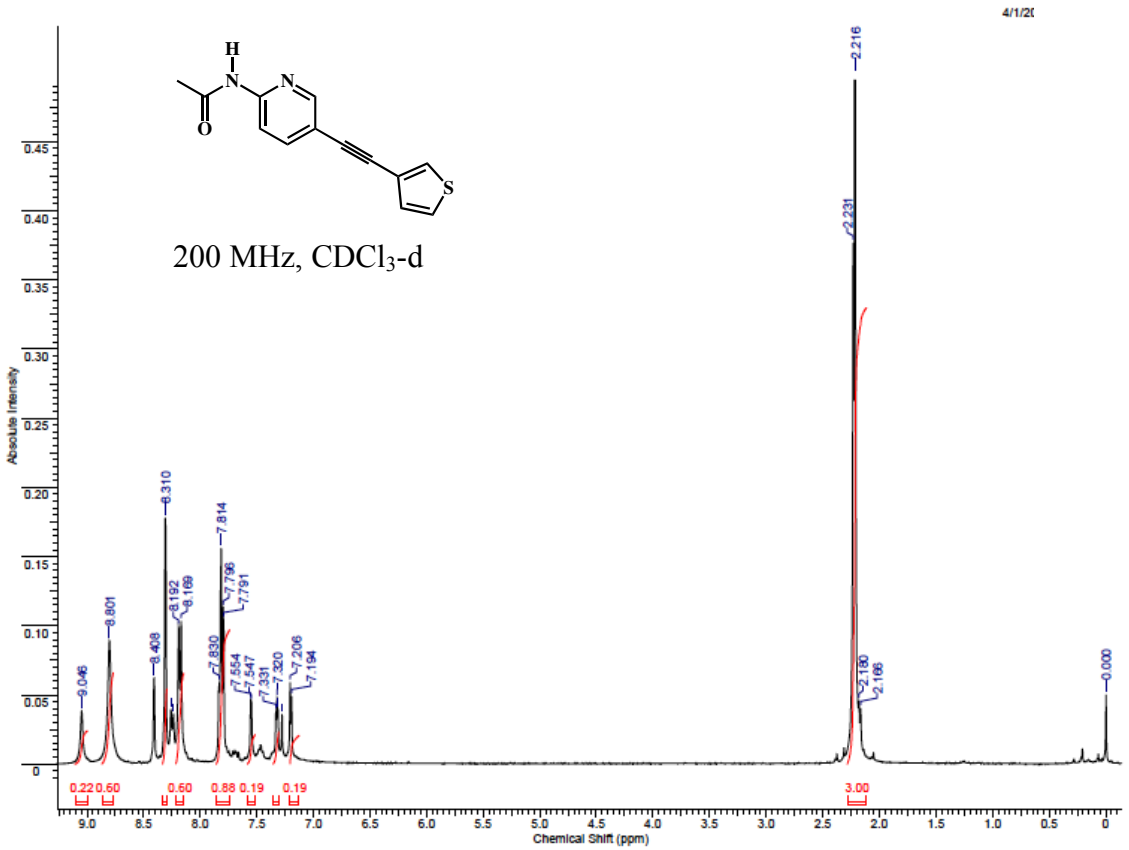

(a)

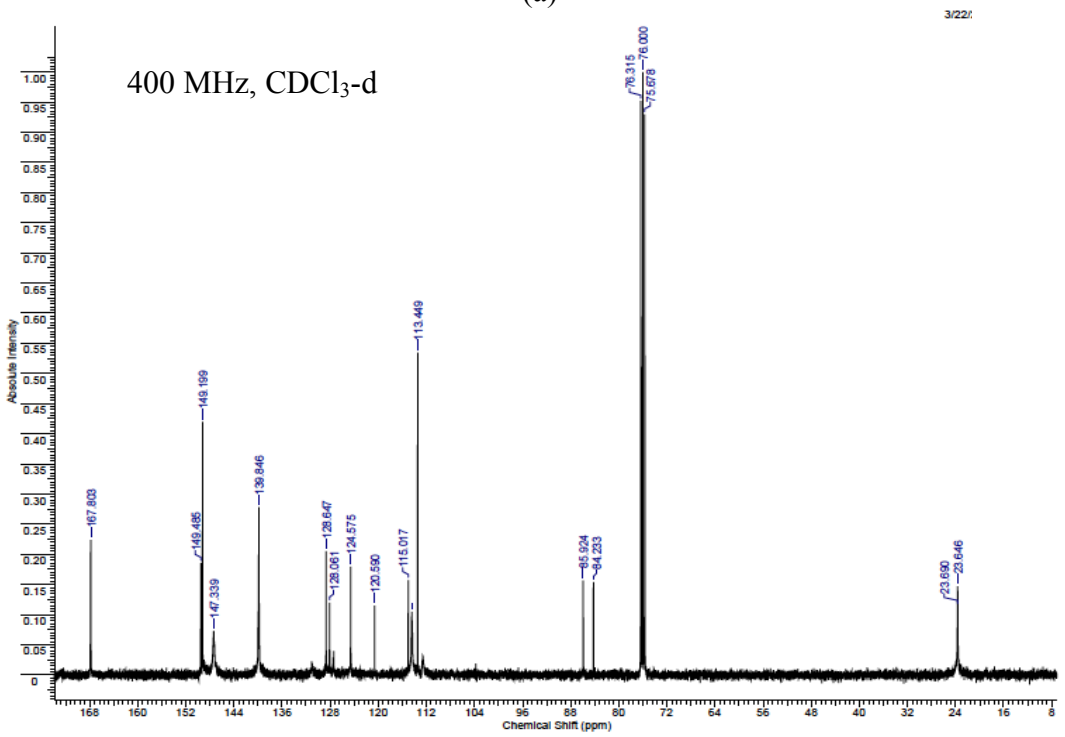

(b)

Figure B.13 (a) ^{1}H and (b) ^{13}C NMR of **13**

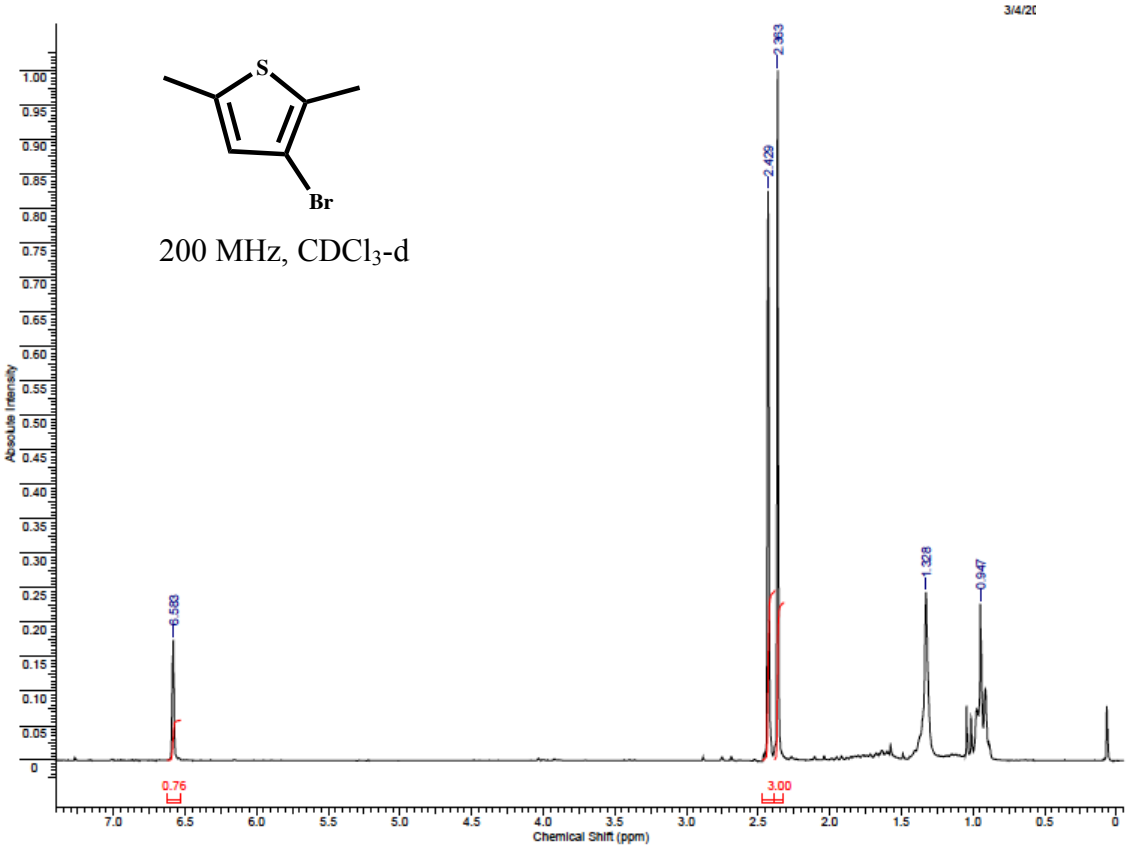

Figure B.14 ^{1}H NMR of **14**

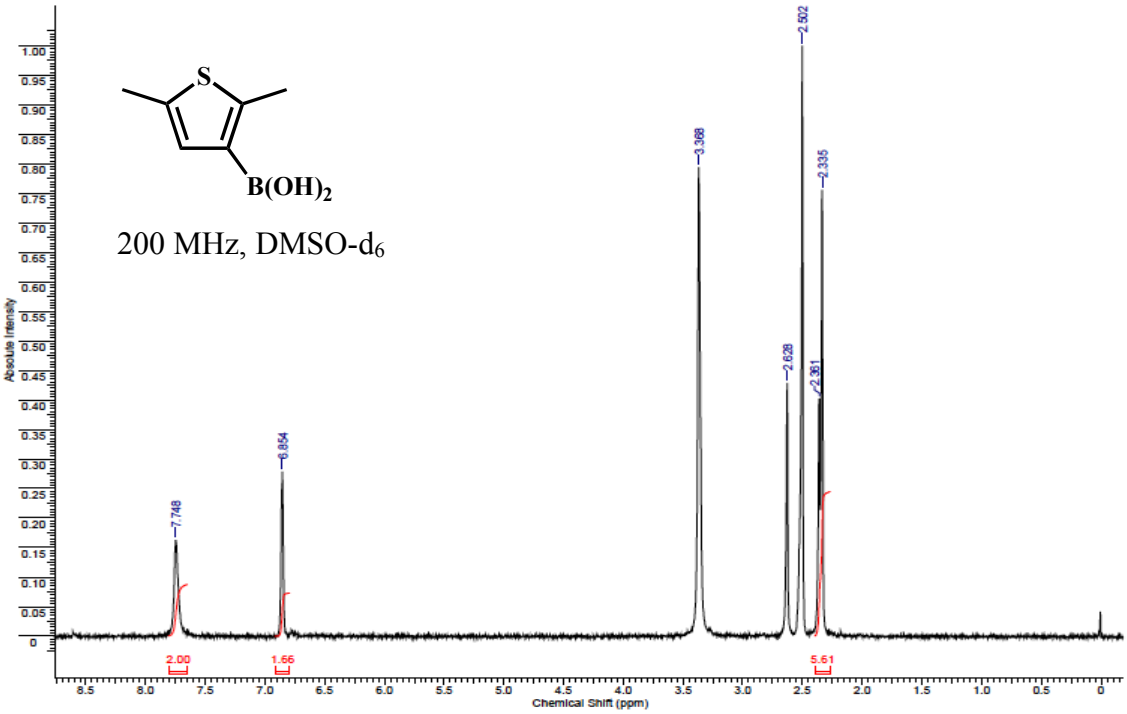

Figure B.15 ^{1}H NMR of **15**

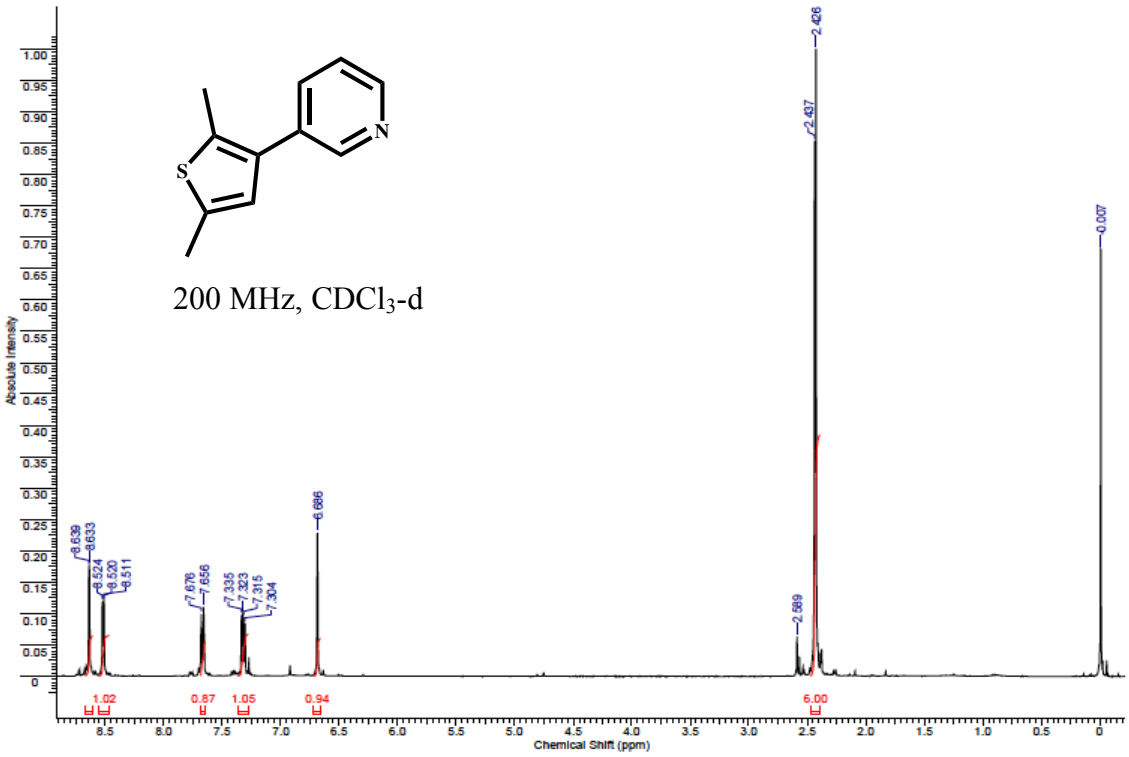

(a)

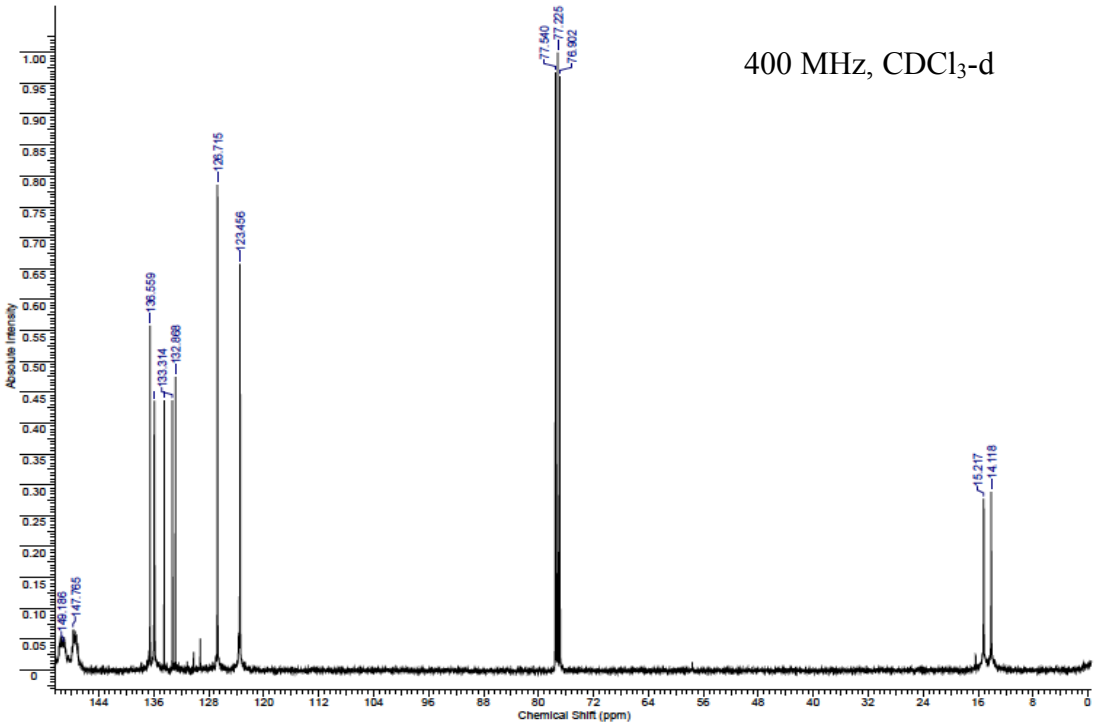

(b)

Figure B.16 (a) ^{1}H and (b) ^{13}C NMR of **16**

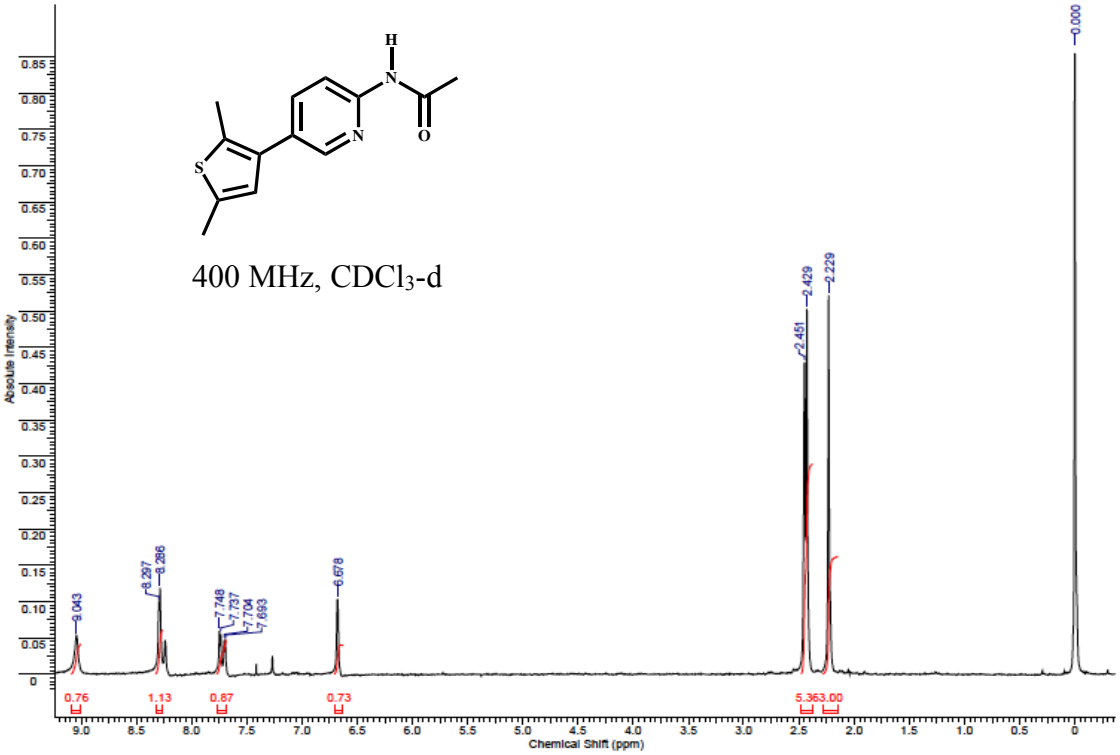

(a)

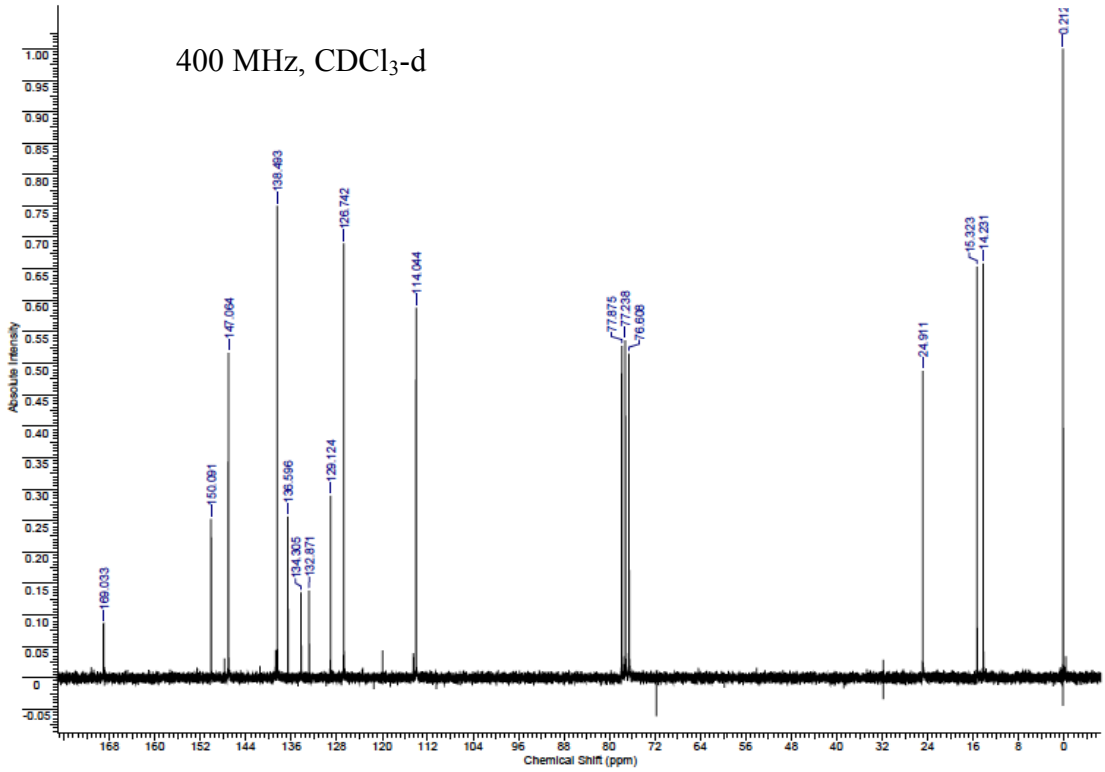

(b)

Figure B.17 (a) ^{1}H and (b) ^{13}C NMR of **17**

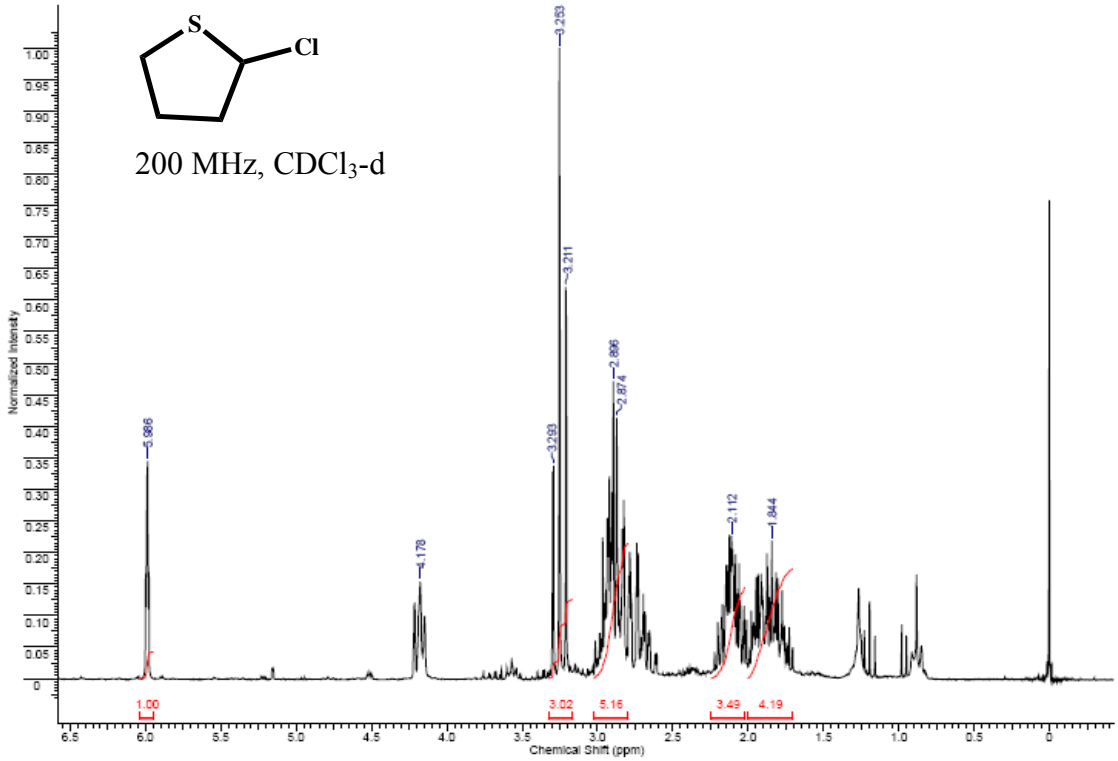

Figure B.18 ^{1}H NMR of **18**

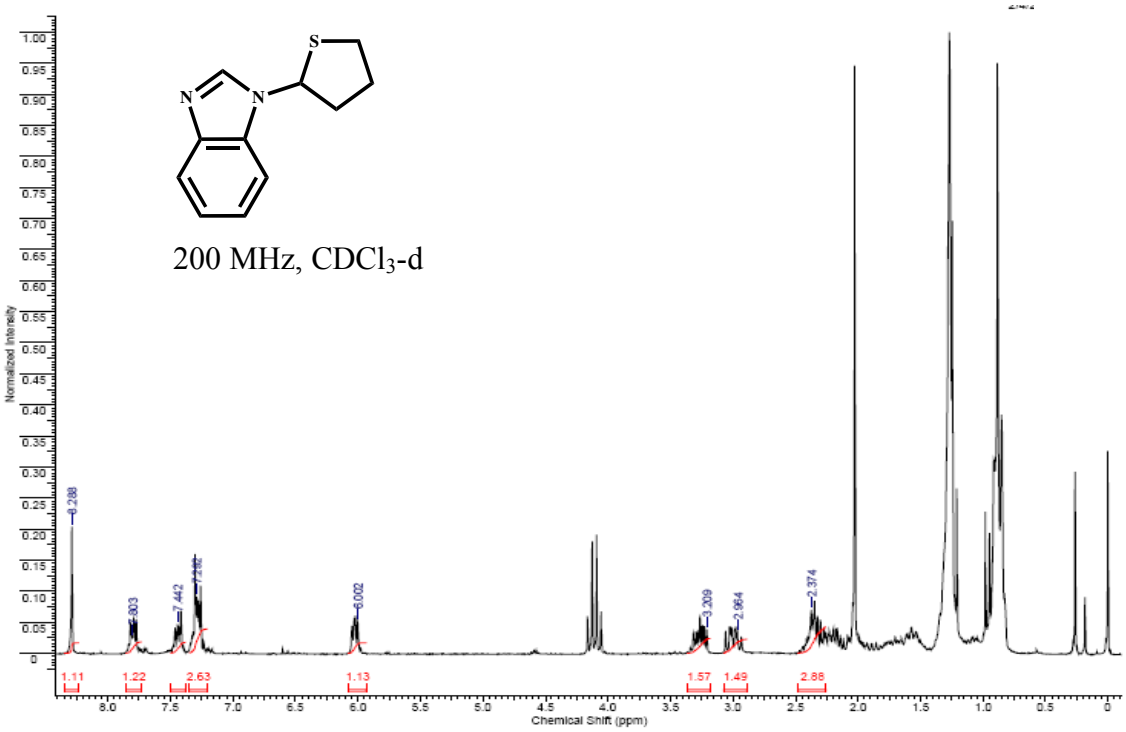

(a)

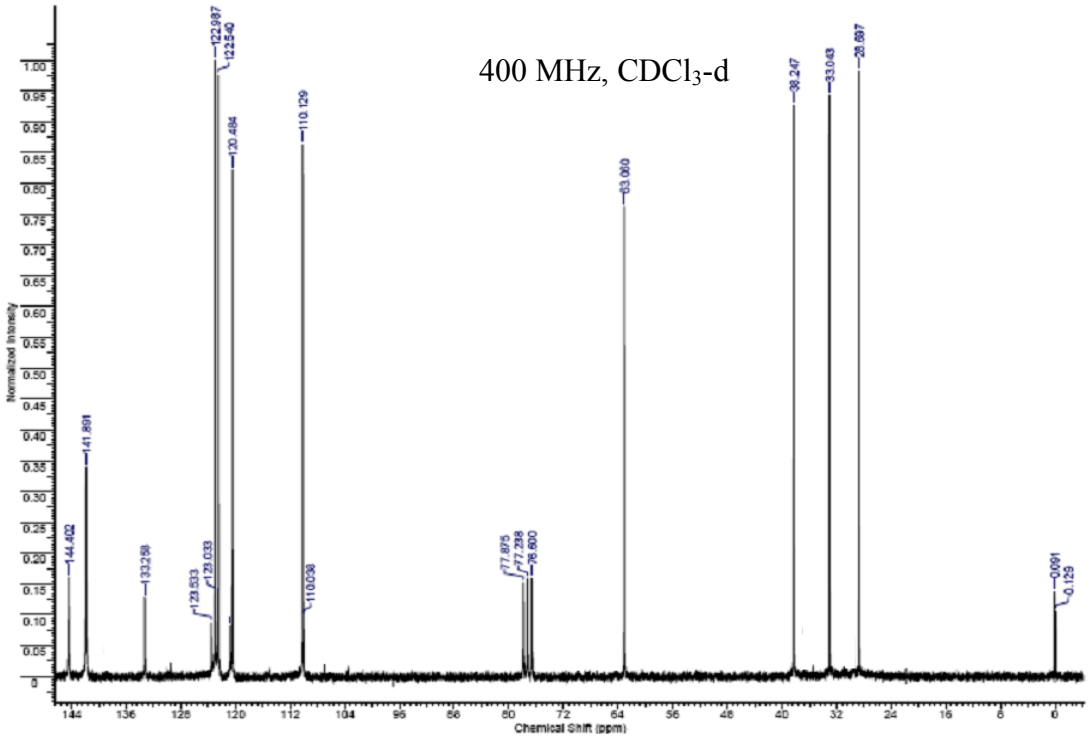

(b)

Figure B.19 (a) ^{1}H and (b) ^{13}C NMR of **19**

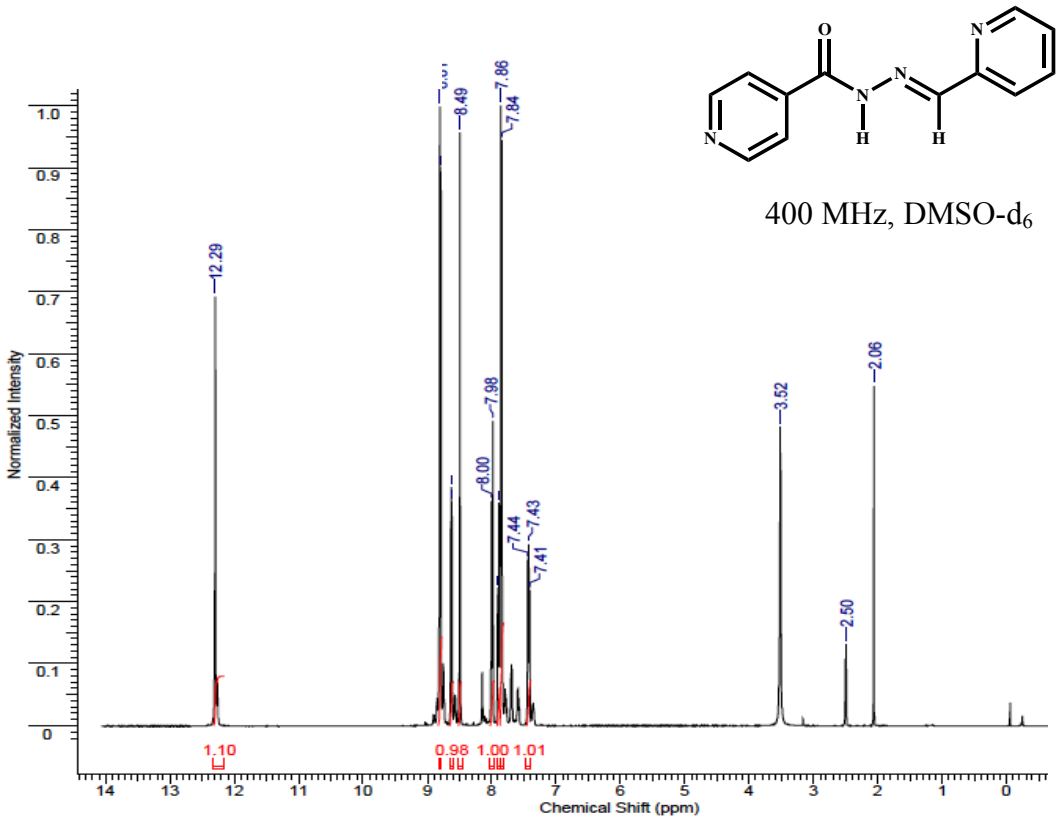

(a)

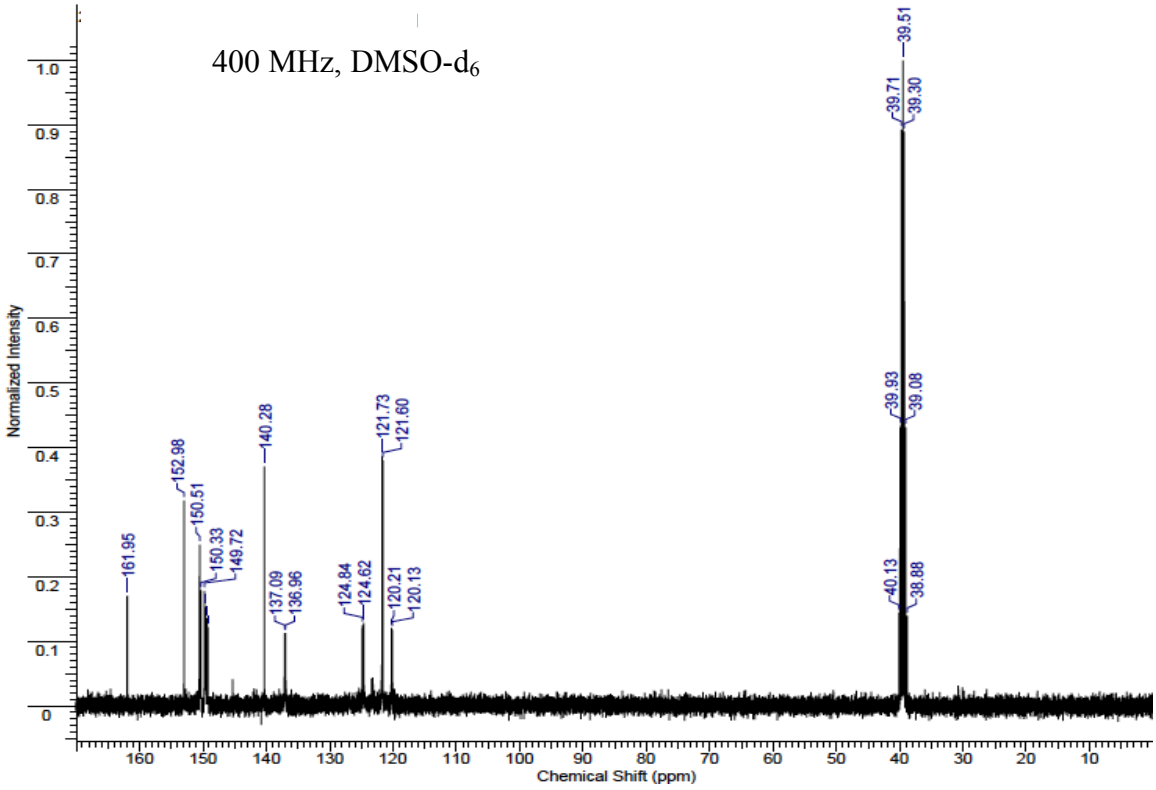

(b)

Figure B.20 (a) ^{1}H and ^{13}C NMR of **20**

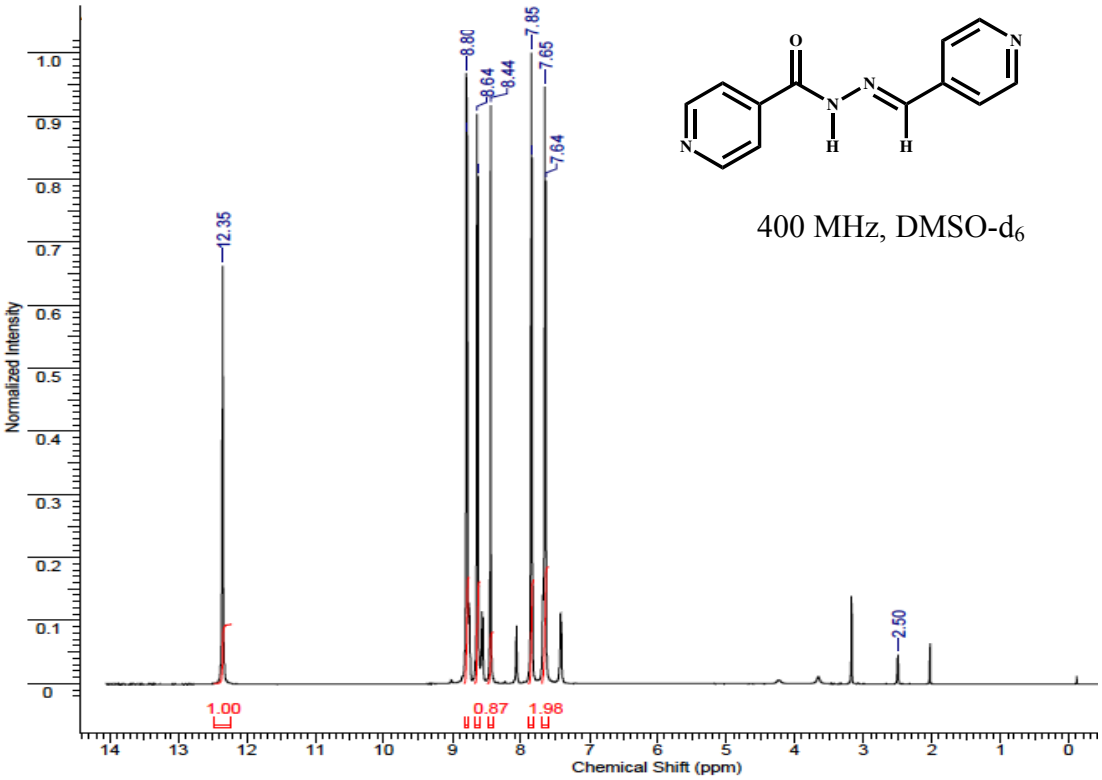

(a)

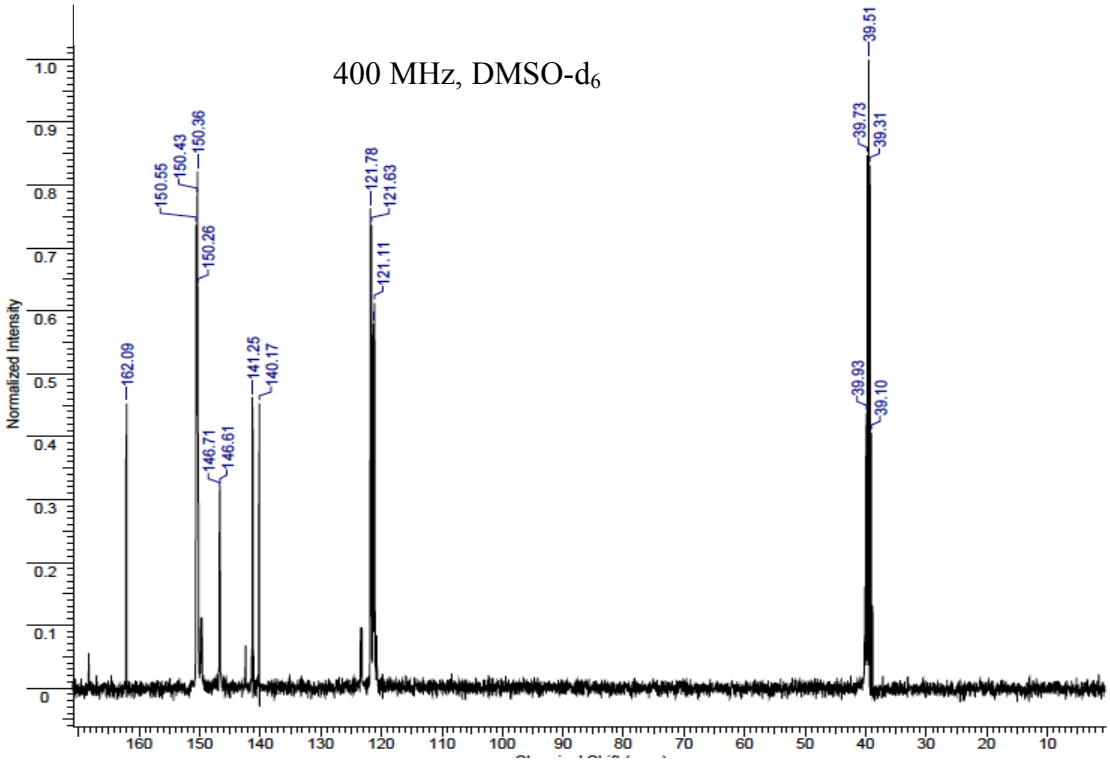

(b)

Figure B.21 (a) ^{1}H and ^{13}C NMR of **21**

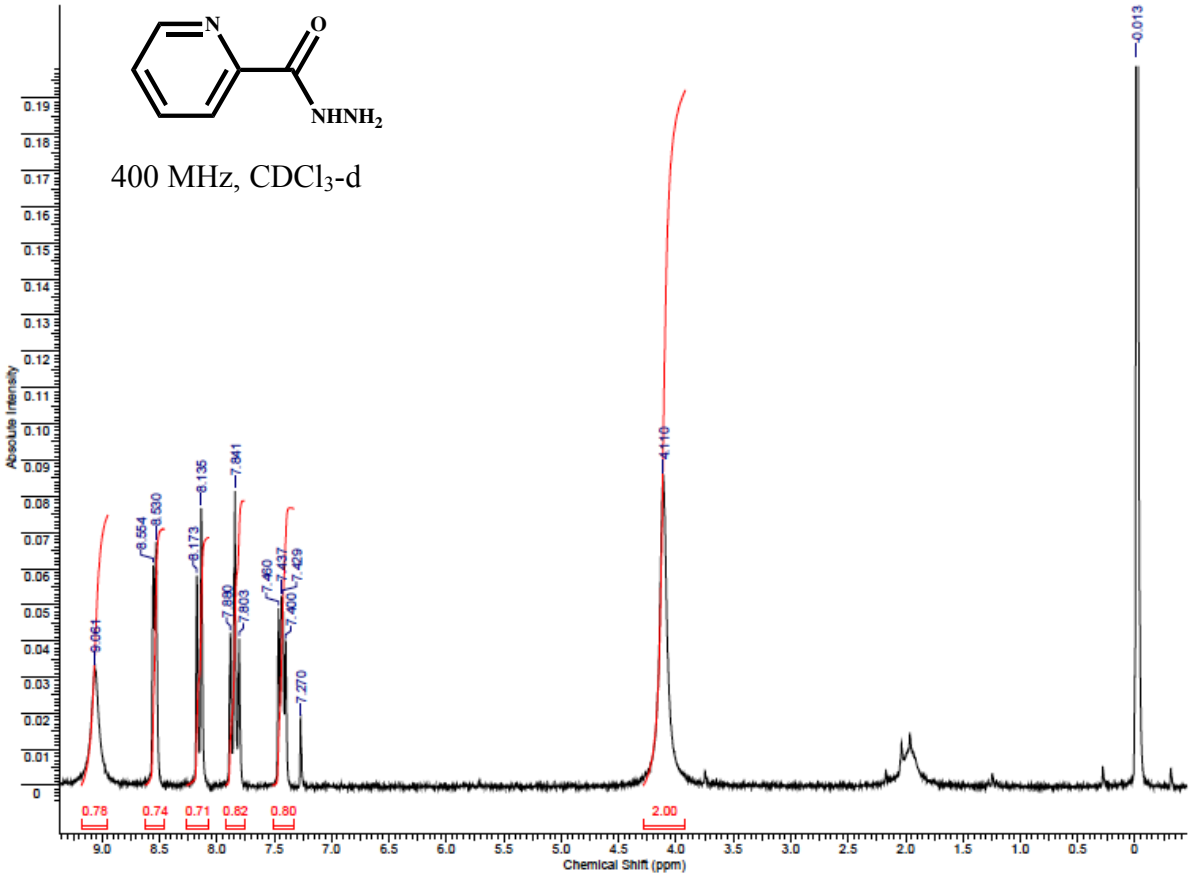

Figure B.22 ^{1}H NMR of **22**

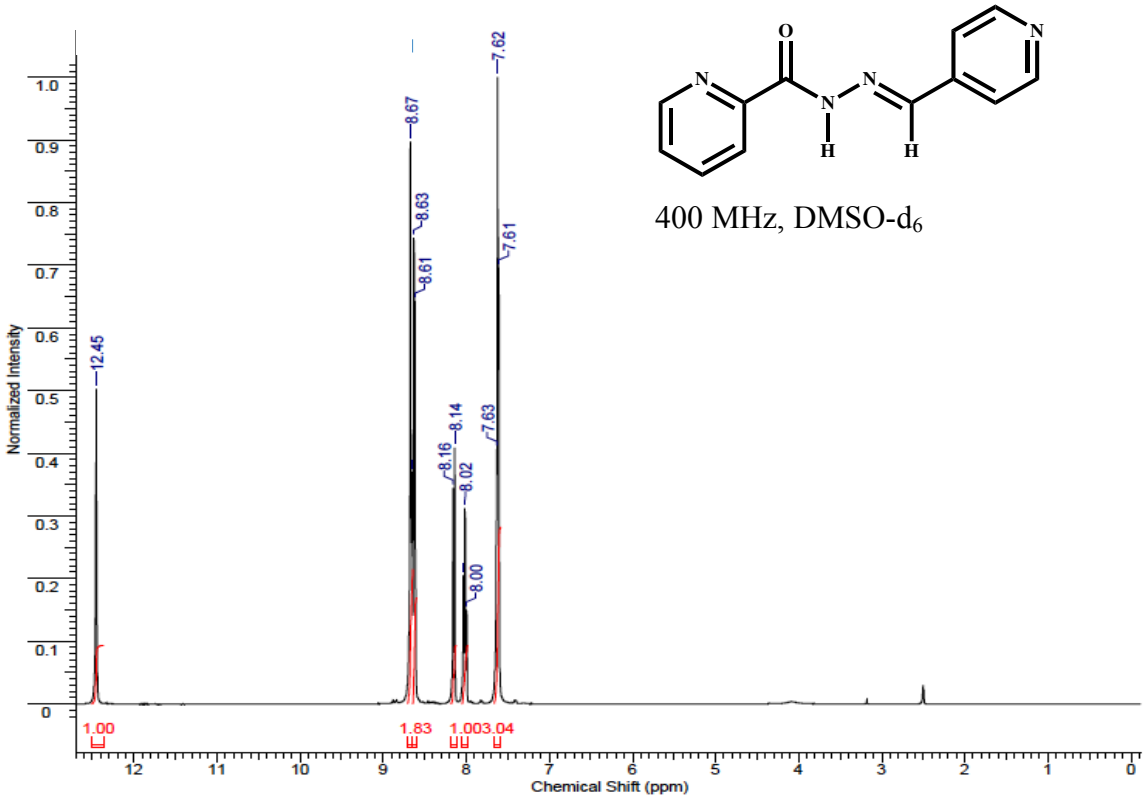

(a)

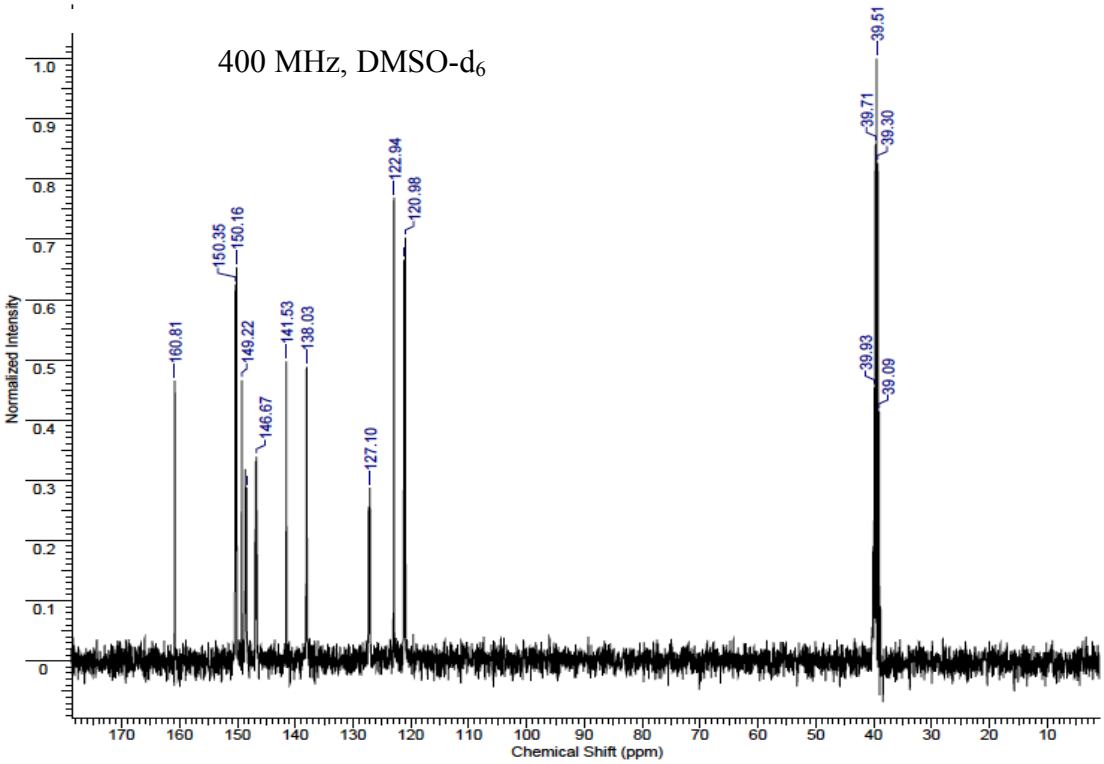

(b)

Figure B.23 (a) ^{1}H and (b) ^{13}C NMR of **23**

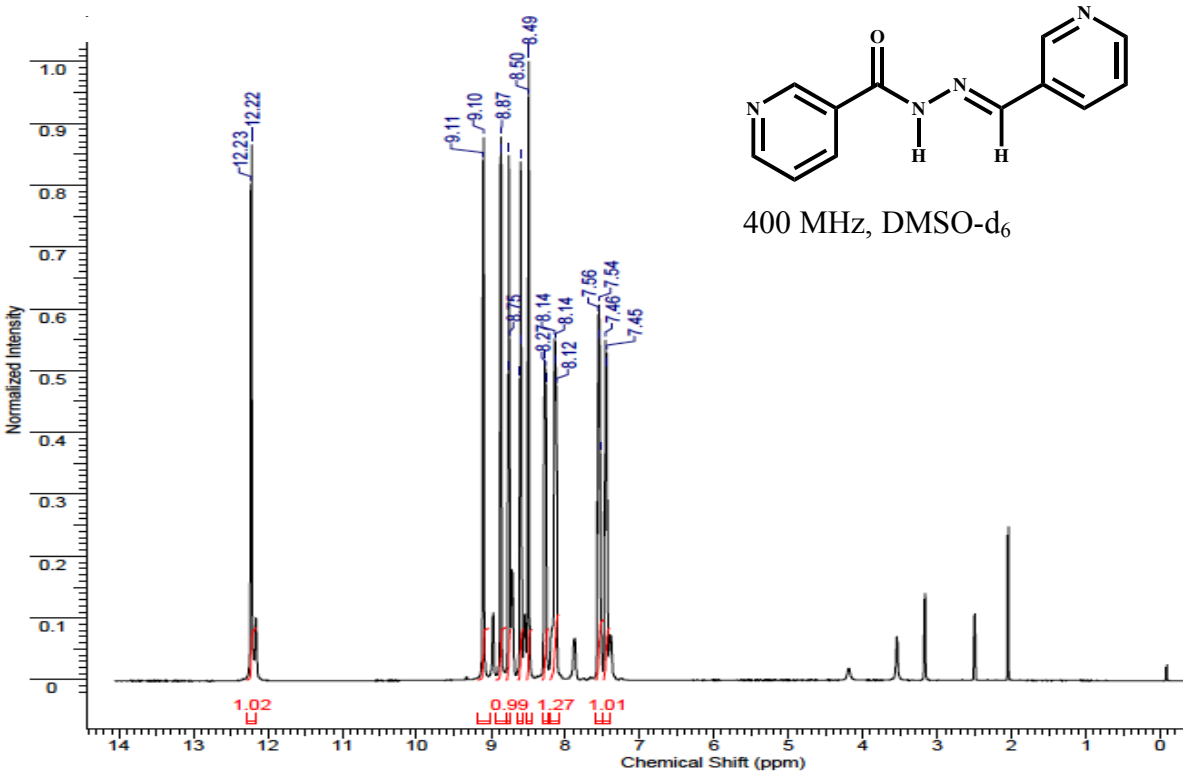

(a)

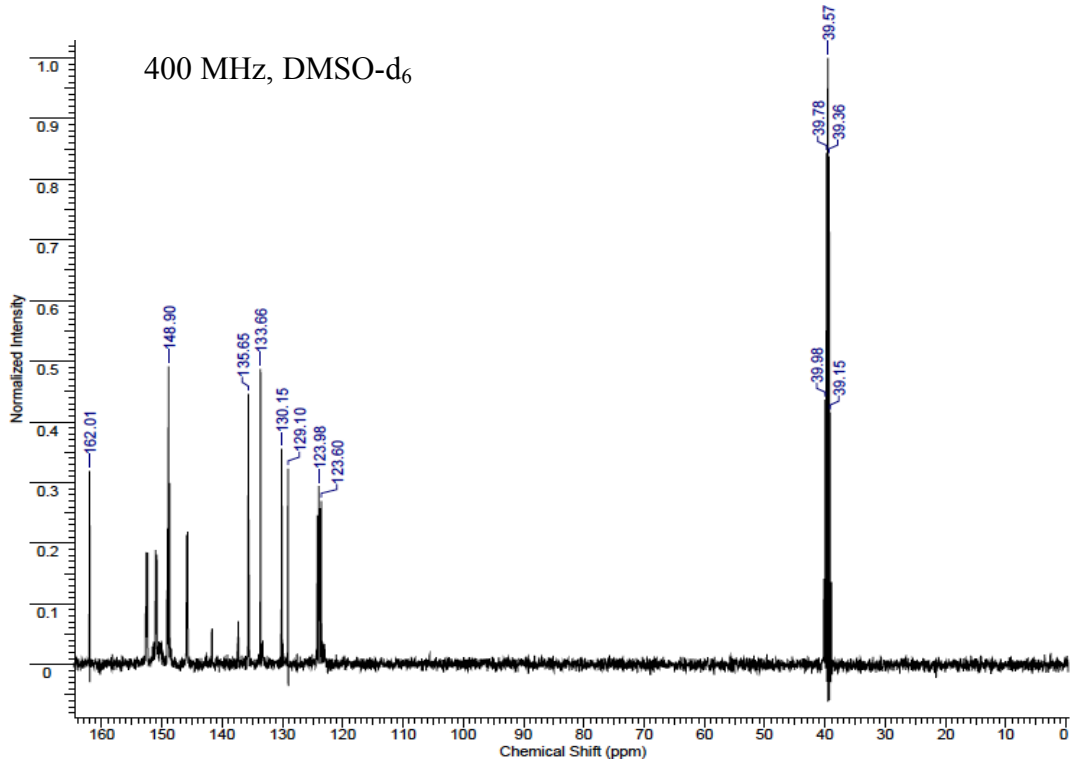

(b)

Figure B.24 (a) ^{1}H and (b) ^{13}C NMR of **24**

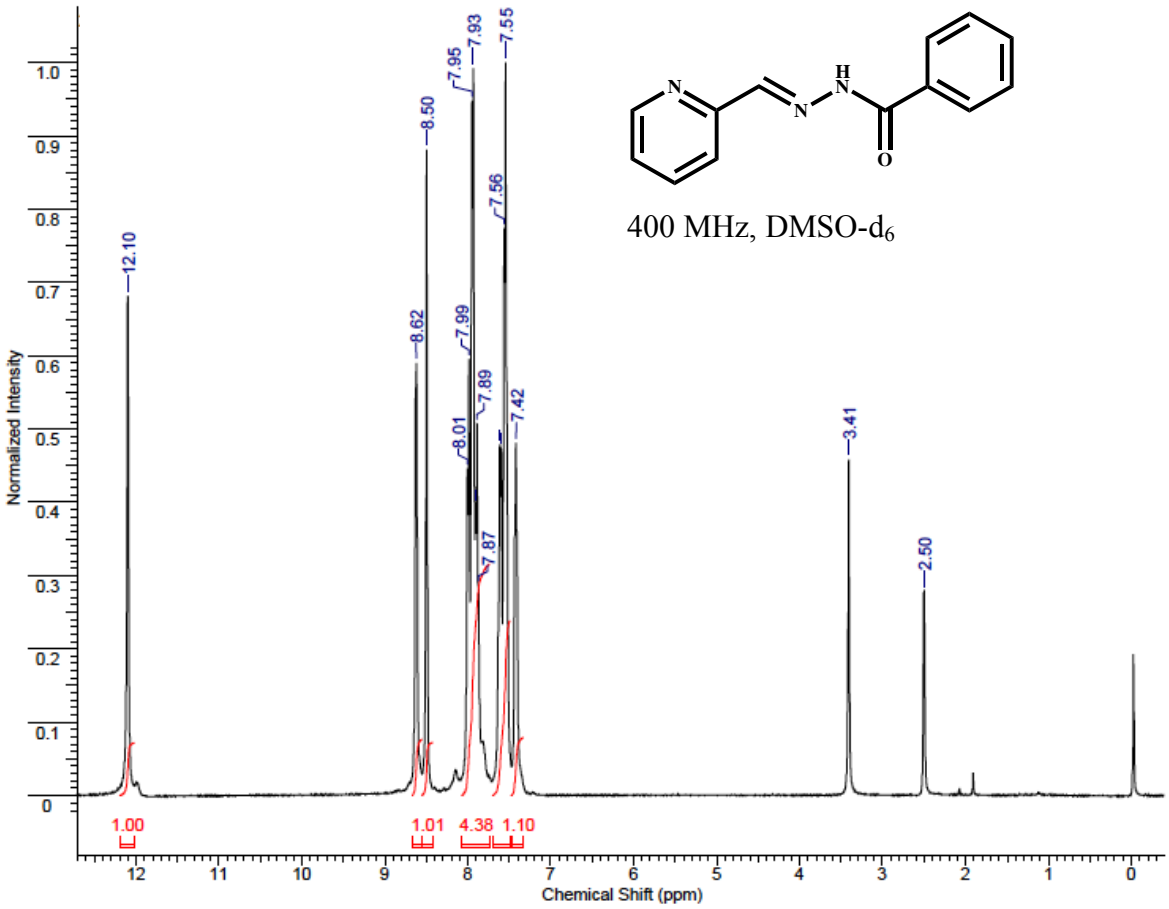

Figure B.25 ^{1}H NMR of **25**

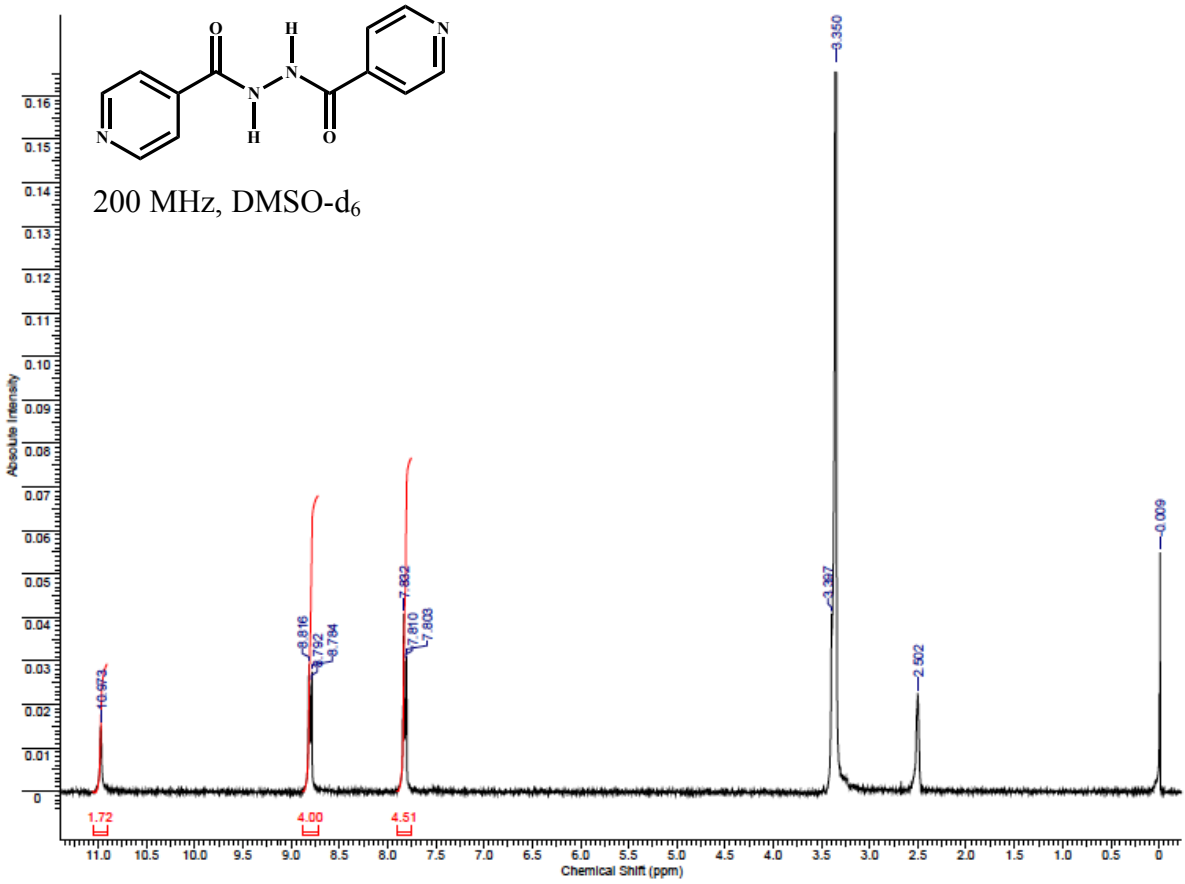

Figure B.26 ^{1}H NMR of **26**

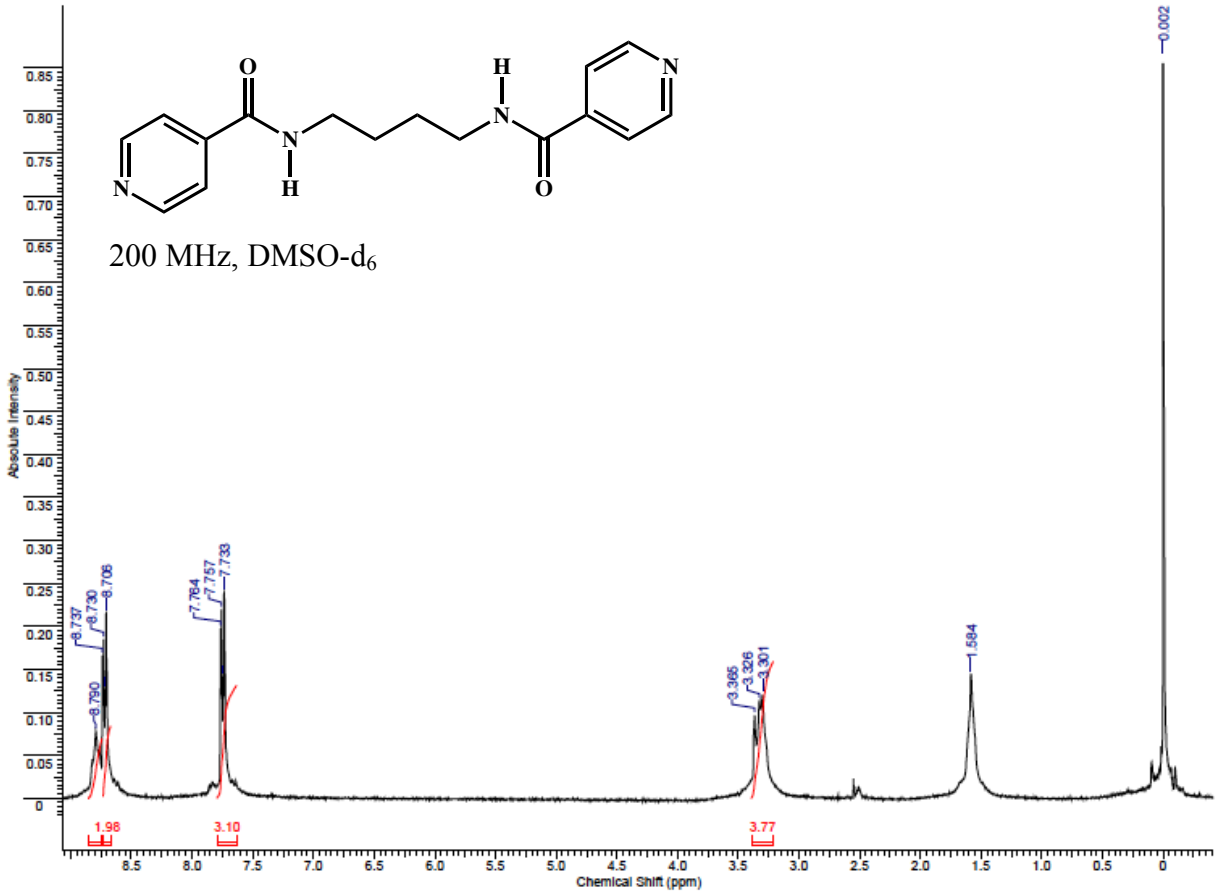

Figure B.27 ^{1}H NMR of **27**

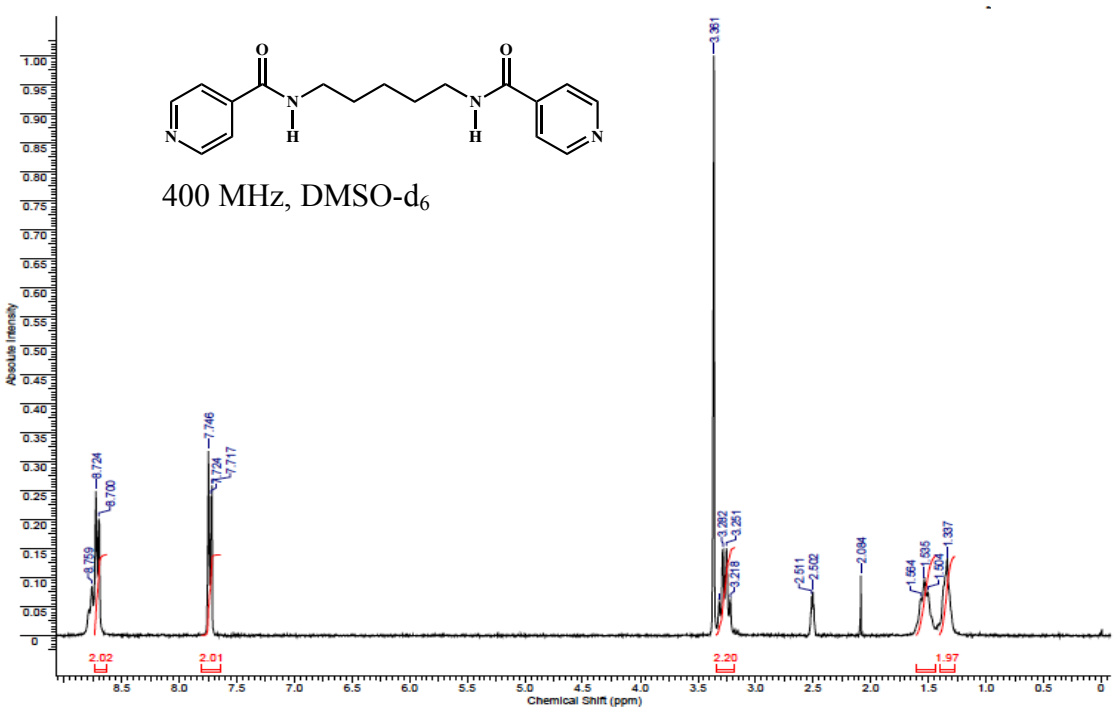

(a)

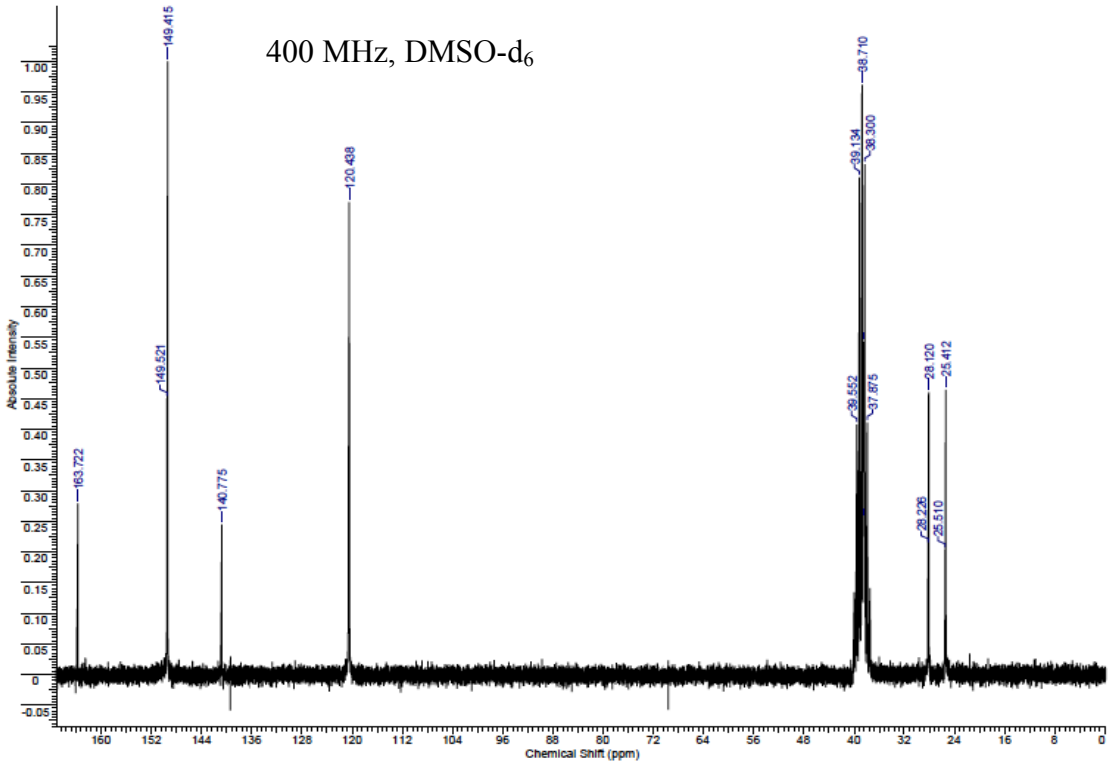

(b)

Figure B.28 (a) ^{1}H and ^{13}C NMR of **28**

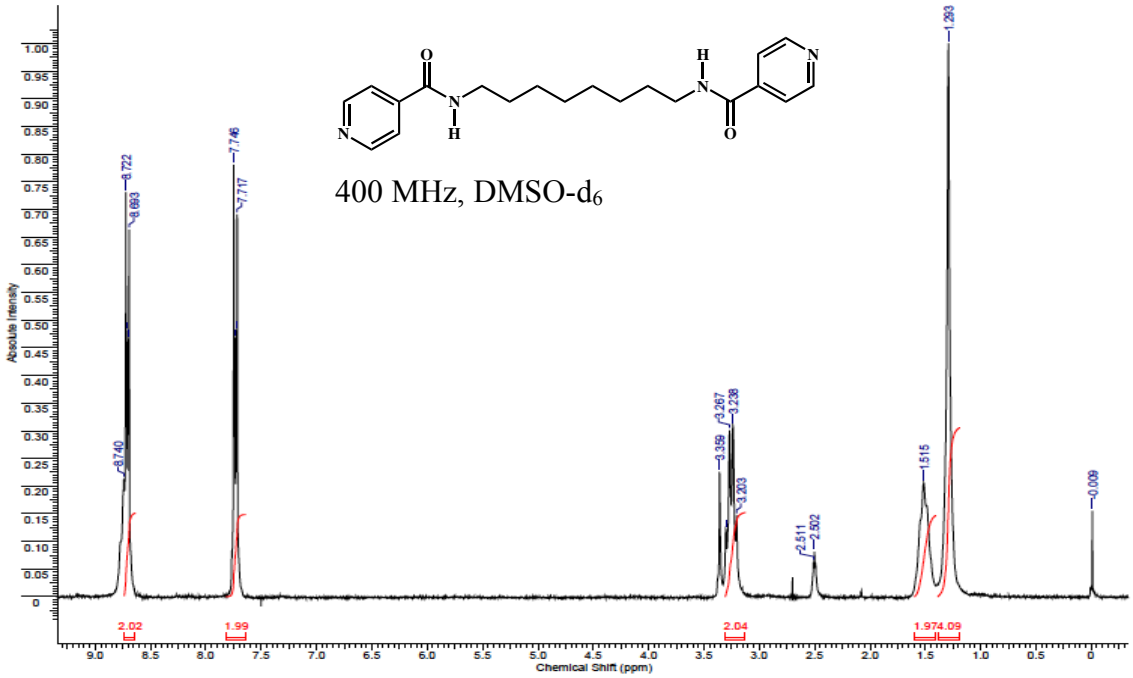

(a)

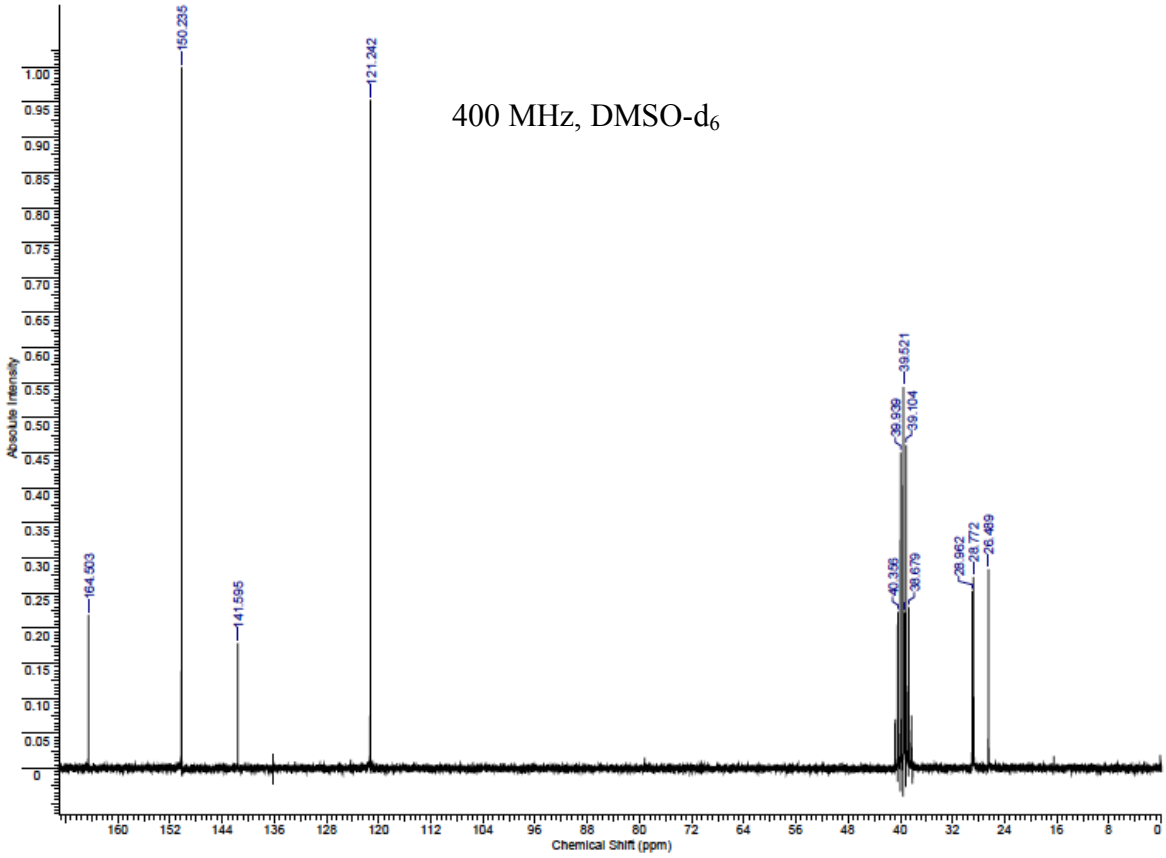

(b)

Figure B.29 (a) ^{1}H and ^{13}C NMR of **29**

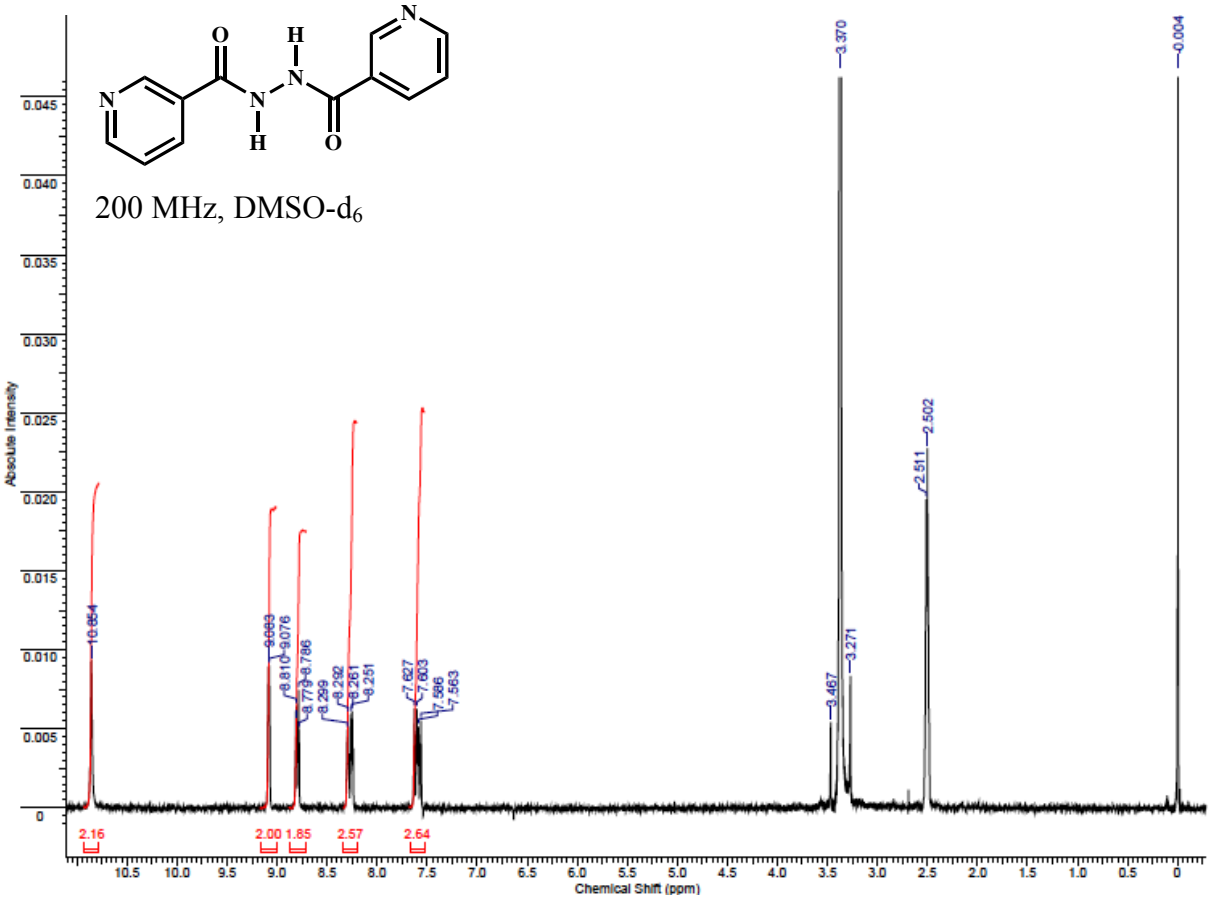

Figure B.30 ^{1}H NMR of **30**

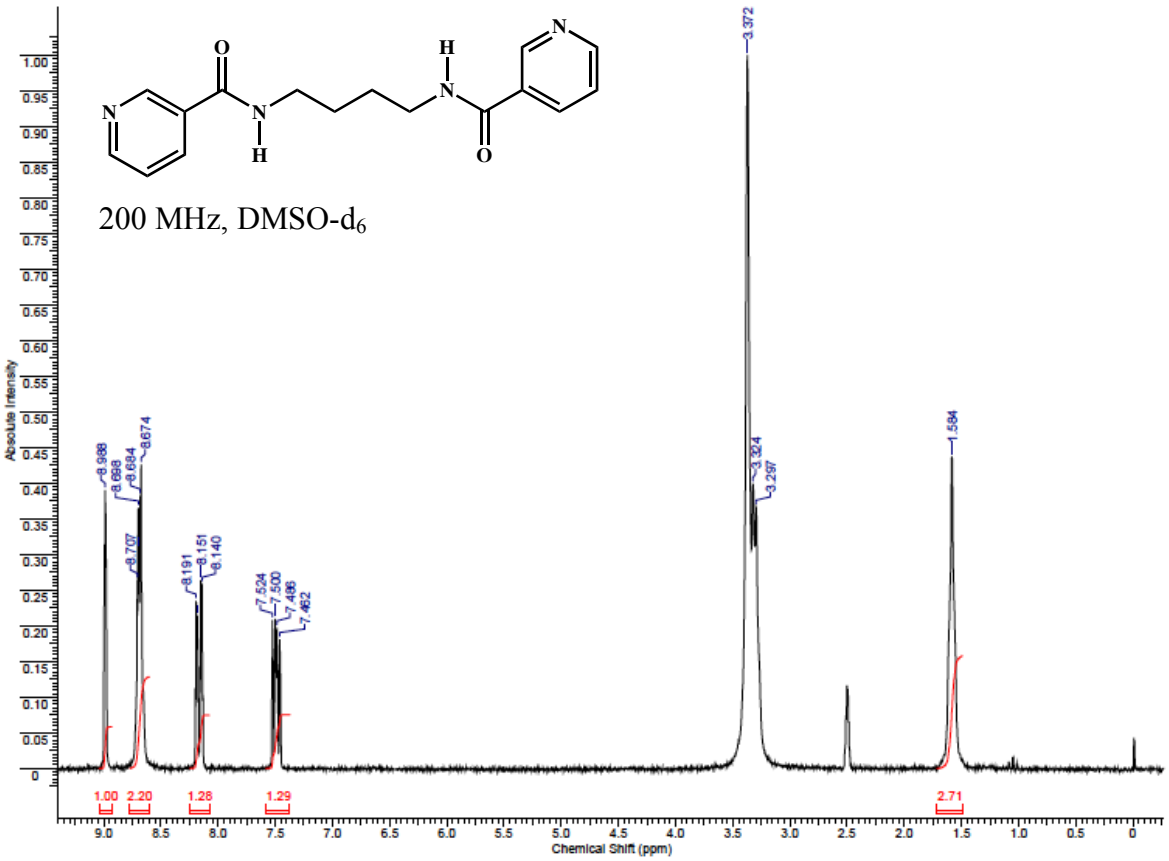

Figure B.31 ^{1}H NMR of **31**

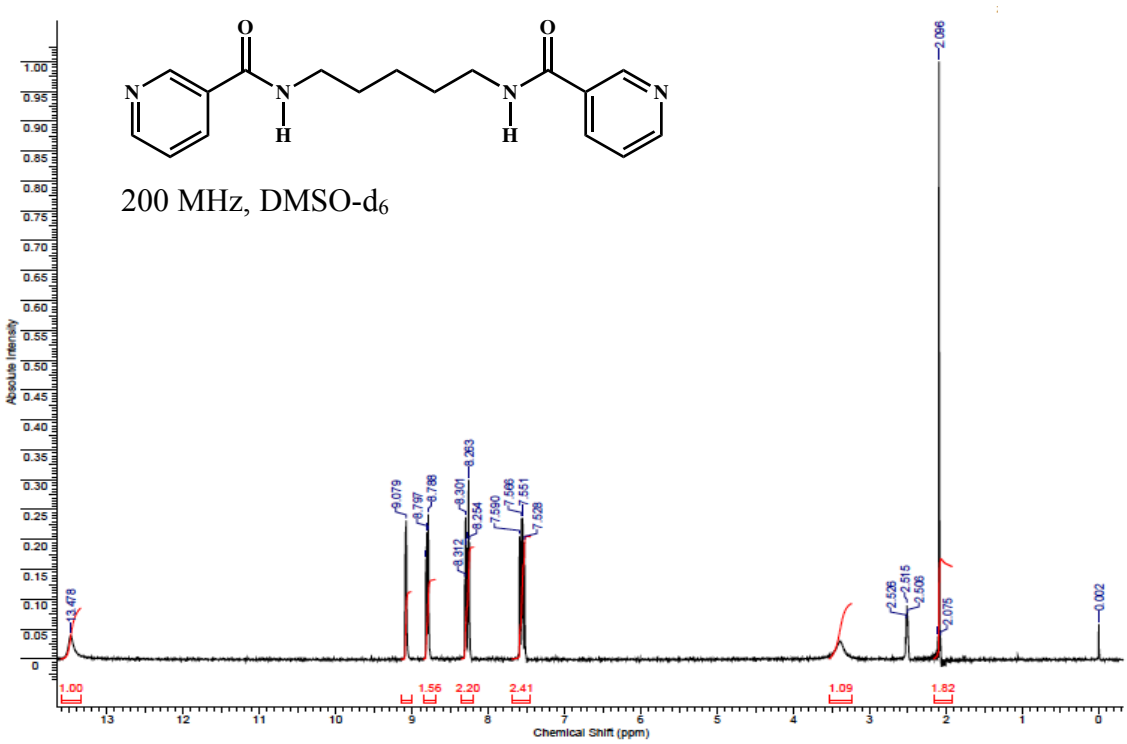

(a)

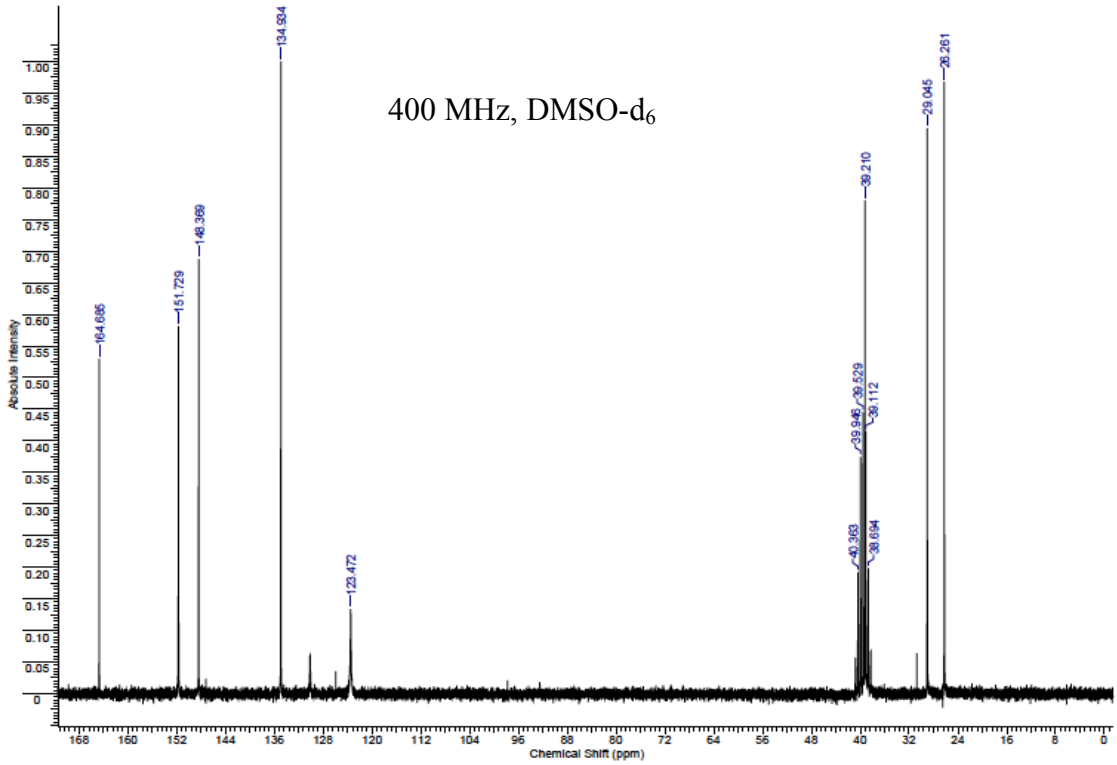

(b)

Figure B.32 (a) ^{1}H and ^{13}C NMR of **32**

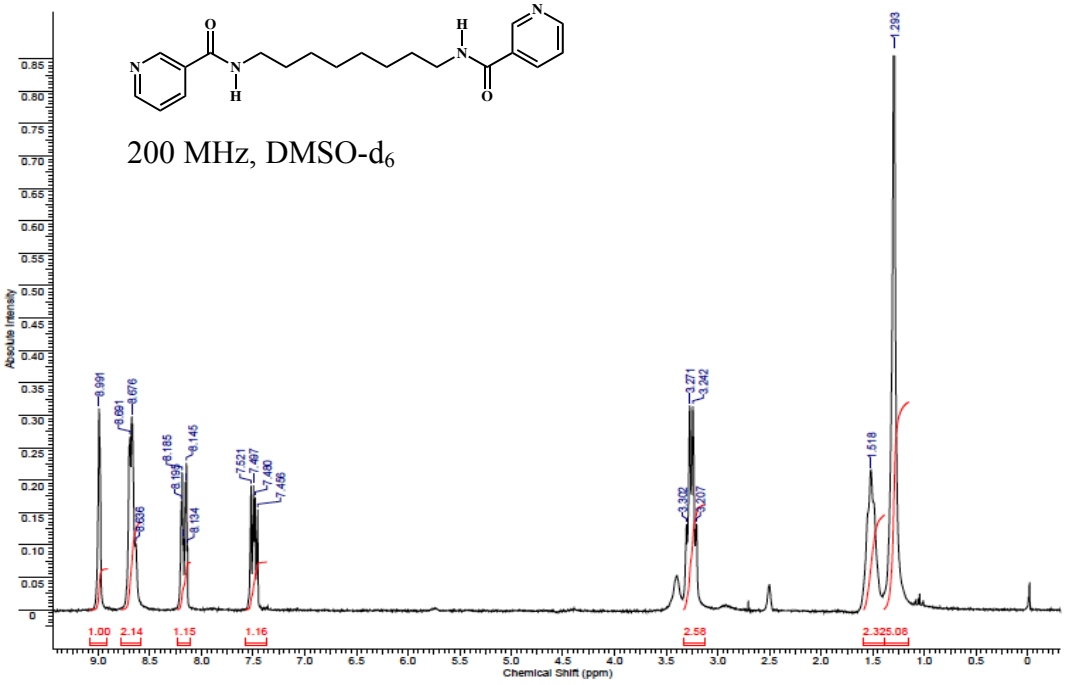

(a)

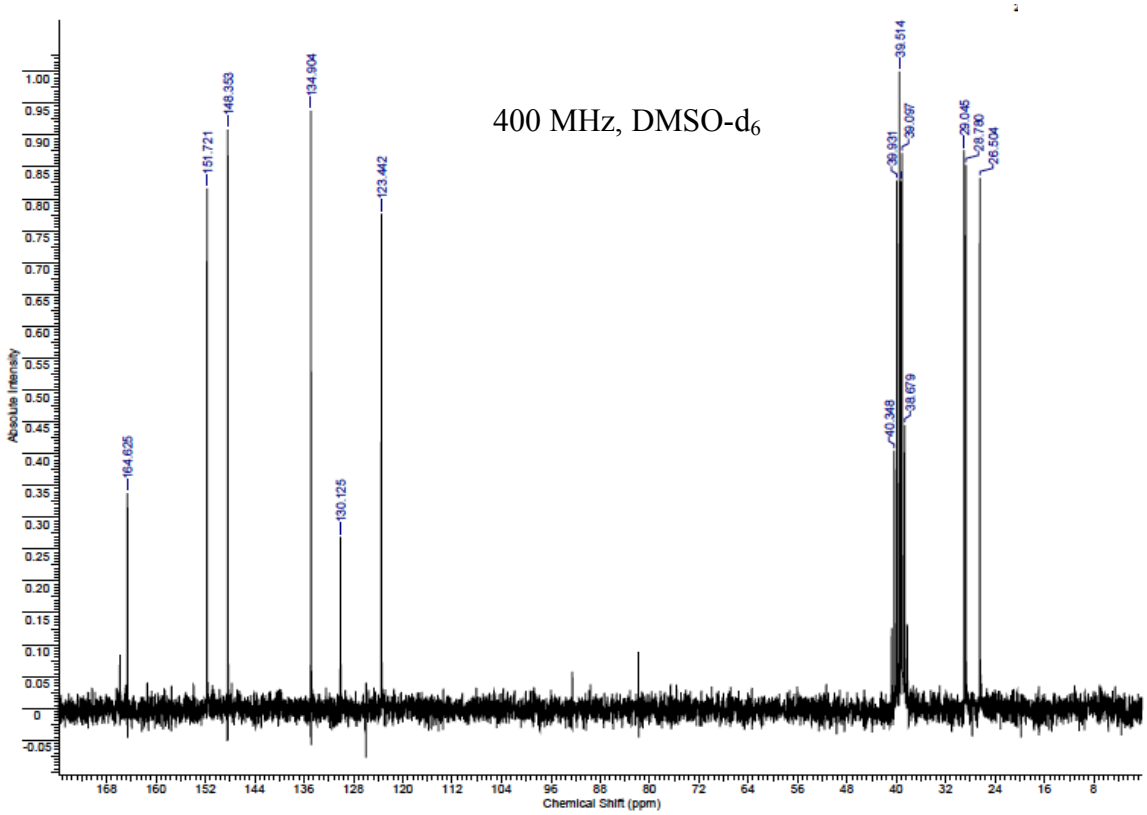

(b)

Figure B.33 (a) ^{1}H and ^{13}C NMR of **33**

Appendix C - Crystallographic Data Tables

Table C.1 Crystal data and structure refinement for **2HG, 2SUB, 2SEB, 3SUC, 3HBA** and **1a-b, 2a, 3a**

2HG

Identification code	sf0601m	
Empirical formula	C12 H16 N2 O5	
Formula weight	268.27	
Temperature	173(2) K	
Wavelength	0.71073 Å	
Crystal system	Triclinic	
Space group	P-1	
Unit cell dimensions	a = 7.1730(8) Å	α= 80.462(7)°.
	b = 7.6117(8) Å	β= 75.807(7)°.
	c = 11.9194(13) Å	γ = 87.896(7)°.
Volume	622.19(12) $Å^3$	
Z	2	
Density (calculated)	1.432 g/cm^3	
Absorption coefficient	0.112 mm^{-1}	
F(000)	284	
Crystal size	0.35 x 0.30 x 0.15 mm^3	
Theta range for data collection	1.79 to 26.37°.	
Index ranges	-8<=h<=8, -9<=k<=9, -13<=l<=14	
Reflections collected	3381	
Independent reflections	2213 [R(int) = 0.0867]	
Completeness to theta = 26.37°	87.3 %	
Absorption correction	None	
Refinement method	Full-matrix least-squares on F^2	
Data / restraints / parameters	2213 / 0 / 182	
Goodness-of-fit on F^2	1.000	
Final R indices [I>2sigma(I)]	R1 = 0.0542, wR2 = 0.1396	
R indices (all data)	R1 = 0.0664, wR2 = 0.1483	
Largest diff. peak and hole	0.442 and -0.291 $e.Å^{-3}$	

Crystal data and structure refinement for **2SUB**.

Identification code	sf0918m	
Empirical formula	C22 H30 N4 O6	
Formula weight	446.50	
Temperature	120(2) K	
Wavelength	0.71073 Å	
Crystal system	Monoclinic	
Space group	P2(1)/n	
Unit cell dimensions	a = 10.0886(7) Å	α= 90°.
	b = 8.6108(6) Å	β= 100.883(3)°.
	c = 25.9765(19) Å	γ = 90°.
Volume	2216.0(3) $Å^3$	
Z	4	
Density (calculated)	1.338 g/cm^3	
Absorption coefficient	0.098 mm^{-1}	
F(000)	952	
Crystal size	0.32 x 0.26 x 0.16 mm^3	
Theta range for data collection	1.60 to 32.56°.	
Index ranges	-15<=h<=11, -11<=k<=13, -39<=l<=38	
Reflections collected	50976	
Independent reflections	7909 [R(int) = 0.0243]	
Completeness to theta = 32.56°	98.2 %	
Absorption correction	None	
Max. and min. transmission	0.9844 and 0.9692	
Refinement method	Full-matrix least-squares on F^2	
Data / restraints / parameters	7909 / 0 / 307	
Goodness-of-fit on F^2	1.052	
Final R indices [I>2sigma(I)]	R1 = 0.0401, wR2 = 0.1134	
R indices (all data)	R1 = 0.0471, wR2 = 0.1186	
Largest diff. peak and hole	0.415 and -0.220 $e.Å^{-3}$	

Crystal data and structure refinement for **2SEB**.

Identification code	sf0602	
Empirical formula	C24 H34 N4 O6	
Formula weight	474.55	
Temperature	100(2) K	
Wavelength	0.71073 Å	
Crystal system	Monoclinic	
Space group	C2/c	
Unit cell dimensions	a = 28.532(3) Å	α= 90°.
	b = 8.2965(8) Å	β= 101.987(2)°.
	c = 10.6120(10) Å	γ = 90°.
Volume	2457.2(4) $Å^3$	
Z	4	
Density (calculated)	1.283 g/cm^3	
Absorption coefficient	0.093 mm^{-1}	
F(000)	1016	
Crystal size	0.22 x 0.32 x 0.42 mm^3	
Theta range for data collection	2.56 to 30.53°.	
Index ranges	-39<=h<=40, -11<=k<=11, -15<=l<=15	
Reflections collected	14481	
Independent reflections	3740 [R(int) = 0.0727]	
Completeness to theta = 30.53°	99.5 %	
Absorption correction	None	
Refinement method	Full-matrix least-squares on F^2	
Data / restraints / parameters	3740 / 0 / 161	
Goodness-of-fit on F^2	1.066	
Final R indices [I>2sigma(I)]	R1 = 0.0555, wR2 = 0.1544	
R indices (all data)	R1 = 0.0661, wR2 = 0.1600	
Largest diff. peak and hole	0.510 and -0.418 $e.Å^{-3}$	

Crystal data and structure refinement for **3SUC**.

Identification code	sf0801m	
Empirical formula	C20 H26 N4 O6	
Formula weight	418.45	
Temperature	120(2) K	
Wavelength	0.71073 Å	
Crystal system	Monoclinic	
Space group	P2(1)/c	
Unit cell dimensions	a = 13.6600(4) Å	α= 90°.
	b = 4.9276(2) Å	β= 110.7620(10)°.
	c = 16.3965(5) Å	γ = 90°.
Volume	1031.99(6) $Å^3$	
Z	2	
Density (calculated)	1.347 g/cm^3	
Absorption coefficient	0.101 mm^{-1}	
F(000)	444	
Crystal size	0.30 x 0.25 x 0.20 mm^3	
Theta range for data collection	2.57 to 32.58°.	
Index ranges	-19<=h<=19, -7<=k<=7, -24<=l<=24	
Reflections collected	11571	
Independent reflections	3694 [R(int) = 0.0229]	
Completeness to theta = 32.58°	98.2 %	
Absorption correction	None	
Max. and min. transmission	0.9801 and 0.9704	
Refinement method	Full-matrix least-squares on F^2	
Data / restraints / parameters	3694 / 0 / 143	
Goodness-of-fit on F^2	1.036	
Final R indices [I>2sigma(I)]	R1 = 0.0403, wR2 = 0.1138	
R indices (all data)	R1 = 0.0461, wR2 = 0.1192	
Largest diff. peak and hole	0.516 and -0.265 $e.Å^{-3}$	

Crystal data and structure refinement for **3HBA**.

Identification code	sf0937m	
Empirical formula	C15 H16 N2 O4	
Formula weight	288.30	
Temperature	120(2) K	
Wavelength	0.71073 Å	
Crystal system	Monoclinic	
Space group	P2(1)/n	
Unit cell dimensions	a = 5.6869(3) Å	α= 90°.
	b = 7.2012(4) Å	β= 93.882(2)°.
	c = 33.5028(18) Å	γ = 90°.
Volume	1368.88(13) $Å^3$	
Z	4	
Density (calculated)	1.399 g/cm^3	
Absorption coefficient	0.103 mm^{-1}	
F(000)	608	
Crystal size	0.32 x 0.24 x 0.14 mm^3	
Theta range for data collection	0.61 to 32.57°.	
Index ranges	-8<=h<=6, -10<=k<=7, -50<=l<=50	
Reflections collected	17775	
Independent reflections	4684 [R(int) = 0.0291]	
Completeness to theta = 30.00°	97.9 %	
Absorption correction	None	
Max. and min. transmission	0.9858 and 0.9679	
Refinement method	Full-matrix least-squares on F^2	
Data / restraints / parameters	4684 / 0 / 204	
Goodness-of-fit on F^2	1.018	
Final R indices [I>2sigma(I)]	R1 = 0.0484, wR2 = 0.1318	
R indices (all data)	R1 = 0.0560, wR2 = 0.1383	
Largest diff. peak and hole	0.666 and -0.278 $e.Å^{-3}$	

Crystal data and structure refinement for **1a**.

Identification code	sf0909m	
Empirical formula	C44 H38 Co N4 O6	
Formula weight	777.71	
Temperature	120(2) K	
Wavelength	0.71073 Å	
Crystal system	Monoclinic	
Space group	P2(1)/c	
Unit cell dimensions	a = 9.5058(5) Å	α= 90°.
	b = 22.1284(11) Å	β= 113.088(2)°.
	c = 9.7478(5) Å	γ = 90°.
Volume	1886.20(17) $Å^3$	
Z	2	
Density (calculated)	1.369 g/cm^3	
Absorption coefficient	0.510 mm^{-1}	
F(000)	810	
Crystal size	0.25 x 0.20 x 0.15 mm^3	
Theta range for data collection	2.45 to 31.50°.	
Index ranges	-13<=h<=13, -31<=k<=32, -14<=l<=14	
Reflections collected	21981	
Independent reflections	6142 [R(int) = 0.0260]	
Completeness to theta = 31.50°	97.8 %	
Absorption correction	None	
Max. and min. transmission	0.9274 and 0.8830	
Refinement method	Full-matrix least-squares on F^2	
Data / restraints / parameters	6142 / 152 / 292	
Goodness-of-fit on F^2	1.043	
Final R indices [I>2sigma(I)]	R1 = 0.0419, wR2 = 0.1117	
R indices (all data)	R1 = 0.0473, wR2 = 0.1162	
Largest diff. peak and hole	0.642 and -0.447 $e.Å^{-3}$	

Crystal data and structure refinement for **1b**.

Identification code	sf0806m	
Empirical formula	C44 H38 N4 Ni O6	
Formula weight	777.49	
Temperature	120(2) K	
Wavelength	0.71073 Å	
Crystal system	Monoclinic	
Space group	P2(1)/c	
Unit cell dimensions	a = 9.3654(6) Å	α= 90°.
	b = 22.1464(15) Å	β= 112.103(2)°.
	c = 9.8255(6) Å	γ = 90°.
Volume	1888.1(2) $Å^3$	
Z	2	
Density (calculated)	1.368 g/cm^3	
Absorption coefficient	0.569 mm^{-1}	
F(000)	812	
Crystal size	0.25 x 0.15 x 0.10 mm^3	
Theta range for data collection	2.35 to 33.14°.	
Index ranges	-14<=h<=13, -34<=k<=34, -14<=l<=15	
Reflections collected	57124	
Independent reflections	7129 [R(int) = 0.0295]	
Completeness to theta = 33.14°	99.1 %	
Absorption correction	None	
Max. and min. transmission	0.9453 and 0.8708	
Refinement method	Full-matrix least-squares on F^2	
Data / restraints / parameters	7129 / 1 / 251	
Goodness-of-fit on F^2	1.049	
Final R indices [I>2sigma(I)]	R1 = 0.0506, wR2 = 0.1466	
R indices (all data)	R1 = 0.0571, wR2 = 0.1535	
Largest diff. peak and hole	1.472 and -0.804 $e.Å^{-3}$	

Crystal data and structure refinement for **2a**.

Identification code	sf0810m	
Empirical formula	C28 H26 Cu F12 N5 O7	
Formula weight	836.08	
Temperature	120(2) K	
Wavelength	0.71073 Å	
Crystal system	Monoclinic	
Space group	P2(1)/c	
Unit cell dimensions	a = 8.6722(5) Å	α= 90°.
	b = 24.6667(14) Å	β= 96.700(4)°.
	c = 9.5859(6) Å	γ = 90°.
Volume	2036.6(2) $Å^3$	
Z	2	
Density (calculated)	1.363 g/cm^3	
Absorption coefficient	0.635 mm^{-1}	
F(000)	844	
Crystal size	0.20 x 0.08 x 0.04 mm^3	
Theta range for data collection	2.29 to 30.51°.	
Index ranges	-12<=h<=12, -35<=k<=33, -11<=l<=13	
Reflections collected	23919	
Independent reflections	6224 [R(int) = 0.0691]	
Completeness to theta = 30.51°	100.0 %	
Absorption correction	None	
Max. and min. transmission	0.9751 and 0.8836	
Refinement method	Full-matrix least-squares on F^2	
Data / restraints / parameters	6224 / 42 / 269	
Goodness-of-fit on F^2	1.524	
Final R indices [I>2sigma(I)]	R1 = 0.0899, wR2 = 0.2423	
R indices (all data)	R1 = 0.1497, wR2 = 0.2649	
Largest diff. peak and hole	1.162 and -0.911 $e.Å^{-3}$	

Crystal data and structure refinement for **3a**.

Identification code	sf0823m	
Empirical formula	C46 H42 Co N4 O6	
Formula weight	805.77	
Temperature	120(2) K	
Wavelength	0.71073 Å	
Crystal system	Monoclinic	
Space group	P2(1)/c	
Unit cell dimensions	a = 12.5711(6) Å	α= 90°.
	b = 15.5146(8) Å	β= 97.011(2)°.
	c = 10.0698(5) Å	γ = 90°.
Volume	1949.28(17) $Å^3$	
Z	2	
Density (calculated)	1.373 g/cm^3	
Absorption coefficient	0.496 mm^{-1}	
F(000)	842	
Crystal size	0.25 x 0.20 x 0.15 mm^3	
Theta range for data collection	2.42 to 32.37°.	
Index ranges	-18<=h<=18, -20<=k<=23, -15<=l<=14	
Reflections collected	31101	
Independent reflections	6869 [R(int) = 0.0249]	
Completeness to theta = 25.00°	99.9 %	
Absorption correction	None	
Max. and min. transmission	0.9293 and 0.8859	
Refinement method	Full-matrix least-squares on F^2	
Data / restraints / parameters	6869 / 0 / 263	
Goodness-of-fit on F^2	1.027	
Final R indices [I>2sigma(I)]	R1 = 0.0317, wR2 = 0.0861	
R indices (all data)	R1 = 0.0375, wR2 = 0.0899	
Largest diff. peak and hole	0.489 and -0.212 $e.Å^{-3}$	

Table C.2 Crystal data and structure refinement for **$4IF_4BA$, $4I_3F_3BA$, 4HBA, $5IF_4BA$, $5BrF_4BA$, 5ABA, 6IBA,** and **6ABA**

$4IF_4BA$

Identification code	sf0832m	
Empirical formula	C11 H5 F4 I N2 O3	
Formula weight	416.07	
Temperature	120(2) K	
Wavelength	0.71073 Å	
Crystal system	Triclinic	
Space group	P-1	
Unit cell dimensions	a = 4.2494(2) Å	α= 110.254(2)°.
	b = 11.6205(6) Å	β= 96.027(2)°.
	c = 13.8376(7) Å	γ = 98.468(2)°.
Volume	625.04(5) $Å^3$	
Z	2	
Density (calculated)	2.211 g/cm^3	
Absorption coefficient	2.625 mm^{-1}	
F(000)	396	
Crystal size	0.46 x 0.28 x 0.22 mm^3	
Theta range for data collection	3.18 to 39.38°.	
Index ranges	-7<=h<=7, -19<=k<=20, -23<=l<=24	
Reflections collected	23438	
Independent reflections	7076 [R(int) = 0.0188]	
Completeness to theta = 30.00°	99.4 %	
Absorption correction	None	
Max. and min. transmission	0.5959 and 0.3814	
Refinement method	Full-matrix least-squares on F^2	
Data / restraints / parameters	7076 / 0 / 190	
Goodness-of-fit on F^2	1.013	
Final R indices [I>2sigma(I)]	R1 = 0.0200, wR2 = 0.0518	
R indices (all data)	R1 = 0.0220, wR2 = 0.0528	
Largest diff. peak and hole	1.436 and -0.852 $e.Å^{-3}$	

Crystal data and structure refinement for **$4I_3F_3B$**.

Identification code	sf0911m	
Empirical formula	C16 H4 F6 I6 N2 O	
Formula weight	1115.61	
Temperature	120(2) K	
Wavelength	0.71073 Å	
Crystal system	Monoclinic	
Space group	Cc	
Unit cell dimensions	a = 12.3402(19) Å	α= 90°.
	b = 13.476(2) Å	β= 110.979(4)°.
	c = 15.223(2) Å	γ = 90°.
Volume	2363.7(6) $Å^3$	
Z	4	
Density (calculated)	3.135 g/cm^3	
Absorption coefficient	7.945 mm^{-1}	
F(000)	1976	
Crystal size	0.24 x 0.12 x 0.08 mm^3	
Theta range for data collection	2.33 to 31.51°.	
Index ranges	-13<=h<=18, -19<=k<=19, -22<=l<=22	
Reflections collected	22414	
Independent reflections	3902 [R(int) = 0.0334]	
Completeness to theta = 31.51°	99.1 %	
Absorption correction	None	
Max. and min. transmission	0.5690 and 0.2515	
Refinement method	Full-matrix least-squares on F^2	
Data / restraints / parameters	3902 / 0 / 149	
Goodness-of-fit on F^2	1.114	
Final R indices [I>2sigma(I)]	R1 = 0.0201, wR2 = 0.0440	
R indices (all data)	R1 = 0.0223, wR2 = 0.0449	
Largest diff. peak and hole	0.780 and -0.833 $e.Å^{-3}$	

Crystal data and structure refinement for **4HBA**.

Identification code	sf0803m	
Empirical formula	C11 H10 N2 O4	
Formula weight	234.21	
Temperature	120(2) K	
Wavelength	0.71073 Å	
Crystal system	Triclinic	
Space group	P-1	
Unit cell dimensions	a = 6.6865(3) Å	α= 85.253(3)°.
	b = 7.2166(4) Å	β= 86.577(3)°.
	c = 10.5803(5) Å	γ = 83.773(3)°.
Volume	505.12(4) $Å^3$	
Z	2	
Density (calculated)	1.540 g/cm^3	
Absorption coefficient	0.120 mm^{-1}	
F(000)	244	
Crystal size	0.25 x 0.25 x 0.15 mm^3	
Theta range for data collection	1.93 to 31.51°.	
Index ranges	-9<=h<=9, -10<=k<=10, -15<=l<=15	
Reflections collected	14329	
Independent reflections	3245 [R(int) = 0.0241]	
Completeness to theta = 31.51°	96.2 %	
Absorption correction	None	
Max. and min. transmission	0.9823 and 0.9707	
Refinement method	Full-matrix least-squares on F^2	
Data / restraints / parameters	3245 / 0 / 160	
Goodness-of-fit on F^2	1.035	
Final R indices [I>2sigma(I)]	R1 = 0.0395, wR2 = 0.1105	
R indices (all data)	R1 = 0.0503, wR2 = 0.1209	
Largest diff. peak and hole	0.531 and -0.234 e.$Å^{-3}$	

Crystal data and structure refinement for **5IF$_4$BA**.

Identification code	sf0829m	
Empirical formula	C15 H13 F4 I N2 O3	
Formula weight	472.17	
Temperature	120(2) K	
Wavelength	0.71073 Å	
Crystal system	Monoclinic	
Space group	P2(1)/c	
Unit cell dimensions	a = 8.9049(10) Å	a= 90°.
	b = 7.9564(9) Å	b= 93.772(4)°.
	c = 23.142(3) Å	g = 90°.
Volume	1636.1(3) Å^3	
Z	4	
Density (calculated)	1.917 Mg/m^3	
Absorption coefficient	2.018 mm^{-1}	
F(000)	920	
Crystal size	0.25 x 0.18 x 0.12 mm^3	
Theta range for data collection	2.71 to 32.58°.	
Index ranges	-13<=h<=13, -12<=k<=10, -34<=l<=31	
Reflections collected	20666	
Independent reflections	5886 [R(int) = 0.0205]	
Completeness to theta = 32.58°	98.8 %	
Absorption correction	None	
Max. and min. transmission	0.7938 and 0.6324	
Refinement method	Full-matrix least-squares on F^2	
Data / restraints / parameters	5886 / 94 / 334	
Goodness-of-fit on F^2	1.057	
Final R indices [I>2sigma(I)]	R1 = 0.0283, wR2 = 0.0677	
R indices (all data)	R1 = 0.0323, wR2 = 0.0702	
Largest diff. peak and hole	0.936 and -0.874 e.Å^{-3}	

Crystal data and structure refinement for **5BrF$_4$BA**.

Identification code	sf0824m	
Empirical formula	C15 H13 Br F4 N2 O3	
Formula weight	425.18	
Temperature	120(2) K	
Wavelength	0.71073 Å	
Crystal system	Monoclinic	
Space group	P2(1)/c	
Unit cell dimensions	a = 8.9124(13) Å	α= 90°.
	b = 7.9267(10) Å	β= 95.717(7)°.
	c = 22.746(3) Å	γ = 90°.
Volume	1598.9(4) Å^3	
Z	4	
Density (calculated)	1.766 g/cm^3	
Absorption coefficient	2.633 mm^{-1}	
F(000)	848	
Crystal size	0.25 x 0.20 x 0.15 mm^3	
Theta range for data collection	2.72 to 32.57°.	
Index ranges	-13<=h<=12, -12<=k<=11, -33<=l<=34	
Reflections collected	17551	
Independent reflections	5657 [R(int) = 0.0273]	
Completeness to theta = 25.00°	99.5 %	
Absorption correction	None	
Refinement method	Full-matrix least-squares on F^2	
Data / restraints / parameters	5657 / 125 / 317	
Goodness-of-fit on F^2	1.061	
Final R indices [I>2sigma(I)]	R1 = 0.0468, wR2 = 0.1298	
R indices (all data)	R1 = 0.0604, wR2 = 0.1372	
Largest diff. peak and hole	0.945 and -1.030 e.Å^{-3}	

Crystal data and structure refinement for **5ABA**.

Identification code	sf0908m	
Empirical formula	C22 H26 N4 O5	
Formula weight	426.47	
Temperature	120(2) K	
Wavelength	0.71073 Å	
Crystal system	Monoclinic	
Space group	P2(1)/c	
Unit cell dimensions	a = 13.0405(8) Å	α= 90°.
	b = 7.2636(5) Å	β= 101.902(3)°.
	c = 23.2647(15) Å	γ = 90°.
Volume	2156.3(2) $Å^3$	
Z	4	
Density (calculated)	1.314 g/cm^3	
Absorption coefficient	0.095 mm^{-1}	
F(000)	904	
Crystal size	0.30 x 0.25 x 0.15 mm^3	
Theta range for data collection	1.60 to 32.03°.	
Index ranges	-14<=h<=19, -10<=k<=10, -34<=l<=34	
Reflections collected	26805	
Independent reflections	7304 [R(int) = 0.0336]	
Completeness to theta = 32.03°	97.3 %	
Absorption correction	None	
Max. and min. transmission	0.9859 and 0.9722	
Refinement method	Full-matrix least-squares on F^2	
Data / restraints / parameters	7304 / 0 / 302	
Goodness-of-fit on F^2	1.095	
Final R indices [I>2sigma(I)]	R1 = 0.0492, wR2 = 0.1307	
R indices (all data)	R1 = 0.0722, wR2 = 0.1435	
Largest diff. peak and hole	0.331 and -0.476 $e.Å^{-3}$	

Crystal data and structure refinement for **6IBA**.

Identification code	sf0917m	
Empirical formula	C17 H13 I N2 O3	
Formula weight	420.19	
Temperature	120(2) K	
Wavelength	0.71073 Å	
Crystal system	Monoclinic	
Space group	P2(1)/c	
Unit cell dimensions	a = 10.1002(7) Å	α= 90°.
	b = 10.7028(8) Å	β= 107.850(3)°.
	c = 15.3637(11) Å	γ = 90°.
Volume	1580.9(2) $Å^3$	
Z	4	
Density (calculated)	1.765 g/cm^3	
Absorption coefficient	2.042 mm^{-1}	
F(000)	824	
Crystal size	0.28 x 0.24 x 0.16 mm^3	
Theta range for data collection	2.12 to 33.14°.	
Index ranges	-15<=h<=15, -16<=k<=10, -22<=l<=23	
Reflections collected	27337	
Independent reflections	5790 [R(int) = 0.0237]	
Completeness to theta = 33.14°	96.0 %	
Absorption correction	None	
Max. and min. transmission	0.7359 and 0.5986	
Refinement method	Full-matrix least-squares on F^2	
Data / restraints / parameters	5790 / 0 / 208	
Goodness-of-fit on F^2	1.068	
Final R indices [I>2sigma(I)]	R1 = 0.0321, wR2 = 0.0882	
R indices (all data)	R1 = 0.0379, wR2 = 0.0919	
Largest diff. peak and hole	1.744 and -1.081 $e.Å^{-3}$	

Crystal data and structure refinement for **6ABA**.

Identification code	sf0805	
Empirical formula	C17 H15 N3 O3	
Formula weight	309.32	
Temperature	100(2) K	
Wavelength	0.71073 Å	
Crystal system	Monoclinic	
Space group	P2(1)/n	
Unit cell dimensions	a = 10.6939(5) Å	α= 90°.
	b = 3.9716(2) Å	β= 92.444(3)°.
	c = 33.8720(19) Å	γ = 90°.
Volume	1437.30(13) $Å^3$	
Z	4	
Density (calculated)	1.429 g/cm^3	
Absorption coefficient	0.101 mm^{-1}	
F(000)	648	
Crystal size	0.32 x 0.203 x 0.188 mm^3	
Theta range for data collection	2.02 to 27.11°.	
Index ranges	-13<=h<=13, -5<=k<=5, -43<=l<=42	
Reflections collected	34351	
Independent reflections	3158 [R(int) = 0.0513]	
Completeness to theta = 25.00°	99.7 %	
Absorption correction	None	
Refinement method	Full-matrix least-squares on F^2	
Data / restraints / parameters	3158 / 0 / 217	
Goodness-of-fit on F^2	1.033	
Final R indices [I>2sigma(I)]	R1 = 0.0437, wR2 = 0.0942	
R indices (all data)	R1 = 0.0895, wR2 = 0.1120	
Largest diff. peak and hole	0.177 and -0.273 $e.Å^{-3}$	

Table C.3 Crystal data and structure refinement for **9**, **17**, **8SUC**, **8IBA**

9

Identification code	sf0720m	
Empirical formula	C11 H10 N2 O S	
Formula weight	218.27	
Temperature	120(2) K	
Wavelength	0.71073 Å	
Crystal system	Monoclinic	
Space group	P2(1)/n	
Unit cell dimensions	a = 5.8014(9) Å	α= 90°.
	b = 24.959(4) Å	β= 111.200(7)°.
	c = 7.4141(10) Å	γ = 90°.
Volume	1000.9(2) $Å^3$	
Z	4	
Density (calculated)	1.449 g/cm^3	
Absorption coefficient	0.294 mm^{-1}	
F(000)	456	
Crystal size	0.25 x 0.15 x 0.10 mm^3	
Theta range for data collection	1.63 to 32.03°.	
Index ranges	-8<=h<=8, -37<=k<=37, -11<=l<=10	
Reflections collected	18161	
Independent reflections	3434 [R(int) = 0.0433]	
Completeness to theta = 32.03°	98.4 %	
Absorption correction	None	
Max. and min. transmission	0.9712 and 0.9301	
Refinement method	Full-matrix least-squares on F^2	
Data / restraints / parameters	3434 / 0 / 140	
Goodness-of-fit on F^2	1.055	
Final R indices [I>2sigma(I)]	R1 = 0.0447, wR2 = 0.1229	
R indices (all data)	R1 = 0.0590, wR2 = 0.1318	
Largest diff. peak and hole	0.606 and -0.486 $e.Å^{-3}$	

Crystal data and structure refinement for **17**.

Identification code	sf0807m	
Empirical formula	C13 H14 N2 O S	
Formula weight	246.32	
Temperature	120(2) K	
Wavelength	0.71073 Å	
Crystal system	Triclinic	
Space group	P-1	
Unit cell dimensions	a = 5.4109(3) Å	α= 90.542(3)°.
	b = 7.3580(4) Å	β= 91.181(3)°.
	c = 15.6259(7) Å	γ = 108.345(3)°.
Volume	590.29(5) $Å^3$	
Z	2	
Density (calculated)	1.386 g/cm^3	
Absorption coefficient	0.258 mm^{-1}	
F(000)	260	
Crystal size	0.25 x 0.05 x 0.02 mm^3	
Theta range for data collection	2.61 to 33.67°.	
Index ranges	-7<=h<=8, -9<=k<=11, -23<=l<=23	
Reflections collected	12962	
Independent reflections	4077 [R(int) = 0.0304]	
Completeness to theta = 25.00°	98.1 %	
Absorption correction	Semi-empirical from equivalents	
Max. and min. transmission	0.9961 and 0.9383	
Refinement method	Full-matrix least-squares on F^2	
Data / restraints / parameters	4077 / 0 / 160	
Goodness-of-fit on F^2	1.034	
Final R indices [I>2sigma(I)]	R1 = 0.0396, wR2 = 0.1075	
R indices (all data)	R1 = 0.0573, wR2 = 0.1175	
Largest diff. peak and hole	0.537 and -0.293 $e.Å^{-3}$	

Crystal data and structure refinement for **8SUC**.

Identification code	sf0802m	
Empirical formula	C22 H20 N2 O4 S2	
Formula weight	440.52	
Temperature	120(2) K	
Wavelength	0.71073 Å	
Crystal system	Monoclinic	
Space group	P2(1)/c	
Unit cell dimensions	a = 7.9134(3) Å	α= 90°.
	b = 5.2495(2) Å	β= 92.786(2)°.
	c = 24.7635(10) Å	γ = 90°.
Volume	1027.49(7) $Å^3$	
Z	2	
Density (calculated)	1.424 g/cm^3	
Absorption coefficient	0.292 mm^{-1}	
F(000)	460	
Crystal size	0.25 x 0.15 x 0.08 mm^3	
Theta range for data collection	3.13 to 34.97°.	
Index ranges	-12<=h<=11, -6<=k<=8, -39<=l<=38	
Reflections collected	18428	
Independent reflections	4280 [R(int) = 0.0224]	
Completeness to theta = 34.97°	94.6 %	
Absorption correction	None	
Max. and min. transmission	0.9770 and 0.9306	
Refinement method	Full-matrix least-squares on F^2	
Data / restraints / parameters	4280 / 10 / 155	
Goodness-of-fit on F^2	1.061	
Final R indices [I>2sigma(I)]	R1 = 0.0352, wR2 = 0.1003	
R indices (all data)	R1 = 0.0405, wR2 = 0.1048	
Largest diff. peak and hole	0.513 and -0.184 $e.Å^{-3}$	

Crystal data and structure refinement for **8IBA**.

Identification code	sf0723	
Empirical formula	C16 H12 I N O2 S	
Formula weight	409.23	
Temperature	100(2) K	
Wavelength	0.71073 Å	
Crystal system	Orthorhombic	
Space group	Pbca	
Unit cell dimensions	a = 16.6606(13) Å	α= 90°.
	b = 6.9866(6) Å	β= 90°.
	c = 25.659(2) Å	γ = 90°.
Volume	2986.7(4) $Å^3$	
Z	8	
Density (calculated)	1.820 g/cm^3	
Absorption coefficient	2.287 mm^{-1}	
F(000)	1600	
Crystal size	0.18 x 0.10 x 0.02 mm^3	
Theta range for data collection	2.44 to 30.53°.	
Index ranges	-23<=h<=23, -9<=k<=9, -36<=l<=35	
Reflections collected	35794	
Independent reflections	4539 [R(int) = 0.0954]	
Completeness to theta = 30.53°	99.8 %	
Absorption correction	None	
Max. and min. transmission	0.9557 and 0.6836	
Refinement method	Full-matrix least-squares on F^2	
Data / restraints / parameters	4539 / 10 / 201	
Goodness-of-fit on F^2	1.020	
Final R indices [I>2sigma(I)]	R1 = 0.0461, wR2 = 0.0849	
R indices (all data)	R1 = 0.0765, wR2 = 0.0938	
Largest diff. peak and hole	1.807 and -1.901 $e.Å^{-3}$	

Table C.4 Crystal data and structure refinement for **20OCT, 20HEX, 20FUM, 20ADI, 20SUB, 20SEB, 20FBA, 20NBA, 20F$_2$BA, 20ABA, 21SUC, 21ADI, 21SUB, 23ADI, 23F$_5$BA, 23FUM, 23GLU, 24ADI, 24SUB**

20OCT

Identification code	sf0603m	
Empirical formula	C20 H28 N4 O4	
Formula weight	388.46	
Temperature	173(2) K	
Wavelength	0.71073 Å	
Crystal system	Triclinic	
Space group	P-1	
Unit cell dimensions	a = 6.6610(8) Å	α= 99.459(8)°.
	b = 8.4541(11) Å	β= 94.349(9)°.
	c = 19.684(2) Å	γ = 107.887(8)°.
Volume	1031.1(2) Å^3	
Z	2	
Density (calculated)	1.251 g/cm^3	
Absorption coefficient	0.088 mm^{-1}	
F(000)	416	
Crystal size	0.40 x 0.10 x 0.10 mm^3	
Theta range for data collection	2.12 to 27.70°.	
Index ranges	-8<=h<=8, -9<=k<=10, -24<=l<=25	
Reflections collected	7356	
Independent reflections	4563 [R(int) = 0.0998]	
Completeness to theta = 27.70°	94.5 %	
Absorption correction	None	
Refinement method	Full-matrix least-squares on F^2	
Data / restraints / parameters	4563 / 0 / 265	
Goodness-of-fit on F^2	0.847	
Final R indices [I>2sigma(I)]	R1 = 0.0679, wR2 = 0.1609	
R indices (all data)	R1 = 0.1322, wR2 = 0.1858	
Largest diff. peak and hole	0.290 and -0.245 e.Å^{-3}	

Crystal data and structure refinement for **20HEX**.

Identification code	sf0608m	
Empirical formula	C18 H24 N4 O4	
Formula weight	360.41	
Temperature	173(2) K	
Wavelength	0.71073 Å	
Crystal system	Triclinic	
Space group	P-1	
Unit cell dimensions	a = 6.6573(13) Å	α= 95.391(10)°.
	b = 8.1256(14) Å	β= 97.999(12)°.
	c = 18.128(3) Å	γ = 104.439(14)°.
Volume	931.9(3) $Å^3$	
Z	2	
Density (calculated)	1.284 g/cm^3	
Absorption coefficient	0.092 mm^{-1}	
F(000)	384	
Crystal size	0.40 x 0.25 x 0.10 mm^3	
Theta range for data collection	1.14 to 27.51°.	
Index ranges	-8<=h<=7, -10<=k<=9, -23<=l<=21	
Reflections collected	6561	
Independent reflections	4031 [R(int) = 0.0855]	
Completeness to theta = 27.51°	94.0 %	
Absorption correction	None	
Refinement method	Full-matrix least-squares on F^2	
Data / restraints / parameters	4031 / 0 / 247	
Goodness-of-fit on F^2	0.894	
Final R indices [I>2sigma(I)]	R1 = 0.0630, wR2 = 0.1541	
R indices (all data)	R1 = 0.1249, wR2 = 0.1825	
Largest diff. peak and hole	0.272 and -0.341 $e.Å^{-3}$	

Crystal data and structure refinement for **20FUM**.

Identification code	sf0712m	
Empirical formula	C28 H24 N8 O6	
Formula weight	568.55	
Temperature	120(2) K	
Wavelength	0.71073 Å	
Crystal system	Monoclinic	
Space group	P2(1)/n	
Unit cell dimensions	a = 4.6444(2) Å	a= 90°.
	b = 26.8514(13) Å	b= 102.395(3)°.
	c = 10.8139(5) Å	g = 90°.
Volume	1317.15(10) $Å^3$	
Z	2	
Density (calculated)	1.434 Mg/m^3	
Absorption coefficient	0.105 mm^{-1}	
F(000)	592	
Crystal size	0.25 x 0.20 x 0.10 mm^3	
Theta range for data collection	2.07 to 30.51°.	
Index ranges	-6<=h<=6, -38<=k<=38, -15<=l<=15	
Reflections collected	33731	
Independent reflections	4030 [R(int) = 0.0631]	
Completeness to theta = 30.51°	99.9 %	
Absorption correction	None	
Max. and min. transmission	0.9896 and 0.9743	
Refinement method	Full-matrix least-squares on F^2	
Data / restraints / parameters	4030 / 0 / 196	
Goodness-of-fit on F^2	1.083	
Final R indices [I>2sigma(I)]	R1 = 0.0464, wR2 = 0.1072	
R indices (all data)	R1 = 0.0712, wR2 = 0.1191	
Largest diff. peak and hole	0.375 and -0.300 $e.Å^{-3}$	

Crystal data and structure refinement for **20ADI**.

Identification code	sf0607m	
Empirical formula	C30 H34 N8 O8	
Formula weight	634.65	
Temperature	173(2) K	
Wavelength	0.71073 Å	
Crystal system	Triclinic	
Space group	P-1	
Unit cell dimensions	a = 6.6047(8) Å	a= 98.182(6)°.
	b = 8.0678(9) Å	b= 101.688(8)°.
	c = 15.3573(18) Å	g = 104.436(9)°.
Volume	759.84(15) $Å^3$	
Z	1	
Density (calculated)	1.387 Mg/m^3	
Absorption coefficient	0.103 mm^{-1}	
F(000)	334	
Crystal size	0.30 x 0.25 x 0.15 mm^3	
Theta range for data collection	1.38 to 28.30°.	
Index ranges	-7<=h<=8, -10<=k<=10, -20<=l<=20	
Reflections collected	9931	
Independent reflections	3529 [R(int) = 0.1503]	
Completeness to theta = 28.30°	93.4 %	
Absorption correction	None	
Refinement method	Full-matrix least-squares on F^2	
Data / restraints / parameters	3529 / 0 / 220	
Goodness-of-fit on F^2	1.070	
Final R indices [I>2sigma(I)]	R1 = 0.0589, wR2 = 0.1523	
R indices (all data)	R1 = 0.0780, wR2 = 0.1713	
Largest diff. peak and hole	0.385 and -0.299 e.$Å^{-3}$	

Crystal data and structure refinement for **20SUB**.

Identification code	sf0605m	
Empirical formula	C32 H38 N8 O8	
Formula weight	662.70	
Temperature	173(2) K	
Wavelength	0.71073 Å	
Crystal system	Triclinic	
Space group	P-1	
Unit cell dimensions	a = 6.6283(9) Å	α= 81.455(11)°.
	b = 8.1784(11) Å	β= 83.602(8)°.
	c = 15.902(2) Å	γ = 74.806(8)°.
Volume	820.29(19) $Å^3$	
Z	1	
Density (calculated)	1.342 g/cm^3	
Absorption coefficient	0.099 mm^{-1}	
F(000)	350	
Crystal size	0.30 x 0.25 x 0.15 mm^3	
Theta range for data collection	2.60 to 27.49°.	
Index ranges	-8<=h<=7, -9<=k<=10, -20<=l<=20	
Reflections collected	6027	
Independent reflections	3569 [R(int) = 0.1203]	
Completeness to theta = 27.49°	94.3 %	
Absorption correction	None	
Refinement method	Full-matrix least-squares on F^2	
Data / restraints / parameters	3569 / 0 / 229	
Goodness-of-fit on F^2	1.096	
Final R indices [I>2sigma(I)]	R1 = 0.0731, wR2 = 0.2228	
R indices (all data)	R1 = 0.0990, wR2 = 0.2502	
Largest diff. peak and hole	0.321 and -0.373 $e.Å^{-3}$	

Crystal data and structure refinement for **20SEB**.

Identification code	sf0703m	
Empirical formula	C34 H42 N8 O8	
Formula weight	690.76	
Temperature	133(2) K	
Wavelength	0.71073 Å	
Crystal system	Triclinic	
Space group	P-1	
Unit cell dimensions	a = 6.5516(4) Å	α= 94.293(3)°.
	b = 8.1666(5) Å	β= 93.041(3)°.
	c = 33.7458(19) Å	γ = 105.225(3)°.
Volume	1732.32(18) $Å^3$	
Z	2	
Density (calculated)	1.324 g/cm^3	
Absorption coefficient	0.096 mm^{-1}	
F(000)	732	
Crystal size	0.25 x 0.20 x 0.08 mm^3	
Theta range for data collection	1.82 to 32.58°.	
Index ranges	-9<=h<=9, -12<=k<=12, -51<=l<=51	
Reflections collected	75728	
Independent reflections	12391 [R(int) = 0.0540]	
Completeness to theta = 32.58°	98.2 %	
Absorption correction	None	
Max. and min. transmission	0.9923 and 0.9763	
Refinement method	Full-matrix least-squares on F^2	
Data / restraints / parameters	12391 / 0 / 475	
Goodness-of-fit on F^2	1.013	
Final R indices [I>2sigma(I)]	R1 = 0.0508, wR2 = 0.1141	
R indices (all data)	R1 = 0.1133, wR2 = 0.1388	
Largest diff. peak and hole	0.508 and -0.254 $e.Å^{-3}$	

Crystal data and structure refinement for **20FBA**.

Identification code	sf0606m	
Empirical formula	C19 H17 F N4 O4	
Formula weight	384.37	
Temperature	173(2) K	
Wavelength	0.71073 Å	
Crystal system	Triclinic	
Space group	P-1	
Unit cell dimensions	a = 6.6065(14) Å	a= 92.457(13)°.
	b = 7.2295(17) Å	b= 97.668(14)°.
	c = 21.354(4) Å	g = 116.706(15)°.
Volume	896.8(3) $Å^3$	
Z	2	
Density (calculated)	1.423 Mg/m^3	
Absorption coefficient	0.109 mm^{-1}	
F(000)	400	
Crystal size	0.40 x 0.20 x 0.05 mm^3	
Theta range for data collection	1.94 to 27.47°.	
Index ranges	-8<=h<=8, -9<=k<=9, -27<=l<=27	
Reflections collected	6657	
Independent reflections	3951 [R(int) = 0.1136]	
Completeness to theta = 27.47°	95.8 %	
Absorption correction	None	
Refinement method	Full-matrix least-squares on F^2	
Data / restraints / parameters	3951 / 0 / 270	
Goodness-of-fit on F^2	0.885	
Final R indices [I>2sigma(I)]	R1 = 0.0624, wR2 = 0.1467	
R indices (all data)	R1 = 0.1720, wR2 = 0.1947	
Extinction coefficient	0.013(4)	
Largest diff. peak and hole	0.285 and -0.258 e.$Å^{-3}$	

Crystal data and structure refinement for **20NBA**.

Identification code	sf0604m	
Empirical formula	C19 H17 N5 O6	
Formula weight	411.38	
Temperature	173(2) K	
Wavelength	0.71073 Å	
Crystal system	Triclinic	
Space group	P-1	
Unit cell dimensions	a = 6.5983(13) Å	α= 81.922(11)°.
	b = 7.2343(14) Å	β= 84.772(14)°.
	c = 19.755(4) Å	γ = 80.711(16)°.
Volume	919.1(3) $Å^3$	
Z	2	
Density (calculated)	1.486 g/cm^3	
Absorption coefficient	0.114 mm^{-1}	
F(000)	428	
Crystal size	0.40 x 0.40 x 0.20 mm^3	
Theta range for data collection	1.04 to 27.45°.	
Index ranges	-8<=h<=8, -9<=k<=8, -25<=l<=25	
Reflections collected	6545	
Independent reflections	3966 [R(int) = 0.0969]	
Completeness to theta = 27.45°	93.9 %	
Absorption correction	None	
Refinement method	Full-matrix least-squares on F^2	
Data / restraints / parameters	3966 / 19 / 306	
Goodness-of-fit on F^2	0.924	
Final R indices [I>2sigma(I)]	R1 = 0.0866, wR2 = 0.2181	
R indices (all data)	R1 = 0.1363, wR2 = 0.2475	
Largest diff. peak and hole	0.784 and -0.291 e.$Å^{-3}$	

Crystal data and structure refinement for **20F$_2$BA**.

Identification code	sf0702m	
Empirical formula	C19 H16 F2 N4 O4.10	
Formula weight	403.96	
Temperature	100(2) K	
Wavelength	0.71073 Å	
Crystal system	Monoclinic	
Space group	C2/c	
Unit cell dimensions	a = 7.4376(2) Å	α= 90°.
	b = 12.3798(4) Å	β= 93.396(2)°.
	c = 39.3480(11) Å	γ = 90°.
Volume	3616.64(18) Å^3	
Z	8	
Density (calculated)	1.484 g/cm^3	
Absorption coefficient	0.120 mm^{-1}	
F(000)	1670	
Crystal size	0.25 x 0.25 x 0.04 mm^3	
Theta range for data collection	3.11 to 30.51°.	
Index ranges	-10<=h<=6, -17<=k<=17, -56<=l<=56	
Reflections collected	34501	
Independent reflections	5339 [R(int) = 0.0500]	
Completeness to theta = 30.51°	96.5 %	
Absorption correction	None	
Max. and min. transmission	0.9952 and 0.9706	
Refinement method	Full-matrix least-squares on F^2	
Data / restraints / parameters	5339 / 0 / 286	
Goodness-of-fit on F^2	1.091	
Final R indices [I>2sigma(I)]	R1 = 0.0540, wR2 = 0.1381	
R indices (all data)	R1 = 0.0713, wR2 = 0.1528	
Largest diff. peak and hole	0.570 and -0.571 e.Å^{-3}	

Crystal data and structure refinement for **20ABA**.

Identification code	sf0722m	
Empirical formula	C19 H19 N5 O4	
Formula weight	381.39	
Temperature	173(2) K	
Wavelength	0.71073 Å	
Crystal system	Monoclinic	
Space group	P2(1)/c	
Unit cell dimensions	a = 8.8995(2) Å	α= 90°.
	b = 14.6202(4) Å	β= 93.198(2)°.
	c = 14.0267(3) Å	γ = 90°.
Volume	1822.21(8) $Å^3$	
Z	4	
Density (calculated)	1.390 g/cm^3	
Absorption coefficient	0.101 mm^{-1}	
F(000)	800	
Crystal size	0.27 x 0.25 x 0.22 mm^3	
Theta range for data collection	3.60 to 27.12°.	
Index ranges	-10<=h<=11, -18<=k<=18, -17<=l<=17	
Reflections collected	23993	
Independent reflections	4009 [R(int) = 0.0552]	
Completeness to theta = 27.12°	99.7 %	
Absorption correction	None	
Max. and min. transmission	0.9787 and 0.9736	
Refinement method	Full-matrix least-squares on F^2	
Data / restraints / parameters	4009 / 0 / 271	
Goodness-of-fit on F^2	1.027	
Final R indices [I>2sigma(I)]	R1 = 0.0420, wR2 = 0.0997	
R indices (all data)	R1 = 0.0673, wR2 = 0.1129	
Largest diff. peak and hole	0.228 and -0.238 $e.Å^{-3}$	

Crystal data and structure refinement for **21SUC**.

Identification code	sf0710m	
Empirical formula	C16 H20 N4 O7	
Formula weight	380.36	
Temperature	120(2) K	
Wavelength	0.71073 Å	
Crystal system	Monoclinic	
Space group	P2(1)/n	
Unit cell dimensions	a = 9.844(2) Å	a= 90°.
	b = 6.8807(14) Å	b= 98.561(2)°.
	c = 26.413(5) Å	g = 90°.
Volume	1769.1(6) $Å^3$	
Z	4	
Density (calculated)	1.428 Mg/m^3	
Absorption coefficient	0.114 mm^{-1}	
F(000)	800	
Crystal size	0.20 x 0.15 x 0.08 mm^3	
Theta range for data collection	8.14 to 30.38°.	
Index ranges	-13<=h<=14, -5<=k<=9, -37<=l<=37	
Reflections collected	26114	
Independent reflections	5152 [R(int) = 0.0792]	
Completeness to theta = 30.38°	96.8 %	
Absorption correction	None	
Max. and min. transmission	0.9910 and 0.9776	
Refinement method	Full-matrix least-squares on F^2	
Data / restraints / parameters	5152 / 0 / 265	
Goodness-of-fit on F^2	1.044	
Final R indices [I>2sigma(I)]	R1 = 0.0580, wR2 = 0.1391	
R indices (all data)	R1 = 0.0970, wR2 = 0.1577	
Largest diff. peak and hole	0.436 and -0.270 $e.Å^{-3}$	

Crystal data and structure refinement for **21ADI**.

Identification code	sf0709m	
Empirical formula	C18 H22 N4 O6	
Formula weight	390.40	
Temperature	120(2) K	
Wavelength	0.71073 Å	
Crystal system	Triclinic	
Space group	P-1	
Unit cell dimensions	a = 6.8908(3) Å	α= 66.395(2)°.
	b = 11.3841(6) Å	β= 89.086(2)°.
	c = 12.6504(6) Å	γ = 84.907(2)°.
Volume	905.54(8) $Å^3$	
Z	2	
Density (calculated)	1.432 g/cm^3	
Absorption coefficient	0.109 mm^{-1}	
F(000)	412	
Crystal size	0.20 x 0.10 x 0.10 mm^3	
Theta range for data collection	1.76 to 30.50°.	
Index ranges	-5<=h<=9, -16<=k<=16, -18<=l<=18	
Reflections collected	15411	
Independent reflections	5258 [R(int) = 0.0366]	
Completeness to theta = 30.50°	95.3 %	
Absorption correction	None	
Max. and min. transmission	0.9892 and 0.9785	
Refinement method	Full-matrix least-squares on F^2	
Data / restraints / parameters	5258 / 0 / 273	
Goodness-of-fit on F^2	1.050	
Final R indices [I>2sigma(I)]	R1 = 0.0550, wR2 = 0.1322	
R indices (all data)	R1 = 0.0848, wR2 = 0.1458	
Largest diff. peak and hole	0.307 and -0.301 $e.Å^{-3}$	

Crystal data and structure refinement for **21SUB**.

Identification code	sf0721m	
Empirical formula	C20 H26 N4 O6	
Formula weight	418.45	
Temperature	120(2) K	
Wavelength	0.71073 Å	
Crystal system	Triclinic	
Space group	P-1	
Unit cell dimensions	a = 6.918(2) Å	a= 67.522(16)°.
	b = 11.800(4) Å	b= 79.851(16)°.
	c = 13.910(5) Å	g = 84.973(16)°.
Volume	1032.6(6) $Å^3$	
Z	2	
Density (calculated)	1.346 Mg/m^3	
Absorption coefficient	0.101 mm^{-1}	
F(000)	444	
Crystal size	0.30 x 0.25 x 0.15 mm^3	
Theta range for data collection	1.60 to 29.57°.	
Index ranges	-9<=h<=9, -12<=k<=16, -19<=l<=19	
Reflections collected	23107	
Independent reflections	5306 [R(int) = 0.0634]	
Completeness to theta = 25.00°	93.8 %	
Absorption correction	None	
Max. and min. transmission	0.9851 and 0.9704	
Refinement method	Full-matrix least-squares on F^2	
Data / restraints / parameters	5306 / 0 / 286	
Goodness-of-fit on F^2	1.024	
Final R indices [I>2sigma(I)]	R1 = 0.0629, wR2 = 0.1621	
R indices (all data)	R1 = 0.1177, wR2 = 0.2042	
Largest diff. peak and hole	0.373 and -0.220 e.$Å^{-3}$	

Crystal data and structure refinement for **23FUM**.

Identification code	sf0819m	
Empirical formula	C28 H24 N8 O6	
Formula weight	568.55	
Temperature	120(2) K	
Wavelength	0.71073 Å	
Crystal system	Triclinic	
Space group	P-1	
Unit cell dimensions	a = 6.4782(3) Å	a= 97.053(2)°.
	b = 8.8918(4) Å	b= 102.589(2)°.
	c = 11.7133(5) Å	g = 90.066(2)°.
Volume	653.24(5) $Å^3$	
Z	1	
Density (calculated)	1.445 Mg/m^3	
Absorption coefficient	0.105 mm^{-1}	
F(000)	296	
Crystal size	0.25 x 0.20 x 0.15 mm^3	
Theta range for data collection	2.31 to 32.55°.	
Index ranges	-9<=h<=9, -13<=k<=13, -17<=l<=17	
Reflections collected	15112	
Independent reflections	4625 [R(int) = 0.0199]	
Completeness to theta = 32.55°	97.1 %	
Absorption correction	None	
Max. and min. transmission	0.9844 and 0.9741	
Refinement method	Full-matrix least-squares on F^2	
Data / restraints / parameters	4625 / 0 / 196	
Goodness-of-fit on F^2	1.041	
Final R indices [I>2sigma(I)]	R1 = 0.0386, wR2 = 0.1139	
R indices (all data)	R1 = 0.0438, wR2 = 0.1184	
Largest diff. peak and hole	0.508 and -0.423 $e.Å^{-3}$	

Crystal data and structure refinement for **23GLU**.

Identification code	sf0932m	
Empirical formula	C17 H18 N4 O5	
Formula weight	358.35	
Temperature	120(2) K	
Wavelength	0.71073 Å	
Crystal system	Orthorhombic	
Space group	Pbca	
Unit cell dimensions	a = 10.4837(6) Å	α= 90°.
	b = 12.1023(8) Å	β= 90°.
	c = 26.5805(16) Å	γ = 90°.
Volume	3372.5(4) $Å^3$	
Z	8	
Density (calculated)	1.412 g/cm^3	
Absorption coefficient	0.106 mm^{-1}	
F(000)	1504	
Crystal size	0.28 x 0.24 x 0.12 mm^3	
Theta range for data collection	1.53 to 32.58°.	
Index ranges	-15<=h<=14, -17<=k<=17, -39<=l<=36	
Reflections collected	34857	
Independent reflections	5877 [R(int) = 0.0862]	
Completeness to theta = 30.00°	100.0 %	
Absorption correction	None	
Max. and min. transmission	0.9874 and 0.9709	
Refinement method	Full-matrix least-squares on F^2	
Data / restraints / parameters	5877 / 0 / 244	
Goodness-of-fit on F^2	1.036	
Final R indices [I>2sigma(I)]	R1 = 0.0704, wR2 = 0.1354	
R indices (all data)	R1 = 0.1261, wR2 = 0.1562	
Largest diff. peak and hole	0.334 and -0.258 $e.Å^{-3}$	

Crystal data and structure refinement for **24ADI**.

Identification code	sf0816m	
Empirical formula	C18 H20 N4 O6	
Formula weight	388.38	
Temperature	120(2) K	
Wavelength	0.71073 Å	
Crystal system	Triclinic	
Space group	P-1	
Unit cell dimensions	a = 6.9702(8) Å	a= 82.412(6)°.
	b = 7.2951(8) Å	b= 86.955(6)°.
	c = 19.794(2) Å	g = 66.582(6)°.
Volume	915.49(17) $Å^3$	
Z	2	
Density (calculated)	1.409 Mg/m^3	
Absorption coefficient	0.108 mm^{-1}	
F(000)	408	
Crystal size	0.30 x 0.20 x 0.10 mm^3	
Theta range for data collection	2.08 to 32.04°.	
Index ranges	-10<=h<=10, -10<=k<=10, -29<=l<=27	
Reflections collected	18462	
Independent reflections	6037 [R(int) = 0.1117]	
Completeness to theta = 25.00°	98.4 %	
Absorption correction	None	
Max. and min. transmission	0.9893 and 0.9684	
Refinement method	Full-matrix least-squares on F^2	
Data / restraints / parameters	6037 / 2 / 267	
Goodness-of-fit on F^2	0.940	
Final R indices [I>2sigma(I)]	R1 = 0.0693, wR2 = 0.1703	
R indices (all data)	R1 = 0.2056, wR2 = 0.2142	
Largest diff. peak and hole	0.479 and -0.335 e.$Å^{-3}$	

Crystal data and structure refinement for **24SUB**.

Identification code	sf0815m	
Empirical formula	C20 H26 N4 O6	
Formula weight	418.45	
Temperature	120(2) K	
Wavelength	0.71073 Å	
Crystal system	Triclinic	
Space group	P-1	
Unit cell dimensions	a = 6.8479(8) Å	α= 92.343(2)°.
	b = 7.5486(8) Å	β= 93.002(2)°.
	c = 21.280(2) Å	γ = 113.883(2)°.
Volume	1002.12(19) $Å^3$	
Z	2	
Density (calculated)	1.387 g/cm^3	
Absorption coefficient	0.104 mm^{-1}	
F(000)	444	
Crystal size	0.15 x 0.15 x 0.10 mm^3	
Theta range for data collection	1.92 to 31.46°.	
Index ranges	-10<=h<=9, -10<=k<=11, -31<=l<=30	
Reflections collected	13812	
Independent reflections	6525 [R(int) = 0.0232]	
Completeness to theta = 31.46°	98.1 %	
Absorption correction	None	
Max. and min. transmission	0.9897 and 0.9846	
Refinement method	Full-matrix least-squares on F^2	
Data / restraints / parameters	6525 / 0 / 286	
Goodness-of-fit on F^2	1.011	
Final R indices [I>2sigma(I)]	R1 = 0.0452, wR2 = 0.1208	
R indices (all data)	R1 = 0.0671, wR2 = 0.1341	
Largest diff. peak and hole	0.487 and -0.323 $e.Å^{-3}$	

Table C.5 Crystal data and structure refinement for **26SUC, 26ADI, 26DOD, 27SUC, 27ADI, 27SUB, 28SUC, 28ADI, 28SUB, 28SEB, 28DOD, 28OXA, 28PIM, 29SUC, 29ADI, 29SUB, 29SEB, 29MAL, 30SEB, 31SUC, 31SUB, 31DOD, 32SUC, 32ADI, 32SUB, 32SEB, 32DOD, 32OXA, 32GLU, 32HEP, 32OCT, 32LAU** and **33UC, 33SUB, 33PIM**

26SUC

Identification code	sf0944m	
Empirical formula	C16 H20 N4 O8	
Formula weight	396.36	
Temperature	120(2) K	
Wavelength	0.71073 Å	
Crystal system	Monoclinic	
Space group	C2/c	
Unit cell dimensions	a = 18.6319(16) Å	α= 90°.
	b = 3.7424(3) Å	β= 99.566(5)°.
	c = 25.545(2) Å	γ = 90°.
Volume	1756.4(3) $Å^3$	
Z	4	
Density (calculated)	1.499 g/cm^3	
Absorption coefficient	0.122 mm^{-1}	
F(000)	832	
Crystal size	0.28 x 0.16 x 0.08 mm^3	
Theta range for data collection	1.62 to 30.45°.	
Index ranges	-22<=h<=26, -5<=k<=5, -36<=l<=35	
Reflections collected	9062	
Independent reflections	2401 [R(int) = 0.0906]	
Completeness to theta = 25.00°	95.0 %	
Absorption correction	None	
Max. and min. transmission	0.9903 and 0.9667	
Refinement method	Full-matrix least-squares on F^2	
Data / restraints / parameters	2401 / 78 / 140	
Goodness-of-fit on F^2	1.503	
Final R indices [I>2sigma(I)]	R1 = 0.1013, wR2 = 0.2416	
R indices (all data)	R1 = 0.1282, wR2 = 0.2609	
Largest diff. peak and hole	0.772 and -0.588 $e.Å^{-3}$	

Crystal data and structure refinement for **26ADI**.

Identification code	sf1004m	
Empirical formula	C18 H20 N4 O6	
Formula weight	388.38	
Temperature	298(2) K	
Wavelength	0.71073 Å	
Crystal system	Triclinic	
Space group	P-1	
Unit cell dimensions	a = 4.8804(3) Å	α= 95.710(4)°.
	b = 7.9736(6) Å	β= 90.985(4)°.
	c = 12.0838(8) Å	γ = 103.099(5)°.
Volume	455.34(5) $Å^3$	
Z	1	
Density (calculated)	1.416 g/cm^3	
Absorption coefficient	0.108 mm^{-1}	
F(000)	204	
Crystal size	0.28 x 0.22 x 0.12 mm^3	
Theta range for data collection	2.64 to 30.03°.	
Index ranges	-6<=h<=6, -11<=k<=11, -17<=l<=17	
Reflections collected	9499	
Independent reflections	2629 [R(int) = 0.0430]	
Completeness to theta = 30.03°	98.7 %	
Absorption correction	None	
Max. and min. transmission	0.9871 and 0.9703	
Refinement method	Full-matrix least-squares on F^2	
Data / restraints / parameters	2629 / 0 / 133	
Goodness-of-fit on F^2	1.723	
Final R indices [I>2sigma(I)]	R1 = 0.0651, wR2 = 0.2399	
R indices (all data)	R1 = 0.0798, wR2 = 0.2486	
Largest diff. peak and hole	0.343 and -0.253 $e.Å^{-3}$	

Crystal data and structure refinement for **26DOD**.

Identification code	sf1001m	
Empirical formula	C24 H32 N4 O6	
Formula weight	472.54	
Temperature	120(2) K	
Wavelength	0.71073 Å	
Crystal system	Triclinic	
Space group	P-1	
Unit cell dimensions	a = 4.6641(12) Å	α= 95.406(6)°.
	b = 7.1147(18) Å	β= 95.778(6)°.
	c = 18.067(5) Å	γ = 91.815(6)°.
Volume	593.3(3) $Å^3$	
Z	1	
Density (calculated)	1.323 g/cm^3	
Absorption coefficient	0.096 mm^{-1}	
F(000)	252	
Crystal size	0.28 x 0.16 x 0.08 mm^3	
Theta range for data collection	2.28 to 31.50°.	
Index ranges	-6<=h<=5, -10<=k<=10, -25<=l<=26	
Reflections collected	11248	
Independent reflections	3909 [R(int) = 0.0607]	
Completeness to theta = 31.50°	98.8 %	
Absorption correction	None	
Max. and min. transmission	0.9924 and 0.9736	
Refinement method	Full-matrix least-squares on F^2	
Data / restraints / parameters	3909 / 0 / 160	
Goodness-of-fit on F^2	1.034	
Final R indices [I>2sigma(I)]	R1 = 0.0560, wR2 = 0.1279	
R indices (all data)	R1 = 0.0942, wR2 = 0.1437	
Largest diff. peak and hole	0.436 and -0.367 $e.Å^{-3}$	

Crystal data and structure refinement for **27SUC**.

Identification code	sf1003m	
Empirical formula	C24 H34 N4 O12	
Formula weight	570.55	
Temperature	120(2) K	
Wavelength	0.71073 Å	
Crystal system	Triclinic	
Space group	P-1	
Unit cell dimensions	a = 4.7321(4) Å	α= 74.877(3)°.
	b = 9.0931(8) Å	β= 85.703(4)°.
	c = 16.0232(14) Å	γ = 76.887(4)°.
Volume	648.15(10) $Å^3$	
Z	1	
Density (calculated)	1.462 g/cm^3	
Absorption coefficient	0.118 mm^{-1}	
F(000)	302	
Crystal size	0.32 x 0.24 x 0.10 mm^3	
Theta range for data collection	2.38 to 32.57°.	
Index ranges	-6<=h<=7, -13<=k<=13, -23<=l<=20	
Reflections collected	13621	
Independent reflections	4352 [R(int) = 0.0424]	
Completeness to theta = 30.00°	98.8 %	
Absorption correction	None	
Max. and min. transmission	0.9883 and 0.9632	
Refinement method	Full-matrix least-squares on F^2	
Data / restraints / parameters	4352 / 0 / 196	
Goodness-of-fit on F^2	1.038	
Final R indices [I>2sigma(I)]	R1 = 0.0513, wR2 = 0.1306	
R indices (all data)	R1 = 0.0739, wR2 = 0.1443	
Largest diff. peak and hole	0.425 and -0.425 $e.Å^{-3}$	

Crystal data and structure refinement for **27ADI**.

Identification code	sf0946m	
Empirical formula	C22 H28 N4 O6	
Formula weight	444.48	
Temperature	120(2) K	
Wavelength	0.71073 Å	
Crystal system	Triclinic	
Space group	P-1	
Unit cell dimensions	a = 5.1160(4) Å	α= 90.704(2)°.
	b = 5.1957(4) Å	β= 93.362(2)°.
	c = 19.5042(16) Å	γ = 91.346(2)°.
Volume	517.36(7) $Å^3$	
Z	1	
Density (calculated)	1.427 g/cm^3	
Absorption coefficient	0.105 mm^{-1}	
F(000)	236	
Crystal size	0.32 x 0.22 x 0.14 mm^3	
Theta range for data collection	3.14 to 32.56°.	
Index ranges	-7<=h<=6, -6<=k<=7, -29<=l<=26	
Reflections collected	8119	
Independent reflections	3505 [R(int) = 0.0163]	
Completeness to theta = 30.00°	98.6 %	
Absorption correction	None	
Max. and min. transmission	0.9854 and 0.9671	
Refinement method	Full-matrix least-squares on F^2	
Data / restraints / parameters	3505 / 0 / 151	
Goodness-of-fit on F^2	1.057	
Final R indices [I>2sigma(I)]	R1 = 0.0375, wR2 = 0.1069	
R indices (all data)	R1 = 0.0437, wR2 = 0.1132	
Largest diff. peak and hole	0.507 and -0.245 $e.Å^{-3}$	

Crystal data and structure refinement for **27SUB**.

Identification code	sf1002m	
Empirical formula	C24 H32 N4 O6	
Formula weight	472.54	
Temperature	120(2) K	
Wavelength	0.71073 Å	
Crystal system	Triclinic	
Space group	P-1	
Unit cell dimensions	a = 5.1221(4) Å	α= 94.963(2)°.
	b = 5.2045(4) Å	β= 95.404(2)°.
	c = 21.5019(14) Å	γ = 91.630(2)°.
Volume	568.12(7) $Å^3$	
Z	1	
Density (calculated)	1.381 g/cm^3	
Absorption coefficient	0.100 mm^{-1}	
F(000)	252	
Crystal size	0.32 x 0.24 x 0.08 mm^3	
Theta range for data collection	3.93 to 32.58°.	
Index ranges	-6<=h<=7, -7<=k<=6, -32<=l<=32	
Reflections collected	10539	
Independent reflections	3669 [R(int) = 0.0198]	
Completeness to theta = 27.50°	97.1 %	
Absorption correction	None	
Max. and min. transmission	0.9920 and 0.9686	
Refinement method	Full-matrix least-squares on F^2	
Data / restraints / parameters	3669 / 0 / 160	
Goodness-of-fit on F^2	1.064	
Final R indices [I>2sigma(I)]	R1 = 0.0429, wR2 = 0.1227	
R indices (all data)	R1 = 0.0529, wR2 = 0.1303	
Largest diff. peak and hole	0.458 and -0.237 $e.Å^{-3}$	

Crystal data and structure refinement for **28SUC**.

Identification code	sf0716m	
Empirical formula	C22 H28 N4 O6	
Formula weight	444.48	
Temperature	120(2) K	
Wavelength	0.71073 Å	
Crystal system	Triclinic	
Space group	P-1	
Unit cell dimensions	a = 5.1754(4) Å	α= 118.826(4)°.
	b = 10.9294(8) Å	β= 91.381(5)°.
	c = 10.9423(8) Å	γ = 99.872(4)°.
Volume	530.11(7) $Å^3$	
Z	1	
Density (calculated)	1.392 g/cm^3	
Absorption coefficient	0.103 mm^{-1}	
F(000)	236	
Crystal size	0.15 x 0.15 x 0.10 mm^3	
Theta range for data collection	2.14 to 30.49°.	
Index ranges	-7<=h<=6, -15<=k<=15, -15<=l<=15	
Reflections collected	12293	
Independent reflections	3228 [R(int) = 0.0513]	
Completeness to theta = 30.49°	99.5 %	
Absorption correction	None	
Max. and min. transmission	0.9898 and 0.9848	
Refinement method	Full-matrix least-squares on F^2	
Data / restraints / parameters	3228 / 0 / 151	
Goodness-of-fit on F^2	1.063	
Final R indices [I>2sigma(I)]	R1 = 0.0605, wR2 = 0.1509	
R indices (all data)	R1 = 0.0993, wR2 = 0.1761	
Largest diff. peak and hole	0.528 and -0.294 $e.Å^{-3}$	

Crystal data and structure refinement for **28ADI**.

Identification code	sf0901m	
Empirical formula	C24 H32 N4 O6	
Formula weight	472.54	
Temperature	120(2) K	
Wavelength	0.71073 Å	
Crystal system	Triclinic	
Space group	P-1	
Unit cell dimensions	a = 5.1412(4) Å	α= 95.094(5)°.
	b = 5.2394(4) Å	β= 95.603(4)°.
	c = 21.3961(17) Å	γ = 91.076(5)°.
Volume	571.10(8) $Å^3$	
Z	1	
Density (calculated)	1.374 g/cm^3	
Absorption coefficient	0.100 mm^{-1}	
F(000)	252	
Crystal size	0.24 x 0.14 x 0.06 mm^3	
Theta range for data collection	2.88 to 31.49°.	
Index ranges	-7<=h<=6, -7<=k<=7, -31<=l<=31	
Reflections collected	9707	
Independent reflections	3695 [R(int) = 0.0336]	
Completeness to theta = 31.49°	97.0 %	
Absorption correction	None	
Refinement method	Full-matrix least-squares on F^2	
Data / restraints / parameters	3695 / 0 / 160	
Goodness-of-fit on F^2	1.095	
Final R indices [I>2sigma(I)]	R1 = 0.0470, wR2 = 0.1167	
R indices (all data)	R1 = 0.0691, wR2 = 0.1293	
Largest diff. peak and hole	0.442 and -0.258 $e.Å^{-3}$	

Crystal data and structure refinement for **28SUB**.

Identification code	sf0705m	
Empirical formula	C26 H36 N4 O6	
Formula weight	500.59	
Temperature	120(2) K	
Wavelength	0.71073 Å	
Crystal system	Triclinic	
Space group	P-1	
Unit cell dimensions	a = 5.1392(5) Å	α= 94.050(3)°.
	b = 5.2412(5) Å	β= 95.222(2)°.
	c = 23.145(2) Å	γ = 91.277(2)°.
Volume	619.02(10) $Å^3$	
Z	1	
Density (calculated)	1.343 g/cm^3	
Absorption coefficient	0.096 mm^{-1}	
F(000)	268	
Crystal size	0.25 x 0.15 x 0.10 mm^3	
Theta range for data collection	1.77 to 30.51°.	
Index ranges	-6<=h<=7, -7<=k<=7, -32<=l<=32	
Reflections collected	17489	
Independent reflections	3780 [R(int) = 0.0297]	
Completeness to theta = 30.51°	99.3 %	
Absorption correction	None	
Max. and min. transmission	0.9905 and 0.9764	
Refinement method	Full-matrix least-squares on F^2	
Data / restraints / parameters	3780 / 0 / 169	
Goodness-of-fit on F^2	1.090	
Final R indices [I>2sigma(I)]	R1 = 0.0372, wR2 = 0.1086	
R indices (all data)	R1 = 0.0424, wR2 = 0.1137	
Largest diff. peak and hole	0.495 and -0.278 $e.Å^{-3}$	

Crystal data and structure refinement for **28SEB**.

Identification code	sf0830m	
Empirical formula	C28 H40 N4 O6	
Formula weight	528.64	
Temperature	120(2) K	
Wavelength	0.71073 Å	
Crystal system	Triclinic	
Space group	P-1	
Unit cell dimensions	a = 5.1506(4) Å	α= 89.647(4)°.
	b = 5.2481(4) Å	β= 87.252(4)°.
	c = 24.5206(16) Å	γ = 88.505(5)°.
Volume	661.82(8) $Å^3$	
Z	1	
Density (calculated)	1.326 g/cm^3	
Absorption coefficient	0.094 mm^{-1}	
F(000)	284	
Crystal size	0.24 x 0.14 x 0.08 mm^3	
Theta range for data collection	3.33 to 33.14°.	
Index ranges	-7<=h<=7, -7<=k<=8, -37<=l<=37	
Reflections collected	16445	
Independent reflections	4947 [R(int) = 0.0338]	
Completeness to theta = 33.14°	98.5 %	
Absorption correction	None	
Refinement method	Full-matrix least-squares on F^2	
Data / restraints / parameters	4947 / 0 / 178	
Goodness-of-fit on F^2	1.057	
Final R indices [I>2sigma(I)]	R1 = 0.0493, wR2 = 0.1271	
R indices (all data)	R1 = 0.0827, wR2 = 0.1420	
Largest diff. peak and hole	0.451 and -0.254 $e.Å^{-3}$	

Crystal data and structure refinement for **28DOD**.

Identification code	sf0928m	
Empirical formula	C30 H44 N4 O6	
Formula weight	556.69	
Temperature	120(2) K	
Wavelength	0.71073 Å	
Crystal system	Triclinic	
Space group	P-1	
Unit cell dimensions	a = 5.1519(4) Å	α= 86.023(6)°.
	b = 5.2778(5) Å	β= 89.386(6)°.
	c = 26.148(3) Å	γ = 88.496(6)°.
Volume	708.99(11) $Å^3$	
Z	1	
Density (calculated)	1.304 g/cm^3	
Absorption coefficient	0.091 mm^{-1}	
F(000)	300	
Crystal size	0.28 x 0.04 x 0.04 mm^3	
Theta range for data collection	2.34 to 32.58°.	
Index ranges	-7<=h<=7, -7<=k<=7, -39<=l<=37	
Reflections collected	16574	
Independent reflections	5028 [R(int) = 0.0726]	
Completeness to theta = 32.58°	97.8 %	
Absorption correction	None	
Max. and min. transmission	0.9964 and 0.9749	
Refinement method	Full-matrix least-squares on F^2	
Data / restraints / parameters	5028 / 0 / 187	
Goodness-of-fit on F^2	1.042	
Final R indices [I>2sigma(I)]	R1 = 0.0650, wR2 = 0.1632	
R indices (all data)	R1 = 0.1159, wR2 = 0.1937	
Largest diff. peak and hole	0.403 and -0.358 $e.Å^{-3}$	

Crystal data and structure refinement for **28OXA**.

Identification code	sf0920m	
Empirical formula	C20 H24 N4 O6	
Formula weight	416.43	
Temperature	120(2) K	
Wavelength	0.71073 Å	
Crystal system	Triclinic	
Space group	P-1	
Unit cell dimensions	a = 5.1134(6) Å	α= 95.992(7)°.
	b = 5.3528(7) Å	β= 91.615(7)°.
	c = 17.611(2) Å	γ = 91.021(7)°.
Volume	479.11(10) $Å^3$	
Z	1	
Density (calculated)	1.443 g/cm^3	
Absorption coefficient	0.108 mm^{-1}	
F(000)	220	
Crystal size	0.26 x 0.16 x 0.08 mm^3	
Theta range for data collection	4.91 to 32.58°.	
Index ranges	-7<=h<=7, -7<=k<=8, -26<=l<=26	
Reflections collected	10093	
Independent reflections	3452 [R(int) = 0.0303]	
Completeness to theta = 25.00°	98.7 %	
Absorption correction	None	
Max. and min. transmission	0.9914 and 0.9724	
Refinement method	Full-matrix least-squares on F^2	
Data / restraints / parameters	3452 / 0 / 143	
Goodness-of-fit on F^2	1.056	
Final R indices [I>2sigma(I)]	R1 = 0.0402, wR2 = 0.1099	
R indices (all data)	R1 = 0.0500, wR2 = 0.1159	
Largest diff. peak and hole	0.472 and -0.236 $e.Å^{-3}$	

Crystal data and structure refinement for **28PIM**.

Identification code	sf0927m	
Empirical formula	C25 H34 N4 O6	
Formula weight	486.56	
Temperature	120(2) K	
Wavelength	0.71073 Å	
Crystal system	Triclinic	
Space group	P-1	
Unit cell dimensions	a = 5.0330(4) Å	α= 82.823(4)°.
	b = 11.9025(9) Å	β= 89.008(4)°.
	c = 20.6795(16) Å	γ = 79.850(4)°.
Volume	1209.86(16) $Å^3$	
Z	2	
Density (calculated)	1.336 g/cm^3	
Absorption coefficient	0.096 mm^{-1}	
F(000)	520	
Crystal size	0.26 x 0.14 x 0.12 mm^3	
Theta range for data collection	2.12 to 32.70°.	
Index ranges	-7<=h<=7, -17<=k<=18, 0<=l<=31	
Reflections collected	17249	
Independent reflections	17249 [R(int) = 0.0000]	
Completeness to theta = 32.70°	97.6 %	
Absorption correction	None	
Max. and min. transmission	0.9885 and 0.9754	
Refinement method	Full-matrix least-squares on F^2	
Data / restraints / parameters	17249 / 0 / 329	
Goodness-of-fit on F^2	1.060	
Final R indices [I>2sigma(I)]	R1 = 0.0547, wR2 = 0.1419	
R indices (all data)	R1 = 0.0810, wR2 = 0.1590	
Largest diff. peak and hole	0.527 and -0.291 $e.Å^{-3}$	

Crystal data and structure refinement for **29SUC**.

Identification code	sf0831m	
Empirical formula	C24 H32 N4 O6	
Formula weight	472.54	
Temperature	120(2) K	
Wavelength	0.71073 Å	
Crystal system	Triclinic	
Space group	P-1	
Unit cell dimensions	a = 5.1072(4) Å	α= 96.134(6)°.
	b = 5.1171(4) Å	β= 94.037(6)°.
	c = 22.119(2) Å	γ = 91.340(6)°.
Volume	573.05(8) $Å^3$	
Z	1	
Density (calculated)	1.369 g/cm^3	
Absorption coefficient	0.099 mm^{-1}	
F(000)	252	
Crystal size	0.24 x 0.14 x 0.08 mm^3	
Theta range for data collection	2.79 to 31.64°.	
Index ranges	-7<=h<=7, -7<=k<=7, 0<=l<=32	
Reflections collected	5484	
Independent reflections	5484 [R(int) = 0.0000]	
Completeness to theta = 31.64°	98.4 %	
Absorption correction	None	
Max. and min. transmission	0.9921 and 0.9765	
Refinement method	Full-matrix least-squares on F^2	
Data / restraints / parameters	5484 / 0 / 161	
Goodness-of-fit on F^2	1.032	
Final R indices [I>2sigma(I)]	R1 = 0.0471, wR2 = 0.1143	
R indices (all data)	R1 = 0.0597, wR2 = 0.1230	
Largest diff. peak and hole	0.403 and -0.250 $e.Å^{-3}$	

Crystal data and structure refinement for **29ADI**.

Identification code	sf0813m	
Empirical formula	C26 H36 N4 O6	
Formula weight	500.59	
Temperature	120(2) K	
Wavelength	0.71073 Å	
Crystal system	Triclinic	
Space group	P-1	
Unit cell dimensions	a = 5.1403(3) Å	α= 93.859(4)°.
	b = 5.2489(3) Å	β= 95.267(4)°.
	c = 22.9829(15) Å	γ = 91.289(4)°.
Volume	615.82(6) $Å^3$	
Z	1	
Density (calculated)	1.350 g/cm^3	
Absorption coefficient	0.097 mm^{-1}	
F(000)	268	
Crystal size	0.25 x 0.10 x 0.05 mm^3	
Theta range for data collection	2.68 to 31.41°.	
Index ranges	-7<=h<=7, -7<=k<=7, -33<=l<=33	
Reflections collected	10595	
Independent reflections	3955 [R(int) = 0.0263]	
Completeness to theta = 31.41°	97.0 %	
Absorption correction	None	
Max. and min. transmission	0.9952 and 0.9763	
Refinement method	Full-matrix least-squares on F^2	
Data / restraints / parameters	3955 / 0 / 169	
Goodness-of-fit on F^2	1.045	
Final R indices [I>2sigma(I)]	R1 = 0.0402, wR2 = 0.1061	
R indices (all data)	R1 = 0.0570, wR2 = 0.1154	
Largest diff. peak and hole	0.439 and -0.213 $e.Å^{-3}$	

Crystal data and structure refinement for **29SUB**.

Identification code	sf0808m	
Empirical formula	C28 H40 N4 O6	
Formula weight	528.64	
Temperature	120(2) K	
Wavelength	0.71073 Å	
Crystal system	Triclinic	
Space group	P-1	
Unit cell dimensions	a = 5.1420(4) Å	α= 89.785(4)°.
	b = 5.2541(4) Å	β= 87.095(4)°.
	c = 24.624(2) Å	γ = 88.590(4)°.
Volume	664.20(9) $Å^3$	
Z	1	
Density (calculated)	1.322 g/cm^3	
Absorption coefficient	0.093 mm^{-1}	
F(000)	284	
Crystal size	0.20 x 0.15 x 0.10 mm^3	
Theta range for data collection	0.83 to 31.88°.	
Index ranges	-7<=h<=7, -7<=k<=7, -27<=l<=36	
Reflections collected	11236	
Independent reflections	4009 [R(int) = 0.0293]	
Completeness to theta = 25.00°	97.2 %	
Absorption correction	None	
Max. and min. transmission	0.9907 and 0.9816	
Refinement method	Full-matrix least-squares on F^2	
Data / restraints / parameters	4009 / 0 / 178	
Goodness-of-fit on F^2	1.005	
Final R indices [I>2sigma(I)]	R1 = 0.0473, wR2 = 0.1230	
R indices (all data)	R1 = 0.0706, wR2 = 0.1384	
Largest diff. peak and hole	0.420 and -0.235 $e.Å^{-3}$	

Crystal data and structure refinement for **29SEB**.

Identification code	sf0936m	
Empirical formula	C30 H44 N4 O6	
Formula weight	556.69	
Temperature	120(2) K	
Wavelength	0.71073 Å	
Crystal system	Triclinic	
Space group	P-1	
Unit cell dimensions	a = 5.1264(6) Å	a= 85.874(4)°.
	b = 5.2432(6) Å	b= 89.354(4)°.
	c = 26.127(3) Å	g = 88.356(4)°.
Volume	700.11(14) $Å^3$	
Z	1	
Density (calculated)	1.320 Mg/m^3	
Absorption coefficient	0.092 mm^{-1}	
F(000)	300	
Crystal size	0.32 x 0.18 x 0.06 mm^3	
Theta range for data collection	3.90 to 33.11°.	
Index ranges	-7<=h<=5, -7<=k<=7, -40<=l<=38	
Reflections collected	11866	
Independent reflections	4577 [R(int) = 0.0393]	
Completeness to theta = 27.50°	96.7 %	
Absorption correction	None	
Max. and min. transmission	0.9945 and 0.9711	
Refinement method	Full-matrix least-squares on F^2	
Data / restraints / parameters	4577 / 0 / 187	
Goodness-of-fit on F^2	1.084	
Final R indices [I>2sigma(I)]	R1 = 0.0614, wR2 = 0.1655	
R indices (all data)	R1 = 0.0956, wR2 = 0.1827	
Largest diff. peak and hole	0.555 and -0.342 e.$Å^{-3}$	

Crystal data and structure refinement for **29MAL**.

Identification code	sf0828m	
Empirical formula	C23 H30 N4 O6	
Formula weight	458.51	
Temperature	120(2) K	
Wavelength	0.71073 Å	
Crystal system	Monoclinic	
Space group	C2/c	
Unit cell dimensions	a = 42.2708(18) Å	α= 90°.
	b = 5.1015(2) Å	β= 115.572(2)°.
	c = 22.9436(10) Å	γ = 90°.
Volume	4463.0(3) $Å^3$	
Z	8	
Density (calculated)	1.365 g/cm^3	
Absorption coefficient	0.100 mm^{-1}	
F(000)	1952	
Crystal size	0.25 x 0.15 x 0.15 mm^3	
Theta range for data collection	4.67 to 32.72°.	
Index ranges	-64<=h<=57, 0<=k<=7, 0<=l<=34	
Reflections collected	15642	
Independent reflections	15642 [R(int) = 0.0000]	
Completeness to theta = 30.00°	98.7 %	
Absorption correction	None	
Max. and min. transmission	0.9852 and 0.9755	
Refinement method	Full-matrix least-squares on F^2	
Data / restraints / parameters	15642 / 0 / 311	
Goodness-of-fit on F^2	1.006	
Final R indices [I>2sigma(I)]	R1 = 0.0570, wR2 = 0.1297	
R indices (all data)	R1 = 0.1087, wR2 = 0.1540	
Largest diff. peak and hole	0.479 and -0.323 $e.Å^{-3}$	

Crystal data and structure refinement for **30SEB**.

Identification code	sf0708m	
Empirical formula	C22 H28 N4 O6	
Formula weight	444.48	
Temperature	120(2) K	
Wavelength	0.71073 Å	
Crystal system	Triclinic	
Space group	P-1	
Unit cell dimensions	a = 4.7236(5) Å	α= 85.161(3)°.
	b = 6.7563(6) Å	β= 82.746(3)°.
	c = 16.9532(16) Å	γ = 89.911(3)°.
Volume	534.78(9) $Å^3$	
Z	1	
Density (calculated)	1.380 g/cm^3	
Absorption coefficient	0.102 mm^{-1}	
F(000)	236	
Crystal size	0.20 x 0.20 x 0.08 mm^3	
Theta range for data collection	3.03 to 30.51°.	
Index ranges	-6<=h<=6, -3<=k<=9, -24<=l<=24	
Reflections collected	8968	
Independent reflections	3155 [R(int) = 0.0575]	
Completeness to theta = 30.51°	96.2 %	
Absorption correction	None	
Max. and min. transmission	0.9919 and 0.9799	
Refinement method	Full-matrix least-squares on F^2	
Data / restraints / parameters	3155 / 18 / 158	
Goodness-of-fit on F^2	1.070	
Final R indices [I>2sigma(I)]	R1 = 0.0652, wR2 = 0.1612	
R indices (all data)	R1 = 0.1205, wR2 = 0.1900	
Largest diff. peak and hole	0.273 and -0.329 $e.Å^{-3}$	

Crystal data and structure refinement for **31SUC**.

Identification code	sf0945m	
Empirical formula	C20 H24 N4 O6	
Formula weight	416.43	
Temperature	120(2) K	
Wavelength	0.71073 Å	
Crystal system	Triclinic	
Space group	P-1	
Unit cell dimensions	a = 10.0264(7) Å	α= 91.733(2)°.
	b = 10.1248(7) Å	β= 107.904(2)°.
	c = 11.0782(8) Å	γ = 110.922(2)°.
Volume	987.11(12) $Å^3$	
Z	2	
Density (calculated)	1.401 g/cm^3	
Absorption coefficient	0.105 mm^{-1}	
F(000)	440	
Crystal size	0.38 x 0.32 x 0.14 mm^3	
Theta range for data collection	2.49 to 32.58°.	
Index ranges	-8<=h<=15, -15<=k<=14, -16<=l<=16	
Reflections collected	16313	
Independent reflections	6661 [R(int) = 0.0212]	
Completeness to theta = 30.00°	98.2 %	
Absorption correction	None	
Max. and min. transmission	0.9854 and 0.9612	
Refinement method	Full-matrix least-squares on F^2	
Data / restraints / parameters	6661 / 0 / 283	
Goodness-of-fit on F^2	1.239	
Final R indices [I>2sigma(I)]	R1 = 0.0525, wR2 = 0.1571	
R indices (all data)	R1 = 0.0645, wR2 = 0.1720	
Largest diff. peak and hole	0.661 and -0.368 $e.Å^{-3}$	

Crystal data and structure refinement for **31SUB**.

Identification code	sf0939m	
Empirical formula	C24 H32 N4 O6	
Formula weight	472.54	
Temperature	120(2) K	
Wavelength	0.71073 Å	
Crystal system	Triclinic	
Space group	P-1	
Unit cell dimensions	a = 5.0982(5) Å	α= 115.707(3)°.
	b = 11.4639(10) Å	β= 98.696(4)°.
	c = 11.4873(11) Å	γ = 100.874(4)°.
Volume	573.10(9) $Å^3$	
Z	1	
Density (calculated)	1.369 g/cm^3	
Absorption coefficient	0.099 mm^{-1}	
F(000)	252	
Crystal size	0.36 x 0.16 x 0.10 mm^3	
Theta range for data collection	2.06 to 31.00°.	
Index ranges	-7<=h<=5, -16<=k<=16, -16<=l<=16	
Reflections collected	9022	
Independent reflections	3570 [R(int) = 0.0278]	
Completeness to theta = 30.00°	98.6 %	
Absorption correction	None	
Max. and min. transmission	0.9901 and 0.9651	
Refinement method	Full-matrix least-squares on F^2	
Data / restraints / parameters	3570 / 0 / 160	
Goodness-of-fit on F^2	1.074	
Final R indices [I>2sigma(I)]	R1 = 0.0445, wR2 = 0.1220	
R indices (all data)	R1 = 0.0601, wR2 = 0.1316	
Largest diff. peak and hole	0.355 and -0.298 $e.Å^{-3}$	

Crystal data and structure refinement for **31DOD**.

Identification code	sf0941m	
Empirical formula	C28 H40 N4 O6	
Formula weight	528.64	
Temperature	120(2) K	
Wavelength	0.71073 Å	
Crystal system	Triclinic	
Space group	P-1	
Unit cell dimensions	a = 5.097(3) Å	α= 86.020(18)°.
	b = 5.486(3) Å	β= 86.521(18)°.
	c = 23.823(13) Å	γ = 87.553(18)°.
Volume	662.8(6) $Å^3$	
Z	1	
Density (calculated)	1.324 g/cm^3	
Absorption coefficient	0.094 mm^{-1}	
F(000)	284	
Crystal size	0.38 x 0.04 x 0.04 mm^3	
Theta range for data collection	2.58 to 28.28°.	
Index ranges	-6<=h<=6, -7<=k<=7, -31<=l<=26	
Reflections collected	10139	
Independent reflections	3194 [R(int) = 0.3225]	
Completeness to theta = 28.28°	97.1 %	
Absorption correction	None	
Max. and min. transmission	0.9963 and 0.9653	
Refinement method	Full-matrix least-squares on F^2	
Data / restraints / parameters	3194 / 0 / 65	
Goodness-of-fit on F^2	1.446	
Final R indices [I>2sigma(I)]	R1 = 0.2077, wR2 = 0.4158	
R indices (all data)	R1 = 0.3885, wR2 = 0.4703	
Largest diff. peak and hole	0.949 and -1.211 $e.Å^{-3}$	

Crystal data and structure refinement for **32SUC**.

Identification code	sf0809m	
Empirical formula	C22 H28 N4 O6	
Formula weight	444.48	
Temperature	120(2) K	
Wavelength	0.71073 Å	
Crystal system	Triclinic	
Space group	P-1	
Unit cell dimensions	a = 5.0275(6) Å	α= 89.749(6)°.
	b = 6.9253(9) Å	β= 81.536(5)°.
	c = 16.058(2) Å	γ = 80.893(6)°.
Volume	545.92(12) $Å^3$	
Z	1	
Density (calculated)	1.352 g/cm^3	
Absorption coefficient	0.100 mm^{-1}	
F(000)	236	
Crystal size	0.25 x 0.25 x 0.15 mm^3	
Theta range for data collection	2.57 to 34.34°.	
Index ranges	-7<=h<=7, -10<=k<=10, -25<=l<=25	
Reflections collected	14151	
Independent reflections	4361 [R(int) = 0.0241]	
Completeness to theta = 25.00°	99.7 %	
Absorption correction	None	
Max. and min. transmission	0.9852 and 0.9755	
Refinement method	Full-matrix least-squares on F^2	
Data / restraints / parameters	4361 / 6 / 161	
Goodness-of-fit on F^2	1.041	
Final R indices [I>2sigma(I)]	R1 = 0.0431, wR2 = 0.1222	
R indices (all data)	R1 = 0.0533, wR2 = 0.1305	
Largest diff. peak and hole	0.473 and -0.225 $e.Å^{-3}$	

Crystal data and structure refinement for **32ADI**.

Identification code	sf1005m	
Empirical formula	C24 H32 N4 O6	
Formula weight	472.54	
Temperature	120(2) K	
Wavelength	0.71073 Å	
Crystal system	Triclinic	
Space group	P-1	
Unit cell dimensions	a = 5.0282(6) Å	a= 98.124(3)°.
	b = 6.7877(8) Å	b= 97.604(3)°.
	c = 17.522(2) Å	g = 94.605(3)°.
Volume	583.82(12) $Å^3$	
Z	1	
Density (calculated)	1.344 Mg/m^3	
Absorption coefficient	0.098 mm^{-1}	
F(000)	252	
Crystal size	0.36 x 0.16 x 0.08 mm^3	
Theta range for data collection	2.37 to 30.49°.	
Index ranges	-7<=h<=6, -8<=k<=9, -24<=l<=24	
Reflections collected	8477	
Independent reflections	3487 [R(int) = 0.0333]	
Completeness to theta = 30.49°	97.8 %	
Absorption correction	None	
Max. and min. transmission	0.9922 and 0.9657	
Refinement method	Full-matrix least-squares on F^2	
Data / restraints / parameters	3487 / 0 / 160	
Goodness-of-fit on F^2	1.084	
Final R indices [I>2sigma(I)]	R1 = 0.0487, wR2 = 0.1270	
R indices (all data)	R1 = 0.0688, wR2 = 0.1400	
Largest diff. peak and hole	0.367 and -0.281 e.$Å^{-3}$	

Crystal data and structure refinement for **32SUB**.

Identification code	sf0934m	
Empirical formula	C26 H36 N4 O6	
Formula weight	500.59	
Temperature	296(2) K	
Wavelength	0.71073 Å	
Crystal system	Triclinic	
Space group	P-1	
Unit cell dimensions	a = 5.1671(13) Å	α= 67.873(11)°.
	b = 11.646(3) Å	β= 80.585(12)°.
	c = 11.779(4) Å	γ = 79.827(12)°.
Volume	642.6(3) $Å^3$	
Z	1	
Density (calculated)	1.294 g/cm^3	
Absorption coefficient	0.093 mm^{-1}	
F(000)	268	
Crystal size	0.28 x 0.18 x 0.08 mm^3	
Theta range for data collection	1.88 to 29.57°.	
Index ranges	-7<=h<=5, -16<=k<=12, -16<=l<=12	
Reflections collected	9851	
Independent reflections	3328 [R(int) = 0.0395]	
Completeness to theta = 27.50°	96.2 %	
Absorption correction	None	
Max. and min. transmission	0.9926 and 0.9745	
Refinement method	Full-matrix least-squares on F^2	
Data / restraints / parameters	3328 / 0 / 169	
Goodness-of-fit on F^2	1.070	
Final R indices [I>2sigma(I)]	R1 = 0.0563, wR2 = 0.1407	
R indices (all data)	R1 = 0.1002, wR2 = 0.1599	
Largest diff. peak and hole	0.251 and -0.293 $e.Å^{-3}$	

Crystal data and structure refinement for **32SEB**.

Identification code	sf0820m	
Empirical formula	C28 H40 N4 O6	
Formula weight	528.64	
Temperature	120(2) K	
Wavelength	0.71073 Å	
Crystal system	Triclinic	
Space group	P-1	
Unit cell dimensions	a = 4.9817(4) Å	a= 93.097(4)°.
	b = 6.8634(6) Å	b= 90.233(4)°.
	c = 20.0493(16) Å	g = 98.285(4)°.
Volume	677.32(10) $Å^3$	
Z	1	
Density (calculated)	1.296 Mg/m^3	
Absorption coefficient	0.092 mm^{-1}	
F(000)	284	
Crystal size	0.25 x 0.15 x 0.10 mm^3	
Theta range for data collection	2.03 to 31.64°.	
Index ranges	-7<=h<=7, -10<=k<=10, -22<=l<=29	
Reflections collected	11823	
Independent reflections	4462 [R(int) = 0.0296]	
Completeness to theta = 31.64°	97.6 %	
Absorption correction	None	
Max. and min. transmission	0.9909 and 0.9775	
Refinement method	Full-matrix least-squares on F^2	
Data / restraints / parameters	4462 / 0 / 178	
Goodness-of-fit on F^2	1.091	
Final R indices [I>2sigma(I)]	R1 = 0.0517, wR2 = 0.1446	
R indices (all data)	R1 = 0.0676, wR2 = 0.1571	
Largest diff. peak and hole	0.626 and -0.322 e.$Å^{-3}$	

Crystal data and structure refinement for **32DOD**.

Identification code	sf0833m	
Empirical formula	C30 H44 N4 O6	
Formula weight	556.69	
Temperature	120(2) K	
Wavelength	0.71073 Å	
Crystal system	Triclinic	
Space group	P-1	
Unit cell dimensions	a = 4.9821(4) Å	α= 87.936(6)°.
	b = 6.8797(6) Å	β= 86.223(6)°.
	c = 21.4410(17) Å	γ = 81.469(5)°.
Volume	724.93(10) $Å^3$	
Z	1	
Density (calculated)	1.275 g/cm^3	
Absorption coefficient	0.089 mm^{-1}	
F(000)	300	
Crystal size	0.28 x 0.12 x 0.06 mm^3	
Theta range for data collection	2.86 to 31.50°.	
Index ranges	-7<=h<=7, -10<=k<=9, -31<=l<=31	
Reflections collected	14792	
Independent reflections	4826 [R(int) = 0.0450]	
Completeness to theta = 31.50°	99.7 %	
Absorption correction	None	
Max. and min. transmission	0.9947 and 0.9755	
Refinement method	Full-matrix least-squares on F^2	
Data / restraints / parameters	4826 / 0 / 187	
Goodness-of-fit on F^2	1.017	
Final R indices [I>2sigma(I)]	R1 = 0.0510, wR2 = 0.1297	
R indices (all data)	R1 = 0.0854, wR2 = 0.1478	
Largest diff. peak and hole	0.479 and -0.300 $e.Å^{-3}$	

Crystal data and structure refinement for **32OXA**.

Identification code	sf0926m	
Empirical formula	C20 H24 N4 O6	
Formula weight	416.43	
Temperature	120(2) K	
Wavelength	0.71073 Å	
Crystal system	Triclinic	
Space group	P-1	
Unit cell dimensions	a = 5.0759(3) Å	α= 77.759(2)°.
	b = 11.9049(8) Å	β= 88.428(3)°.
	c = 16.5104(11) Å	γ = 84.804(2)°.
Volume	970.97(11) $Å^3$	
Z	2	
Density (calculated)	1.424 g/cm^3	
Absorption coefficient	0.107 mm^{-1}	
F(000)	440	
Crystal size	0.32 x 0.26 x 0.20 mm^3	
Theta range for data collection	1.26 to 32.52°.	
Index ranges	-7<=h<=7, -17<=k<=15, -22<=l<=24	
Reflections collected	20512	
Independent reflections	6627 [R(int) = 0.0266]	
Completeness to theta = 30.00°	98.9 %	
Absorption correction	None	
Max. and min. transmission	0.9790 and 0.9666	
Refinement method	Full-matrix least-squares on F^2	
Data / restraints / parameters	6627 / 0 / 283	
Goodness-of-fit on F^2	1.088	
Final R indices [I>2sigma(I)]	R1 = 0.0447, wR2 = 0.1295	
R indices (all data)	R1 = 0.0565, wR2 = 0.1379	
Largest diff. peak and hole	0.403 and -0.280 $e.Å^{-3}$	

Crystal data and structure refinement for **32GLU**.

Identification code	sf0907m	
Empirical formula	C28 H38 N4 O10	
Formula weight	590.62	
Temperature	120(2) K	
Wavelength	0.71073 Å	
Crystal system	Triclinic	
Space group	P-1	
Unit cell dimensions	a = 5.2223(3) Å	α= 92.069(3)°.
	b = 11.4288(7) Å	β= 100.203(3)°.
	c = 12.4175(7) Å	γ = 102.989(3)°.
Volume	708.52(7) $Å^3$	
Z	1	
Density (calculated)	1.384 g/cm^3	
Absorption coefficient	0.106 mm^{-1}	
F(000)	314	
Crystal size	0.26 x 0.22 x 0.15 mm^3	
Theta range for data collection	3.34 to 32.57°.	
Index ranges	-7<=h<=7, -17<=k<=17, -18<=l<=17	
Reflections collected	14555	
Independent reflections	5113 [R(int) = 0.0240]	
Completeness to theta = 32.57°	99.2 %	
Absorption correction	None	
Max. and min. transmission	0.9843 and 0.9730	
Refinement method	Full-matrix least-squares on F^2	
Data / restraints / parameters	5113 / 0 / 199	
Goodness-of-fit on F^2	1.050	
Final R indices [I>2sigma(I)]	R1 = 0.0406, wR2 = 0.1169	
R indices (all data)	R1 = 0.0539, wR2 = 0.1267	
Largest diff. peak and hole	0.441 and -0.279 $e.Å^{-3}$	

Crystal data and structure refinement for **32HEP**.

Identification code	sf0916m	
Empirical formula	C32 H50 N4 O6	
Formula weight	586.76	
Temperature	120(2) K	
Wavelength	0.71073 Å	
Crystal system	Triclinic	
Space group	P-1	
Unit cell dimensions	a = 5.0819(4) Å	a= 71.273(4)°.
	b = 12.1581(11) Å	b= 87.334(4)°.
	c = 13.7060(11) Å	g = 80.885(4)°.
Volume	791.87(11) $Å^3$	
Z	1	
Density (calculated)	1.230 Mg/m^3	
Absorption coefficient	0.085 mm^{-1}	
F(000)	318	
Crystal size	0.32 x 0.24 x 0.14 mm^3	
Theta range for data collection	1.57 to 31.49°.	
Index ranges	-7<=h<=7, -10<=k<=17, -19<=l<=20	
Reflections collected	12589	
Independent reflections	4649 [R(int) = 0.0222]	
Completeness to theta = 27.50°	95.1 %	
Absorption correction	None	
Refinement method	Full-matrix least-squares on F^2	
Data / restraints / parameters	4649 / 0 / 197	
Goodness-of-fit on F^2	1.113	
Final R indices [I>2sigma(I)]	R1 = 0.0496, wR2 = 0.1411	
R indices (all data)	R1 = 0.0643, wR2 = 0.1513	
Largest diff. peak and hole	0.301 and -0.315 e.$Å^{-3}$	

Crystal data and structure refinement for **32OCT**.

Identification code	sf0922m	
Empirical formula	C34 H54 N4 O6	
Formula weight	614.81	
Temperature	120(2) K	
Wavelength	0.71073 Å	
Crystal system	Triclinic	
Space group	P-1	
Unit cell dimensions	a = 5.1476(9) Å	α= 71.870(5)°.
	b = 11.756(2) Å	β= 89.300(6)°.
	c = 14.714(3) Å	γ = 79.313(5)°.
Volume	830.6(3) $Å^3$	
Z	1	
Density (calculated)	1.229 g/cm^3	
Absorption coefficient	0.084 mm^{-1}	
F(000)	334	
Crystal size	0.22 x 0.16 x 0.12 mm^3	
Theta range for data collection	4.03 to 32.58°.	
Index ranges	-7<=h<=7, -17<=k<=17, -22<=l<=21	
Reflections collected	12360	
Independent reflections	5396 [R(int) = 0.0319]	
Completeness to theta = 30.00°	95.7 %	
Absorption correction	None	
Max. and min. transmission	0.9900 and 0.9817	
Refinement method	Full-matrix least-squares on F^2	
Data / restraints / parameters	5396 / 0 / 206	
Goodness-of-fit on F^2	1.033	
Final R indices [I>2sigma(I)]	R1 = 0.0521, wR2 = 0.1385	
R indices (all data)	R1 = 0.0764, wR2 = 0.1544	
Largest diff. peak and hole	0.392 and -0.243 $e.Å^{-3}$	

Crystal data and structure refinement for **32LAU**.

Identification code	sf0914m	
Empirical formula	C42 H70 N4 O6	
Formula weight	727.02	
Temperature	120(2) K	
Wavelength	0.71073 Å	
Crystal system	Triclinic	
Space group	P-1	
Unit cell dimensions	a = 4.9566(9) Å	α= 86.710(7)°.
	b = 6.8438(12) Å	β= 88.938(8)°.
	c = 30.988(6) Å	γ = 80.797(7)°.
Volume	1035.9(3) $Å^3$	
Z	1	
Density (calculated)	1.165 g/cm^3	
Absorption coefficient	0.077 mm^{-1}	
F(000)	398	
Crystal size	0.26 x 0.14 x 0.04 mm^3	
Theta range for data collection	2.63 to 31.00°.	
Index ranges	-7<=h<=7, -5<=k<=9, -43<=l<=44	
Reflections collected	21462	
Independent reflections	6407 [R(int) = 0.0664]	
Completeness to theta = 31.00°	97.4 %	
Absorption correction	None	
Max. and min. transmission	0.9969 and 0.9802	
Refinement method	Full-matrix least-squares on F^2	
Data / restraints / parameters	6407 / 0 / 241	
Goodness-of-fit on F^2	1.179	
Final R indices [I>2sigma(I)]	R1 = 0.0760, wR2 = 0.1926	
R indices (all data)	R1 = 0.1217, wR2 = 0.2117	
Largest diff. peak and hole	0.464 and -0.308 $e.Å^{-3}$	

Crystal data and structure refinement for **33SUC**.

Identification code	sf0935m	
Empirical formula	C24 H32 N4 O6	
Formula weight	472.54	
Temperature	296(2) K	
Wavelength	0.71073 Å	
Crystal system	Monoclinic	
Space group	P2/n	
Unit cell dimensions	a = 5.6265(5) Å	a= 90°.
	b = 5.0514(4) Å	b= 93.156(5)°.
	c = 41.791(4) Å	g = 90°.
Volume	1185.98(18) $Å^3$	
Z	2	
Density (calculated)	1.323 Mg/m^3	
Absorption coefficient	0.096 mm^{-1}	
F(000)	504	
Crystal size	0.36 x 0.14 x 0.06 mm^3	
Theta range for data collection	3.84 to 30.11°.	
Index ranges	-5<=h<=7, -7<=k<=5, -58<=l<=58	
Reflections collected	12813	
Independent reflections	3407 [R(int) = 0.0609]	
Completeness to theta = 30.11°	97.6 %	
Absorption correction	None	
Max. and min. transmission	0.9943 and 0.9663	
Refinement method	Full-matrix least-squares on F^2	
Data / restraints / parameters	3407 / 0 / 160	
Goodness-of-fit on F^2	1.042	
Final R indices [I>2sigma(I)]	R1 = 0.0547, wR2 = 0.1379	
R indices (all data)	R1 = 0.1196, wR2 = 0.1632	
Largest diff. peak and hole	0.208 and -0.198 e.$Å^{-3}$	

Crystal data and structure refinement for **33SUB**.

Identification code	sf0919m	
Empirical formula	C28 H40 N4 O6	
Formula weight	528.64	
Temperature	120(2) K	
Wavelength	0.71073 Å	
Crystal system	Triclinic	
Space group	P-1	
Unit cell dimensions	a = 4.9897(14) Å	α= 94.517(9)°.
	b = 6.8639(18) Å	β= 92.960(10)°.
	c = 20.045(5) Å	γ = 99.537(9)°.
Volume	673.5(3) $Å^3$	
Z	1	
Density (calculated)	1.303 g/cm^3	
Absorption coefficient	0.092 mm^{-1}	
F(000)	284	
Crystal size	0.28 x 0.14 x 0.08 mm^3	
Theta range for data collection	3.10 to 32.58°.	
Index ranges	-7<=h<=6, -10<=k<=8, -30<=l<=29	
Reflections collected	11396	
Independent reflections	4516 [R(int) = 0.0399]	
Completeness to theta = 30.00°	97.2 %	
Absorption correction	None	
Max. and min. transmission	0.9927 and 0.9747	
Refinement method	Full-matrix least-squares on F^2	
Data / restraints / parameters	4516 / 0 / 178	
Goodness-of-fit on F^2	1.042	
Final R indices [I>2sigma(I)]	R1 = 0.0547, wR2 = 0.1314	
R indices (all data)	R1 = 0.0957, wR2 = 0.1495	
Largest diff. peak and hole	0.325 and -0.259 $e.Å^{-3}$	

Crystal data and structure refinement for **33PIM**.

Identification code	sf0925m	
Empirical formula	C34 H50 N4 O10	
Formula weight	674.78	
Temperature	120(2) K	
Wavelength	0.71073 Å	
Crystal system	Triclinic	
Space group	P-1	
Unit cell dimensions	a = 5.1587(3) Å	α= 86.165(3)°.
	b = 11.5313(7) Å	β= 80.328(3)°.
	c = 14.8862(9) Å	γ = 78.897(3)°.
Volume	856.06(9) $Å^3$	
Z	1	
Density (calculated)	1.309 g/cm^3	
Absorption coefficient	0.096 mm^{-1}	
F(000)	362	
Crystal size	0.28 x 0.20 x 0.12 mm^3	
Theta range for data collection	2.78 to 31.50°.	
Index ranges	-7<=h<=7, -16<=k<=16, -21<=l<=21	
Reflections collected	20473	
Independent reflections	5667 [R(int) = 0.0416]	
Completeness to theta = 31.50°	99.3 %	
Absorption correction	None	
Max. and min. transmission	0.9885 and 0.9735	
Refinement method	Full-matrix least-squares on F^2	
Data / restraints / parameters	5667 / 0 / 226	
Goodness-of-fit on F^2	1.072	
Final R indices [I>2sigma(I)]	R1 = 0.0459, wR2 = 0.1279	
R indices (all data)	R1 = 0.0657, wR2 = 0.1411	
Largest diff. peak and hole	0.435 and -0.250 $e.Å^{-3}$	

Appendix D - Infrared Spectra of cocrystals of 27-29

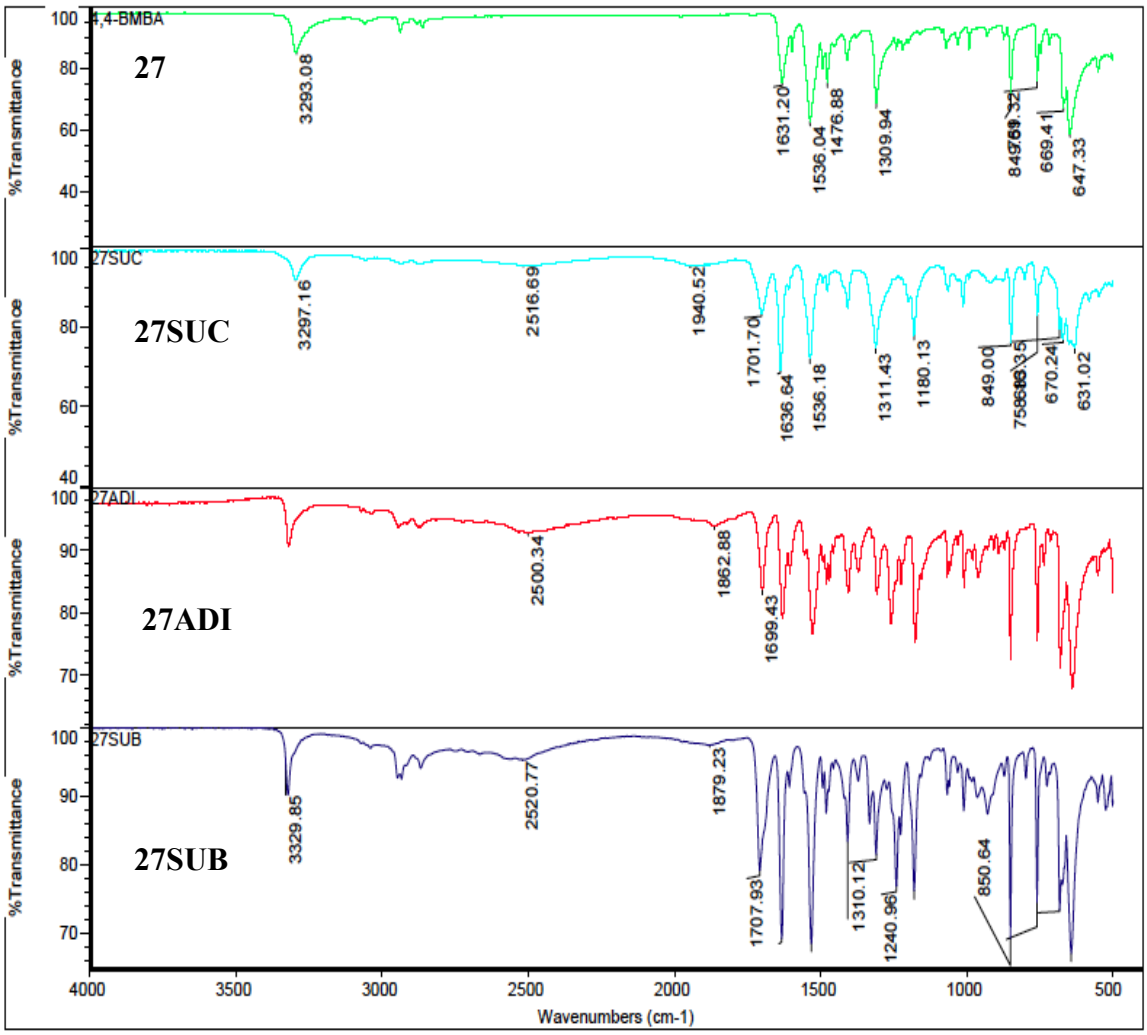

Figure D.1 FT-IR of **27** (green), **27SUC** (turquoise), **27ADI** (red) and **27SUB** (blue).

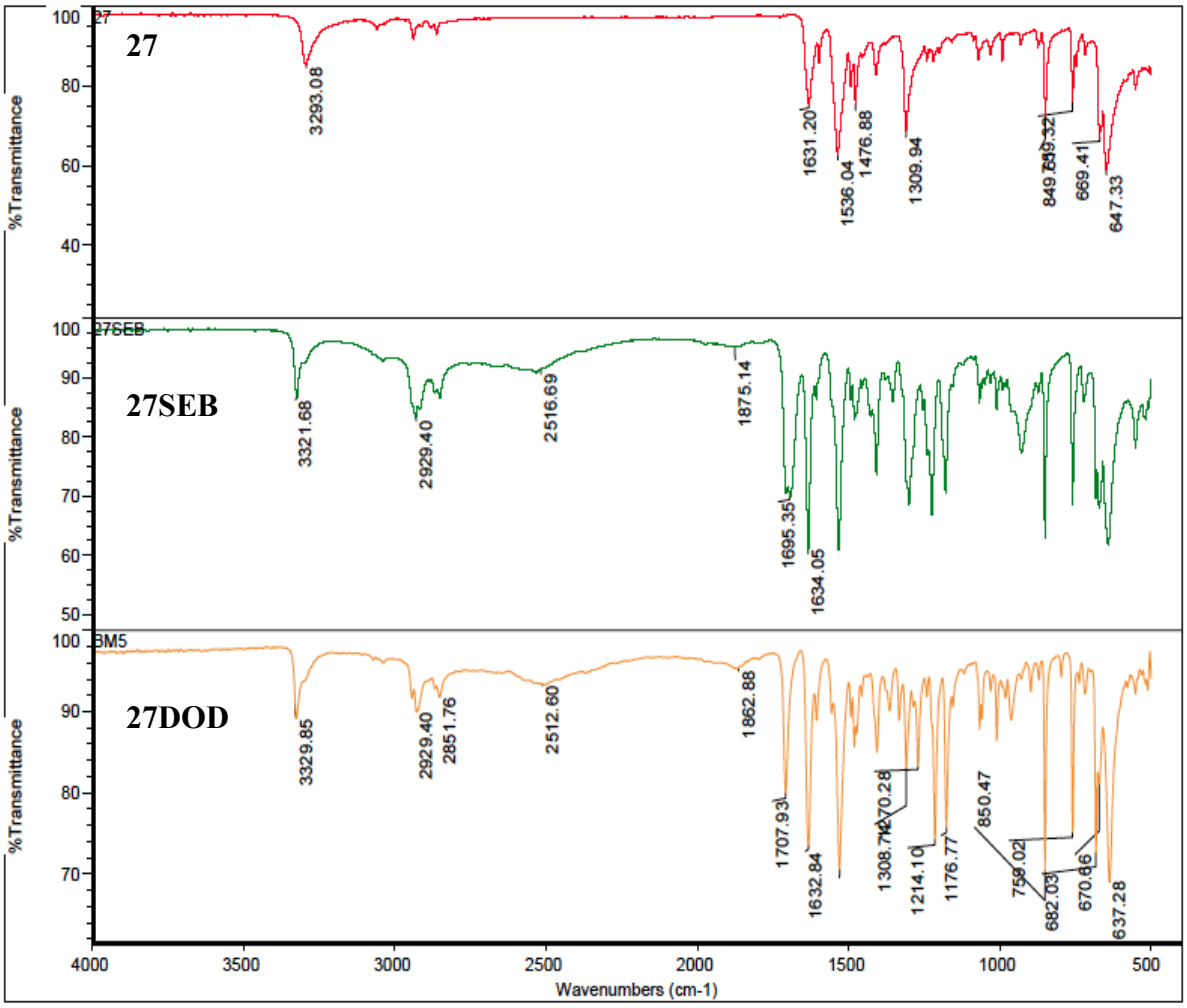

Figure D.2 FT-IR of **27** (red), **27SEB** (green) and **27DOD** (orange).

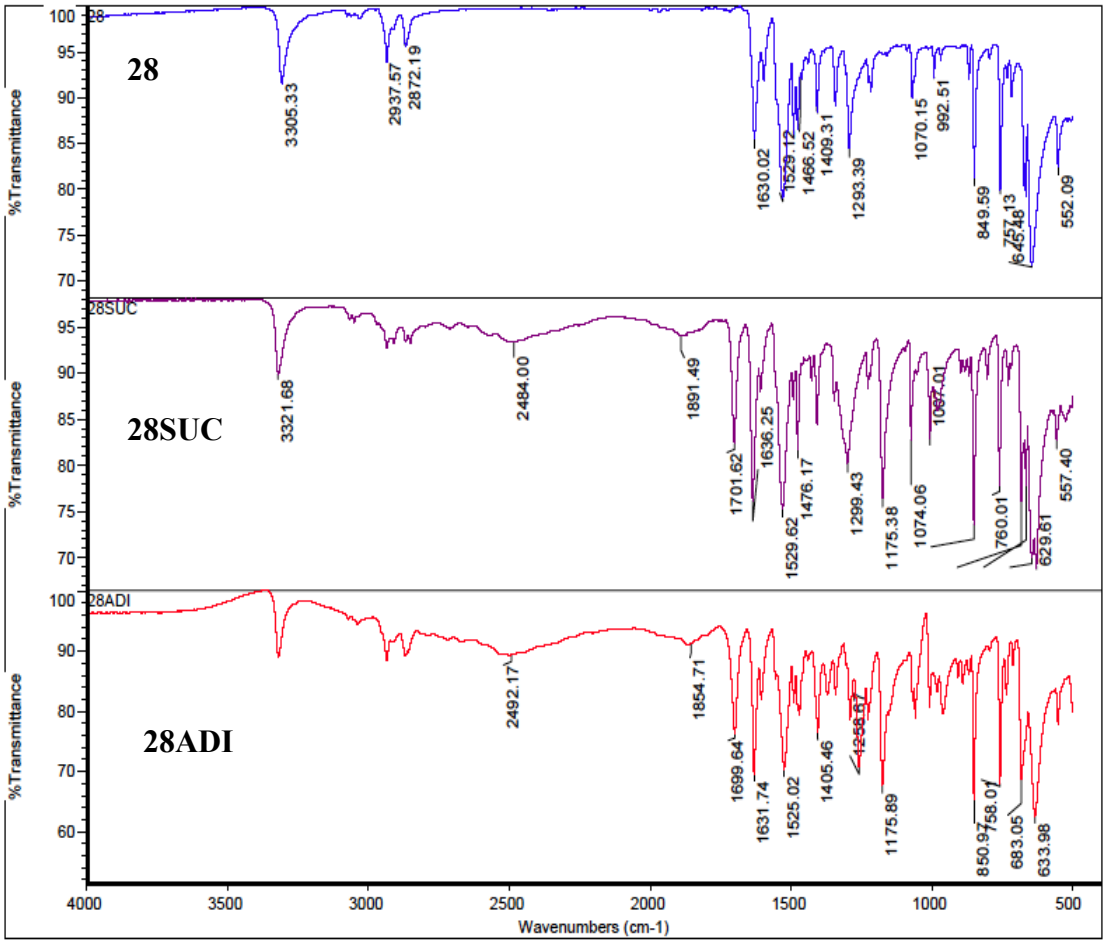

Figure D.3 FT-IR of **28** (blue), **28SUC** (purple) and **28ADI** (red).

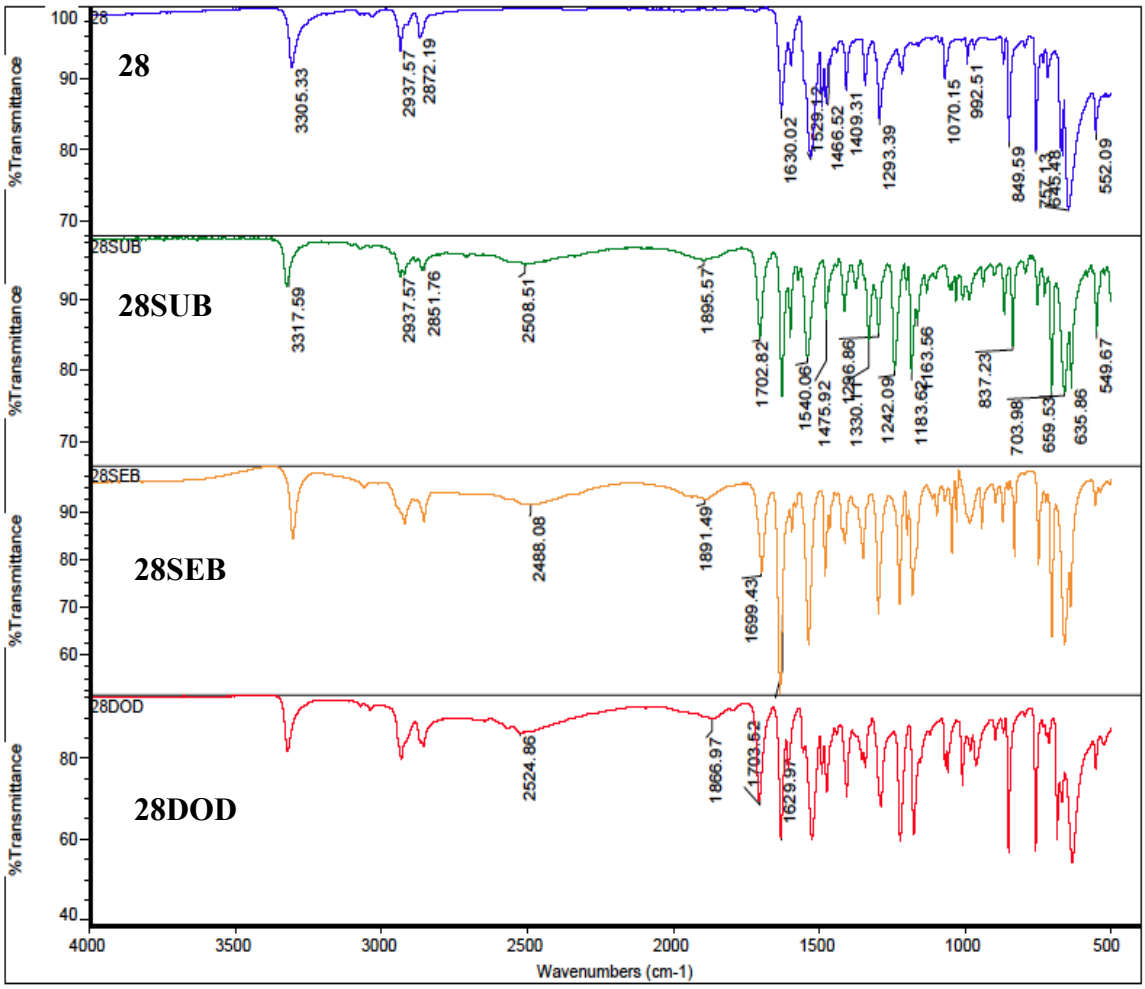

Figure D.4 FT-IR of **28** (blue), **28SUB** (green), **28SEB** (orange) and **28DOD** (red).

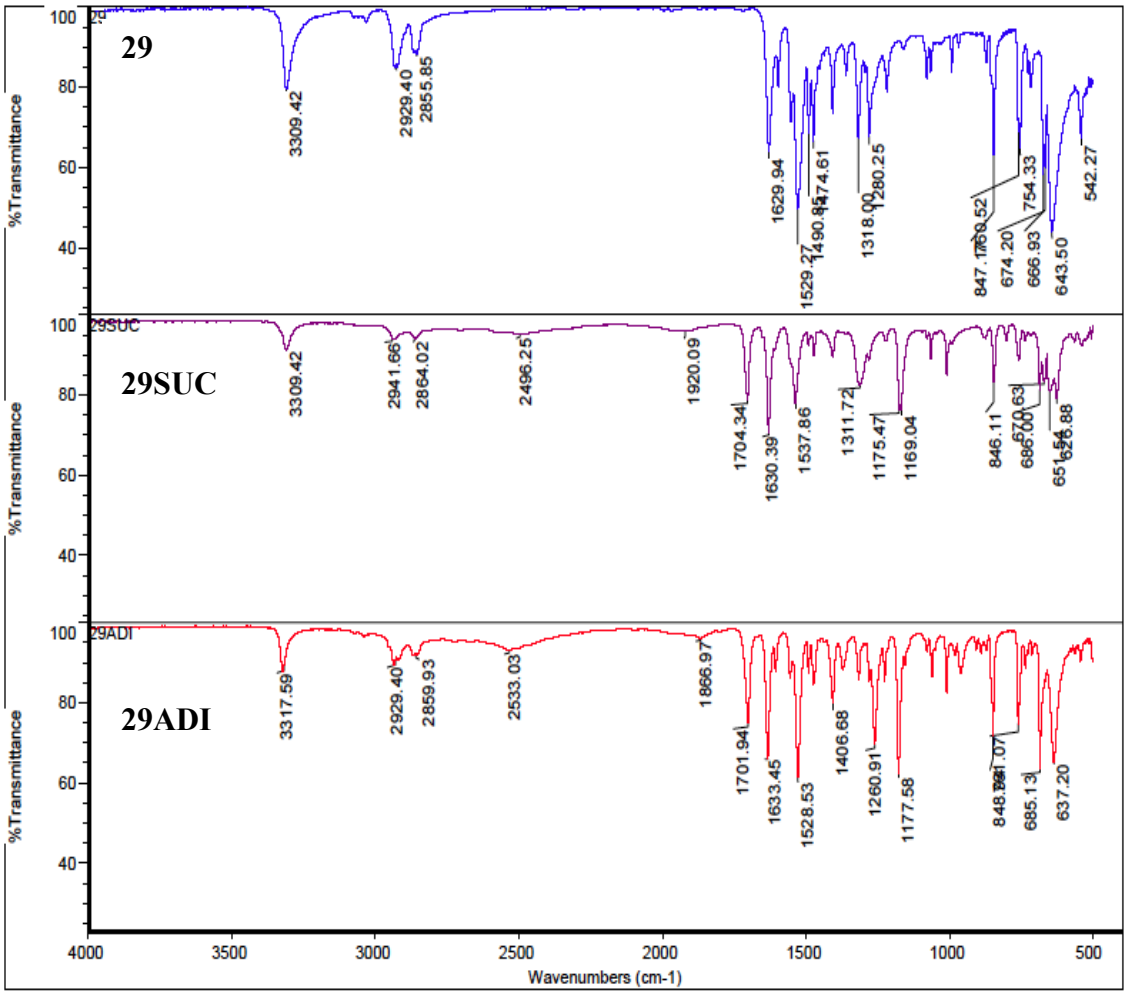

Figure D.5 FT-IR of **29** (blue), **29SUC** (purple), **29ADI** (red).

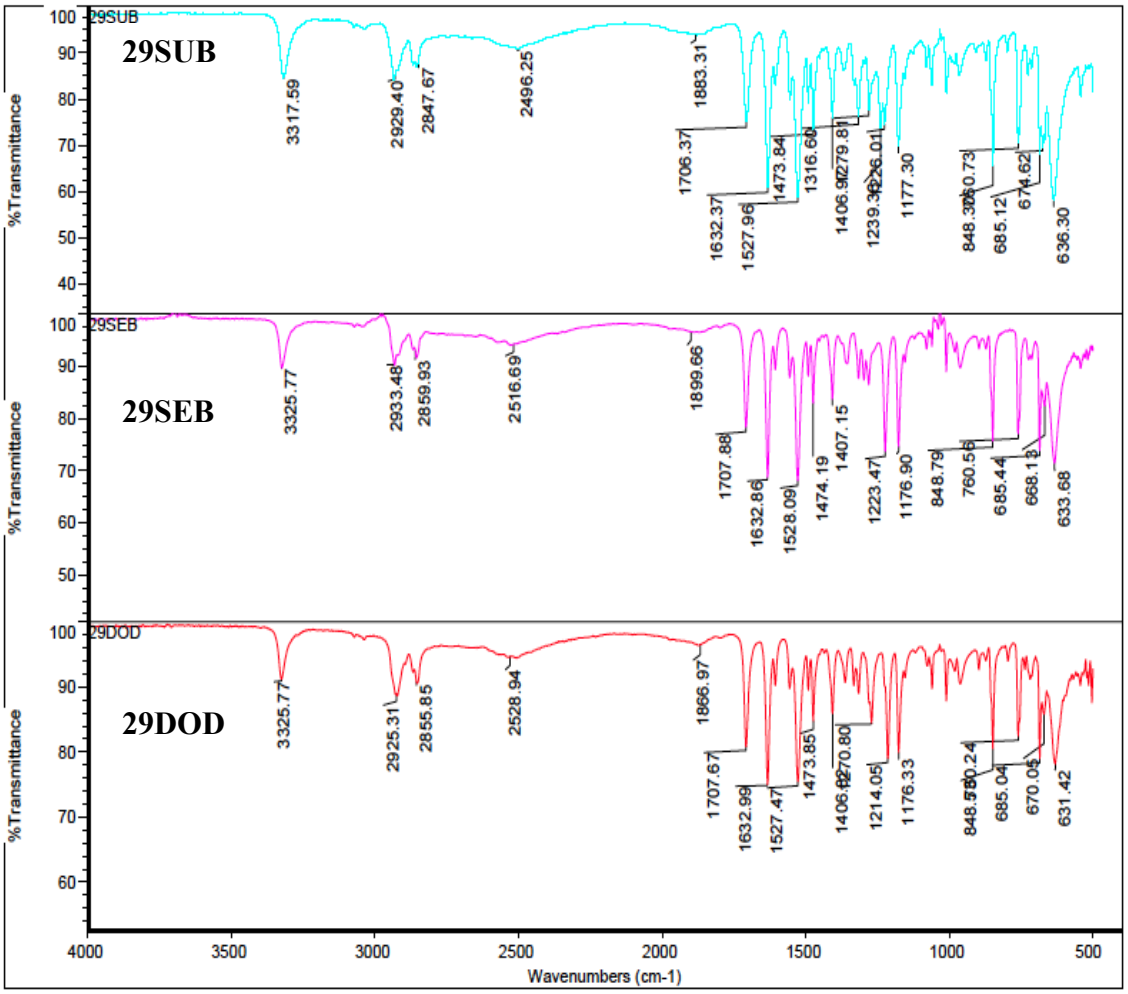

Figure D.6 FT-IR of **29SUB** (turquoise), **29SEB** (pink), **29DOD** (red).

Appendix E - Solubility data for cocrystals of 28 and 29

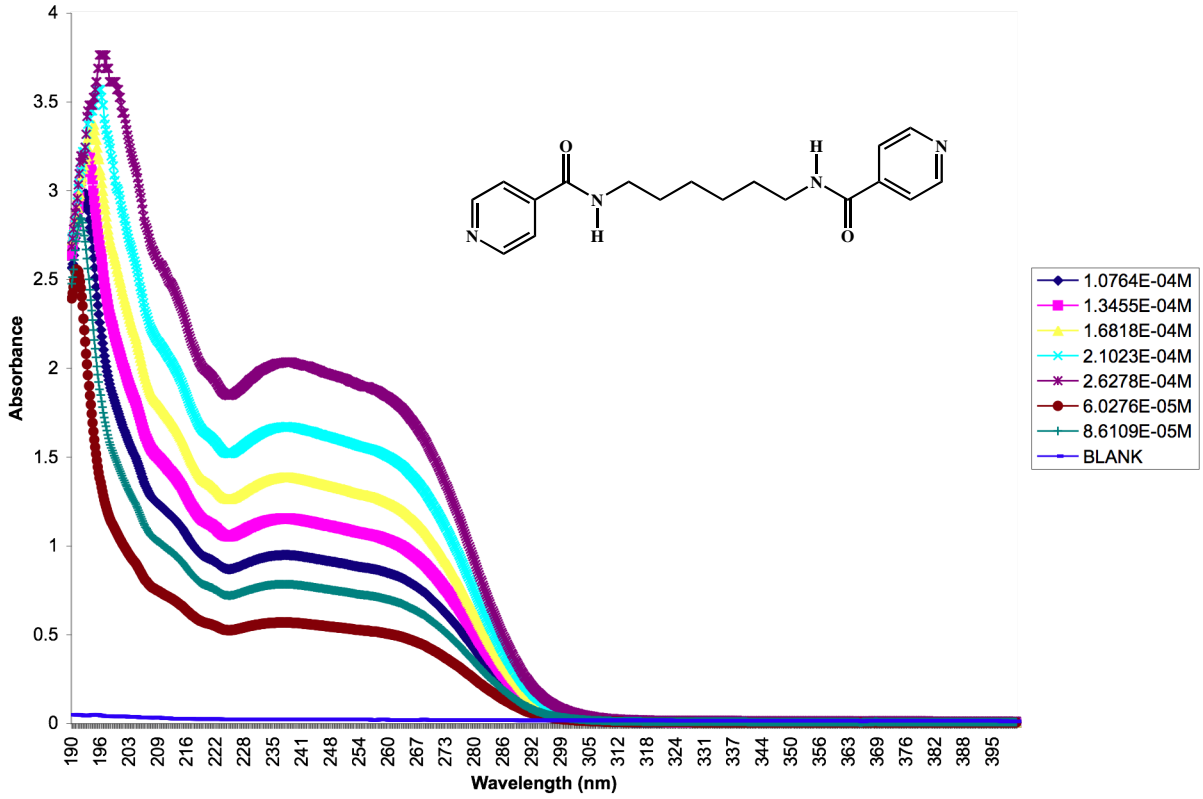

Figure E.1 UV-Vis profile for **28**

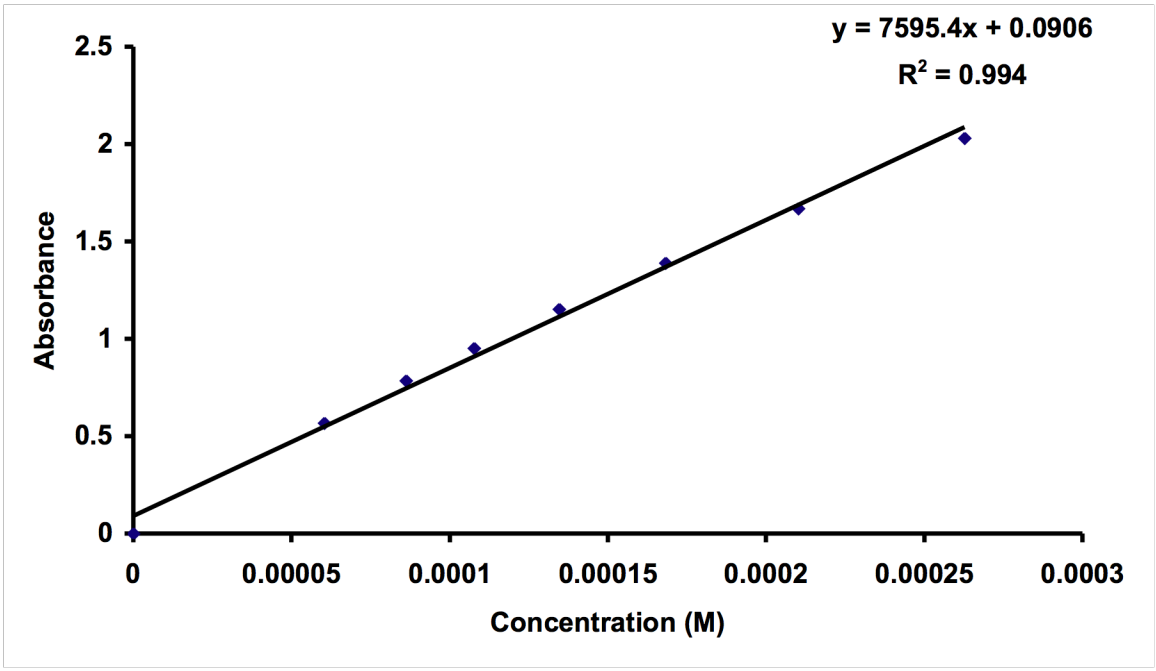

Figure E.2 Calibration curve of **28**

Table E.1 Solubility of cocrystals **28SUC-28DOD** and single component crystals, **28** in water at T = 25°C

Sample	Solubility (g/L)
28	0.2151± 0.0209
28SUC	0.5122± 0.0024
28ADI	0.3594± 0.0052
28SUB	0.2820± 0.0038
28SEB	0.0371± 0.0032
28DOD	0.0222± 0.0001

Solubility values are the mean ± standard deviation of n = 4

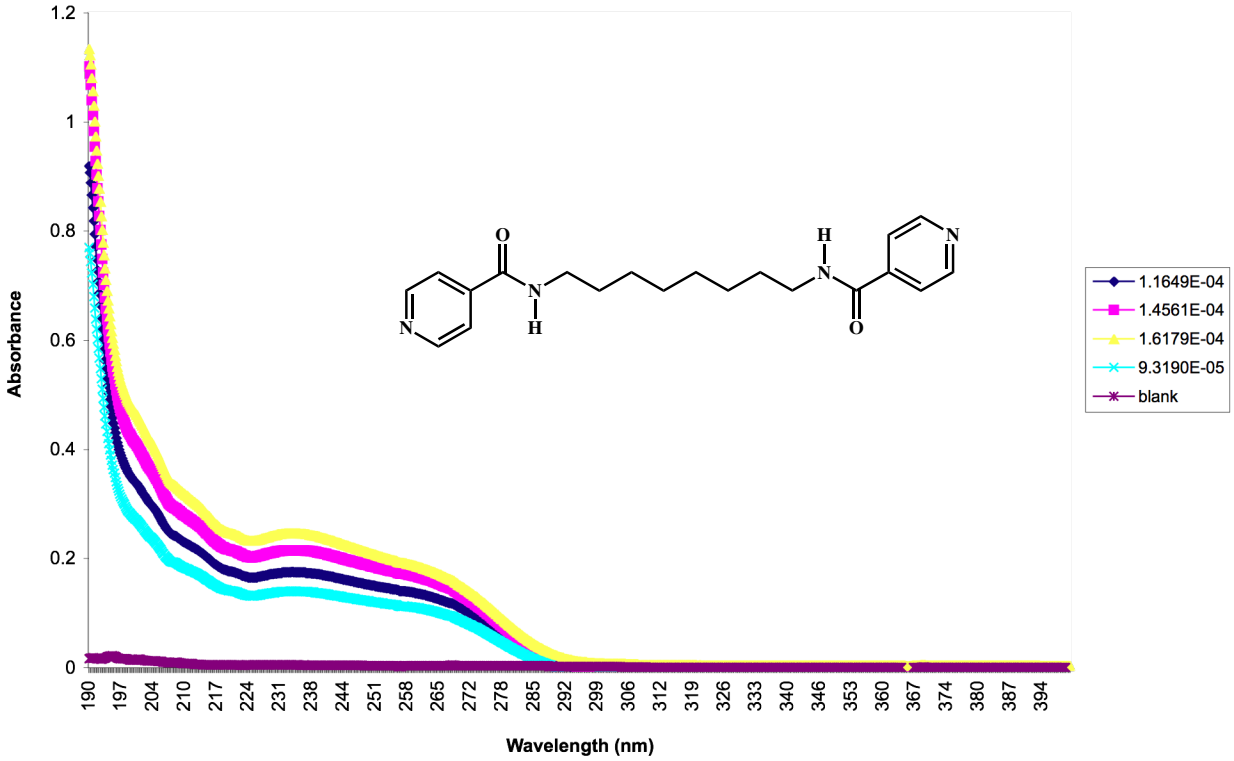

Figure E.3 UV-Vis profile of **29**

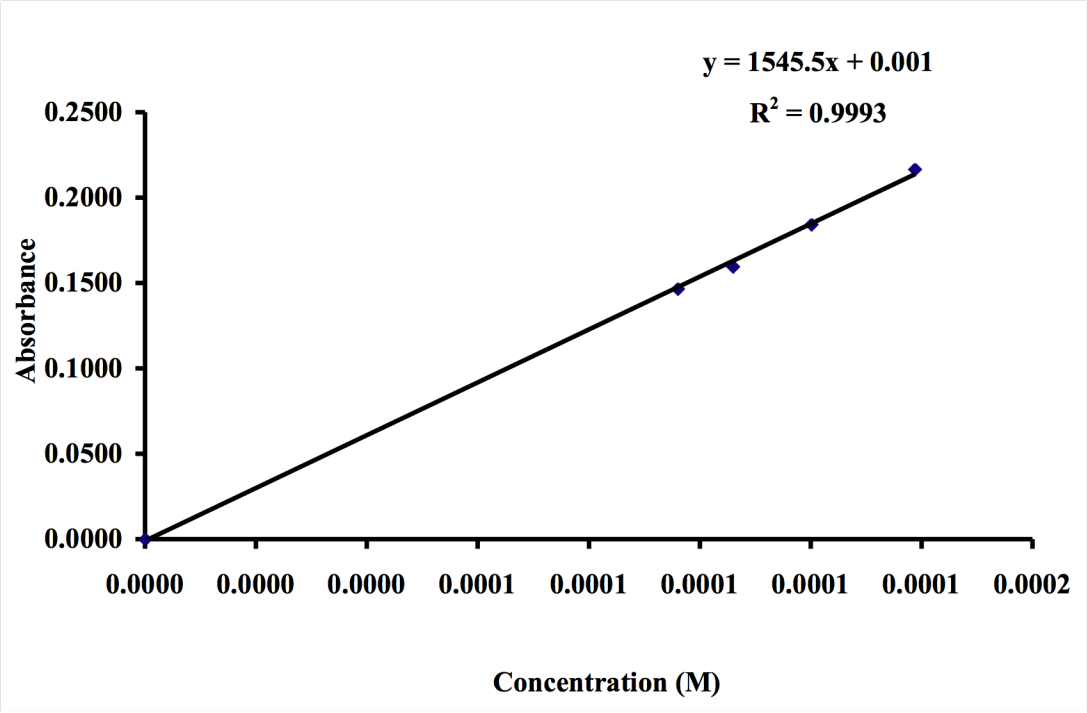

Figure E.4 Calibration curve of **29**

Table E.2 Solubility of cocrystals **29SUC-29DOD** and single component crystals, **29** in water at T = 25°C

Sample	Solubility (g/L)
29	0.0412 ± 0.04118
29SUC	0.1786± 0.001
29ADI	0.1076± 0.002
29SUB	0.0877± 0.002
29SEB	0.0523± 0.002
29DOD	0.0530± 0.001

Solubility of values are the mean ± standard deviation n = 4.